STRATIGRAPHIC INVESTIGATIONS OF THE WOLFCAMP GROUP IN CORE, OUTCROP, AND WELL LOGS IN THE PERMIAN BASIN OF WEST TEXAS

A Dissertation

by

BENJAMIN HENRY RICHARDS

Submitted to the Graduate and Professional School of
Texas A&M University
in partial fulfillment of the requirements for the degree of

DOCTOR OF PHILOSOPHY

Chair of Committee,	Michael C. Pope
Co-Chair of Committee,	Arthur D. Donovan
Committee Members,	Nicholas D. Perez
	Michael J. King
Head of Department,	Julie Newman

December 2021

Major Subject: Geology

ABSTRACT

The Lower Permian Wolfcamp Group in the West Texas Permian Basin is recognized as an economically significant unit that has extremely complex stratigraphy. These deposits were historically well studied only in isolated regions where data was abundant, as is the case on the highly developed Eastern Shelf of Midland Basin (a sub-region of the Greater Permian Basin) or in outcrop exposures. More recently, data has become abundant in the basinal occurrences of the Wolfcamp Group, first in Midland Basin and then in Delaware Basin. This work integrates a variety of data sets to delineate the regional stratigraphy of the Wolfcamp Group in multiple settings across the Permian Basin.

First, two extended (>1000' thick) cores through the Wolfcamp Group in Southern Midland Basin and their XRF-derived chemofacies are interpreted through a novel stratigraphic model which posits that siliceous deposition and carbonate deposition can, under certain conditions, reflect highstand and lowstand conditions, respectively. This differs from the implementation of the traditional reciprocal-sedimentation model, which often assumes that significant detrital sediment is available, and that inherited topographies are such that shallow (photic zone) carbonate factories have reduced surface area during sea level lowstands.

Second, proximal deposits in the Wolf Camp Hills type-locality outcrops were studied using traditional stratigraphic techniques combined with drone photogrammetry and handheld gamma-ray spectroscopy to document two large-scale (3rd-order)

sequences occurring in the Lower Wolfcamp Formation. These sequences are bounded by unconformities and associated carbonate-clast conglomerate deposition and create a framework into which chemostratigraphic data are placed.

Third, available well log data is used to correlate chronostratigraphic surfaces in the Wolfcamp Group from the tectonically complex and understudied Southern Delaware Basin near the type section outcrops to the Southern Midland Basin (west-east correlations) and to the central Delaware Basin (south-north correlations). These correlations create a chronostratigraphic framework into which absolute age dates can be extrapolated with confidence across the Greater Permian Basin.

In summary, the results of these studies reinforce the complex nature of Wolfcamp Group stratigraphy, which varies dramatically as a function of its position within the Greater Permian Basin. Specifically, distal, basin floor strata contain thick and complex lowstand sedimentary packages, sometimes carbonate-rich, which are expressed as unconformities overlain by carbonate-clast conglomerates in proximal strata. Conversely, transgressive and highstand system tracts result in the deposition of highly radioactive (>100 API units) mudstone intervals, often siliceous in composition, which are apparent on well logs and can be correlated regionally, including from the basin center onto the Southern Shelf. These correlated surfaces connect studied cores in Southern Midland Basin with the outcrops in Southern Delaware Basin, and provide a unifying framework for the Wolfcamp Group in the Greater Permian Basin.

DEDICATION

This dissertation is dedicated to my family – my wife, my son, and my parents.

Thank you for everything.

ACKNOWLEDGEMENTS

I would like to express my utmost gratitude to the many individuals and organizations which made this dissertation possible. First, I would like to thank my advisors, Drs. Mike Pope and Art Donovan, who gave me this opportunity. This gratitude extends to committee members Drs. Nick Perez and Mike King, whose unique perspectives and rigorous thinking made our interactions stimulating and productive.

Several individuals associated with University Lands were also key players and enthusiastic partners in these investigations. I would especially like to thank Brian Casey, now at the Bureau of Economic Geology, and John Tackett for their many contributions. In 2017, prior to my formal start at Texas A&M, Brian also played a unique role mentoring myself and others in the creation of a 3D static model which added real value while being an incredibly informative experience for myself. I would also like to thank the Berg-Hughes Center for their support, including the previous and current directors Drs. Dengo and Bhatia.

Finally, the many people I met in the department were universally friendly, bright and eager to help. In particular I would like to thank the former and current students Philipp Tesch, Connor Moore, Matt Wehner, Roy Conte, Chris Griffith, Jake Sleight, Maria Gutierrez, Eric Peavey, Eileah Sims, and Nick Dusak. I am honored to have been a colleague of theirs.

CONTRIBUTORS AND FUNDING SOURCES

Contributors

This dissertation was supervised by Drs. Michael Pope and Arthur Donovan (Chair and Co-Chair), as well as Dr. Nicholas Perez of the Depart of Geology & Geophysics, and Dr. Michael King of the Department of Petroleum Engineering.

The data sets for the core-based research came from Fleur de Lis Energy, Sable Permian Resources, University Lands, and W.D. Von Gonten Laboratories. Original X-Ray Fluorescence data for this work was collected with the assistance of colleagues Matthew Wehner and Conor Sullivan. Outcrop data from the Lenox Hills is from colleagues Eric Peavey and Nicholas Dusak. Data for well log-based research came from Enverus, MJ Systems, and University Lands. All other work conducted for the dissertation was completed by the student independently.

Funding Sources

The Geology & Geophysics Department, as well as the Berg-Hughes Center, both provided direct and generous financial support. Additional financial support came from the American Association of Petroleum Geologists Milliken Memorial Grant (2018), the Houston Geological Society Calvert Memorial Scholarship (2019-2021). Additional support came the Geology and Geophysics Department's Mary & Michael Blackwell '73 Endowed Scholarship (2020) and the ConocoPhillips/HEEP Endowment Graduate Fellowship (2020).

NOMENCLATURE

AAPG	American Association of Petroleum Geology
Al	Aluminum
API	American Petroleum Institute
BEG	Bureau of Economic Geology
Ca	Calcium
DOM	Digital Outcrop Model
GR	Gamma-Ray
HEB	Hybrid Event Bed
HST	Highstand System Tract
IFP	Institut Français du Pétrole
ILD	Deep Induction (wireline log tool)
k.y.	Thousand year(s), duration
LLD	Laterolog (wireline log tool)
LST	Lowstand System Tract
Ma	Million year (Age)
Mo	Molybdenum
MWU	Mid-Wolfcamp Unconformity
Ni	Nickel
Ohmm	Ohm * meter(s)
PeF	Photoelectric Factor
ppm	Parts per million

SB	Sequence Boundary
Si	Silicon
TOC	Total Organic Content
TST	Transgressive System Tract
WCH	Wolf Camp Hills
XRD	X-Ray Diffraction
XRF	X-Ray Fluorescence
Zr	Zirconium

TABLE OF CONTENTS

Page

LIST OF FIGURES

Page

LIST OF TABLES

Page

CHAPTER I

INTRODUCTION

Background

The term “Wolfcamp” was originally applied to a Lower Permian formation cropping out in the eponymous Wolf Camp Hills (Udden, 1917) at the foot of the Glass Mountains in Brewster County in West Texas. Having later been adopted as a series name on the geologic timescale (Adams et al., 1939), the Wolfcampian Series in the Glass Mountains was recognized as containing two distinct formations, the lower Neal Ranch Formation in the Wolf Camp Hills, and the upper Lenox Hills Formation in the nearby Lenox Hills (Ross, 1963) but these formation names were never widely adopted in the subsurface, and this study therefore refers to the combined Wolfcamp Group.

These Lower Permian rocks had been reasonably well studied in outcrop where they are carbonate-rich (e.g., King, 1931) and later in the subsurface of the Greater Permian Basin where they are mudstone-rich (e.g., Hall, 1956), but their importance as a hydrocarbon source rock which could be targeted by oil-and-gas operators directly was not fully realized until around 2009 (Fairhurst and Hanson, 2012). Since then, interest and development around these rocks have grown exponentially, in both the western Delaware Basin and the eastern Midland Basin, both part of the Greater Permian Basin. While it was readily apparent that the Wolfcamp Group in the basin is extremely heterogeneous (e.g., Hamlin and Baumgardner, 2012), the controls on its basinal stratigraphy, and how it ties to the historically studied carbonate-rich outcrops, remained poorly understood.

Early stratigraphic models first developed for the Wolfcamp Group on the shallowly dipping Eastern Shelf of Midland Basin (e.g., Van Siclen, 1958) where individual clinoforms and their internal facies transitions were readily observed on extremely tightly spaced well logs. In other basins, models developed which predicted the development of carbonate strata in proximal settings at high sea levels, and the deposition of detrital silica in basinal settings during low sea levels and associated sediment bypass of fluvial input (Wilson, 1967). Building on this model, carbonate deposits observed on the basin floors were then often assumed to be the result of highstand shedding by carbonate factories (Droxler and Schlager, 1985).

Sequence stratigraphy evolved greatly with the advent of seismic data which enabled the visualization of true chronostratigraphic surfaces (e.g., Vail et al., 1977), often flooding surfaces capping individual clinoforms. When recognized, these surface prevent the lithostratigraphic grouping of seemingly similar facies tracts between adjacent rocks of distinct age, but seismic data taken on behalf of industry operators is often not publicly available and is not available for use in this study.

This study investigates the stratigraphy of the Wolfcamp Group in the Greater Permian Basin using cores in Reagan County, outcrops in Brewster County and with well log data spanning the region. These data are investigated in order to explore the controls of sedimentation in the basin, to identify and correlate chronostratigraphically significant markers between depositional environments, and to determine how the stratigraphy of the Wolfcamp Group varies across these sub-regions and over the course of its deposition, as a function of its position within the Greater Permian Basin.

References

Adams, J. E., M. G. Cheney, R. K. DeFord, R. I. Dickey, C. O. Dunbar, J. M. Hills, R. E. King, E. R. Lloyd, A. K. Miller, and C. E. Needham, 1939, Standard Permian section of North America: AAPG Bulletin, v. 23, no. 11, p. 1673-1678, doi: 10.1306/3D933136-16B1-11D7-8645000102C1865D.

Droxler, A. W., and W. Schlager, 1985. Glacial versus interglacial sedimentation rates and turbidite frequency in the Bahamas: Geology, v. 13, no. 11, p. 799-802.

Fairhurst, B., and M. Hanson, 2012, Evolution and Development of the WolfBone Play, Southern Delaware Basin, West Texas: An Emerging Frontier, An Oil-Rich Unconventional Resource: AAPG Search and Discovery Article, no. 10411.

Hall, W. E., 1956, Marathon folded belt in Big Bend area of Texas: AAPG Bulletin, v. 40, p. 2247-2255.

Hamlin, H. S., and R. W. Baumgardner, 2012, Wolfberry Play, Midland Basin, West Texas: AAPG Search and Discovery Article, no. 10419.

King, P. B., 1931, Geology of the Glass Mounatins, Part I, Descriptive Geology: Univ. Texas Bull. 3038, p. 51-90.

Ross, C. A., 1963, Standard Wolfcampian Series (Permian), Glass Mountains, Texas: Geol. Soc. America Mem. 88, 205 p.

Udden, J. A., 1917, Notes on the Geology of the Glass Mountains, Texas University Bulletin 1753, p. 3-59.

Van Siclen, D. C., 1958, Depositional topography—examples and theory: AAPG Bulletin v. 42, no. 8, p. 1897-1913.

Vail, P. R., R. M. Mitchum, and S., III, Thompson, 1977, Seismic stratigraphy and global changes of sea level, part four: global cycles of relative changes of sea level: American Association of Petroleum Geologists Memoir 26, p. 83–98.

Wilson, J. L., 1967, Cyclic and reciprocal sedimentation in Virgilian strata of southern New Mexico: Geological Society of America Bulletin, v. 78, no. 7, p. 805–818.

CHAPTER II

AN INTEGRATED CHEMO- AND SEQUENCE STRATIGRAPHIC ANALYSIS OF EXTENDED (>1000 FT) LOWER PERMIAN WOLFCAMP CORES, REAGAN COUNTY, WEST TEXAS

Abstract

Two 1000'+ (300 m) cores of Lower Permian (Wolfcampian) strata from Midland Basin, Texas were described bed-by-bed to establish an integrated lithostratigraphic, chemostratigraphic, and sequence stratigraphic framework. Ten lithofacies, where mudstones were defined as being finer than coarse silt in size, include: 1) dolostone, 2) floatstone, 3) graded skeletal grainstone, 4) graded skeletal wackestone and packstone, 5) graded calcisiltstone, 6) siliceous siltstone, 7) carbonate mudstone, 8) mixed siliceous-carbonate mudstone, 9) siliceous mudstone and 10) argillaceous mudstone. Using this framework, in conjunction with significant stratigraphic surfaces, four depositional sequences were identified and correlated between the two cores. Each sequence transitions up section from carbonate-rich intervals interpreted as lowstand deposits upward into siliceous mudstone beds where the dominant source of silica is biogenic, interpreted as pelagic transgressive to highstand deposits. This differs from the traditional deep-water reciprocal sedimentation model where quartz-rich strata are interpreted as lowstand deposits, and carbonate-rich strata are interpreted as transgressive to highstand deposits.

Introduction

The Wolfcamp Group in the Permian Basin, and in both the Delaware and Midland sub-basins (Figure II-1A), contains a series of stacked, tight-oil reservoirs intercalated with organic-rich mudstones. Since 2012, this stratigraphic unit has become one of the primary zones of unconventional reservoir exploitation by industry (Gaswirth, 2018). However, despite significant historical and ongoing interest in the Wolfcamp Group (e.g., Candelaria et al., 1992; Fitchen, 1997; Ross and Ross, 1997; Saller et al. 1999, Ruppel, 2001; Mary Van Der Loop; 2017; Thompson et al., 2018), its detailed basinal stratigraphy, as well as its relationship to more proximal shelf stratigraphy, are still not fully understood. Presently, some difficulty remains in determining the controls on sedimentation in the basin. This stems partially from the difficulty in applying traditional sequence stratigraphic models, which require the presence of fluvial systems along the basin margins to provide siliciclastic sediments to the basin during sea-level falls. Where fluvial systems are not present, the classic reciprocal sedimentation model does not apply. This inability to sub-divide the Wolfcamp Group into silicliclasitic-prone lowstand sediments and carbonate-rich transgressive to highstand sediments negatively impacts the ability of operators and public agencies to predict the occurrence and distribution of Wolfcampian sediments in the subsurface. Additionally, strata coeval to the Wolfcamp Group in the subsurface do not crop out near southern Midland Basin. Fortunately, extensive well data in this basin, coupled with an abundance of new core control, provides excellent insight into the Wolfcamp Group in the subsurface.

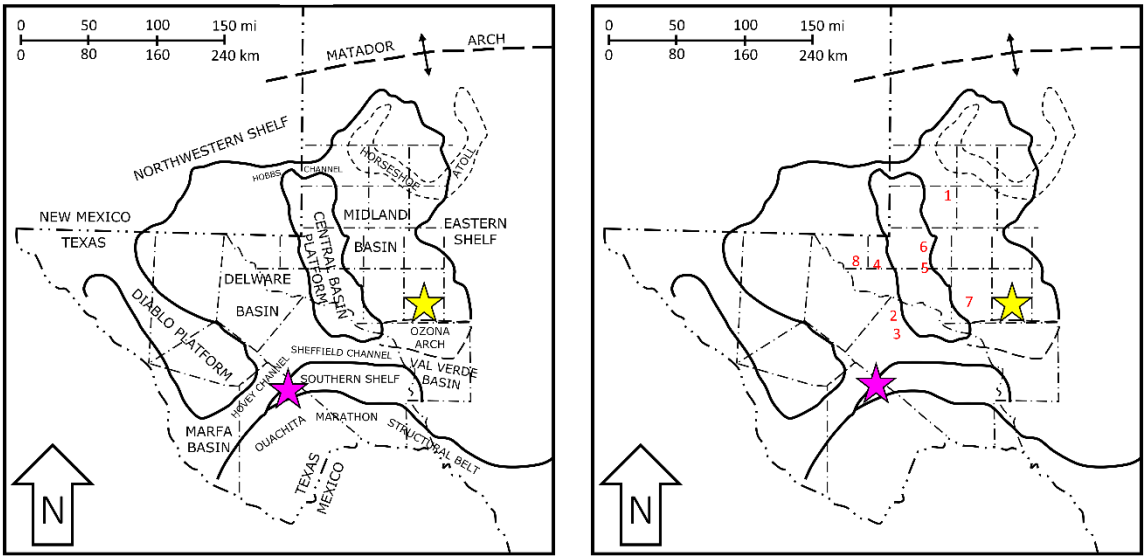

Figure II-1 (A) Map of the Permian Basin (left) with labelled Late Paleozoic features (modified from McKee and Oriel, 1967). The yellow star in Reagan County approximates the location of cored wells. The purple star in Brewster County approximates the location of the Wolf Camp Hills type outcrops. The red numbers (right) indicate a selection of historic Wolfcamp fields including the 1) Adair, 2) Coyanosa, 3) Gomez, 4) War Wink, 5) Fasken, 6) Parker, 7) Tippett, and 8) Morton fields.

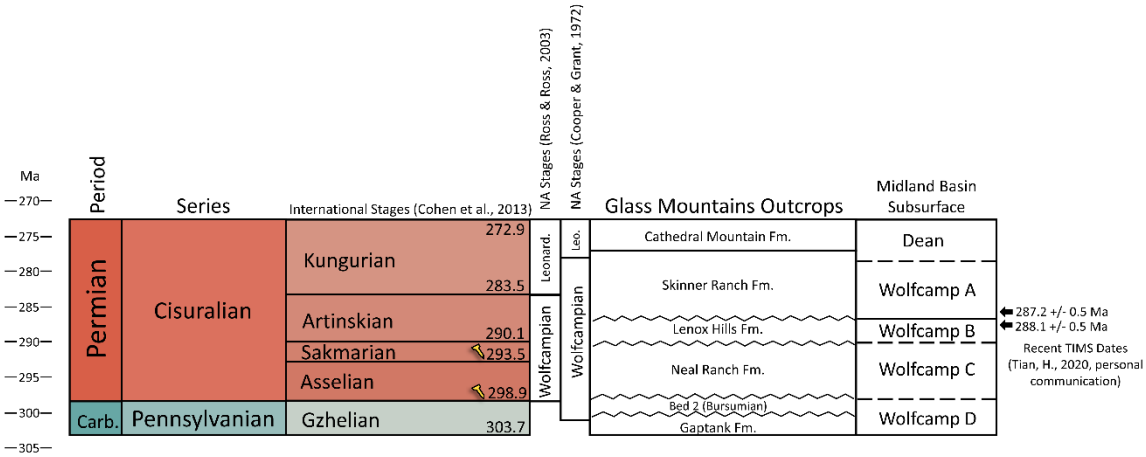

Figure II-1 (B) Stratigraphic chart for the Lower Permian Wolfcamp Group outcrops in the Glass Mountains, with correlative international stages and Midland Basin subsurface stratigraphy. Debate over biostratigraphic correlations necessitates absolute age dating; two recently determined dates (e.g. Thermal Ionization Mass Spectrometry) are shown at right from bentonite-derived zircon crystals near the Wolfcamp A/B boundary (Tian, H., 2020, personal communication). International stage ages from (Cohen et al., 2013; updated), note that the bases of both the Asselian and the Sakmarian have defined GSSPs.

Operators have used various schemes for sub-dividing the Wolfcamp Group in the subsurface using inconsistent top-down wireline log markers. The most commonly used scheme divides the Wolfcamp from the top down into the Wolfcamp A, B, C, and D (Figure II-1B), which are typically hundreds to thousands of feet thick (100's of meters). Unfortunately, the markers chosen as boundaries often vary within and among operators, as well as across the region (Figure II-2B). Additionally, some of the log markers may be lithostratigraphic boundaries that may not have any regional chronostratigraphic significance.

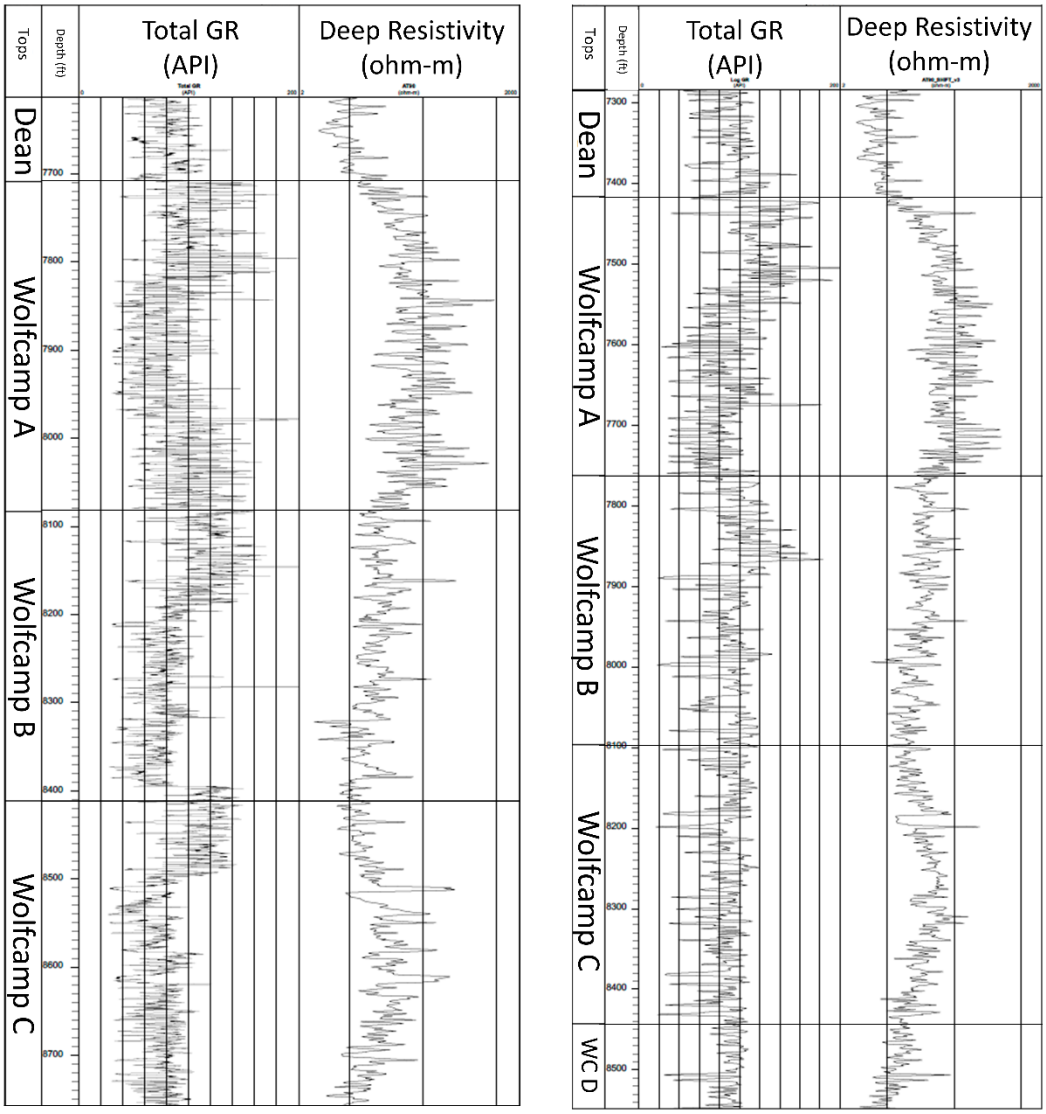

Figure II-2 Total gamma-ray and deep resistivity logs along cored intervals shown with subsurface names and core depth (core 1 on left; core 2 on right).

This research focused on a succession of basinal mudrock and carbonate facies through the Wolfcamp Group in two extended, continuous cores on state-owned University Lands acreage in southern Midland Basin, Reagan County, Texas (Figure 1). Potential stratigraphic implications of the resulting facies patterns also are also

discussed. The description of these cores includes high-resolution handheld XRF data which is crucial to understanding mudrock facies as well as providing organic and potential detrital indicators.

Geologic Setting and Context

The type section for the Wolfcamp Group, as defined in this paper, is in the Wolf Camp Hills (Udden, 1917), at the southern edge of the Glass Mountains in Brewster County, Texas (Figure II-1B). The type outcrops were later divided (Ross, 1959; Cooper and Grant, 1972) into multiple formations (e.g., Neal Ranch Formation, Lenox Hills Formation). The term "Wolfcampian" was also adapted to define the lowermost Permian Wolfcampian Series in North America (Ross, 1963; Childs, 1985). Strata mapped as the Wolfcamp Group in the subsurface became an important conventional reservoir in the subsurface beginning in the 1950's. Early oil fields producing from the "Wolfcampian" in the Permian Basin include the Adair Field discovered in 1950 in Terry County, which was followed by several others (e.g. Fasken, Parker, Amacker-Tippett, and Morton fields) mostly exploiting carbonate platform and proximal slope facies in both Midland and Delaware Basin and their adjacent shelves (Figure II-1A). Later exploration focused on fields in deeper slope and toe-of-slope basinal carbonate facies, including Coyanosa, Gomez, and War Wink fields (Dutton et al., 2004) and lateral facies variation in the Wolfcamp Group was documented along the eastern margin of Midland Basin using tightly spaced electric logs (Van Siclen, 1958).

Traditionally, the base of the North American Wolfcampian (Permian) was placed at an unconformity in outcrop (Adams et al., 1939). With the adoption of the International Commission on Stratigraphy Geologic Time Scale (Cohen et al., 2013), the current base of the Asselian (Permian) is now placed chronostratigraphically higher, at what appears to be a maximum flooding surface. The traditional North American base Wolfcampian (Permian) placement now resides in the Uppermost Pennsylvanian (Lucas, 2013).

In the subsurface the Wolfcamp Group has traditionally been interpreted as being Lower Permian (Böse, 1917; King, 1931; Ross, 1959). However, recent subsurface biostratigraphic work (Kohn, 2016; Barrick and Wahlman, 2019) suggests that some of the basal portions of the Wolfcamp Group, as presently mapped in the subsurface by some operators, are also Latest Pennsylvanian (North American Virgilian Stage), or equivalent to Gzhelian Stage (Aretz et al., 2020), based on the latest version of the geologic time scale (Cohen et al., 2013).

Additionally, there is no consensus as to where to carry the top of the Wolfcamp Group (base Leonard Group), at their type localities along the Glass Mountains. Ross and Ross (2003) place the base of the Leonardian at the base of the Skinner Ranch Formation (Figure II-1B). This interpretation places the base of the North American Leonardian Stage at or near the base of the international Kungurian Stage (Figure II-1B). However, Cooper and Grant (1972) place the base of the Leonardian at the base of the Cathedral Mountain Formation (Figure II-1B). This interpretation places the base of the North American Leonardian Stage within the middle Kungurian (Figure II-1B).

In the subsurface, the top of the Wolfcamp Group is likely Kungurian in age based on biostratigraphic work on the mudstones immediately below the basinal Dean Sandstone, towards the top of an interval known informally as the "Wolfcamp A" (Wilde, 1975, 1990; Mazzullo et al., 1987; Reid et al., 1988). Preliminary results of Thermal Ionization Mass Spectrometry (TIMS) geochronology of Upper Wolfcamp zircons (Tian, 2020, personal communication) suggest that bentonites dated from the lowermost Wolfcamp A and uppermost B are Artinskian (287 and 288 Ma, respectively).

This article follows the traditional subsurface definition of the Wolfcamp Group in the Midland Basin. Strata situated between the Dean Formation (above) and the Cisco Group (below) are mapped as the Wolfcamp Group. Future work of the Texas A&M Unconventional Reservoir & Outcrop (TAMU UROC) group will focus on tying the subsurface and surface stratigraphy of the Wolfcamp Group.

Finally, previous sequence stratigraphic interpretations of Wolfcamp Group stratigraphy largely focused on the proximal stratigraphy, as occurs on the Central Basin Platform (Saller et al., 1993; Ross and Ross, 2003). Newer work attempts to tease out subtle changes in relative accommodation in the basin (Bohacs and Schwalbach, 1992) as they relate to the occurrence of calciturbidites and debrites (Thompson et al., 2018). Specifically, calcidebrites were interpreted as a possible response to drops in relative sea level specifically for the Wolfcamp Group (Thompson et al., 2018) and in other settings (Reijmer et al., 2012). Calciturbidites too, were interpreted as potentially occurring more frequently during higher relative sea levels during the Wolfcampian (Thompson et al.,

2018). Other workers have focused on the distribution of lithofacies as a function of depositional processes type on the basin floor, while deemphasizing the role of relative sea level (Kvale et al., 2020).

Data and Methodology

Core data (Figure II-2) includes two nearly continuous cores (core 1 is 1145 ft [349 m] in length and core 2 is 1263 ft [385 m] in length) in Reagan County, in the southern Midland Basin just north of the Ozona Arch (Figure II-1A), a paleo-high during deposition (Flawn et al., 1961). Descriptions of the core slabs were performed bed-by-bed and sedimentary processes were interpreted at the log-scale for each bed. Additional data provided by the operators include core photographs under normal and ultraviolent light, a comprehensive well log suite from each borehole and 210 Total Organic Carbon (LECO TOC) measurements (variable spacing, intervals averaging 15 ft or 5 m) from W.D. Van Gonten Laboratories. For this study XRF data was measured at the bed scale, resulting in a total of 1149 XRF measurements taken every foot (30 cm) on core 1 and 2380 XRF measurements on core 2 taken approximately every 0.5 feet (15 cm). Major and minor elements were measured using a hand-held Bruker Tracer III for core 1, and an Olympus Delta Professional for core 2. All photo, log, XRF, and geochemical data and descriptions are integrated in the core logging software EasyCore. Sequence stratigraphic surfaces are interpreted directly on the core slab, as well as from lithofacies trends and the logs.

Results

Core Descriptions, X-Ray Fluorescence Data, and Lithofacies

The two cores record 2,408 feet (734 m) of described core, of which 2,179 feet (664 m) belong to the Wolfcamp Group (Figure II-2). Detailed core descriptions focus on bed and well log-scale features, facies analysis, and 3,529 original XRF measurements (Figure II-3).

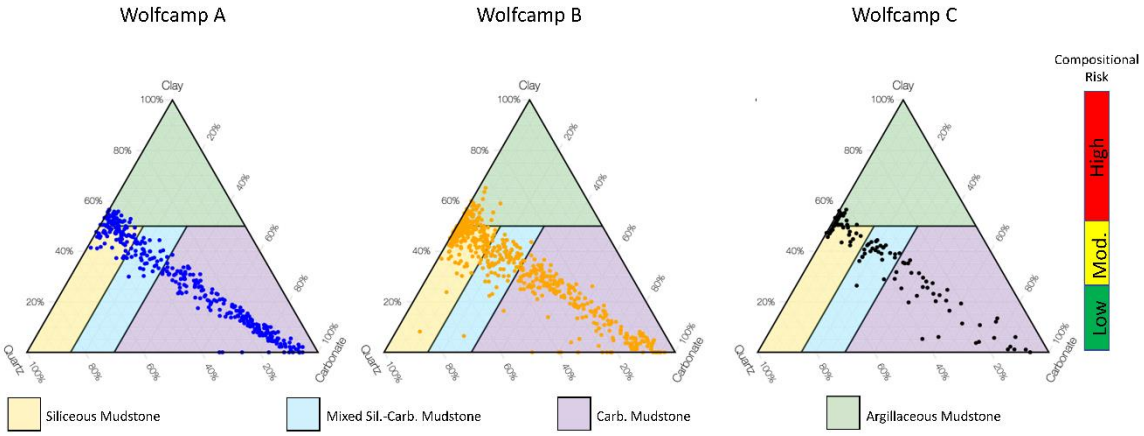

Figure II-3 (A) All XRF data points in the Wolfcamp Group (n=1029) from core 1 are plotted in ternary diagrams (for each sub-unit) with compositional (geomechanical) risk as a function of clay content (*sensu* Donovan et al., 2017).

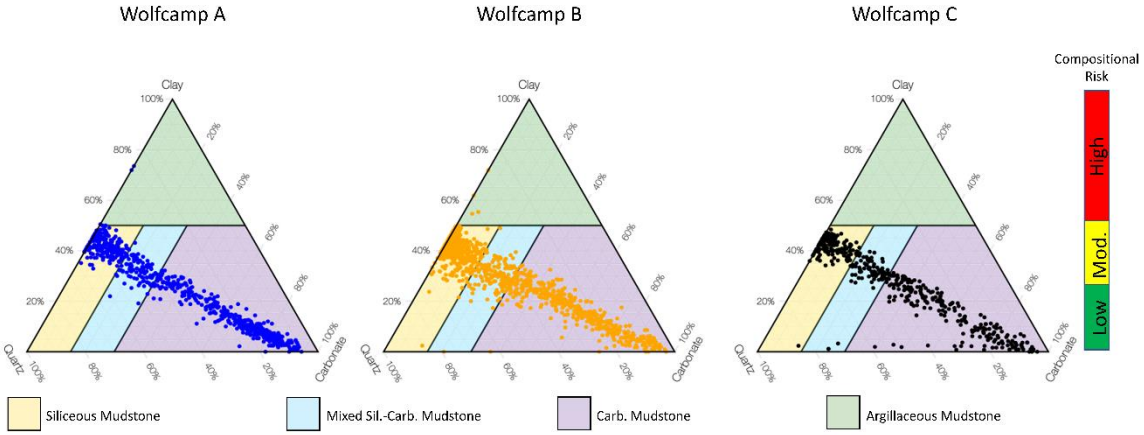

Figure II-3 (B) All XRF data points in the Wolfcamp Group (n=2182) from core 2 are plotted in ternary diagrams (for each sub-unit) with compositional (geomechanical) risk as a function of clay content (*sensu* Donovan et al., 2017).

Aluminum, calcium and silicon are interpreted as effective proxies for clay, carbonate and silicate mineral content, respectively, by comparing original XRF measurements with 74 provided X-Ray Diffraction (XRD) measurements through Wolfcamp Group from core 2 (Figure II-4). XRF compositional data through the Wolfcamp Group in core 1 and 2 (n = 1029 and 2182, respectively) are applied to Carbonate-Clay-Quartz (CCQ) Ternary Diagrams (Evenick, 2016; Donovan et al., 2017).

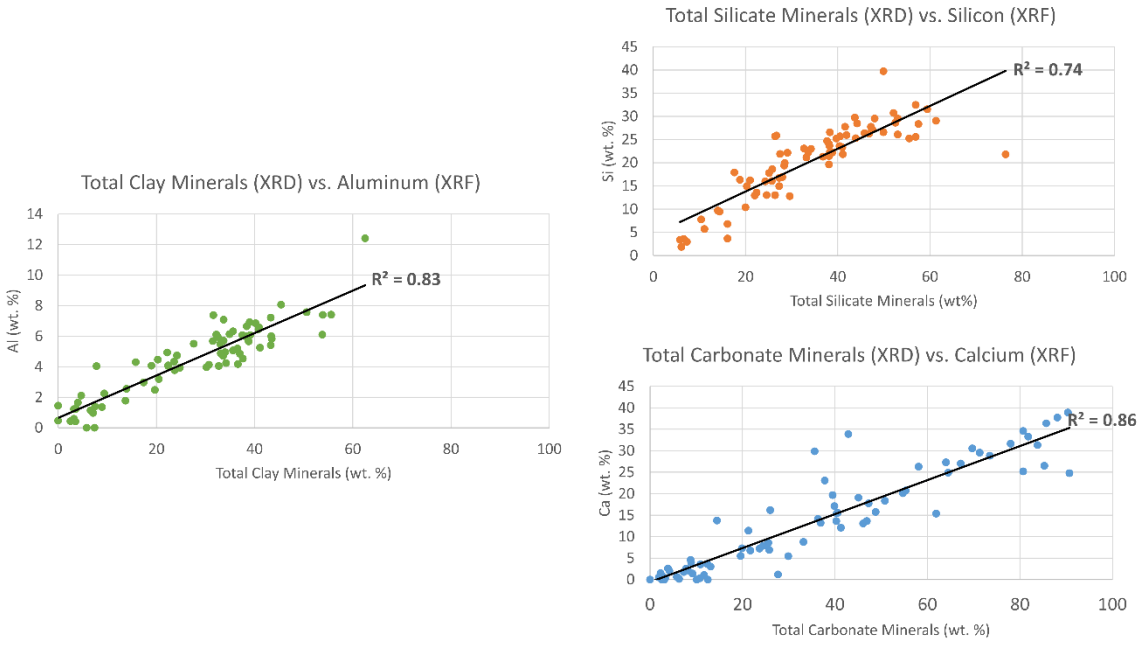

Figure II-4 XRF elemental data for aluminum, silicon and calcium are shown to be effective proxies for clay, silicate and carbonate minerals as shown by cross-plots with XRD.

The dominant lithologies include various limestone beds, typically two feet thick or less, that often are normally graded, and interbedded with high gamma-ray mudstone beds (Figure II-5). The four mudstone lithofacies are difficult to consistently distinguish

in core visually but are readily identified with XRF data (Figure II-5). Bioturbation is common in the overlying Dean Formation but rarely visible at core-scale in the Wolfcamp Group. The most common sedimentary structures include massive bedding, planar lamination, and low-angle asymmetric ripples (Figure II-6). Crinoid, fusulinid, and brachiopod skeletal fragments are common grain types in the limestone beds (Figure II-6). Fossilized plant material (identified as the terrestrial peltasperm *Germaropteris martinsii*) also occurs in the Wolfcamp A of core 1; this is consistent with work finding increased abundance of terrestrial input, and *Germaropteris martinsii* specifically, in the Wolfcamp A and B (Baumgardner et al., 2016; Kvale et al., 2020 and others). Large-scale (10's to 100's of feet) chemostratigraphic variations are delineated in the XRF data, including trends in calcium, silica, aluminum, nickel, molybdenum, magnesium and other elements (Figure II-7).

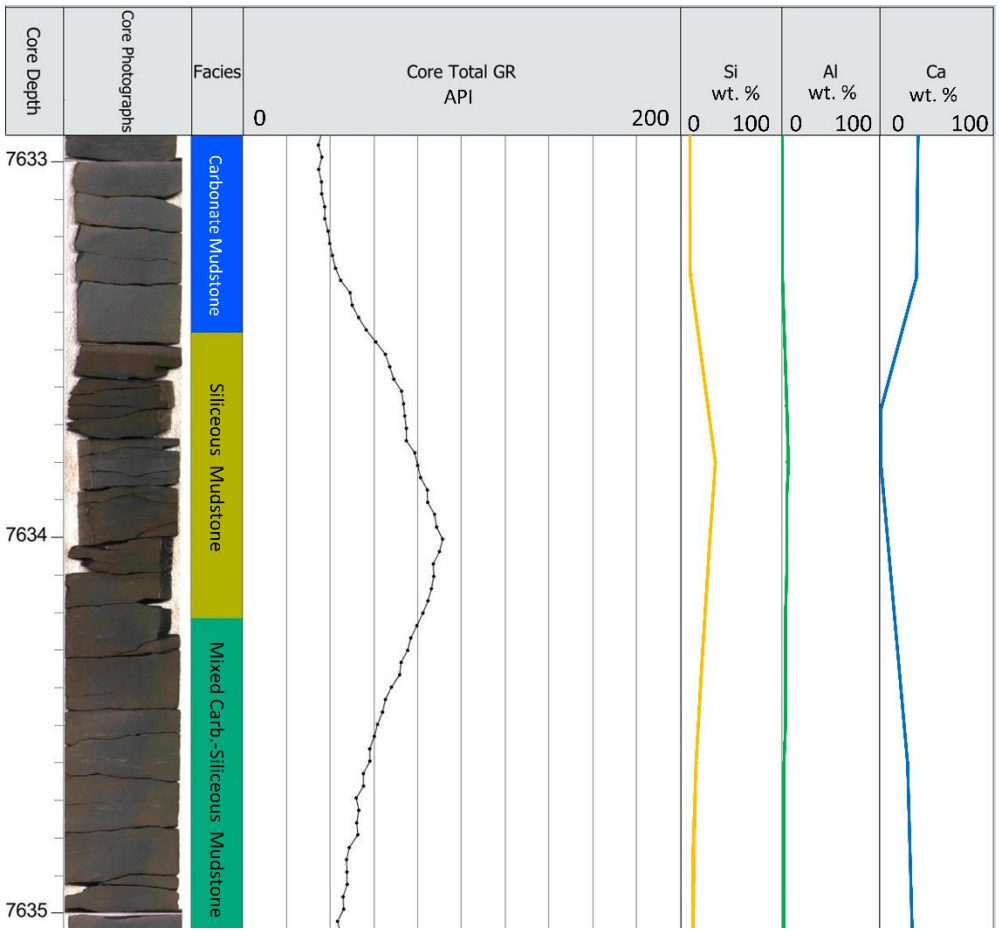

Figure II-5: Three adjacent mudstone lithofacies from core 2, towards base of Wolfcamp A. Some color differences and gamma-ray differences between mudstone lithofacies but XRF clearly distinguishes mudstone composition (note that lithofacies 10, the argillaceous mudstone lithofacies, is the most rare mudstone lithofacies and not shown here).

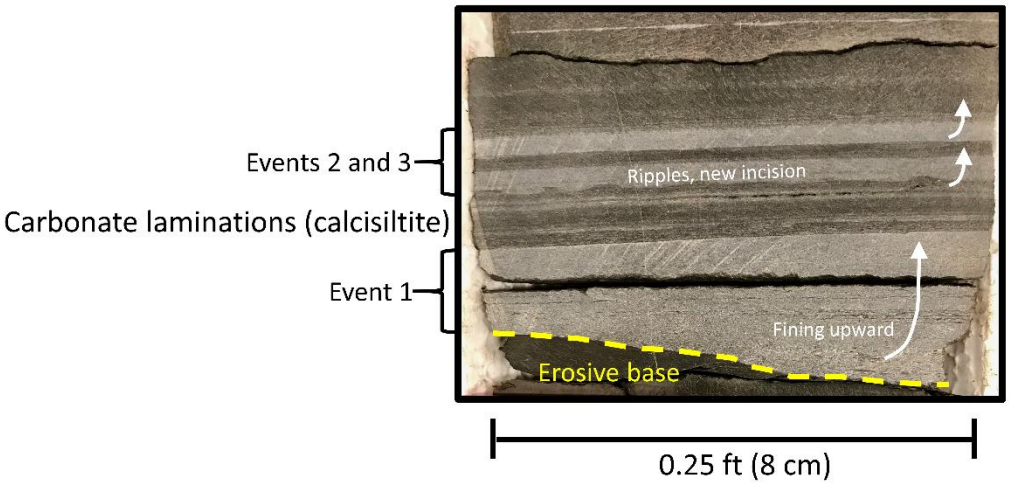

Figure II-6 (A) Typical fining upward carbonate beds shown, interpreted as calciturbidites (core 2, 8401.5 ft).

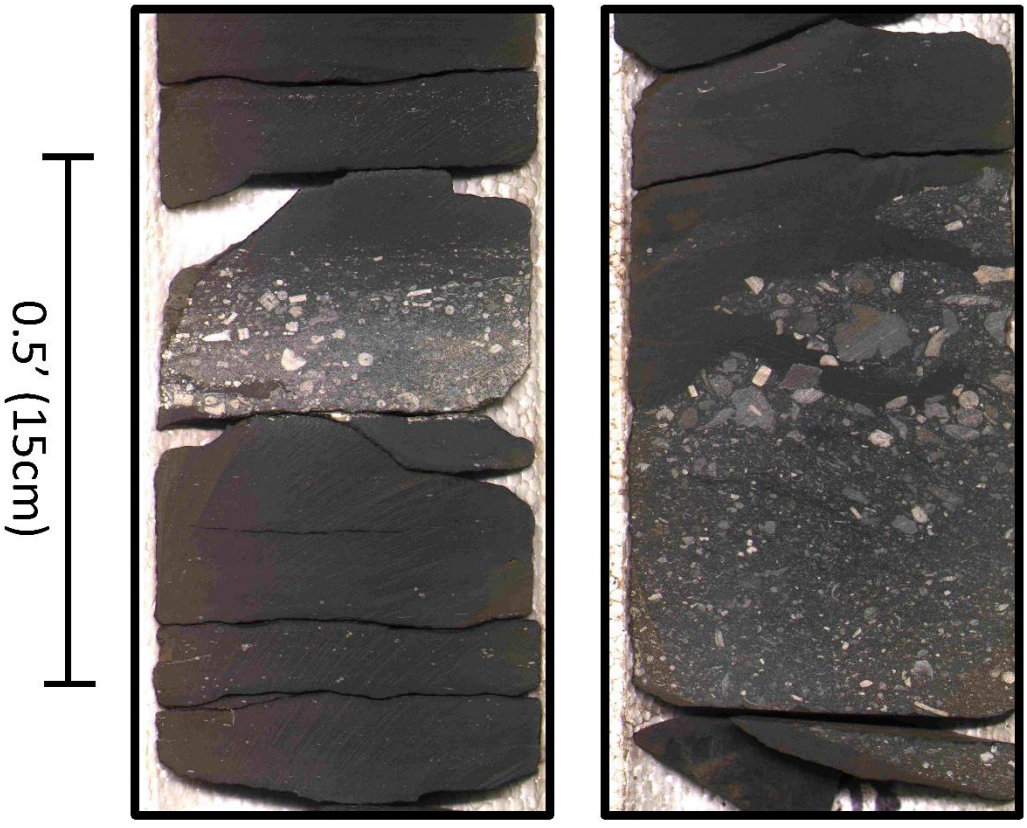

Figure II-6 (B) Coarse (>2 mm) carbonate grains more common in Wolfcamp C, D and lowermost Wolfcamp B. A typical coarse crinoidal fining-upward event bed is shown (left,

core 2 – 8046 ft) and a typical coarse grained, coarsening-upward and deformed event bed (right, core 2 – 8278 ft) is interpreted as a debrite.

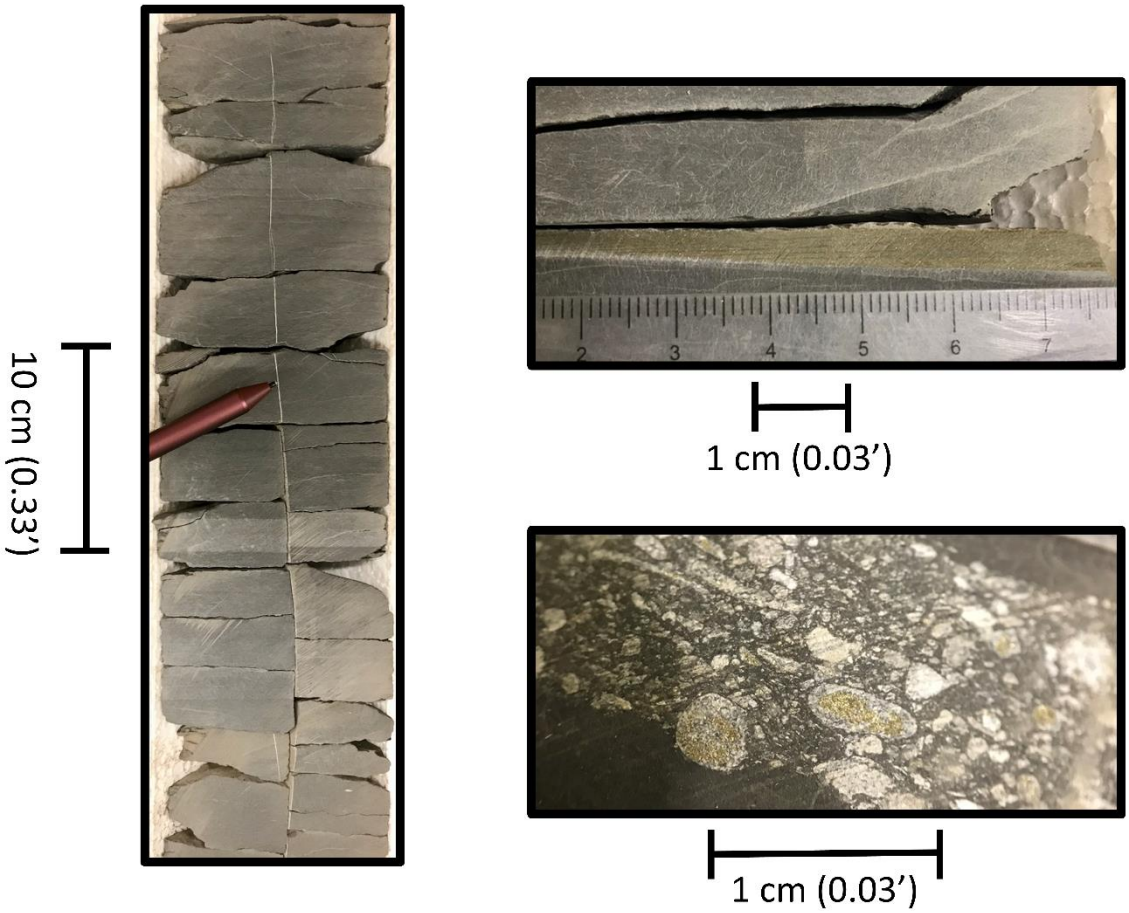

Figure II-6 (C) Other sedimentary features in cores 1 and 2. Left, healed fracture (core 1 – 8463 ft). Upper right, pyritized laminations (core 2 – 8030 ft). Lower right, pyritized fusulinid fragments (core 2 – 8051 ft). Pyritization is common in siliceous mudstone beds.

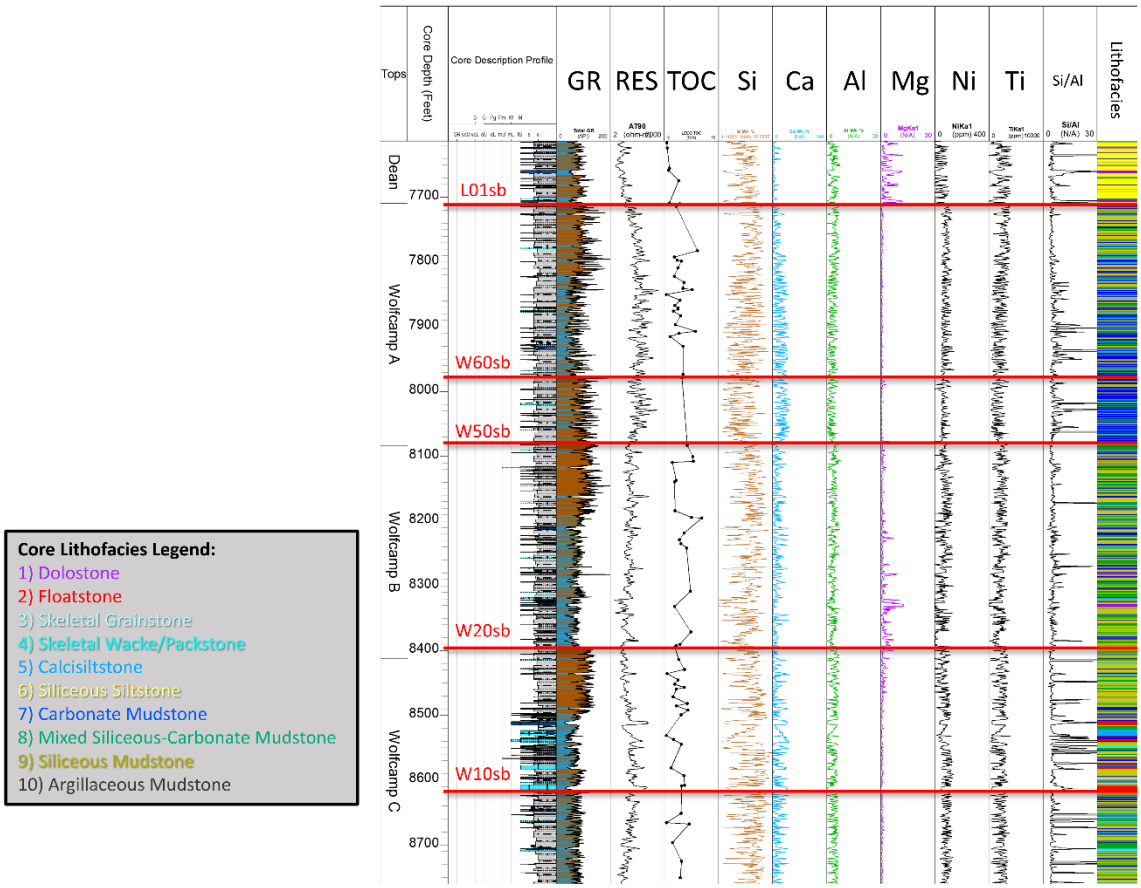

Figure II-7 (A) Core 1 with key well logs, tops, XRF elements, and lithofacies. From left to right, columns include subsurface tops, core depth, simplified core description, total gamma-ray (GR) where <50 API is blue, >100 API is brown, 50-100 API is transitional, deep resistivity (RES), LECO TOC (TOC). Columns 7 through 13 are key XRF elemental data, including silicon (Si), calcium (Ca), aluminum (Al), magnesium (Mg), nickel (Ni), titanium (Ti), and silicon to aluminum ratio (Si/Al). Column 14 shows lithofacies, which are color-coded per the legend. Sequence boundaries shown with red horizontal lines.

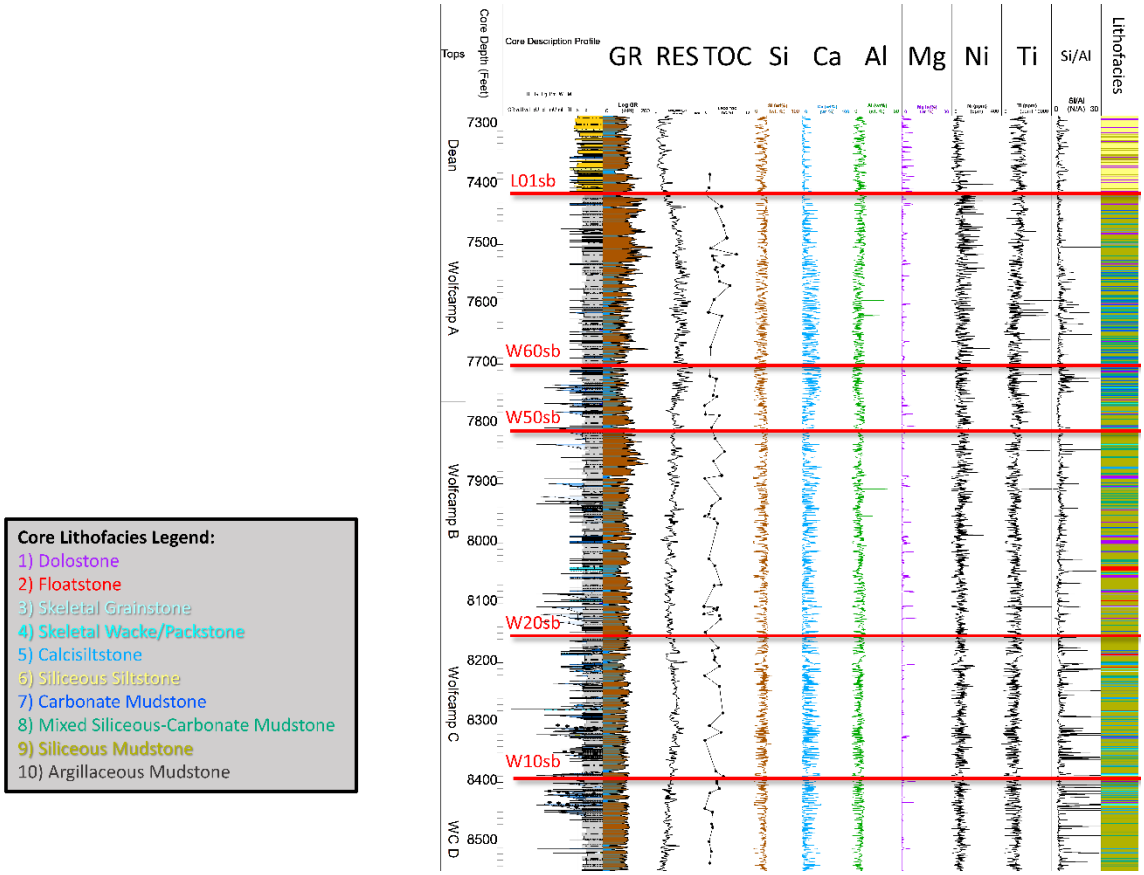

Figure II-7 (B) Core 2 with key well logs, tops, XRF elements, and lithofacies. From left to right, columns include subsurface tops, core depth, simplified core description, total gamma-ray (GR) where <50 API is blue, >100 API is brown, 50-100 API is transitional, deep resistivity (RES), LECO TOC (TOC). Columns 7 through 13 are key XRF elemental data, including silicon (Si), calcium (Ca), aluminum (Al), magnesium (Mg), nickel (Ni), titanium (Ti), and silicon to aluminum ratio (Si/Al). Column 14 shows lithofacies, which are color-coded per the legend. Sequence boundaries shown with red horizontal lines.

Ten lithofacies (Table 1) are proposed for the Wolfcamp Group strata in these cores. They include, 1) dolostone, 2) floatstone, 3) graded skeletal grainstone, 4) graded skeletal wackestone and packstone, 5) graded calcisiltstone, 6) siliceous siltstone, 7) carbonate mudstone, 8) mixed siliceous-carbonate mudstone, 9) siliceous mudstone, and 10) argillaceous mudstone. Mudstone grain size is here defined as grains less than or

equal to 16 microns in diameter (Donovan et al., 2017) thereby including clay and fine silt grain sizes and excluding medium to coarse silt grain sizes. Other workers (e.g., Dunham, 1962; Wright, 1992) have used grain size cutoffs between 20 and 62 microns in diameter as the upper limit for mud grain sizes and the decision to exclude medium and coarse silt from mudstone grain sizes was used to enable greater differentiation within fine-grained sedimentary successions. For additional context, the floatstone facies in this paper is defined as being supported by a generally muddy matrix with gravel-sized skeletal grains and could be alternatively termed a "coarse-grained wackestone".

Name	Photo	Description	Process	Name	Photo	Description	Process
Dolostone		Light to medium grey, occasional blue-grey color. Occasional faint parallel laminations, often massive. Individual grains rarely visible. Upper and lower contacts often diffuse or gradational. Often corresponds to highest RHOB values. XRF shows elevated magnesium values. XRD data show primary minerals are dolomite and ankerite (XRD data shows up to 80% dolomite and iron dolomite/ankerite by weight).	Burial Dolomitization (sensu Mazzullo, 1994)	Siliceous Siltstone		Light to medium brown. Lighter brown intervals contain more visible grains (silt) and are interbedded with darker brown mudstone beds. Many intervals show mottled textures and pervasive horizontal burrowing with little bedding. Planar to inclined lamina are also common. Some inclined, asymetric ripples. Laminations often discontinuous. XRD data show quartz and clays as the dominant constituents (44 wt % and 33 wt % of core 2, respectively). Dominant lithofacies in Dean Formation rare in Wolfcamp Group. Silt grains sizes are primarily medium and coarse silt with rare fine sand.	Sediment Gravity Flows (Proximal or Medial)
Floatstone		Least common lithofacies. Poorly sorted, with inconsistent grading. Skeletal bioclasts are dominant grain type. 10 to 50% of grains exceed 2mm in diameter (granules and pebbles, no cobbles or boulders). Matrix supported. Matrix grains are typically mud-sized, rarely coarse silt to sand-sized. Coarse grains are skeletal (primarily disarticulated crinoid fragments). Mud clasts also present. Soft sediment deformation and convolute bedding. Lower contacts are sub-horizontal and sharp. Intervals meet criteria by Embrey and Kloven (1972).	Debris Flows, Slumps, MTDs	Carbonate Mudstone		Light to dark grey. Often massive or structure-less. Rare, faint planar laminations. Upper and lower contacts often gradational. Upper contacts often grade into mixed-siliceous/carbonate mudstone lithofacies or siliceous mudstone lithofacies. XRD data show calcite is the primary mineral (85 wt % in core 2). Mud grain sizes are defined here as fine silt and clay (16 microns and under) to separate medium and coarse silt lithofacies. Carbonate content ranges from 30 to 90% by weight.	Sediment Gravity Flows (possibly Low-Density Turbidites)
Graded Skeletal Grainstone		Rare relative to skeletal wackestone/packstone beds. Typically very thin (less than .5') and sharp based. Commonly normally graded into overlying skeletal packstone or caclisilite beds. Grains are skeletal, most often crinoidal fragments with secondary foram and unidentifiable populations. Rare asymmetric ripples are present. Skeletal grains are sand-sized (.065 to 2 mm).	Sediment Gravity Flows (possible high-density turbidites sensu Lowe, 1982)	Mixed Silc.-Carb. Mudstone		Often medium brown to medium grey, with gradational upper and lower contacts. Often overlain by siliceous mudstone lithofacies. Occasional mottled texture and possible burrowing. Rare phosphate nodules and pyritized skeletal fragments. Calcite is the dominant mineral (45 wt % in core 2) but with significant quartz (24 wt % in core 2). Mud grain sizes are defined here as fine silt and clay (16 microns and under) to separate medium and coarse silt lithofacies. Carbonate content ranges from 15 to 30%.	Sediment Gravity Flows (possibly Low-Density Turbidites)
Graded Skeletal Wacke/Packstone		Common carbonate lithofacies showing inconsistent grading. Grains are skeletal and mostly sand-sized. Where identifiable, crinoidal fragments appear to be common. Some intervals contain up to 10% granule-sized grains. Typically matrix supported with rare grain support. Often sharp-based with gradational upper contacts. Calcite is the dominant mineral (87 wt % in core 2). Skeletal grains are sand-sized (.065 to 2 mm).	Sediment Gravity Flows	Siliceous Mudstone		Most common Wolfcamp lithofacies. Medium to dark brown. Common pyritized laminations, skeletal fragments, and phosphate nodules. Rare, faint laminations present but massive texture is dominant. Mottled textures are rare. Burrow traces are rarely visible at core (macro) scale. XRD data show quartz is dominant but with a significant clay component (38 wt % for quartz, and 37 wt % for all clay minerals in core 2). Carbonate content ranges from 0 to 15%. Mud grain sizes are defined here as fine silt and clay (16 microns and under) to separate medium and coarse silt lithofacies.	Background Sedimentation (pelgaic and hemipelgaic plumes, algal blooms and marine snow)
Graded Calcisiltstone		Typically off-white to light grey, with some medium grey intervals. Planar laminations are common, often faint. Some laminations are discontinuous. Grains are primarily medium and coarse silt (16 to 62.5 microns). Lower contacts are sharp, often horizontal to sub-horizontal. Upper contacts are often gradational into various mudstone facies. Calcite is the primary mineral (53 wt % in core 2) with a secondary quartz component (22 wt % in core 2). Grains are medium-coarse silt (16-62.5 microns).	Sediment Gravity Flows	Argillaceous Mudstone		Mudstone with >50% clay mineral content by weight. Least common mudstone lithofacies. Light to medium grey. Faint laminations present, but massive bedding dominants. Upper contacts often sharp but lower contacts often gradational. Burrow traces are rare to absent. Difficult to distinguish visually from other mudstone lithofacies. Associated with highest GR values of all lithofacies. Molybdenum and TOC values lower than siliceous mudstone. XRF data show significant silicon content but more aluminum than siliceous mudstone.	Background Sedimentation (pelgaic and hemipelgaic plumes, more distal fluvial influence than siliceous mudstone)

Table II-1 (A) Lithofacies with photos, descriptions and interpreted processes. Note that all pictured cores are 0.3 ft (9 cm) wide.

	Log Indicators		Occurrence		Reservoir Properties		Selection of XRF Elemental Data					
Lithofacies	Avg. Total GR (API)	Avg. RHOB (g/cm^3)	Avg. Lithofacies Thickness (ft)	Proportion of Lithofacies (%)	Avg. Effective Porosity (%)	Avg.LECO TOC (wt. %)	Avg. Si (wt. %)	Avg. Ca (wt. %)	Avg. Al (wt. %)	Avg. Ti (ppm)	Avg. Mo (ppm)	Avg. Si/Al Ratio
Dolostone	57	2.64	1.6	2.6	5.7	1.10	5	2	0	260	5	25.1
Floatstone	53	2.61	1.3	1.9	3.4	2.01	15	20	2	1614	3	8.2
Skeletal Grainstone	46	2.60	0.3	1.2	4.5	No Data	7	33	0	980	3	24.5
Skeletal Wacke/Packstone	53	2.57	0.5	2.8	4.9	0.33	12	27	1	1038	2	23.8
Calcisiltstone	62	2.58	0.6	16.1	4.8	1.86	13	24	2	1507	4	12.2
Siliceous Siltstone	87	2.59	3.4	2.5	7.0	1.08	20	4	4	3781	5	5.9
Carbonate Mudstone	76	2.59	1.0	16.4	5.1	1.84	12	18	2	1355	5	9.1
Mixed Silc.-Carb. Mudstone	79	2.55	1.0	19.2	6.0	2.92	18	15	3	2362	8	6.3
Siliceous Mudstone	89	2.54	1.8	33.5	6.5	3.24	26	4	6	3223	23	5.2
Argillaceous Mudstone	103	2.54	0.8	3.8	6.7	0.03	24	1	8	4174	12	3.5

Table II-1 (B) Lithofacies with log indicators (average total GR, RHOB), lithofacies occurrences (average thickness, relative proportion of total lithofacies), reservoir properties (average effective porosities & LECO TOC weight percent), selection of key elemental data (average concentration of silicon, calcium, aluminum, titanium, molybdenum, and silicon/aluminum ratio).

The resulting facies scheme is compatible with, but more detailed than, published petrophysically-determined log facies (Casey et al., 2020) which may distinguish six or seven analogous facies using standard petrophysical suites (gamma-ray, resistivity, sonic, density & neutron logs, or "quad combos", in addition to photoelectric factor or PEF logs). Petrophysically-determined facies schemes can struggle to differentiate carbonate grain sizes (Casey et al., 2020), thus potentially lumping core lithofacies 3, 4, and 5 (skeletal grainstone, skeletal wacke/packstone, and calcisiltstone). Analysis of well logs alone may also be insufficient to detect subtle compositional variations in mudstones detected by XRF data in core, potentially lumping core lithofacies 8 (mixed siliceous-carbonate mudstone) with end-member carbonate or siliceous mudstone facies (core lithofacies 7 and 9, respectively).

Additionally, both cores record several instances of a sudden upward transition from siliceous mudstone-prone intervals (Facies 6) to various carbonate facies (especially Facies 2 and 7), these intervals are also seen on total gamma-ray curves (Figure II-2) where a sharp (20 to 80 API unit) upward drop in gamma-ray values is observed, including at approximately 7985', 8085', 8400', and 8615' in Core 1 (Figure II-2).

XRF-based Correlations with Organofacies

Mudstone lithofacies also are correlated with organofacies and with source rock compositional risk (Figure II-3). There are many risk elements associated with source rock quality, including TOC content, maturity, source rock thickness, pressure and

structural complexity (Donovan et al., 2017). Compositional risk is defined as a function of clay content where higher clay contents are associated with less favorable geomechanical properties for the purposes of hydraulic fracturing (Evenick, 2016; Donovan et al., 2017). Mudstone lithofacies 7) carbonate mudstone, 8) mixed siliceous-carbonate mudstone, and 9) siliceous mudstone are all common in the Wolfcamp Group and are correlated with organofacies A and B (Figure II-3), which are derived from oil-prone marine algae (equivalent to type II/IIS organic matter types by IFP classification). This applies for all tested Wolfcamp Group sub-divisions, Wolfcamp A through Wolfcamp C. Lithofacies 10), the argillaceous mudstone lithofacies, is the least common mudstone type in the Wolfcamp Group, and is correlated with gas-prone organofacies D/E/F (equivalent to type III/IV organic matter types by IFP classification). Organofacies A and B are oil-prone and associated with low to moderate interpreted compositional risk, wherein source rocks contain less than 50 wt. % clay and are geomechanically favorable source rocks (i.e., less ductile and more conducive to hydraulic fracturing). Conversely, organofacies D, E and F are associated with clay content above 50 wt. %, and therefore have interpreted high compositional risk (Donovan et al., 2017). Finally, given the dominance of organofacies A and B, the distribution of organic content throughout the Wolfcamp Group must be controlled by variations in both marine algal productivity and preservation. Resulting sequence stratigraphic models should account for this.

Discussion

Depositional Models and Sequence Stratigraphy

The sequence stratigraphic interpretation of this interval is based on large-scale facies trends, XRF derived elemental trends and well log interpretations. Within this framework, sharp drops in gamma-ray values (20-80 API units) associated with an influx of carbonate facies (e.g., Figure II-7A at approximately 7980', 8,400', and 8,620') are interpreted as potential sequence boundaries. This interpretation is made because the higher gamma-ray mudstone beds (Siliceous Mudstone, Facies 9) record a lower energy depositional environment and the sudden shift to a lower gamma-ray facies reflects a rapid basinward shift in facies where toe-of-slope carbonate sediment gravity flows (Facies 1 through 5, and Facies 7) cap siliceous mudstone (Facies 9). Conversely, the siliceous mudstone deposits in the basin would reflect quiescent highstand sedimentation because the carbonate sedimentary system (the autogenic factory and its allochthonous downslope deposits) had shifted away from the center of the basin during relative sea level highs (Figure II-8).

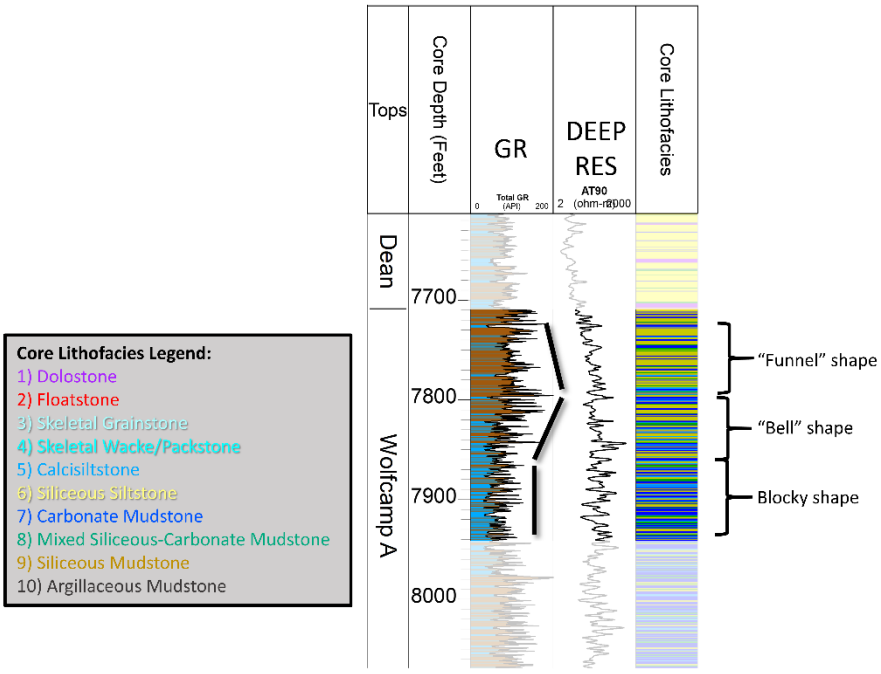

Figure II-8 (A) An idealized complete sequence in Wolfcamp A, core 1, with lithofacies and log shape interpretation. Note transition from carbonate to siliceous mudstone.

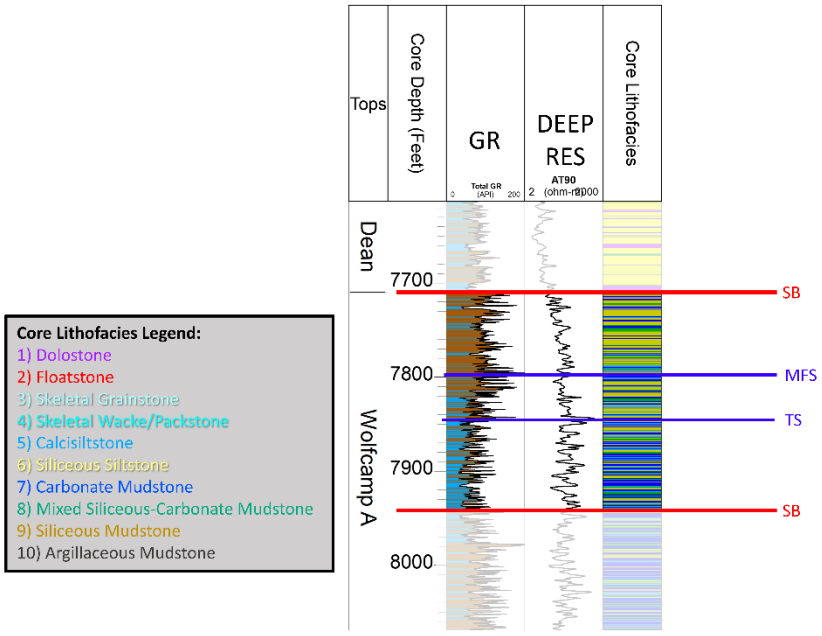

Figure II-8 (B) In this interpretation the "blocky" interval is interpreted as the lowstand system tract, the "bell" shaped interval is interpreted as the transgressive system tract, and the "funnel" interval is interpreted as highstand system tract.

As such, five sequence boundaries (SB) are interpreted in each core (Figure II-9) at similar places through the Wolfcamp Group stratigraphy, indicating a correlation between the two cores. Four Wolfcampian depositional sequences are informally named in ascending order, including W10, W20, W50 and W60. In this naming scheme the base of depositional sequence W50 would be the W50 sequence boundary, identified as a candidate for a basinal expression of the mid-Wolfcamp unconformity (Ross, 1963; Candelaria et al., 1992, and others) identified in proximal Wolfcampian strata. These sequence boundaries can be identified in well logs by sharp drops in gamma-ray values, interpreted to represent a sudden change in facies from high gamma-ray pelagic fallout

to low gamma-ray lowstand fan. The distribution of lithofacies within each interpreted sequence and across interpreted sequence boundaries show distinct patterns.

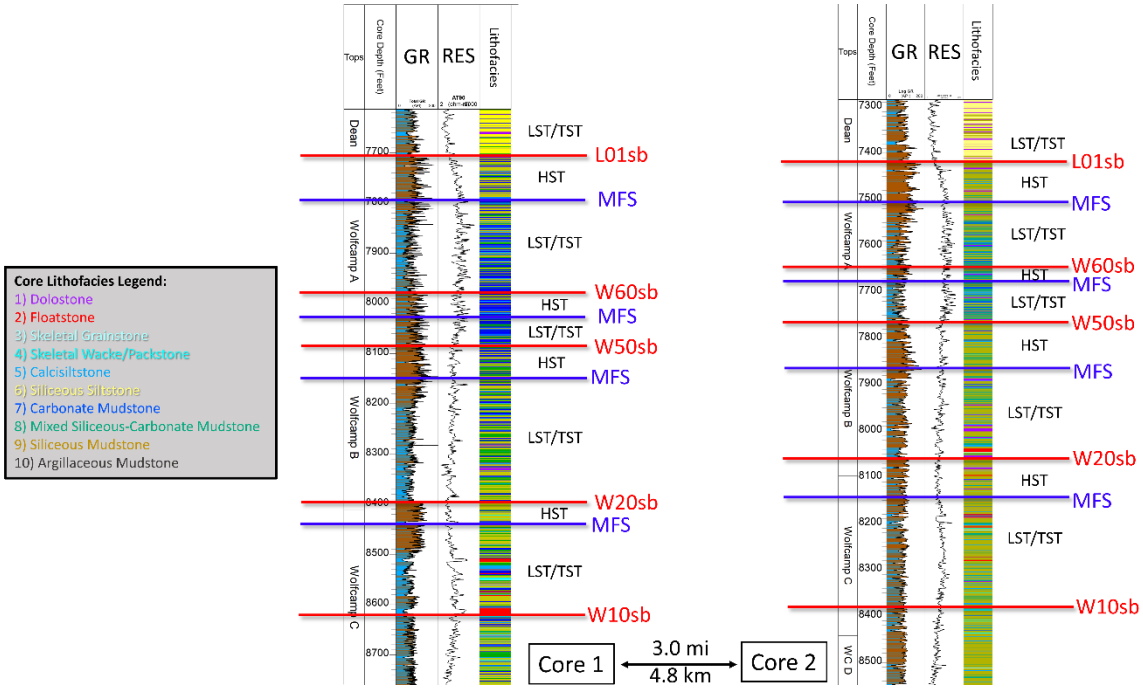

Figure II-9 (A) Core 1 and 2 with complete stratigraphic interpretations using the proposed carbonate-rich lowstand fan model. Sequence boundaries shown with red horizontal lines while each blue line represents a maximum flooding surface (MFS).

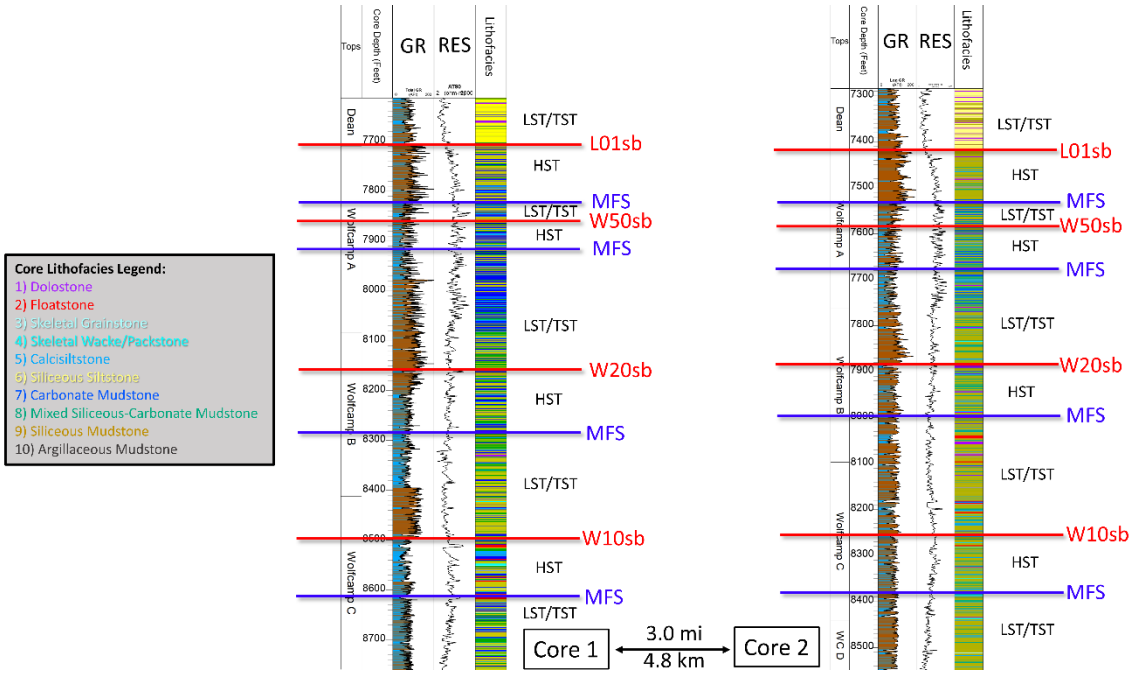

Figure II-9 (B) Core 1 and 2 with complete stratigraphic interpretations using the traditional reciprocal model (assumes carbonate-rich intervals represent highstand shedding). Sequence boundaries shown with red horizontal lines while each blue line represents a maximum flooding surface (MFS).

Specifically, the lower half of each sequence contains more carbonate beds (various lithofacies) and the upper half of each sequence has a higher concentration of siliceous mudstone beds. This trend is well developed in the uppermost Wolfcamp sequence, roughly aligned with the operator designated Wolfcamp A. Here the carbonate-prone facies concentrated at the base of each sequence are interpreted as belonging to a basinal expression of a relative sea level fall as a result of shelf-derived, carbonate grain bypassed from the shelf margin. Conversely, the concentrated siliceous mudstone beds at the top of the sequence are interpreted as resulting from a relative sea level high and coinciding with fewer carbonate clasts available for deposition in the basin (Figure II-10).

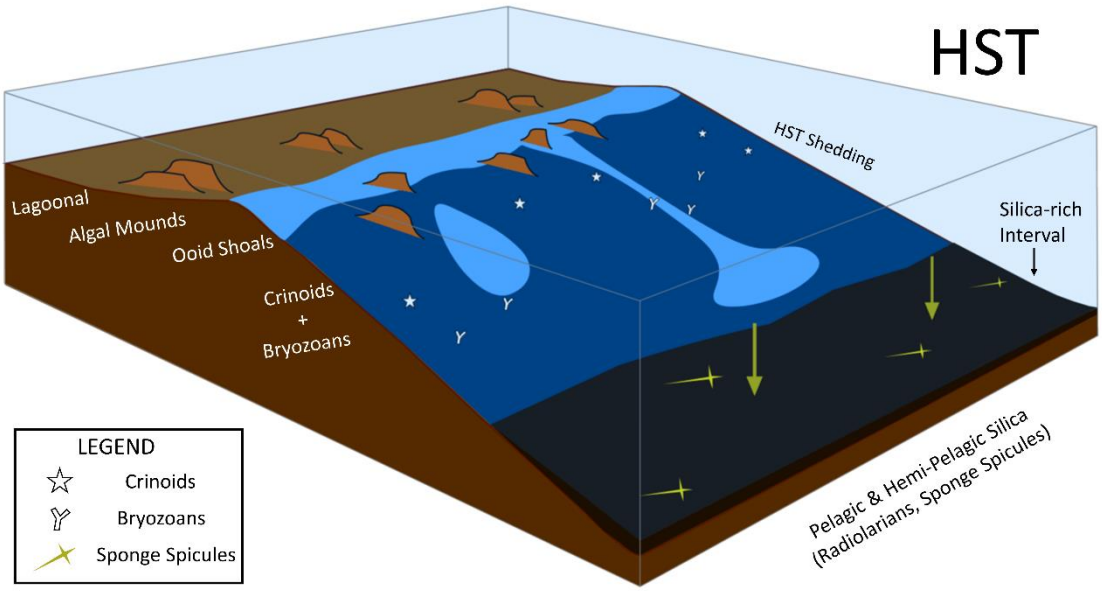

Figure II-10 (A) Block diagram for proposed depositional model - highstand (HST) scenario. Note productive carbonate factories in landward environments and associated highstand shedding and carbonate fans on the adjacent slope. Also note that some calciturbidites make it to the basin floor but the factories are farther landward during highstands and most of the shed material is not delivered far out into the basin

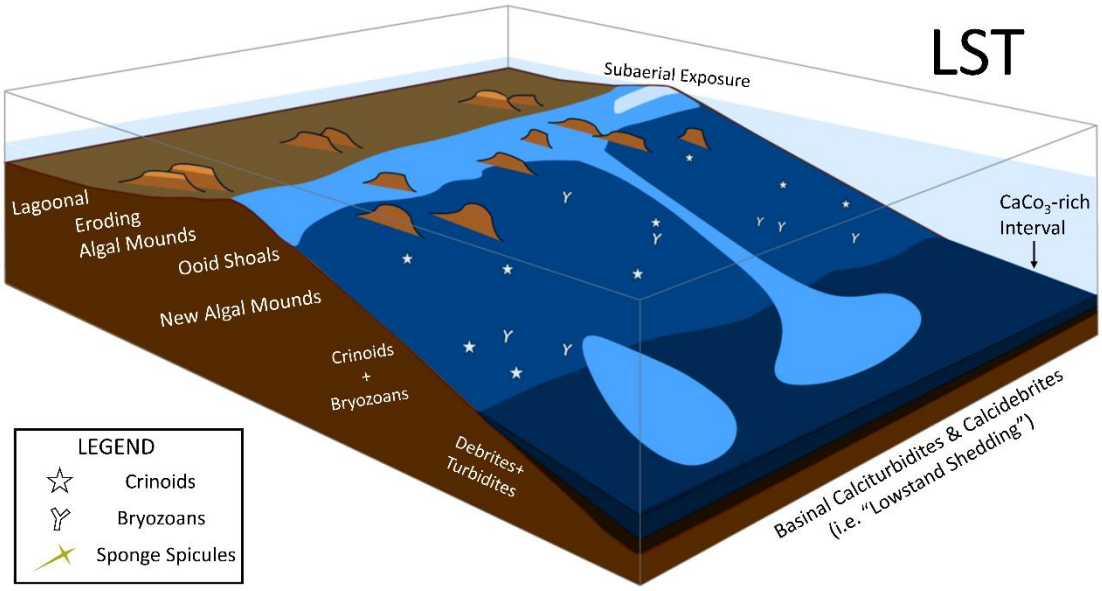

Figure II-10 (B) Block diagram for proposed depositional model - lowstand (LST) scenario. Note the presence of carbonate-rich basin floor fans associated with downdip migration of productive carbonate factories. In ramp settings lacking a pronounced shelf break the shallow area available for carbonate factory development does not decrease with a drop in sea level (such that factories move seaward rather than shut-down) and produced sediment is closer to the basin floor (i.e. "Lowstand shedding"). Subaerial erosion of previous highstand carbonate factories can generate carbonate sediments in both ramp and platform settings.

The concurrence of high-silica, high-TOC, and fine-grained mudstones in the in the organic-rich mudstone facies of the Wolfcamp Group are interpreted as resulting from a biogenic source of the silica content, associated with high organic productivity. The Siliceous Mudstone facies (Facies 9) has the highest average TOC of all the facies, and the Mixed Siliceous-Carbonate Mudstone facies (Facies 8) has the second highest average TOC (Table 1B). The fine-grained (finer than coarse silt) siliceous intervals observed in this study are interpreted as fundamentally different than the coarser grained detrital quartz input normally associated with lowstands in younger Permian strata, as in the Delaware Mountain Group (Wilson, 1967; Silver and Todd, 1969; Handford, 1981).

Recent study of the younger Delaware Mountain Group has also attributed significant basinal siliciclastic (> medium silt sized) input to eolian transport (Motanated and Tice, 2016). If eolian siliceous input to the basin was also significant during the Wolfcampian, this would also dilute the signal associated with fluvially-derived siliceous input into the basin. Though thin sections could not be taken for this study, other recent petrographic analyses (Driskill et al., 2018; Thompson et al., 2018; Wilson et al., 2020) indicates significant biogenic silica content in the Wolfcamp Group, supplied by radiolarians, sponge spicules, and agglutinated foraminifera. Silicon to zirconium ratios have been used to distinguish biogenic and detrital silica in the Wolfcamp Group (Wilson et al., 2020) where elevated Si/Zr values in the Wolfcamp Group versus the overlying Spraberry were interpreted as corresponding to biogenic (or authigenic) quartz. In these cores, Si/Zr is also consistently higher than in the overlying Dean Formation, rarely exceeding 0.15 and never exceeding 0.2, conversely almost the entire Wolfcamp Group exceeds a Si/Zr ratio of 0.15. Silicon to aluminum ratios have also been employed in the Wolfcamp Group (Driskill et al., 2018) with elevated values were interpreted as indicating biogenically-sourced silica, although in these cores the Si/Al ratio is most elevated in carbonates facies lacking any clay content and is therefore not useful for distinguishing between clastic and biogenically-sourced siliceous facies here. Various absolute elemental concentrations used as detrital indicators (e.g. zircon, and to a lesser extent titanium) in these cores do show consistently lower values in siliceous mudstone beds in the Wolfcamp Group compared with the siliceous siltstones in the overlying Dean. Additionally, the regional lateral continuity of the siliceous intervals seems to

support a basin-wide depositional process for quartz-rich intervals, rather than an unevenly distributed point-sourced (fluvial-deltaic) model (Reading, 1991; Playton et al., 2010; Bhattacharya et al., 2019).

Recent modeling work shows a variety of common stratigraphic architectures can be replicated entirely using autogenic variables when external controls or allogenic variables (e.g. eustasy and sediment supply) are held constant (Hajek and Straub, 2017). When these allogenic and autogenic processes are superimposed, allogenic trends are more easily observed at larger spatial or temporal scales (Wang et al., 2011). When allogenic signals are drowned out by autogenic signals, this is termed "signal shredding" (Jerolmack and Paola, 2010). Individual event beds in the basin cannot be definitively interpreted as evidence of externally-controlled cyclicity. Specific carbonate lithologies also be indicative of re-deposition. For example, "mega-breccias" were interpreted as lowstand deposits and "calci-turbidites" as highstand shedding (Spence and Tucker, 1997) and skeletal-grain-rich calciturbidites were interpreted as lowstand deposits (Reijmer et al., 2012). Others have interpreted carbonate deposition in the Permian Basin as occurring during sea level lows in the absence of significant siliciclastic input (Saller et al., 1993). The proposed model would cease to function in the presence of significant siliceous detrital input, as at the interpreted sequence boundary between the Wolfcamp Group and the overlying Dean Formation (Figure II-11) which marks the influx of significant detrital silica, interpreted as a traditional siliciclastic lowstand (Handford, 1981).

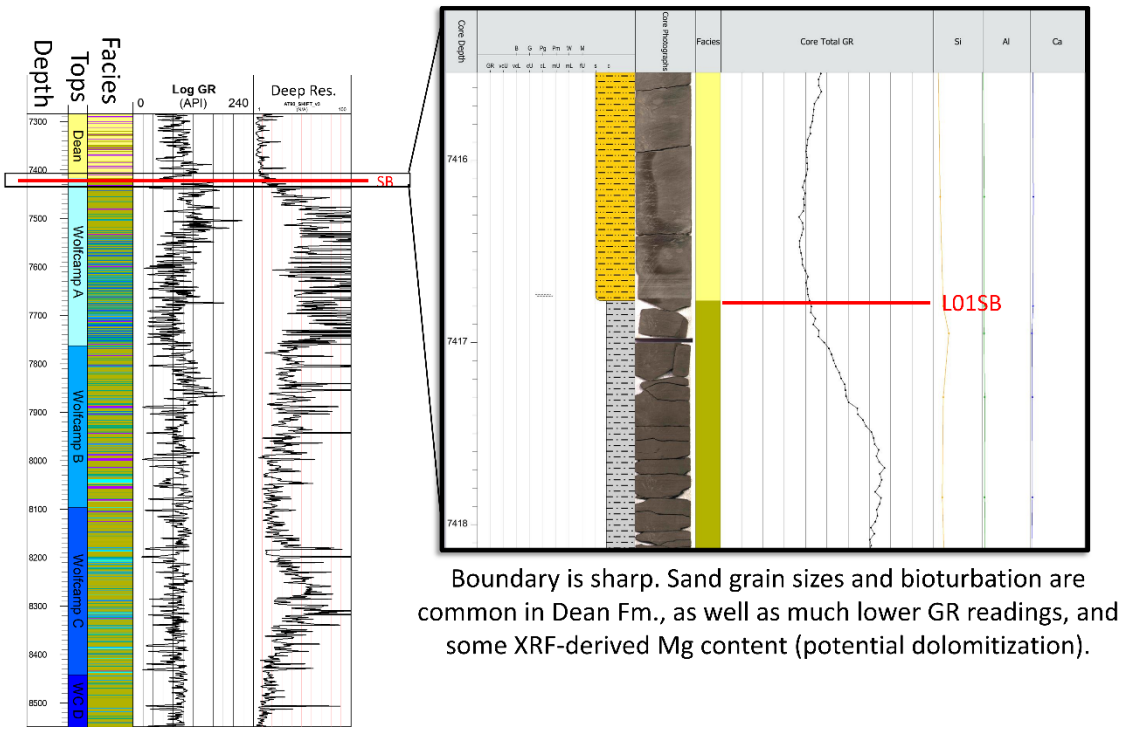

Figure II-11 (A) Sequence boundary (correlative conformity) example in core, base of siliciclastic lowstand fan at Dean-Wolfcamp boundary. Note that this sequence boundary does not require invoking LST carbonate deposition, as interpreted for intra-Wolfcamp Group sequence boundaries.

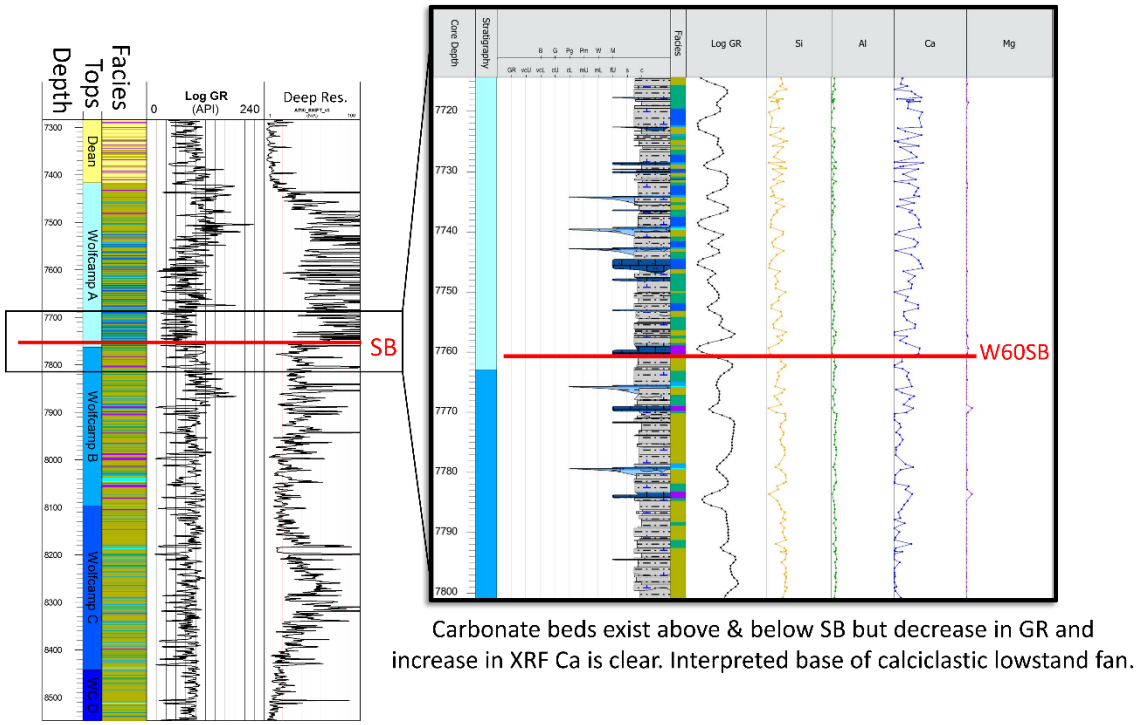

Figure Chapter II-11 (B) Sequence boundary (correlative conformity) example in core, intra-Wolfcamp example, base of calciclastic lowstand fan.

Quantifying Carbonate Bed Dimensions as Lithofacies

A better and more quantitative understanding of the constituent lithofacies and their dimensions in the Wolfcamp Group, as well as the associated stratigraphic processes, will facilitate subsurface modeling where only 1D data (i.e. well logs) are used to extrapolate facies in 3D. In particular, object-based modeling allows as an input the size and shape of prototypical geobodies for a given facies (Strebelle, 2006; Deveugle et al., 2014; Wang et al., 2018, but this information is best gained where the rocks can be observed directly, as in core or outcrop. The distribution and dimensions of the carbonate facies in the Wolfcamp Group, for example, are poorly constrained and therefore difficult to model (Casey et al., 2018).

While lateral and vertical dimensions of individual carbonate geobodies can be inferred from well logs, especially at the bedset scale, more precise measurements can be made with core data which enable direct observation of individual lamina, lamina sets, and beds at the sub-log scale in one or multiple cores. In the studied cores (Figure II-12), limestone beds are described and interpreted as recording sediment gravity flows, e.g. calciturbidites and as calcidebrites (*sensu* Reijmer et al., 2012). The beds are typically between 0.5 and 1.5 ft (15-46 cm) thick as measured directly in the cores and they tend to be continuous between the cores based on the identical and near identical thickness, frequency, and lithologies of carbonate beds between them. This requires the sediment gravity flow basinal fan deposits to be at least 3 miles (4.8 km) across (Figure II-13). These results can be added and compared to the limited literature on the dimensions of calciturbidites and calcidebrites.

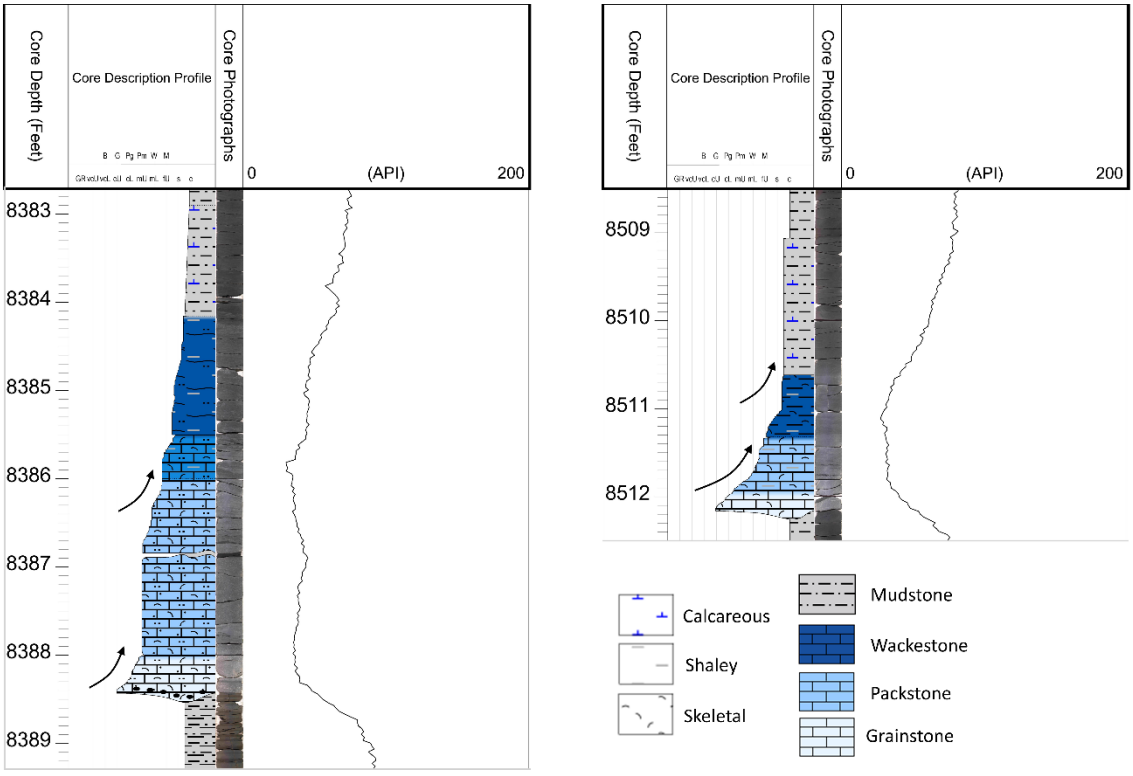

Figure II-12 Typical normally graded event beds (calciturbidites) from core 2. Two examples shown, both grading upward from basal grainstone intervals (light blue) to packstone, wackestone intervals (medium to dark blue), and carbonate-rich mudstone intervals (grey with blue).

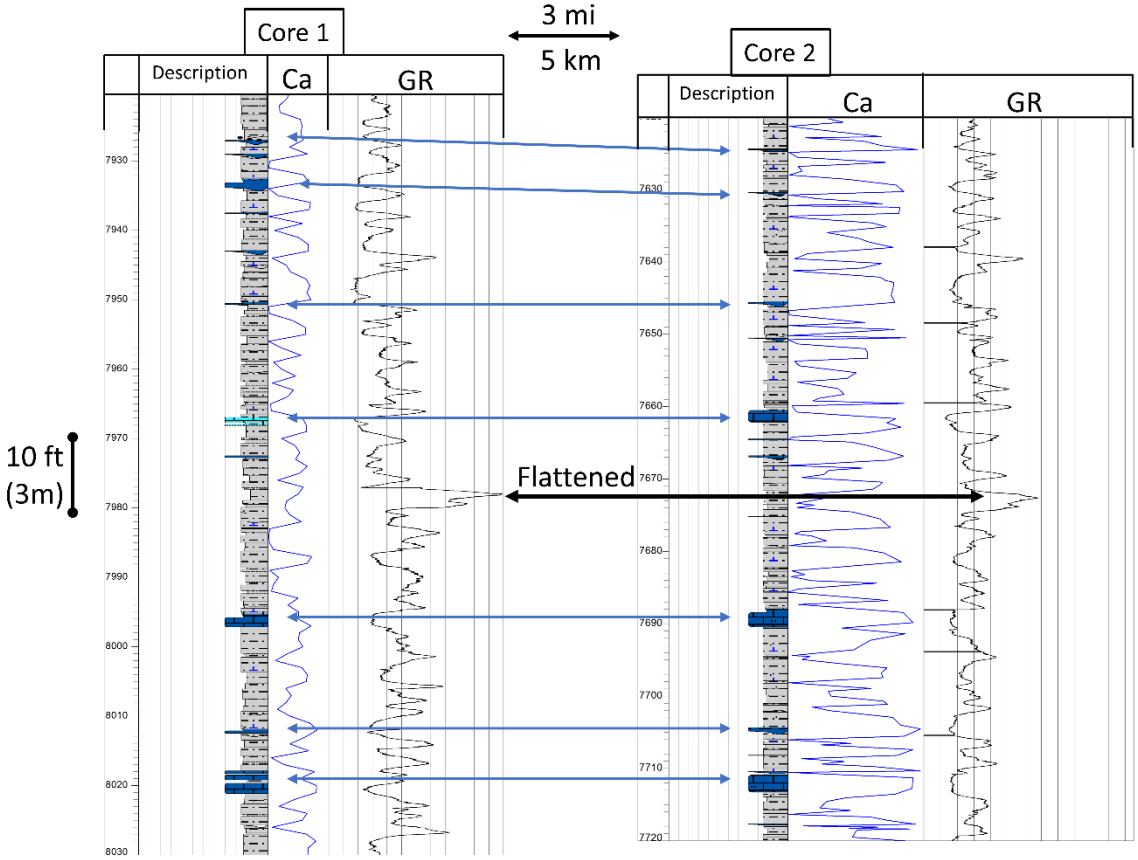

Figure II-13 One-to-one correlation of individual detrital limestone beds at log and sub-log scale between cores 1 and 2 in lower Wolfcamp A shown with GR, XRF-Ca and simplified descriptions. Note that each blue arrow shows an event present in both cores, and the black arrow shows a local high gamma-ray mudstone datum used for this correlation.

Some studies have focused on the dimensions of entire fans, which offers useful upper bounds for expect dimensions of individual beds comprising basin floor fans. For example, carbonate fans were classified into those which are less than 6 miles (10 km) across, those which are 6 to 22 miles (10-35 km) across, and those which are greater than 31 miles (50 km) across (Payros and Pujalte, 2008). Individual carbonate beds from Devonian outcrops in Utah, interpreted as lower slope debrites, were shown to be

typically between 0.2 and 3 ft (5-90 cm) thick and between 400 and 2000 ft (120-610 m) across (Sheehan et al., 1993). Wolfcamp Group hybrid-event beds were shown in northern Delaware Basin cores (Kvale et al., 2020) formed as part of off-axis and lateral fringe deposition in a mixed lithology fan and is thought to be the best, though more proximal, analog to the cores studied here. There, detrital carbonate hybrid-event beds (HEB's) were generally < 2 ft (0.6 m) thick but they were not correlated between cores and their lateral dimensions are therefore unknown. Generally, transported carbonate beds associated with debris-, grain- and mud-dominated deposits range from 10's to 100's to 1000's of meters across (~33 to 3280 ft), where finer grained systems show greater lateral continuity associated with lower energy deposition (Playton et al., 2010). The larger lateral dimensions reported for fine-grained (distal) detrital carbonate beds (Playton et al., 2010) are consistent with observations from this study. For comparison, mudstone intervals of comparable thickness (1-10 feet, or meter-scale) are created by many events over time such that similar patterns of mudstone facies between both cores might be explained by analogous depositional histories reflecting similar seafloor conditions rather than requiring each hemipelagic event to span the distance between the cores.

Comparing Nickel, Molybdenum, and Uranium as proxies for TOC

Three elements (nickel, molybdenum, and uranium) were hypothesized as potential organic proxies for the Wolfcamp Group mudstone units (Figure II-14). XRF measurements were correlated with operator-provided LECO TOC measurements

(Figure 14). Nickel was moderately correlated with Total Organic Content (TOC) with an R^2 of 0.64, molybdenum was weakly correlated with TOC (R^2 of 0.25), and uranium was not correlated with TOC (R^2 of 0.03). Calcium (as a proxy for carbonate minerals) was hypothesized as potentially inversely correlated with TOC reflecting dilution by carbonate beds of organic-rich siliceous mudstone beds but showed no correlation (R^2 of 0.13) when including all lithofacies. For comparison, total gamma-ray measurements made via a core scanner have a weak to moderate correlation with TOC (R^2 of 0.41).

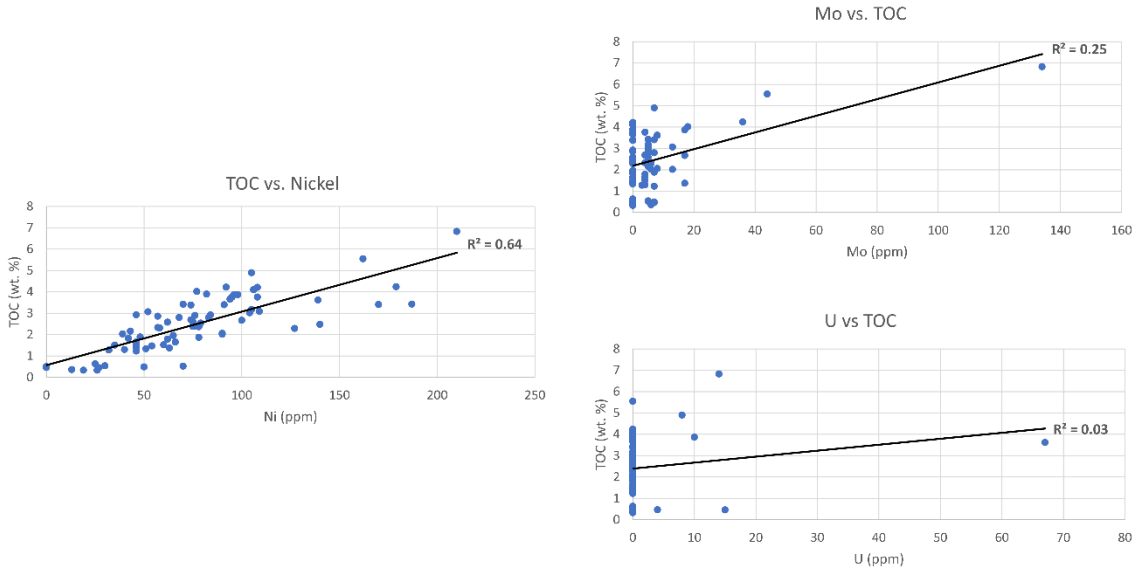

Figure II-14 While nickel (shown) is a good proxy for total organic content (TOC), with a moderate linear correlation ($R^2 = 0.64$), molybdenum and uranium (not shown) have poor to no correlation with TOC ($R^2 = 0.25$ and 0.03, respectively) and are therefore poor proxies in the Wolfcamp Group.

Average calcium content within only Wolfcamp Group mudstone facies, however, does show an inverse relationship with TOC (Table 1) where lithofacies 9, siliceous mudstone, has an average calcium content of 4 ppm and average TOC of 3.2 wt. %, lithofacies 8, mixed siliceous-carbonate mudstone, has an average calcium

content of 15 ppm and average TOC of 2.9 wt. %, lithofacies 7, carbonate mudstone, has an average calcium content of 18 ppm and average TOC of 1.8 wt. %. Between these mudstone lithofacies, there is a moderate inverse correlation between calcium content and TOC (R^2 of 0.65), therefore suggesting a potential dilution effect between these lithofacies. Lithofacies 10, argillaceous mudstone, is rare in the Wolfcamp Group and has both low carbonate content and low TOC (1 ppm carbonate content and 0 wt. % TOC). The relationship also breaks down in the overlying Dean Formation where siliceous siltstones beds have low average calcium content and low average TOC (4 ppm and 1.1 wt. %). The dilution interpretation for the Wolfcamp Group mudstone in these cores agrees with observations of the Wolfcamp Group by previous workers (Baumgardner et al., 2014). Spectral Gamma-Ray measurements of the core also were tested as organic proxies, both total and uranium gamma-ray readings show low to moderate correlation with TOC (R^2 of 0.41, for total and uranium gamma-ray). To summarize, XRF data reveals two key insights into organic-rich source rocks and organic content in the Wolfcamp Group. One, nickel is an effective proxy for TOC and two, that carbonate content shows a moderate negative correlation between Wolfcamp Group lithofacies, here interpreted as a dilution effect.

Long Term Intra-Wolfcamp Group Trends

Recent work (Montañez et al., 2016; Chen et al., 2018) has shown that peak global icehouse conditions were present at the end of the Pennsylvanian and the beginning of the Permian (Gzhelian and Asselian stages). After this period of peak

glaciation and associated high-amplitude eustatic fluctuations, icehouse conditions decreased during the Lower Permian. Therefore, it was hypothesized that large-scale shifts in facies cyclicity through the Lower Permian stratigraphy in these cores may reflect a shift away from peak ice-house conditions. It should also be noted that a coincident external control involves the collision of Laurentia and Gondwana associated with the assembly of Pangea and subsequent tectonically-controlled subsidence of the Midland and Delaware Basins through the latest Pennsylvanian and earliest Permian (Yang and Dorobek, 1995).

Some large-scale trends in litho- and chemofacies variations do occur upward through the Wolfcamp Group (Figure II-7). First, average bed thickness was measured for the Wolfcamp A, B and C but no clear trends in thickness were observed, with beds in the Wolfcamp C averaging 1.2 ft (37 cm), beds in the Wolfcamp B averaging 1.4 ft (43 cm), and beds in the Wolfcamp A averaging 1.1 ft (34 cm). Thorium content, however, measured by spectral gamma-ray and by XRF, shows a significant decrease upward, from the Wolfcamp C to the Wolfcamp B and especially to the Wolfcamp A. Also, lithofacies 2, the floatstone lithofacies, is exclusive to the Wolfcamp C, Wolfcamp D and lowermost Wolfcamp B; conversely, they are absent in the Wolfcamp A of both core 1 and core 2. Lithofacies 3 and 4, skeletal grainstone and skeletal wacke/packstone, also decrease significantly upsection. The relative proportions of mudstone facies show a decrease in lithofacies 8, 9, and 10 (mixed, siliceous and argillaceous mudstone facies, respectively) and an increase in lithofacies 7 (carbonate mudstone) upsection and into the Wolfcamp A (Figure II-15).

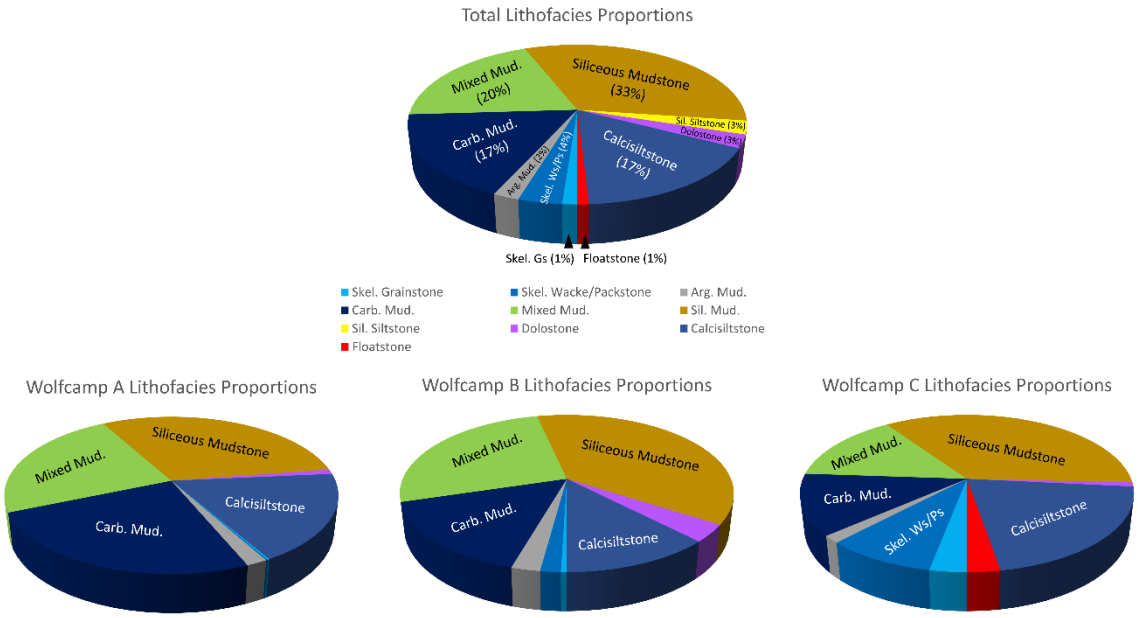

Figure II-15 Lithofacies proportions throughout the entire Wolfcamp, aggregated from both cores. Total proportions shown on top, and proportions for Wolfcamp A, B, and C shown below. Note that minor lithofacies are only labelled on topmost pie graph for the total proportions. Note that lithofacies change dramatically between the Wolfcamp A, B and C. Lithofacies 7, Carbonate Mudstone, is far more common in the Wolfcamp A, lithofacies 4, wacke/packstone, is far more common in Wolfcamp B and C. Lithofacies 2 and 3, floatstone and grainstone, are rare but most common in the Wolfcamp C and almost entirely missing from Wolfcamp A. Lithofacies 5, calcisiltstone, is common throughout the Wolfcamp. In aggregate, a significant trend towards finer carbonate facies is observed up-section, through the Wolfcamp Group and is interpreted as reflecting backstepping of carbonate factories, aligned with published eustasy curves for the Wolfcamp Group in the Lower Permian (Ross and Ross, 1987).

In aggregate these trends demonstrate a clear fining of carbonate facies upsection through the Wolfcamp Group, potentially indicating a relative landward migration of carbonate factories associated with long-term eustatic rise (i.e. backstepping). This agrees with long term (2nd-order) eustatic rise shown by previous workers (Ross and Ross, 1987). This longer-term trend would also be correlated with a shift away from peak icehouse conditions and the maximal extent of global glaciation associated with the

earliest Permian. Alternatively, the decline in tectonism associated with the Ouachita-Marathon orogeny during the Wolfcampian could also be invoked as a potential causal mechanism explaining the upward fining of carbonate facies.

Conclusions

Over 2,000 ft (>600 meters) of cored Wolfcamp Group stratigraphy were described bed-by-bed, and combined with high-resolution XRF elemental data resulting in ten distinct lithofacies, including four compositionally-defined mudstone facies. The Wolfcamp Group, which shows a consistently low clay content (< 50 wt. %) and a consistent clay to quartz ratio, varies as a function of carbonate content. By virtue of their composition the Wolfcamp Group mudstone beds are shown to be associated with marine organofacies A and B (IFP Type I and II organic matter equivalent). The efficacy of elemental data, in particular aluminum, calcium, and silicon, as mineralogic proxies where mineralogy data (i.e., XRD data) is absent, is demonstrated. X-ray fluorescence is therefore consistently able to distinguish the spectrum of mudstone facies occurring throughout the Wolfcamp Group.

The limestone lithofacies are interpreted as calciturbidites and calcidebrites, and consistently correlate bed-by-bed between cores 1 and 2. Quantification of the lithofacies, especially for 3D object modeling of the subsurface, indicates these thin-bedded limestone beds in the Wolfcamp Group are < 2 ft (< 0.6 meters) thick and at least 3 miles (4.8 kilometers) across.

Several elemental proxies were tested as proxies for total organic content or TOC including nickel, molybdenum and uranium, but only nickel is shown to have a moderate positive correlation with TOC (R^2 of 0.64). Other tested elements from XRF analyses perform worse than core-run total gamma-ray measurements which does show a weak correlation with TOC (R^2 of 0.41).

Additionally, four depositional sequences (W10, W20, W50 and W60) are interpreted between cores 1 and 2 within the Wolfcamp Group using a depositional model that interprets the source of silica in siliceous mudstone intervals as being primarily the result of biogenic (as opposed to detrital) silica. Similarly, the carbonate-prone intervals are interpreted as resulting from either the up-dip erosion of carbonate platforms or the basinward shift of carbonate factories during lowstands. This bioclastic lowstand model differs from the traditional reciprocal sedimentation model and provides a useful alternative framework for defining interpreted lowstand deposits where coarse (sand-sized) siliciclastic input is absent, as in the case of the Wolfcamp Group in southern Midland Basin. Importantly, this model demonstrates that alternative explanations for silica-rich and carbonate-rich alternating strata exist, and that research invoking the traditional reciprocal sedimentation model should attempt to demonstrate that the silica is predominately detrital (specifically fluvial) in nature. Similarly, the presence of detrital carbonate deposits in the basin not inherently diagnostic of relative sea level highstands, as some workers historically assumed.

Finally, several large-scale shifts in litho- and chemofacies are observed from the lower Wolfcamp to the upper Wolfcamp Group. In particular, an increase in thorium

occurs in both spectral gamma-ray and in XRF, and a fining of carbonate facies away from skeletal wacke/packstone and toward carbonate mudstone is observed. These shifts correlate with declining icehouse conditions in the Lower Permian although the decline in tectonism is also a possible causal mechanism for these trends.

References

Adams, J. E., M. G. Cheney, R. K. DeFord, R. I. Dickey, C. O. Dunbar, J. M. Hills, R. E. King, E. R. Lloyd, A. K. Miller, and C. E. Needham, 1939, Standard Permian section of North America: AAPG Bulletin, v. 23, no. 11, p. 1673-1678, doi: 10.1306/3D933136-16B1-11D7-8645000102C1865D.

Aretz, M., H. G. Herbig, X. D. Wang, F. M. Gradstein, F. P. Agterberg, and J. G. Ogg, 2020, The Carboniferous Period, *in* Geologic Time Scale 2020, p. 811-874. Elsevier, doi: 10.1016/B978-0-12-824360-2.00023-1.

Barrick, J. E., and G. P. Wahlman, 2019, Conodont and fusulinid biostratigraphy of the Strawn Group (Desmoinesian, Middle Pennsylvanian) and lower part of the" Wolfcamp Shale" (Missourian-Virgilian, Late Pennsylvanian) in the northern Midland Basin, West Texas: Stratigraphy, v. 16, no. 2, p. 65-86, doi: 10.2110/sepmsp.111.11.

Baumgardner Jr, R. W., H. S. Hamlin, and H. D. Rowe, 2014, High-Resolution Core Studies of Wolfcamp/Leonard Basinal Facies, Southern Midland Basin, Texas: Search and Discovery Article # 10607.

Baumgardner Jr, R. W., W. A. DiMichele, and N. de Siqueira Vieira, 2016, An early Permian coastal flora dominated by Germaropteris martinsii from basinal sediments in the Midland Basin, West Texas: Palaeogeography, Palaeoclimatology, Palaeoecology, 459, p. 409-422, doi: 10.1016/j.palaeo.2016.07.024.

Barrick, J. E., and G. P. Wahlman, 2019, Conodont and fusulinid biostratigraphy of the Strawn Group (Desmoinesian, Middle Pennsylvanian) and lower part of the" Wolfcamp Shale"(Missourian-Virgilian, Late Pennsylvanian) in the northern Midland Basin, West Texas: Stratigraphy, v. 16, no. 2, p. 65-86, doi: 10.29041/strat.16.2.65-86.

Bhattacharya, J. P., A. D. Miall, C. Ferron, J. Gabriel, N. Randazzo, D. Kynaston, B. R. Jicha, and B. S. Singer, 2019, Time-stratigraphy in point sourced river deltas:

Application to sediment budgets, shelf construction, and paleo-storm records: Earth-Science Reviews, v. 199, 102985, doi: 10.1016/j.earscirev.2019.102985.

Bohacs, K. M., and J. R. Schwalbach, 1992, Chapter II – Sequence stratigraphy of fine-grained rocks with special reference to the Monterey Formation, *in* J.R. Schwalbach, K.M. Bohacs, L.D. White (Eds.), Sequence stratigraphy in fine-grained rocks: Examples from the Monterey Formation. SEPM 70, p. 7-19.

Böse, E., 1917, The Permo-Carboniferous Ammonoids of the Glass Mountains, West Texas and Their Stratigraphical Significance: Univ. Texas Bull. 1762, p. 1-241.

Campbell, C. V., 1967, Lamina, laminaset, bed and bedset: Sedimentology, v. 8, no. 1, p. 7-26, doi: 10.1111/j.1365-3091.1967.tb01301.x.

Candelaria, M. P., J. F. Sarg, and G. L. Wilde, 1992, Wolfcampian sequence stratigraphy of the eastern Central Basin platform. Permian Basin exploration and production strategies: Applications of sequence-stratigraphic and reservoir characterization concepts: West Texas Geological Society Publication, v. 92(91), p. 27-44.

Casey, B., M. Wehner, B. H. Richards, and C. Moore, 2018, Wolfcamp Geologic Reservoir Modeling Challenges: Proceedings of the 6th Unconventional Resources Technology Conference, Houston, Texas, July 23-25, p. 270-280, doi:10.15530/urtec-2018-2901856.

Casey, B., R. Dommisse, D. Carr, H. S. Hamlin, A. Gherabati, L. Horne, and I. Yurchenko, 2020, Geologic Modeling of Wolfcamp and Bone Spring Formations, Delaware Basin, AAPG ACE 2020.

Chen, J., I. P. Montañez, Y. Qi, S. Shen, and X. Wang, 2018, Strontium and carbon isotopic evidence for decoupling of *p*CO2 from continental weathering at the apex of the late Paleozoic glaciation: Geology, v. 46, no. 5, p. 395-398, doi: 10.1130/G40093.1.

Childs, O. E., 1985, Correlation of stratigraphic units of North America—COSUNA: AAPG Bulletin, v. 69, no. 2, p. 173-180.

Cohen, K. M., S. C. Finney, P. L. Gibbard, and J.X. Fan, 2013; updated, The ICS International Chronostratigraphic Chart: Episodes v. 36: p. 199-204.

Cooper, G. A., and R. E. Grant, 1972, Permian brachiopods of west Texas, I. Smithsonian contributions to Paleobiology, doi: 10.5479/si.00810266.14.1.

Deveugle, P. E., M. D. Jackson, G. J. Hampson, J. Stewart, M. D. Clough, T. Ehighebolo, M. E. Farrell, C. S. Calvert, and J. K. Miller, 2014, A comparative

study of reservoir modeling techniques and their impact on predicted performance of fluvial-dominated deltaic reservoirs: AAPG bulletin, v. 98(4), p. 729-763.

Donovan, A., J. Evenick, and L. Banfield, 2017, An Organofacies-Based Mudstone Classification for Unconventional Tight Rock & Source Rock Plays: Proceedings of the 5th Unconventional Resources Technology Conference, Austin, Texas, July 24-26, p. 3683-3697, doi: 10.15530/URTEC-2017-2715154/.

Driskill, B., J. Pickering, and H. Rowe, 2018, Interpretation of high resolution XRF data from the Bone Spring and Upper Wolfcamp, Delaware Basin, USA: Proceedings of the 6th Unconventional Resources Technology Conference, Houston, Texas, July 23-25, p. 2861-2888, doi: 10.15530/URTEC-2018-2901968.

Dunham, R. J., 1962, Classification of carbonate rocks according to depositional textures, *in* W.E. Ham., ed., Classification of Carbonate Rocks - a symposium: AAPG Memoir 1, p. 108-121.

Dutton, S. P., E. M. Kim, R. F. Broadhead, C. L. Breton, W. D. Raatz, S. C. Ruppel, and C. Kerans, 2004, Play analysis and digital portfolio of major oil reservoirs in the Permian Basin: Application and transfer of advanced geological and engineering technologies for incremental production opportunities: DOE Report DE-FC26-02NT15131, 408 p.

Embry III, A. F., and J. E. Klovan, 1971, A late Devonian reef tract on northeastern Banks Island, NWT: Bulletin of Canadian Petroleum Geology, v. 19, no. 4, p. 730-781.

Evenick, J., 2016, Evaluating source rock organofacies and paleodepositional environments using bulk rock compositional data and pristane/phytane ratios: Marine and Petroleum Geology, v. 78, p. 507-515, doi: 10.1016/j.marpetgeo.2016.10.008.

Fitchen, W. M., 1997, Lower Permian sequence stratigraphy of the western Delaware Basin margin. Sierra Diablo, west Texas, Ph.D. dissertation, University of Texas at Austin, Austin, Texas, 263 p.

Flawn, P. T., A. Jr. Goldstein, P. B. King, and C. E. Weaver, 1961, The Ouachita System: Texas Univ. Pub. 6120, 401 p.

Gaswirth, S. B., K. L. French, J. K. Pitman, K. R. Marra, T. J. Mercier, H. M. Leathers-Miller, C. J. Schenk, M. E. Tennyson, C. A. Woodall, M. E. Brownfield, and T. M. Finn, 2018, USGS National and Global Oil and Gas Assessment Project-Permian Basin Province, Delaware Basin, Wolfcamp Shale and Bone Spring Assessment

Units and Input Data: U.S. Geological Survey Data Release, doi: 10.5066/P9WOUJD3.

Hajek, E.A., and K.M. Straub, 2017, Autogenic sedimentation in clastic stratigraphy: Annual Review of Earth and Planetary Sciences 45, p. 681-709, doi: 10.1146/annurev-earth-063016-015935.

Handford, C. R., 1981, Sedimentology and genetic stratigraphy of Dean and Spraberry formations (Permian), Midland Basin, Texas: AAPG Bulletin, v. 65, no. 9, p. 1602–1616.

Henderson, C. M., V. I. Davydov, B. R. Wardlaw, F. M. Gradstein, and O. Hammer, 2012, The Permian Period, *in* The Geologic Time Scale, p. 653-679. Elsevier.

Jerolmack, D. J., and C. Paola, 2010, Shredding of environmental signals by sediment transport: Geophysical Research Letters 37, no. 19, doi: 10.1029/2010GL044638.

King, P. B., 1931, Geology of the Glass Mounatins, Part I, Descriptive Geology: Univ. Texas Bull. 3038, p. 51-90.

Koch, J. T., and T. D. Frank, 2011, The Pennsylvanian-Permian Transition in the low-latitude carbonate record and the onset of major Gondwanan glaciation: Paleogeography, Paleoclimatology, Palaeoecology, v. 308, p. 362-372, doi: 10.1016/j.palaeo.2011.05.041.

Kohn, J. L., 2016, Late Pennsylvanian (Virgilian) to early Permian (Leonardian) conodont biostratigraphy of the “Wolfcamp Shale,” Northern Midland Basin, Texas: M.S. thesis, Texas Tech University, Lubbock, Texas, 112 p.

Kvale, E. P., C. M. Bowie, C. Flenthrope, C. Mace, J. M. Parrish, B. Price, S. Anderson, and W. A. DiMichele, 2020, Facies variability within a mixed carbonate–siliciclastic sea-floor fan (upper Wolfcamp Formation, Permian, Delaware Basin, New Mexico): AAPG Bulletin, v. 104, no. 3, p. 525-563, doi: 10.1306/06121917225**.**

Lucas, S. G., 2013, Reconsideration of the base of the Permian System: New Mexico Museum of Natural History and Science Bulletin 60, p. 230-232.

Lucas, S. G., and S. Z. Shen, 2018, The Permian chronostratigraphic scale: history, status and prospectus. Geological Society, London, Special Publications, v. 450(1), p. 21-50, doi: 10.1144/SP450.3.

Mazzullo, S. J., A. M. Reid, and L. J. Mazzullo, 1987, Basinal Lower Permian Facies, Permian Basin: Part I-Stratigraphy of the Wolfcampian-Leonardian Boundary. Bulletin-West Texas Geological Society, v. 26, p. 5-9.

Mazzullo, S. J., 1994, Dolomitization of periplatform carbonates (Lower Permian, Leonardian), Midland Basin, Texas. Carbonates and Evaporites, v. 9, no. 1, p. 95-112.

McKee, E. D., and S. S. Oriel, 1967, Paleotectonic investigations of the Permian System in the United States: U.S. Geol. Survey Prof. Paper 515, 271 p., doi: 10.3133/pp515.

Motanated, K., and M. M. Tice, 2016, Siltstone Geochemical Compositions: Applications for Event Size and Correlation: International Journal of Geosciences, v. 7, no. 02, p. 189, doi: 10.4236/ijg.2016.72015.

Montañez, I. P., J. C. McElwain, C. J. Poulsen, J. D. White, W. A. DiMichele, J. P. Wilson, G. Griggs, and M. T. Hren, 2016, Climate, *p*CO 2 and terrestrial carbon cycle linkages during late Palaeozoic glacial–interglacial cycles: Nature Geoscience, v. 9, no. 11, p. 824-828, doi: 10.1038/ngeo2822.

Payros, A., and V. Pujalte, 2008, Calciclastic submarine fans: An integrated overview: Earth-Science Reviews, v. 86 (1-4), p. 203-246, doi: 10.1016/j.earscirev.2007.09.001.

Pearce, T. J., and I. Jarvis, 1992, Composition and provenance of turbidite sands: late Quaternary, Madeira Abyssal Plain: Marine Geology, v. 109(1-2), p. 21-51, doi: 10.1016/0025-3227(92)90219-8.

Playton, T. E., X. Janson, C. Kerans, N. P. James, and R. W. Dalrymple, 2010, Carbonate slopes, *in* Facies models 4, p. 449-476.

Reading, H. G., 1991, The classification of deep-sea depositional systems by sediment caliber and feeder system: Journal of the Geological Society, v. 148(3), p. 427-430, doi: 10.1144/gsjgs.148.3.0427.

Reid, A. M., S. T. Reid, S. J. Mazzullo, and S. T. Robbins, 1988, Revised fusulinid biostratigraphic zonation and depositional sequence correlation, subsurface Permian basin: AAPG Bulletin, v. 72, p. 102.

Reijmer, J. J., P. Palmieri, and R. Groen, 2012, Compositional variations in calciturbidites and calcidebrites in response to sea-level fluctuations (Exuma Sound, Bahamas): Facies, v. 58, no. 4, p. 493-507, doi: 10.1007/s10347-011-0291-z.

Reijmer, J. J., P. Palmieri, R. Groen, and M. Floquet, 2015, Calciturbidites and calcidebrites: Sea-level variations or tectonic processes?: Sedimentary Geology, v. 317, p. 53-70, doi: 10.1016/j.sedgeo.2014.10.013.

Ross, C. A., 1959, The Wolfcamp series (Permian) and new species of fusulinids, Glass Mountains, Texas: Journal of the Washington Academy of Sciences, v. 49, no. 9, p. 299-316.

Ross, C. A., 1963, Standard Wolfcampian Series (Permian), Glass Mountains, Texas: Geol. Soc. America Mem. 88, 205 p.

Ross, C. A., and J. R. P. Ross, 1987, Late Paleozoic sea levels and depositional sequences: Cushman Foundation for Foraminiferal Research, p. 137.

Ross, C. A., and J. R. P. Ross, 1997, Nealian and Lenoxian (Wolfcampian, Lower Permian) Depositional Sequences, Fusulinid Facies and Biostratigraphy, Glass Mountains, Texas: Cushman Foundation for Foraminiferal Research, p. 125.

Ross, C. A., and J. R. P. Ross, 2003, Sequence evolution and sequence extinction: Fusulinid biostratigraphy and species level recognition of depositional sequence, Lower Permian, Glass Mountains, west Texas, U.S.A., *in* H.C. Olson and R. M. Leckie, eds., Micropaleontologic proxies for sea level change and stratigraphic discontinuities: Society for Sedimentary Geology Special Publication 75, p. 317–359.

Ruppel, S. C., 2001, Stratal Architecture and Facies Development in a Middle Wolfcampian Platform Carbonate Reservoir: University Block 9 Field, Andrews County, Texas, *in* Permian Basin SEPM Field Trip and Core Workshop, Austin, Texas: Bureau of Economic Geology.

Sageman, B. B., and T. W. Lyons, 2003, Geochemistry of fine-grained sediments and sedimentary rocks, Vol. 7, 407 p.

Saller, A. H., M. J. Frankforter, and S. A. Boyd, 1993, Depositional setting of lowstand carbonates in the BC (Canyon) field, Howard County, Texas, *in* R.E. Crick, ed., Transactions and Abstracts: AAPG Southwest Section Geological Convention Abstracts, p. 81-89.

Saller, A. H., J. A. D. Dickson, E. T. Rasbury, and T. Ebato, 1999, Effects of long-term accommodation change on short-term cycles, upper Paleozoic platform limestones, west Texas, *in* P. M. Harris, A. H. Saller, and J. A. Simo, eds., Advances in carbonate sequence stratigraphy, application to reservoirs, outcrops and models: Society for Sedimentary Geology (SEPM) Special Publication 63, p. 227–246.

Sheehan, P. M., J. M. Pandolfi, and K. B. Ketner, 1993, Isolated carbonate bodies composed of stacked debris-flow deposits on a fine-grained carbonate lower slope of Devonian age, Antelope Peak, Elko County, Nevada, USGS Bulletin 1988-E, 11 p.

Silver, B. A., and R. G. Todd, 1969, Permian cyclic strata, northern Midland and Delaware Basins, West Texas and southeastern New Mexico: AAPG Bulletin, v. 53, no. 11, p. 2223-2251, doi: 10.1306/5D25C94D-16C1-11D7-8645000102C1865D.

Spence, G. H., and M. E. Tucker, 1997, Genesis of limestone megabreccias and their significance in carbonate sequence stratigraphic models: a review: Sedimentary Geology, 112, no. 3-4, p. 163-193.

Strebelle, S. B., 2006, Sequential simulation for modeling geological structures from training images, *in* T. C. Coburn, J. M. Yarus, and R. L. Chambers, eds., Stochastic modeling and geostatistics: Principles, methods, and case studies, volume II: AAPG Computer Applications in Geology 5, p. 139-149, doi: 10.1306/1063812CA53231.

Thompson, M., J. Pickering, P. Desjardins, and B. Driskill, 2018, An integrated view of the petrology, sedimentology, and sequence stratigraphy of the Wolfcamp Formation, Delaware Basin, Texas: Proceedings of the 5th Unconventional Resources Technology Conference, Houston, Texas, July 23-25, p. 311-318.

Turner, B. W., J. A. Tréanton, and R. M. Slatt, 2016, The use of chemostratigraphy to refine ambiguous sequence stratigraphic correlations in marine mudrocks. An example from the Woodford Shale, Oklahoma, USA: Journal of the Geological Society, 173(5), p. 854-868, doi: 10.1144/jgs2015-125.

Udden, J. A., 1917, Notes on the Geology of the Glass Mountains, Texas University Bulletin 1753, p. 3-59.

Van Der Loop, M., 2017, Proposed Stratigraphic Correlation Framework for Wolfcamp of Delaware Basin, West Texas. Proceedings of the 2017 Southwest Section AAPG Annual Convention.

Van Siclen, D. C., 1958, Depositional topography—examples and theory: AAPG Bulletin v. 42, no. 8, p. 1897-1913.

Wang, Y. C., M. J. Pyrcz, O. Catuneanu, and J. B. Boisvert, 2018, Conditioning 3D object-based models to dense well data: Computers & Geosciences, v. 115, p. 1-11, doi: 10.1016/j.cageo.2018.02.006.

Wang, Y. C., K. M. Straub, and E. A. Hajek, 2011, Scale-dependent compensational stacking: an estimate of autogenic time scales in channelized sedimentary deposits: Geology, v. 39, no. 9, p. 811-814.

Wilde, G. L., 1975, Fusulinid-defined Permian stages: West Texas Geological Society and Permian Basin Section, Society of Economic Paleontologists and Mineralogists Publication, v. 75, no. 65, p. 67-83.

Wilde, G. L., 1990, Practical fusulinid zonation: the species concept; with Permian Basin emphasis: West Texas Geological Society Bulletin, v. 29, no. 7, p. 5-34.

Wilson, J. L., 1967, Cyclic and reciprocal sedimentation in Virgilian strata of southern New Mexico: Geological Society of America Bulletin, v. 78, no. 7, p. 805–818.

Wilson, R. D., J. Chitale, K. Huffman, P. Montgomery, and S. J. Prochnow, 2020, Evaluating the depositional environment, lithofacies variation, and diagenetic processes of the Wolfcamp B and lower Spraberry intervals in the Midland Basin: Implications for reservoir quality and distribution. AAPG Bulletin v.104, no. 6., p. 1287-1321, doi: 10.1306/12031917358.

Wright, V. P., 1992, A revised classification of limestones: Sedimentary Geology 76, no. 3-4, p. 177-185.

Yang, K, and S. L. Dorobek, 1995, The Permian Basin of west Texas and New Mexico: Tectonic history of a “composite” foreland basin and its effects on stratigraphic development, *in* Dorobek, S.L. and Ross, G.M., eds., Stratigraphic evolution of foreland basins: SEPM (Society for Sedimentary Geology) Special Publication No. 52, p. 149-174, doi: 10.2110/pec.95.52.0149.

CHAPTER III SEQUENCE STRATIGRAPHY OF THE LOWER WOLFCAMP FORMATION IN THE WOLF CAMP HILLS AT THE SOUTHERN MARGIN OF DELAWARE BASIN, BREWSTER COUNTY, WEST TEXAS

Abstract

The Lower Wolfcamp Formation (Asselian to Sakmarian) is defined, described, and interpreted at the Wolf Camp Hills type locality along the southern margin of the Delaware Basin in Brewster County, Texas. Six sections were measured and used to create a new 622 foot (190 meter) composite type section for the Lower Wolfcamp Formation. These sections are tied into a digital outcrop model created with drone photogrammetry documenting lap-out relationships. The base of the Lower Wolfcamp Formation is placed at an angular unconformity (W10sb), which also marks the top of the Bursumian (Newwellian) substage. The top of the Lower Wolfcamp Formation is placed at a distinct angular unconformity (W50sb) overlain by prominent, stacked, carbonate-clast conglomerate bedsets, which contain normally-graded cobble to boulder-sized clasts. Two depositional sequences (W10 and W20) are interpreted, each marked by a basal conglomerate interval potentially reflecting a relative sea-level fall, as well as tectonic activity associated with coeval Marathon-Ouachita thrusting. Two major transgressive surfaces are also identified and marked by a sharp change from limestones (below) to mudstones (above), coinciding with sharp increases in gamma-ray values. Significant lateral thinning to the east (N70E) is interpreted as resulting from differential truncation under the tectonically-enhanced angular unconformity (W50sb) located at the

top of the Lower Wolfcamp Formation. Lithologies are grouped into seven facies interpreted as occurring along a moderate relief carbonate depositional profile capable of transporting coarse clasts during relative sea level falls. Lithoclasts are interpreted as the byproduct of updip erosion of the shallowest (upper foreset and topset) portions within each depositional sequence. This unique depositional profile may be a function of the proximal foredeep or "wedge top" setting adjacent to the Ouachita-Marathon orogenic wedge, and is rarely preserved.

Introduction

Despite ongoing interest in Wolfcamp Group across the greater Permian Basin region (Gaswirth et al., 2018), its detailed regional stratigraphy is still poorly understood. Historically, the Wolfcamp Group was studied in both proximal, limestone-rich outcrops and more recently in mudstone-rich strata, due to the growth in the availability of subsurface data from basinal settings. Adding complexity to the understanding of the basinal stratigraphy has been the use of industry-specific, informal stratigraphic terms in the subsurface and more provincial terms in outcrop. Furthermore, arbitrary and variable lithostratigraphic assignments of units in the subsurface, as well as the inconsistent use of sequence stratigraphic concepts (Nelson et al. 2013), have prevented the development of a unified chronostratigraphic framework across the basin for units like the Wolfcamp Group.

The original use of the term Wolfcamp was as the Wolfcamp Formation (Udden, 1917, King, 1931). It was defined at its type locality, the Wolf Camp Hills, located at the

foot of the Glass Mountains in Brewster County, Texas (Udden, 1917). These strata were subsequently divided into two formations (i.e., the Neal Ranch and Lenox Hills Formations) by Ross (1959), essentially elevating the Wolfcamp to Group level. Cooper and Grant (1972) proposed adding younger (Kungurian) strata, which they named the Skinner Ranch Formation, into the Wolfcamp Group (Figure III-1). Thus, along the Glass Mountain outcrops, there is no consensus as to the chronostratigraphic placement of the top of the Wolfcamp Group. Furthermore, the exact stratigraphic placement of the base of the Wolfcamp Group has also been debated. King (1931) placed it at the base of his Gray Limestone Unit (Figure III-1). However, Ross (1959, 1963) placed the base of the Wolfcamp Group at the top of the Gray Limestone Unit (Figure III-1).

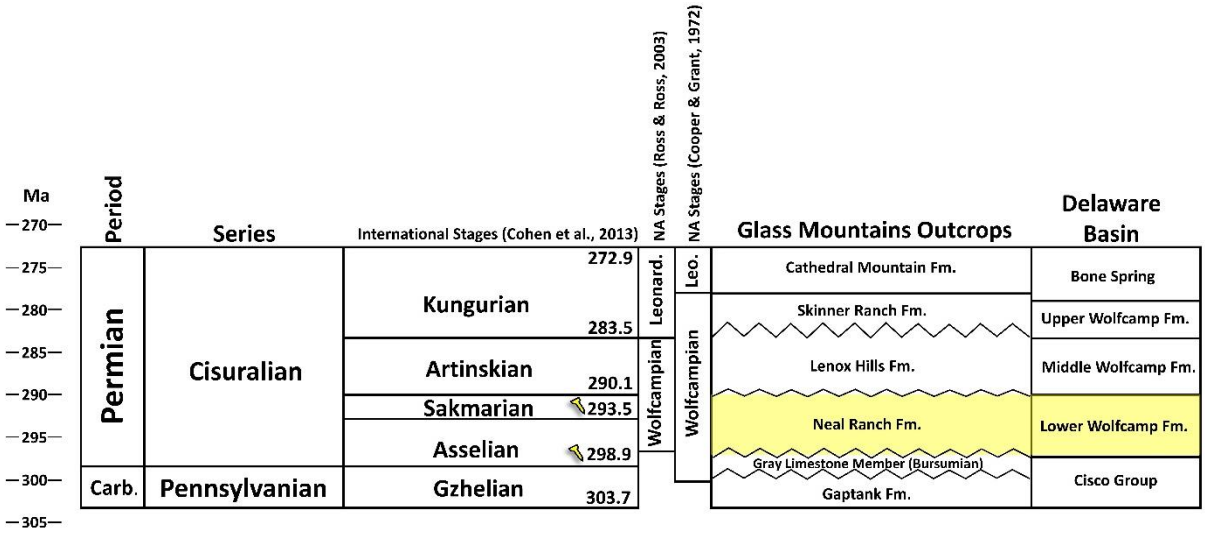

Figure III-1 Stratigraphic chart with international and North American stages, legacy Glass Mountains stratigraphy, and the proposed nomenclature. International stage ages from (Cohen et al., 2013; Lucas and Shen, 2018), note that the base of the Asselian and Sakmarian have defined GSSPs. Yellow highlight indicates focus of this study.

This paper supports the tri-partite stratigraphic framework of the Wolfcamp Group proposed by Cooper and Grant (1972) but here the provincial terms of Neal Ranch, Lenox Hills, and Skinner Ranch, which lack any sense of superposition, are replaced, respectively, by the terms Lower, Middle, and Upper Wolfcamp Formations.

Additionally, the term Wolfcamp has also been used to convey time, specifically as the Lowermost North American Permian Stage and later, the Lowermost North American Series (Adams, 1939; King, 1942; Ross, 1963). However, the global standardization of the geologic time scale (Cohen et al., 2013), has made these provincial North American Stage names somewhat obsolete. Currently the Lower Permian stages include, from the base up, the international Asselian, Sakmarian, Artinskian, and Kungurian Stages. These stages approximately correspond to the classic North American Wolfcampian and Leonardian Stages. However, ICS stage boundaries are typically defined in conformable, biostratigraphically-defined condensed sections (Cowie et al., 1986; Lucas, 2013), while the classic North American stages are based on unconformities, so the relative position of stage, series, and systems boundaries in North America are now all in a state of flux. The original base of the Wolfcampian no longer aligns with the base of the Permian (Lucas, 2013) and the Lowermost Wolfcampian strata (the "Gray Limestone Member") previously included within the Permian (e.g., King, 1937) are now considered Latest Pennsylvanian in age based on the International Geologic Time Scale (Cohen et al., 2013). These Uppermost Pennsylvanian (Cohen et al., 2013) strata have been referred to as the Bursumian Stage or Substage (Ross and Ross, 1987; Ross and Ross, 1994), as well as the Newwellian Substage (Wilde, 2002).

These strata, now considered Latest Pennsylvanian, are excluded from the Wolfcamp Group in this article.

Geologic Setting

Permian rocks, first recognized in the Ural Mountains (Murchison, 1841), also outcrop in the portion of Texas west of the Pecos river known as the Trans-Pecos region (Hill, 1887). The geology of the Trans-Pecos region is complex and includes several small mountain ranges, including the Glass Mountains which form an east-west trending cuesta or homocline comprised largely of Permian rocks dipping gently to the north and northwest (Hill, 1903). The Wolf Camp Hills are at the foot of the Glass Mountains in Brewster County approximately 19 kilometers northeast of the town of Marathon, and contain rocks from the Late Pennsylvanian and Early Permian (Böse, 1917; Udden, 1917; King, 1931; Ross, 1959).

The Latest Pennsylvanian and Earliest Permian rocks of the Wolf Camp Hills and the Glass Mountains were deposited in a tectonically and climatically dynamic Late Paleozoic environment (Galley, 1958; Adams, 1965; Ewing, 1984; Hills, 1985). The Middle Paleozoic proto-Permian Basin was the Tobosa Basin and its depositional units, such as the organic-rich Devonian Woodford Formation, were deposited in relatively quiescent waters, bounded by a passive continental margin to the south (Galley, 1958; Yang and Dorobek, 1995; Tai and Dorobek, 2003). In the Carboniferous, this broad shallow basin was sub-divided into a series of smaller basins and uplifts (notably the deeper, western Delaware Basin, the Central Basin Platform, and the shallower, eastern Midland Basin) associated with the closing of the Rheic Ocean, the eventual collision of

Gondwana and Laurasia, and the assembly of Pangea (Galley, 1958, Adams, 1965; Ewing, 1984, Hills, 1985). This continental suturing produced the Marathon-Ouachita Orogeny, which involved significant loading and subsequent flexure on the North American plate in the Marathon (Trans-Pecos) region (Yang and Dorobek, 1995; Poole et al., 2005). The thrusting was directed to the northwest (Ross, 1986) creating the larger Permian Basin with several uplifts and sub-basins (Yang and Dorobek, 1995). The greater Permian Basin is a peripheral (i.e., collisional) foreland basin located above the subducted passive margin, where the Rheic Ocean crust was subducted beneath the continent of Gondwana. Additional relevant paleogeographic features in the vicinity of the Glass Mountains include the Diablo Platform to the west of Delaware Basin (named for the present-day Sierra Diablo Mountains), and the Orogrande Basin in New Mexico, which also contains significant Wolfcampian stratigraphy (Oriel and McKee, 1967; Wahlman et al., 2013).

There also are several other current small mountain ranges bounding the perimeter of Delaware Basin including, clockwise from the southern Glass Mountains, the Davis, Apache, Delaware, and Guadalupe Mountains which also contain documented Late Paleozoic stratigraphy (e.g., Blanchard and Davis, 1929; Crandall, 1929; King et al., 1965; Sarg, 1989; Sonnenfeld and Cross, 1993; Fitchen, 1997; Playton and Kerans, 2002; Janson et al., 2007). Rocks in these localities have a variety of distinct lithologies and provincial formation names, and their precise time-relationship to the Wolfcamp Group in the Glass Mountains is disputed (Richardson, 1904; Lee and Girty, 1909; Hills, 1942; King, 1942; Fitchen, 1997; Lucas et al., 1998; Lucas et al., 2014).

The Permian strata in the Glass Mountains were interpreted as being deposited on a southern shelf of the Delaware Basin (Figure III-2), and bounded by the Hovey Channel to the northwest, the Marfa Basin to the southwest, the greater Delaware Basin to the north, and the Sheffield Channel and Val Verde Foredeep Basin to the northeast (Flawn et al., 1961; McKee and Oriel, 1967; Cooper and Grant, 1972; Hills, 1972; Ross, 1986). The southern shelf is notably narrower compared with the northwest shelf of Delaware Basin and the eastern shelf of Midland Basin. The Glass Mountains outcrops are immediately north of the thin-skinned Ouachita-Marathon thrust-and-fold belt (Ewing, 1993), which was a significant source of sediment during the Pennsylvanian and Permian (Wuellner et al., 1986; Hamlin, 2009; Soto-Kerans et al., 2020). Peak subsidence in the Delaware and Midland Basins is estimated to have occurred during deposition of the Wolfcampian strata (Hills, 1984; Horak, 1985; Ewing, 1993). Major thrust faults (e.g., the Dugout Creek Thrust) in the region are not exposed in the Wolf Camp Hills or the Glass Mountains, although their subsurface expression tips out just below the Glass Mountains, as documented in well data (King, 1980; Ross, 1986; Ross and Ross, 2003).

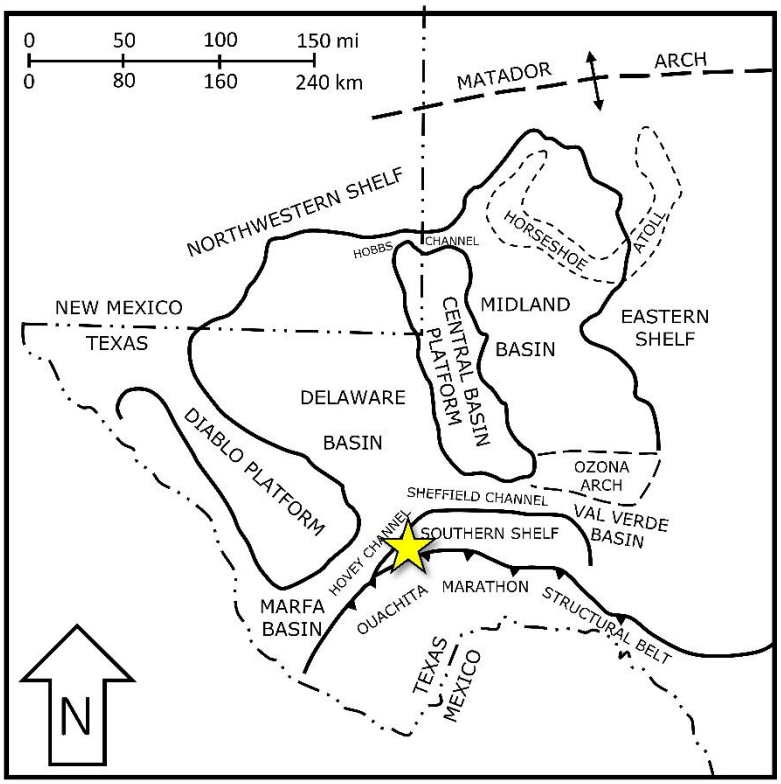

Figure III-2 Map of the Permian Basin with Late Paleozoic features (after McKee and Oriel, 1967). The yellow star in Brewster County approximates location of Wolf Camp Hills at foot of Glass Mountains.

The Permian Basin was located on the western side of the supercontinent Pangea where it was connected to the Panthalassic ocean at low, equatorial latitudes (±5 degrees latitude from the equator) during the Earliest Permian (Ross and Ross, 1990; Scotese and Langford, 1995; Tabor and Montañez, 2002; Tabor and Montañez, 2004; Tabor et al., 2008; Koch and Frank, 2011). The Permian Basin likely was influenced by westerly trade winds (Tabor and Montañez, 2002; Miall, 2019). Study of paleosols from the region indicate a transition from Late Pennsylvanian wet climate to an increasingly arid climate in the Early Permian (Tabor and Montañez, 2004). Globally, the Permian

coincided with a long-term transition away from peak icehouse conditions and recent work indicates the maximum extent of glaciation occurred near the Pennsylvanian-Permian boundary, from approximately 303 to 297 Ma (Montañez et al., 2016; Chen et al., 2018). In the Latest Pennsylvanian, even low latitudes may have been sufficiently cold to support widespread glaciation (Soreghan et al., 2008). Historically, workers interpreted higher frequency cyclicity and higher magnitude eustasy associated with icehouse conditions compared with greenhouse conditions, potentially representing 4th-order depositional sequences (Heckel, 1986; Ross and Ross, 2003; Holterhoff, 2010). Global eustatic interpretations for the Lower Wolfcampian (North American Bursumian and Nealian stages) based on the Paleozoic outcrops from the Glass Mountains show several short term (3rd-order) eustatic fluctuations (10's of meters). superimposed on a longer-term sea-level rise of approximately 30 meters through the Lower Wolfcamp Formation before a final, major drop of sea level at the top of the Lower Wolfcamp Formation potentially exceeding 50 meters (Ross and Ross, 1987; Ross and Ross, 1995). Many recent global eustatic composite curves (e.g., Rygel et al., 2008) leverage the eustatic interpretations from the Permian Basin region (Ross and Ross, 1987). The magnitude of eustasy in the Late Pennsylvanian is estimated to be up to 50 meters by recent workers (Montañez and Poulsen, 2013), although some interpret smaller swings between 10 and 20 meters (Sweet and Soreghan, 2012). Historically some workers concluded between up to 150 meters of fluctuation was possible (Read, 1998; Rygel et al., 2008; Montañez and Poulsen, 2013). Other workers show a shift from eustatic fluctuations of approximately 110 meters during the Latest Pennsylvanian shifting to

Permian eustatic swings of approximately 70 meters (Koch and Frank, 2011). Atmospheric pCO_2 is interpreted as the primary driver of climate and glacioeustasy in the Late Paleozoic (Royer et al., 2004; Montañez et al., 2016), especially on longer time scales (millions of years), although orbital forcing (i.e., Milankovitch cycles on 10's or 100's kiloyear scales) is an important shorter-term driver as well (Heckel, 1986; Montañez and Poulsen, 2013). Recent work also suggested the possibility of short term (<1 million years) atmospheric pCO_2-driven cyclicity which might overprint orbitally-driven cyclicity (Montañez et al., 2016). Orbital eccentricity (100-400 kyr cycles) in particular was cited as the dominant driver of short-term icehouse climate cyclicity (Heckel, 1986; Markello et al., 2008). Note that pCO_2 increased from approximately 300 to 900 ppm between 300 and 290 Ma (Montañez et al., 2007; Montañez et al., 2016; Chen et al., 2018). Plant fossils in Wolfcampian rocks in the subsurface also support the interpretation of a semi-arid climate in the Early Permian for the Permian Basin (Baumgardner et al., 2016; Kvale et al., 2020), although some Early Permian plant fossils from the Glass Mountains show an inconclusive mixture of wet- and arid climate-favoring floral assemblages (Glasspool et al., 2013). The oceans were primarily aragonitic during the Latest Pennsylvanian and the Earliest Permian, and algae were the dominant reef builders, with lesser contributions from *Tubiphytes*, microbes, and bryozoans (Markello et al., 2008).

Finally, the significant variation in Paleozoic carbonate profiles around the Permian Basin should also be taken into account, as they likely record different responses to relative sea level change and the resulting sediment delivery to the basin, or the local

tectonics of the area. The Leonardian Hess Formation, which is strongly aggradational, forms of the bulk of the southern face of the Glass Mountains above the Wolf Camp Hills (Ross et al., 1987). The earliest Wolfcampian phylloid-algal mounds aggrade less, create less relief, and tend to create more ramp-like profiles (Ross et al., 1987; Mazzullo and Reid, 1989; Wahlman and Tasker, 2013; Sleight et al., in press). The Sierra Diablo mountains show various Mid-Late Wolfcampian profiles, including low gradient (1 to 2º) distally-steepened ramps which are, in some places, tectonically-enhanced and steepened up to 7º gradients, adding hundreds of meters of relief (Playton and Kerans, 2006).

Data and Methodology

Data includes six measured sections through the western Wolfcamp Hills where the Lower Wolfcamp Formation is well exposed (Figure III-3). The sections include spectral gamma-ray measurements (n=1,112) made with a handheld gamma-ray spectrometer (Radiation Solutions RS-230 BGO Super-SPEC). Section A is 47 feet (14 meters) thick, section B is 145 feet (44 meters), section C is 297 feet (91 meters), section D is 265 feet (81 meters), section E is 590 feet (180 meters) thick, and section F is 148 feet (45 meters) thick. Total length of the composite measured section is 620 feet (190 meters). Measured sections focus on bed and bed-set scale features (Campbell, 1967), both carbonate and mudstone lithology, sedimentary structures, process sedimentology, and bedding surfaces. Fossil assemblages also are noted (Figure III-4). Silicification of fossils commonly is observed and consistent with previous studies (e.g., Ross, 1963).

Major bedding surfaces and lithologic breaks with potential chronostratigraphic significance are documented in detail. Measured section and spectral gamma-ray data are integrated in the software EasyCore™. Raw spectral gamma-ray data include potassium (%), uranium (ppm), and thorium (ppm) which were later used to derive the total gamma-ray values in API units (Crain, 1986). The primary use of the measured section data was to document in detail the lithologies, surfaces and cyclicity occurring during deposition of the Lower Wolfcamp Formation. Extensive biostratigraphic data (Sims and Belanger, 2020, in review) and chemostratigraphic data (Gutierrez et al., 2021, in prep) also were collected throughout the Lower Wolfcamp Formation for analysis, and are integrated into this stratigraphic framework.

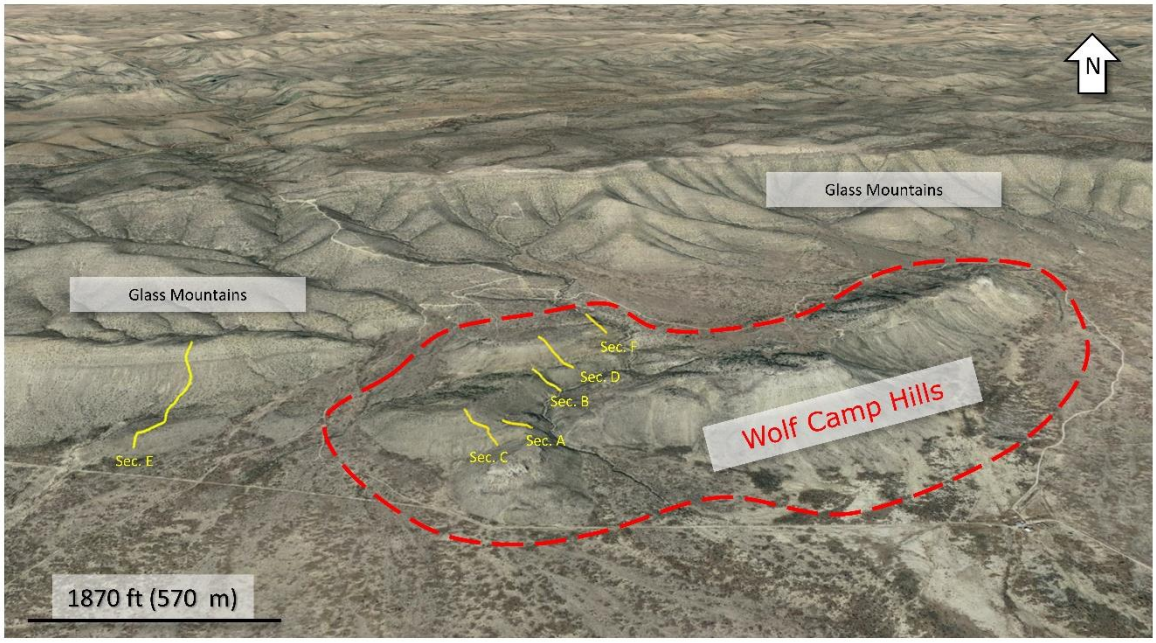

Figure III-3 Six measured sections (A through F) across Wolf Camp Hills (foreground, circled in red) at the foot of the Glass Mountains (background). Wolfcampian stratigraphy outcrops on west side of hills. View is towards the north.

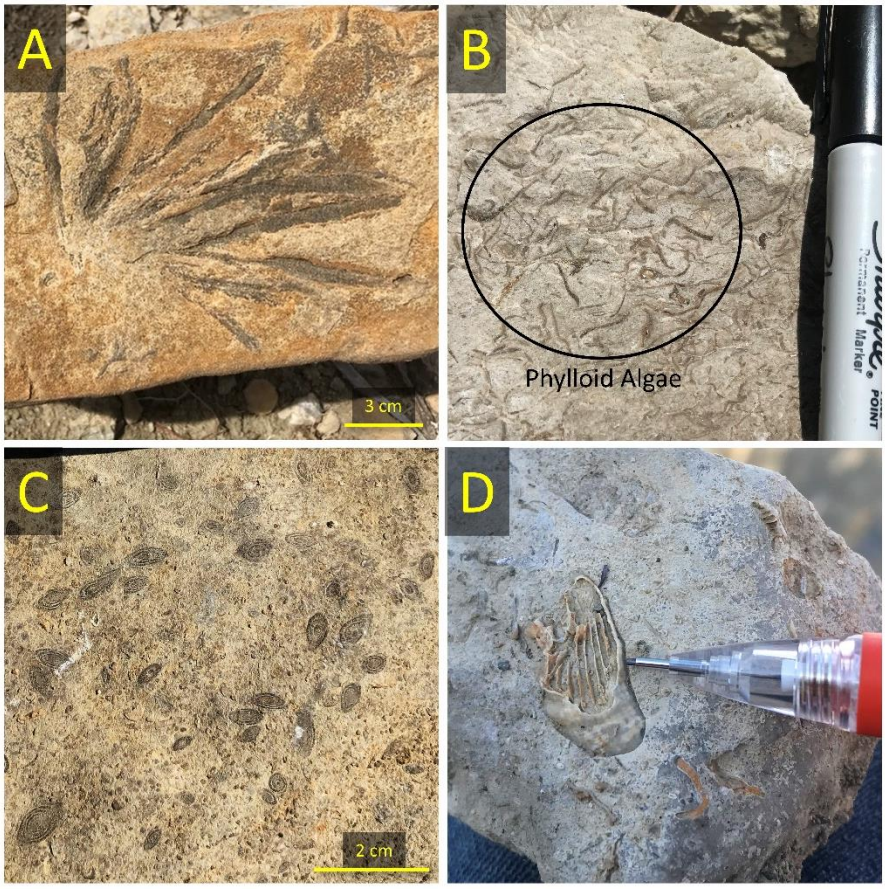

Figure III-4 Field photos of fossil assemblage. Gastropods, sponges and brachiopods (not shown) also are present. From left to right: A) Terrestrial plants in siltstone beds. B) Phylloid algae. C) Fusulinid tests. D) Rugose coral with visible septa.

Seventy-four polished fist-sized hand samples from the Wolf Camp Hills collected throughout the Lower Wolfcamp Formation aided in detailed facies description and were used to create thin sections. Thin sections are especially essential for accurate description of carbonate lithologies, particularly for those which are at least partially recrystallized or dolomitized (Laya and Tucker, 2012). Carbonate lithologies are classified according to Dunham (1962) with the modifications by Embrey and Kloven

(1972) to account for coarser-grained (>2 millimeter) lithologies. Mudstone exposures (Figure III-5) were sampled and mudstone facies were classified compositionally, according to Donovan et al. (2017). Siliceous mudstone is defined as having <15% carbonate and <50% clay (by volume), mixed siliceous-carbonate mudstone is defined as having <50% clay and 15 to 30% carbonate, carbonate mudstone is defined as having >30% carbonate and <50% clay, and finally argillaceous mudstone is defined as having >50% clay. Where possible, thin sections of mudrock facies were generated to aid in descriptions of facies, for example, in determination of relative quantities of silica and clay grains. In total, 73 thin sections were prepared and described of the Lower Wolfcamp Formation lithologies (Figure III-6).

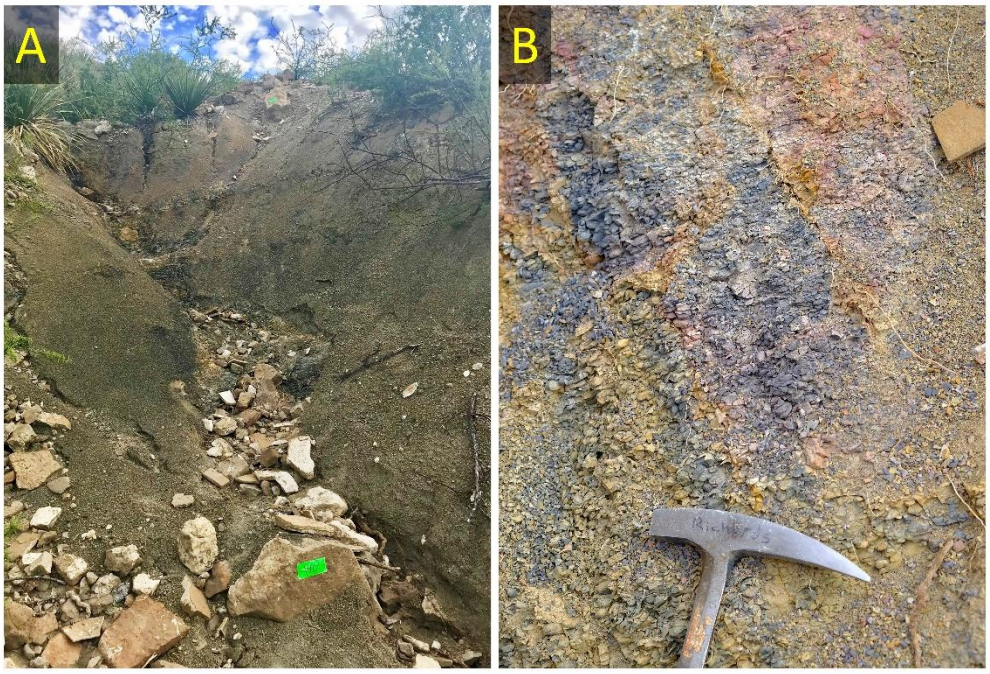

Figure III-5 Mudstone exposures in outcrop. A) Permian Wolfcamp Group mudstone exposure from approximately 140 ft (43 m) to 160 ft (49 m) in the composite section. B) Close up example with standard size rock hammer.

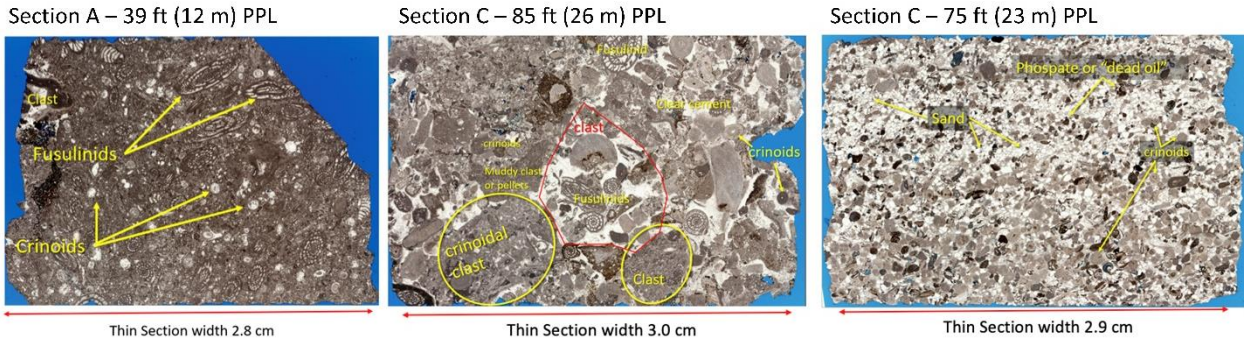

Figure III-6 Three thin section examples from measured sections A and C. From left to right, they are interpreted as a fusulinid packstone, a carbonate-clast conglomerate, and a sandy crinoidal grainstone.

Photogrammetry was gathered using a DJI Phantom 4 Pro drone for the purpose of identifying and documenting in detail the relevant lateral geometries and lap-out relationships for the Lower Wolfcamp Formation, including stratal on-lap and truncation (*sensu* Zahm et al., 2016). Oblique and overhead 20-megapixel images (n=2,260) were used in the creation of a georeferenced point cloud, which was ultimately built into a 3D DOM (Digital Outcrop Model) in Agisoft Metashape™ Professional Edition photogrammetry software (Figure III-7) for the westernmost Wolf Camp Hills. Resolution is around 5 centimeters per pixel, enabling the interpretation of bed-scale features. This 3D model also is tied to the measured sections for stratigraphic and facies control, and enables interpretation of the geobodies and bounding surfaces at seismic-scale both between and away from the measured sections.

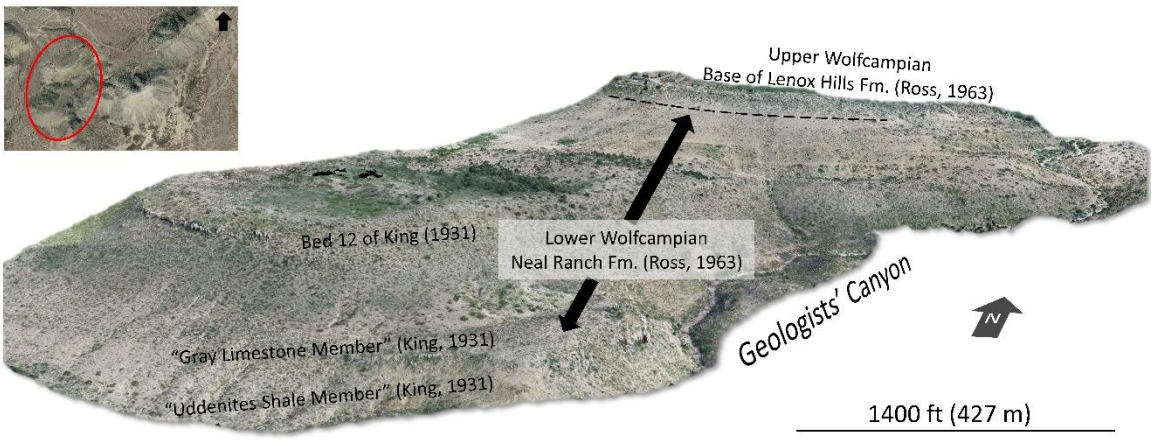

Figure III-7 Georeferenced 3D DOM (Digital Outcrop Model) of the western end of the Wolf Camp Hills created in Agisoft Metashape™ Professional Edition with overlapping 20-megapixel images (n=2,260) captured with a DJI Phantom 4 Pro. Resolution is approximately 5 centimeters per pixel. Shown with historic names of features for reference. Inset made in Google Earth.

Results

Measured Sections

The six measured sections (A, B, C, D, E and F) have varying degrees of vertical overlap and, in aggregate, capture the entirety of the stratigraphy through the Lower Wolfcamp Formation in its type locality (Udden, 1917; King, 1931; Ross, 1963) on the western side of the Wolf Camp Hills. Sections C, E and F are used in the composite section (Figure III-8). Generally speaking, the sections record intervals of thin, ridge-forming limestone beds dipping nine to twelve degrees towards the northwest that alternate with slope-forming mudstone intervals. The lowest point in the stratigraphy captured in these sections is a modestly exposed mudstone outcrop in the *Uddenites*-bearing shale member (Böse, 1917; Udden, 1917) of the uppermost Pennsylvanian Gaptank Formation (*Uddenites* is an ammonite genus discovered in a prominent

mudstone saddle on the western side of the southern mouth of Geologists' Canyon). Previous type sections for the original Wolfcamp Formation and the later Neal Ranch Formation both followed reasonably well exposed outcrops over 0.6 miles (1.0 kilometers) on the west side of the north-south trending Geologists' Canyon (Ross, 1963) and five of the six measured sections in this study also used these same exposures. Section E, however, was measured 0.8 miles (1.2 kilometers) further west in order to capture lateral thickness variation of the Lower Wolfcamp Formation and measures the upper half of the Lower Wolfcamp Formation. The uppermost section stratigraphically, Section F, measures 150 feet (46 meters) into prominent carbonate conglomerate beds at the base of the Lenox Hills Formation (Ross, 1963), here termed the Middle Wolfcamp Formation, which are distinct from the coarse carbonate lithologies in the Lower Wolfcamp Formation.

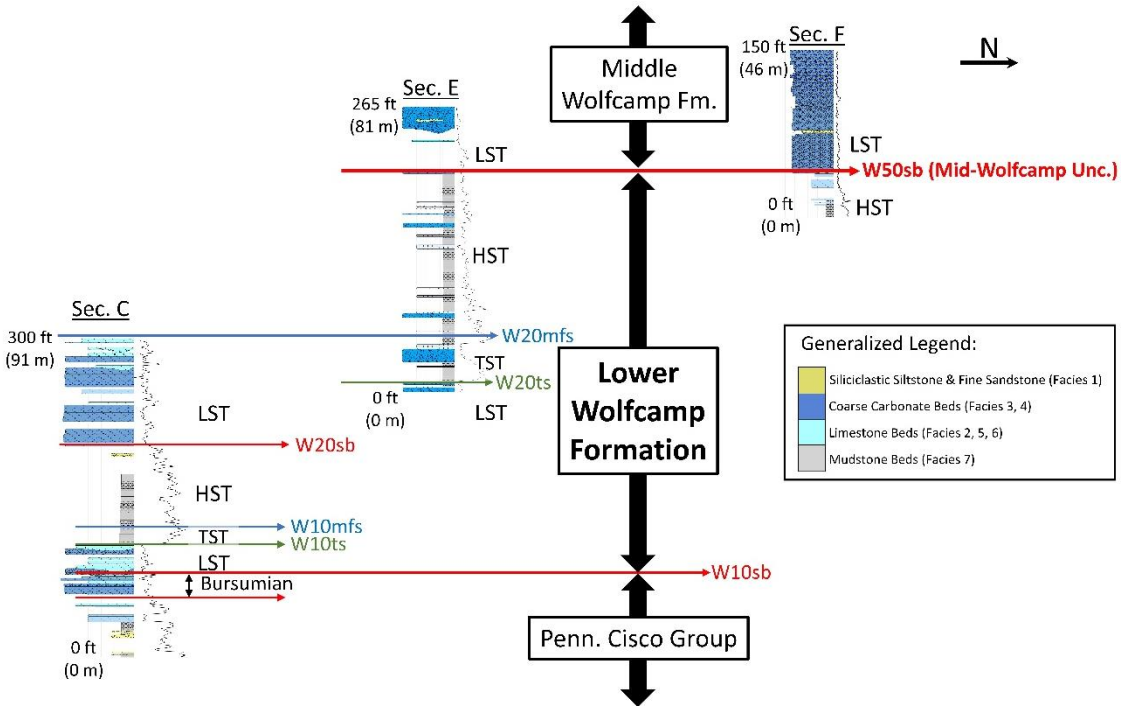

Figure III-8 Three measured sections (C, E, F) used to construct the new composite section for the Lower Wolfcampian. Total gamma ray values show from 0 to 200 API units (higher values are to the right). North is to the right.

Composite Section

These measured sections were combined to create a 622 foot (190 meter) composite section which captures the entire Lower Wolfcamp Formation (Figure III-9). The first section used for the composite, Section C, captures the lower half of the Lower Wolfcamp Formation, the second, Section D, captures the upper half of the Lower Wolfcamp Formation, and the third section for the composite, F, captures the transition to and lowermost stratigraphy of the Middle Wolfcamp Formation. From the base of the stratigraphy, the first 100 feet (30 meters) capture a prominent limestone bedset (the Uppermost Pennsylvanian Gray Limestone Member of King, 1931) which contains the

conglomeratic base of the Lower Wolfcamp Formation, then sharply transitions to a 100 foot (30 meter) thick interval of primarily mudstone beds. This gradually transitions to 115 feet (35 meters) of limestone beds (beds 7 through 11 of Ross, 1963 and beds 9 through 12 of King, 1931), and then ultimately transitions to a 200 foot (60 meter) interval of primarily mudstone beds with some thin, interbedded limestone beds. The Lower Wolfcamp Formation is then, where exposed, sharply and unconformably overlain by the Middle Wolfcamp Formation. Note that total gamma-ray readings are consistently higher in mudstone lithologies (typically 100 to 150 API units) than limestone lithologies (typically 25 to 50 API units). Potassium, thorium and uranium gamma-ray components are all also individually elevated in mudstone lithologies compared with limestone lithologies, although the increases in uranium values are less prominent between lithologies.

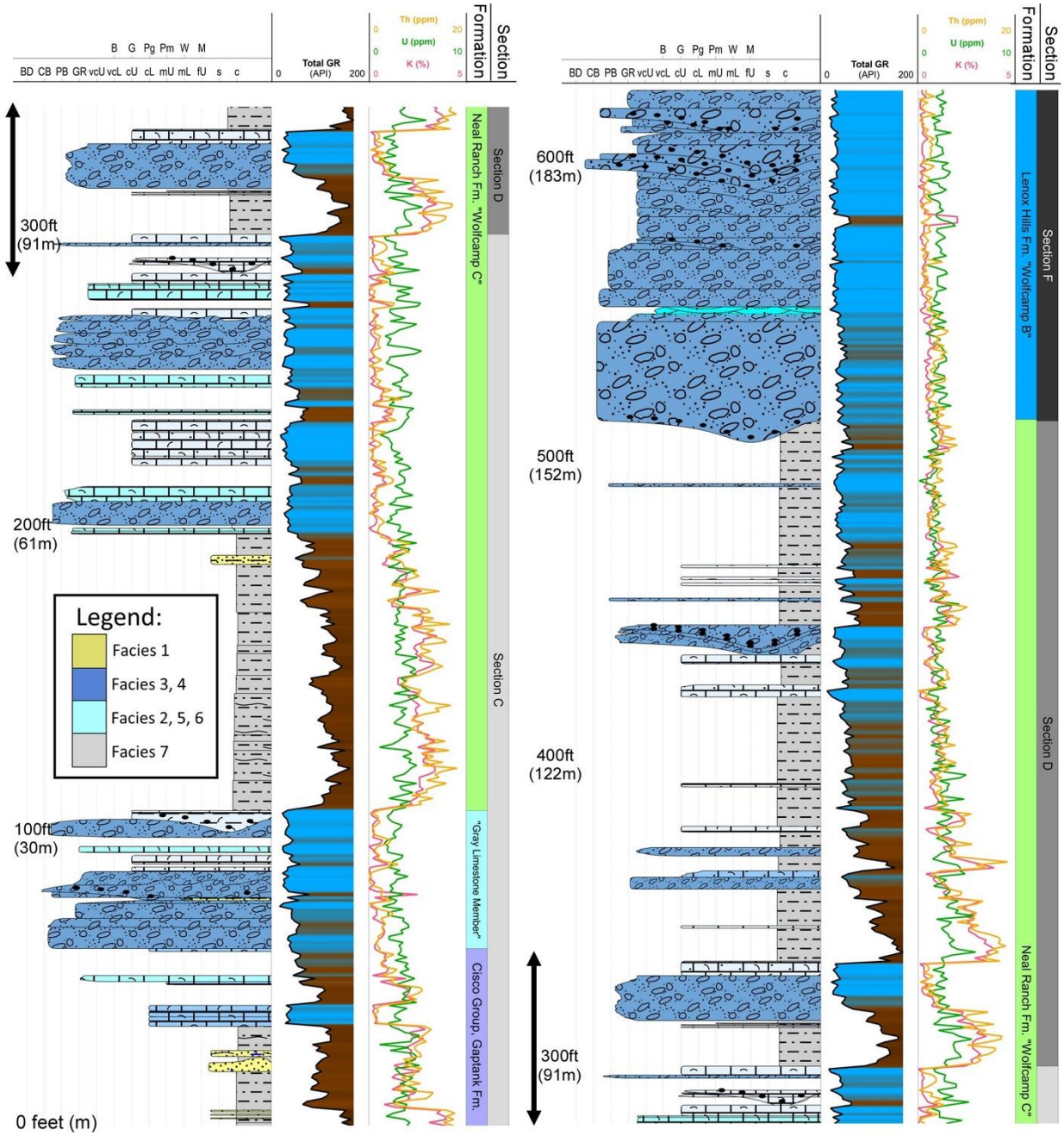

Figure III-9 Composite measured section for the Lower Wolfcamp Formation. Total gamma-ray colored such that low values (<50 API) are blue and higher values (>75 API) are brown. For the spectral gamma-ray track, note that orange is thorium, green is uranium and red is potassium.

Facies

Seven facies are described and interpreted for the Lower Wolfcamp Formation (summarized in Table 1). An eighth facies is a distinct, coarser carbonate-clast conglomerate facies (Facies 4B) occurring only in the basal portion of the Middle Wolfcamp Formation. The facies include 1) siliciclastic siltstone and fine sandstone, 2) phylloid algal boundstone, 3) skeletal rudstone, 4A) red-brown cobble-pebble graded carbonate-clast conglomerate, 4B) light gray boulder-cobble graded carbonate-clast conglomerate, 5) skeletal grainstone, 6) skeletal wackestone and packstone, and 7) siliceous mudstone.

Facies	Description	Interpreted Environment
1) Siliciclastic Siltstone & Fine Sandstone	Light to medium brown and thinly bedded (10's of cm or less). Fine siltstone (≤16μ) excluded from facies. Sand grain sizes are fine to very fine. Rare symmetric ripples in outcrop. Thin sections show occasional inclined laminations and normal grading. Interbedded with mudstone. Occasional carbonate cements. Minor carbonate skeletal grains intermixed examples. Massive to faint planar laminations. One bed with plant fossils. Rare in Wolfcamp, common in Pennsylvanian.	Shefal (potentially hyperpycnites), in storm wave base where symmetric ripples present. Plant fragments indicate increased terrestrial input. Lesser quantities mixed with mudstone in basinal setting.
2) Phylloid Algal Boundstone	Phylloid algae (sensu Pray and Wray, 1963) show curvilinear shape, dark color in plane-polarized light in thin section. Fenestral bryozoan and crinoid fragments also observed in thin section. Some mud visible. Potential coatings around algae also observed in hand sample. Non-phylloid algae also present rarely. Re-worked phylloid algal boundstone clasts occurs in Wolfcampian conglomerate beds. Primarily in Pennsylvanian.	Shelfal or isolated upper slope algal mound buildups or their flanks.
3) Skeletal Rudstone	Grains are skeletal or bioclastic, not lithoclasts (sensu Embry and Kloven, 1972). Light to medium grey, weathering orange-brown. Thick bedded (meter scale). Normal grading occurs rarely. Crinoid columnal fragments dominate, some partially articulated but usually completely disarticulated. Matrix is medium to dark grey, consists of smaller (sand-sized) skeletal fragments and carbonate mud. Common.	Near or part of crinoidal banks, or on the flanks of patch reefs, outer shelf environment. Bioclasts likely transported some distance (i.e. not deposited in in-situ growth position).
4A) Gray-Brown Carbonate-Clast Conglomerate	Polymictic, clasts are primarily lithoclasts. Non-imbricated, typically clast supported but floating clasts also found. Clasts are sub-angular to sub-rounded, cobble to pebble sized, often comprised of skeletal packstone or grainstone or phylloid algal boundstone. Traction structures rare to absent. Weathering removes clasts, leaving fissile med. brown matrix. Inconsistently graded, poorly-moderately sorted. Bed bases sharp where exposed. Occurs in several beds through the Lower Wolfcamp.	Marine debris flows resulting from up-dip subaerial erosion of limestones.
4B) Light Gray Carbonate-Clast Conglomerate	Polymictic, similar clasts to Facies 4A but lithoclasts and matrices are lighter in color, and clasts are coarser (cobbles to boulders) and are more thickly bedded. Non-imbricated. Occasional cross bedding, other traction structures rare. Normal grading and sharp base of beds is also more prominent than red-brown pebble-cobble carbonate clast conglomerate beds from Lower Wolfcamp. Some possible red silty interbeds, locally. Exclusive to base of Upper Wolfcamp in single 150 ft+ (46 m+) bedset.	Conglomeratic braided streams or incised valleys, sourced by subaerial erosion of up-dip carbonate factories.
5) Skeletal Grainstone	Skeletal grains are fusulinids and crinoids primarily, secondary bryozoan, algae, brachiopod and bivalve fragments. Generally heterozoan assemblage. Medium grey to medium brown. Crinoid fragments small (<2 mm), disarticulated. Peloidal grainstone beds occur rarely. Occasional quartz grains intermixed, as high as 40% in rare beds (74 ft or 23 m in Section C, within Gray Limestone Member). Occasional normal grading. Beds typically 1 to 4 ft (0.3 - 1.2 m). Common.	Subtidal, medium to high energy grain-rich shoals or patch reefs on middle shelf.
6) Skeletal Wacke- and Packstone	Typically red-brown to medium gray in outcrop. Grains types vary, but heterozoan skeletal grains dominate, especially crinoid and fusulinid fragments. Lesser population of fenestrate bryozoans and gastropods. Rare packstone beds with significant transported phylloid algal content. Minor dolomitization occurs (<10% by volume). Geopetal structures from sediment fill in foraminifera tests. Isolated quartz sand grains. Common, often interbedded with mudstone beds.	Deep subtidal, low energy setting on outer shelf or medium energy on uppermost slope. Downdip from local bioherms or patch reefs.
7) Siliceous Mudstone	Often covered, or slope forming but exposed in local drainages. Freshest exposures show grey-blue color, weathering red-brown with rare, planar laminations. Interbedded with thin, flaggy siltstone and wackestone beds. Thin sections show siliceous sponge spicules, detrital quartz silt, clays and organic matter. Preliminary geochemical analyses show varied composition, but siliceous mudstone (<15% carb., <50% clay) dominates. Common in Lower Wolfcamp & Cisco.	Low energy open marine setting below storm wave base, deposited by hemipelagic plumes on lower slope or in basinal setting.

Table III-1 Summary of all 8 facies with descriptions and interpreted depositional environments.

Note that the limestone and mudstone facies dominate the stratigraphy for the Lower Wolfcamp Formation. Total gamma-ray measurements consistently differentiate gross lithologies, where limestone beds (Facies 2 through 6) are often under 50 API units, whereas siliciclastic siltstone and sandstone beds (Facies 1) typically are between 50 and 100 API units, and mudstone beds (Facies 7) often exceed 100 API units. Siliciclastic siltstone and sandstone beds (Facies 1) and phylloid algal boundstone beds (Facies 2) are more common in the underlying Pennsylvanian Cisco Group. Coarse carbonate facies (with grain diameters exceeding 2mm) are separated between those which are primarily bioclastic (Facies 3, skeletal rudstone) and those which are primarily comprised of lithoclasts (Facies 4, carbonate-clast conglomerate). The carbonate-clast conglomerate facies are split into light gray boulder to cobble carbonate-clast conglomerate (Facies 4A) which only occurs at the base of the Middle Wolfcamp Formation and red-brown cobble to pebble carbonate-clast conglomerate (Facies 4B), which occurs in several locations through the Lower Wolfcamp Formation. Some rudstone beds are almost entirely dominated by crinoid fragments, usually but not always disarticulated (Figure III-10), and could alternately be classified as an encrinite facies (*sensu* Ausich, 1997). Finally, fine siltstone (<16μ) is distinguished from medium and coarse siltstone (Figure III-11) and instead grouped with mudstone facies. This is similar to the Dunham (1962) classification which also grouped fine silt sized carbonate particles with carbonate mud.

Figure III-10 A) Example of rudstone facies (Facies 3) from outcrop dominated almost entirely by crinoid columnal fragments. Note that bed could also be classified as a coarse encrinite. The term “encrinite” refers to packstones or grainstones composed of >50% crinoidal debris (Ausich, 1997). This particular bed crops out towards the base of Section E (base of interpreted W20 depositional sequence). B) An example of a pebble-cobble conglomerate (Facies 4A) for comparison. Note that it is primarily composed of limestone lithoclasts with rare skeletal bioclasts mixed in.

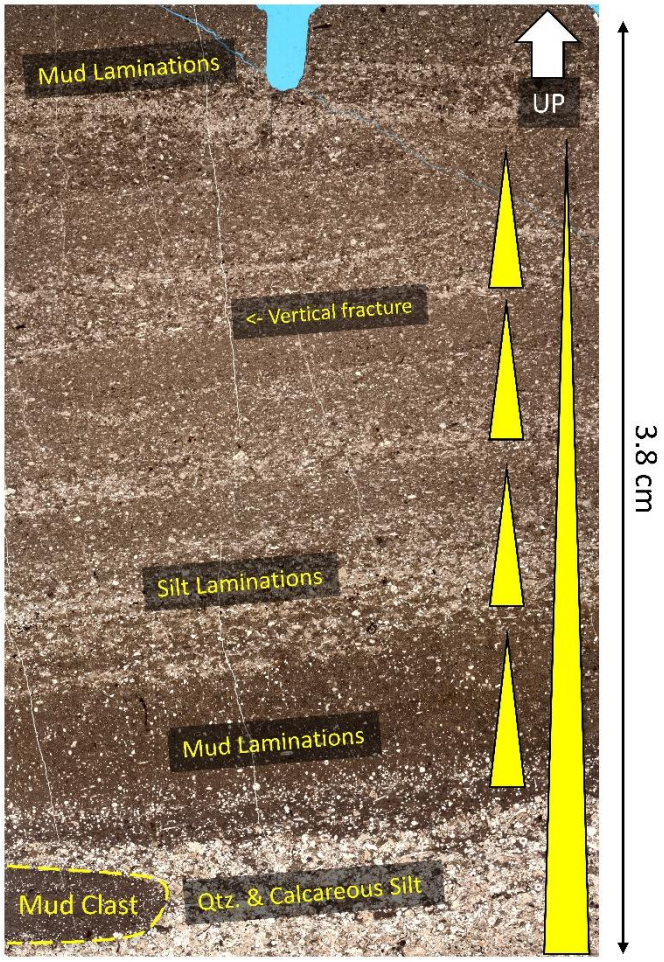

Figure III-11 Thin section (PPL) example of siltstone facies (Facies 7) from thin siltstone bed interbedded with mudstone. Lateral equivalent of measured section C along western edge of Geologists' Canyon. Note inclined laminations which alternate between mud, quartz silt and fine sand. Also note normal grading, and single mud clast at bottom. Notch signifies upward direction.

Description of Major Surfaces

Six surfaces of varying prominence occur within the Lower Wolfcamp Formation. They include four surfaces in which carbonate-clast conglomerate beds (Facies 4A, 4B) sharply overlie limestone (Facies 5, 6) or mudstone facies (Facies 7) and are marked by sharp drops in gamma-ray values (>50 API units where contacts are well

exposed). From the base of the composite section stratigraphy, the surfaces include the onset of carbonate-clast conglomerate beds 59 feet (18 meters) up from the base of the composite section (the base of Uppermost Pennsylvanian Gray Limestone Member), and the onset of another carbonate-clast conglomerate bed 77 feet (23 meters) above the base of the composite section (W10sb, the base of the Wolfcampian). A third, similar surface (W20sb) occurs 200 feet (61 meters) above the base of the composite section, also occurring 10 feet (3 meters) above a significant siltstone bed (Facies 1) enriched in plant fossils. The floral specimens were previously documented in detail (Glasspool et al., 2013) and coincides with Bed 12 of the Neal Ranch Type Section (Ross, 1963). The fourth surface (W50sb), at 512 feet (156 meters), is the most prominent and marks the onset of the Middle Wolfcamp Formation carbonate-clast conglomerate beds which lie unconformably above the Lower Wolfcamp Formation.

Two additional surfaces are distinct in that they mark the sharp onset of thick mudstone intervals (10's of feet, 6 meters or more) above limestone beds and coincide with significant breaks in topography which expose the uppermost planar contact with the underlying limestone beds. The first of these surfaces occurs 105 feet (32 meters) above the base of the composite section (W10ts) and is marked by a very sharp increase in all spectral gamma-ray values, although uranium is somewhat less increased. This occurs at the top of the "Gray Limestone Member" (King, 1931). Another surface occurs approximately 295 feet (90 meters) above the base of the composite section (W20mfs) and also is marked by sharp increases in all gamma-ray values, although again, uranium values increase less sharply than thorium or potassium. The thickness of this mudstone

interval (320-350 feet, 98-107 meters) is less substantial than the previous mudstone interval, it is nonetheless a prominent transition, also coinciding with a major break in topography, and again forming a broad terrace above the preceding limestone bed. This surface shows an extensive but thin (centimeter-scale) iron-oxide crust capping the limestone beds, immediately below the overlying mudstone interval (Figure III-12).

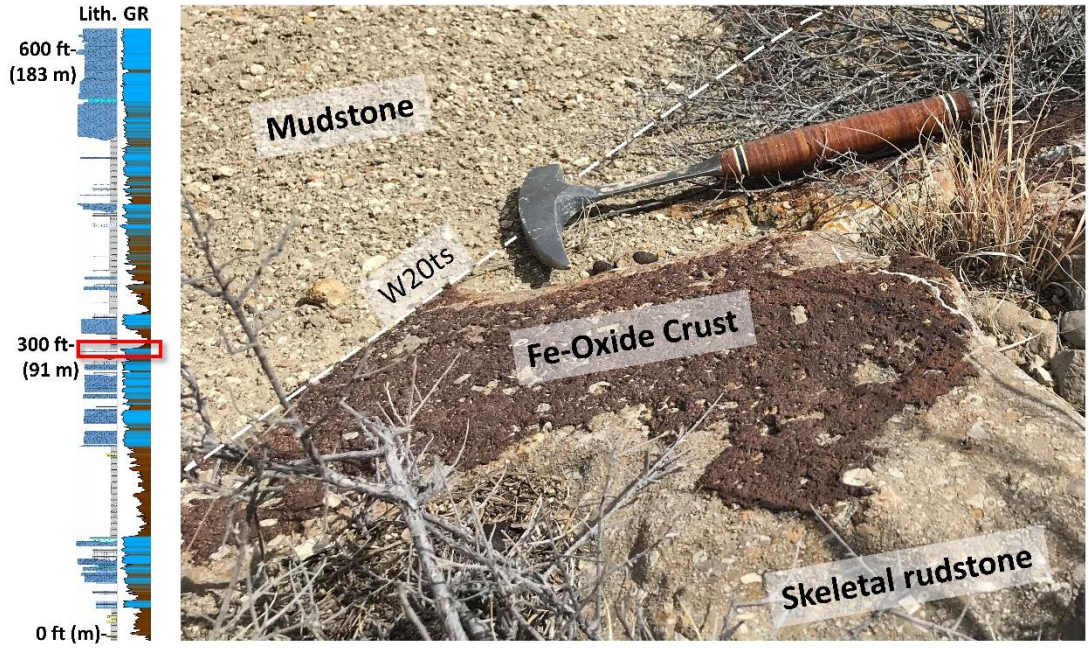

Figure III-12 Prominent mudstone-limestone bed contact occurring at W20 maximum flooding surface (W20mfs). Here, mudstone beds are eroded and slope forming but underlying limestone is intact. Also note iron oxide crust, interpreted as a hardground.

Lateral Thinning of the Lower Wolfcamp Formation

The Lower Wolfcamp Formation thins considerably to the east (Figure III-13). The westernmost section, Section E, shows a 66 foot (20 meter) increase in thickness 0.8 miles (1.2 kilometers) west of Geologists' Canyon in the Wolf Camp Hills, across a north-south trending ephemeral drainage and ranch road. Measurements were made

upwards from a continuous surface (W20mfs), which marks a sudden shift from limestone to mudstone facies and coincides with a sharp break in topography. This surface was walked-out and utilized as a local datum in order to compare sections laterally. Stratal terminations are interpreted at the top of the Lower Wolf Camp Group under the lowermost bedset(s) of off-white carbonate-clast conglomerate beds in the Upper Wolfcamp Group. These stratal terminations are not continuously exposed as the ridge-forming conglomerate from the overlying Middle Wolfcamp Formation sheds clasts and these contacts commonly are obscured.

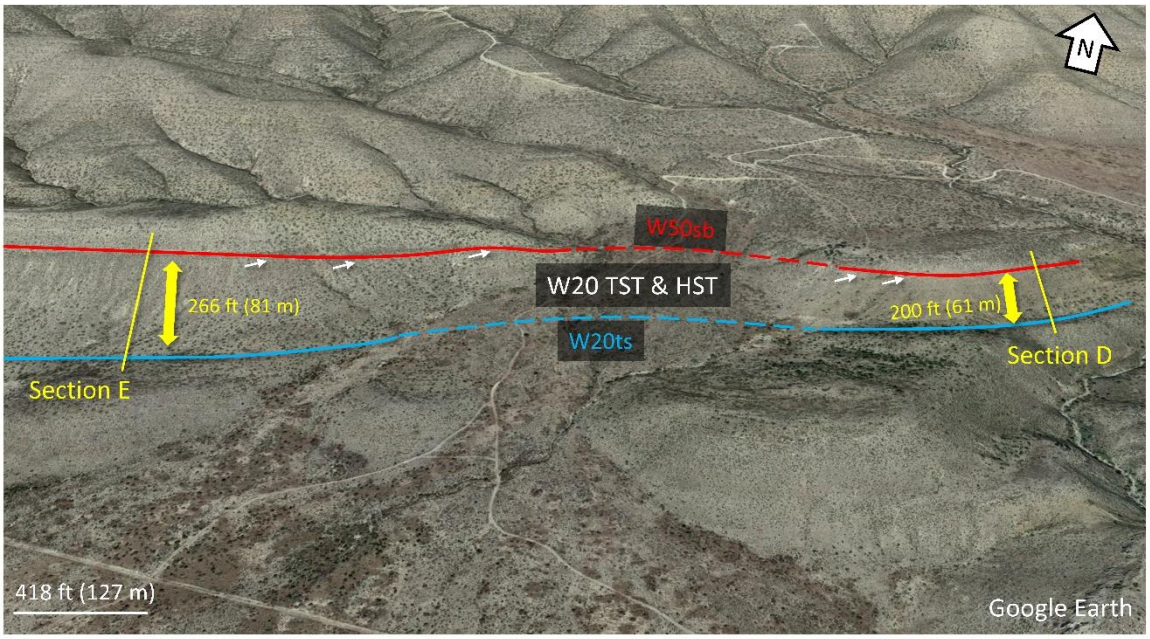

Figure III-13 Oblique view of far west side of Wolf Camp Hills showing eastward thinning of Lower Wolfcamp Formation (W20 depositional sequence) due to differential truncation under the Mid-Wolfcamp Unconformity (W50sb). Distance shown for each section is true stratigraphic thickness between transgressive surface below (W20ts) and unconformity above (W20sb). Truncation of W20 depositional sequence under sequence boundary (W50sb) shown with white arrows.

The Lower Wolfcamp Formation also shows thinning of ~51 feet (16 meters) between Section B to the northeast (0.3 miles, or 0.5 kilometers into Geologists' Canyon), and Section C to the southwest (0.15 miles or 0.25 kilometers west of the mouth of Geologists' Canyon). Thinning between Sections B and C is measured down from the local datum (W20mfs) in the middle of Section C and the top of Section B, and coincides with stratal terminations of the Lower Wolfcamp Formation against the underlying "Gray Limestone Member" (King, 1931).

Sharp Transition to Overlying Carbonate-Clast Conglomerate Beds

The Lower Wolfcamp Formation is unconformably overlain by the lowermost bed-set of the Middle Wolfcamp Formation. The overlying conglomerate interval is at least 150 feet (46 meters) thick, and consists of light gray or off-white carbonate-clast conglomerate beds (Facies 4B) outcropping exclusively in this interval, comprised primarily of cobble to boulder sized limestone clasts of various limestone lithologies. The component lithologies in individual clasts often match facies observed in lower limestone beds (e.g., skeletal grainstone, phylloid algal boundstone clasts). Individual beds often show clear grading from boulder- or cobble-sized clasts upwards into pebble-sized clasts (Figure III-14). The contact with the underlying Lower Wolfcamp Formation is very sharp and irregular (Figure III-15), where best exposed shows stratal terminations and relief up to 66 feet (20 meters), but individual clasts create a thick apron or cover of scree below the in-situ Middle Wolfcamp Formation, thereby obscuring this contact across much of the Wolf Camp Hills. The underlying Lower Wolfcamp Formation often

contains reddish brown to orange-brown limestone beds which are distinct in color from the off-white conglomerate beds comprising the Middle Wolfcamp Formation, aiding in inference of the contact where the contact itself is covered. Thin sections of limestone beds (Facies 5) underlying this unconformity contain dissolution features (Figure III-15).

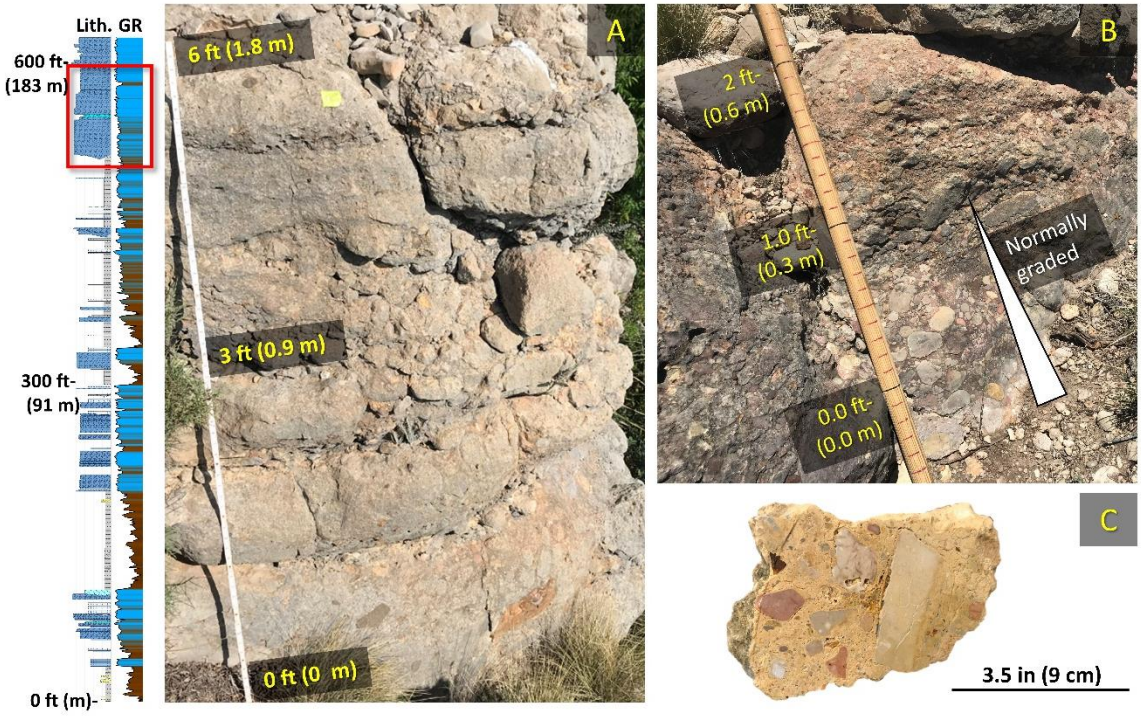

Figure III-14 A) Basal 151 ft+ (46 m) of the basal Middle Wolfcamp Formation composed entirely of light gray carbonate-clast conglomerates (Facies 4B). Note sharp bases of beds. B) Bisected rock face showing grading. C) Polished hand sample with visible, defined lithoclasts.

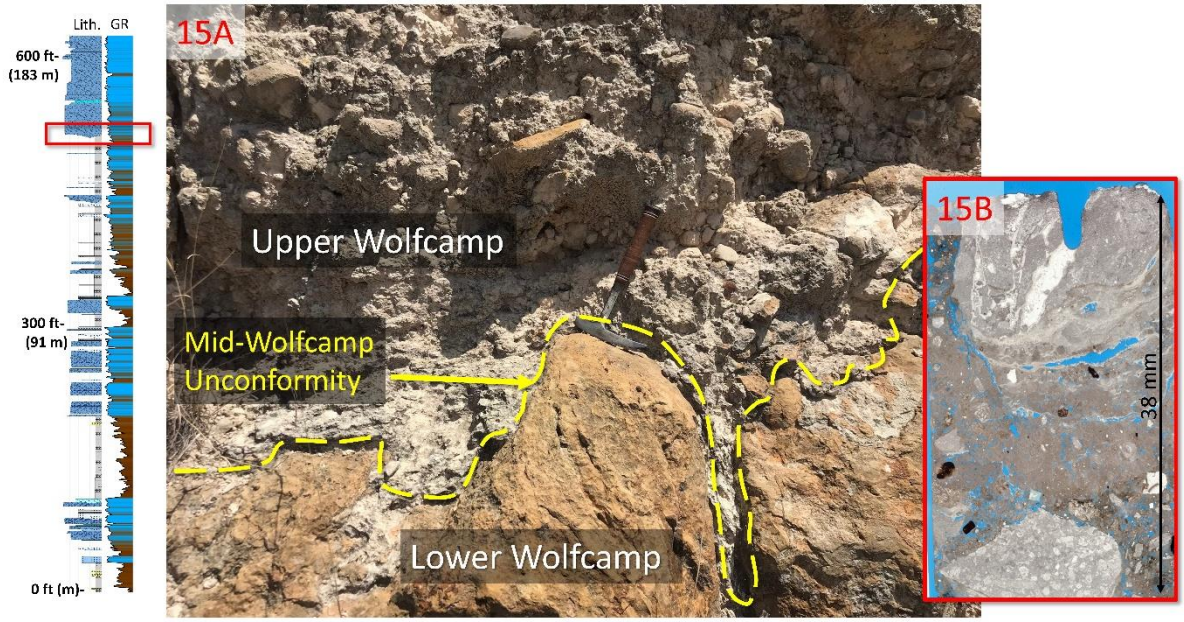

Figure III-15 Exposed contact between Middle and Lower Wolfcamp Formations interpreted as the Mid-Wolfcamp Unconformity (W50sb). Underlying lithologies vary from limestone, as shown, to mudstone. Thin section from overlying limestone shows signs of dissolution, potentially reflecting a compound sequence boundary with stepped (repeated) drops in relative sea level.

Discussion

Depositional Profile for the Lower Wolfcampian Southern Shelf

Wolfcampian depositional profiles vary across the greater Permian Basin both as a function of location and through time. In terms of location, Wolfcampian carbonate factories in the Permian Basin region developed in a variety of tectonic settings. This includes the margins of steep, fault-bounded uplifts on the western margin of the Central Basin Platform, or across the low relief Eastern Shelf of Midland Basin (e.g., Dorobek, 1995; Fitchen, 1996). The southern shelf described in this study is unique in the greater Permian Basin in that it formed on the proximal margin of the foredeep associated with the Ouachita-Marathon Thrust system (Ross, 1986). This is the “wedge-top” depozone

described in foreland basins by previous workers (DeCelles and Giles, 1996). Carbonate-platforms classified according to their tectonic setting include so-called "foreland margin platforms" (Bosence, 2005) but they typically are positioned on the distal foredeep, whose shallower depositional profile and reduced sediment input are conducive to carbonate production. Rare examples of carbonate factories on the proximal side of the foredeep include Holocene reefs formed in the Persian Gulf (Purser, 1973) and ancient reefs atop paleo-highs in Cenozoic strata in the southern Pyrenees (Luterbacher et al., 1991). There, paleo-highs conducive to carbonate production were controlled by blind thrust faults created by the advancing orogenic wedge (Luterbacher et al., 1991). Other examples of carbonate factories perched on tectonically controlled (often terraced) paleo-highs on active margins include reef deposits documented in southern Cyprus (Robertson et al., 1991). These examples also closely resemble the "thrust-top platform" model of Bosence (2005) and is consistent with the wedge-top (*sensu* DeCelles and Giles, 1996) tectonic setting of the southern shelf with regards to Ouachita-Marathon foreland system.

Regarding variation in carbonate profiles through the Wolfcampian over time, regional studies in the Permian Basin indicate that Lower Wolfcampian carbonate profiles were more ramp-like, as opposed to the higher relief Upper Wolfcampian carbonate profiles (e.g., Ross, 1987; Mazzullo and Reid, 1989; Sarg, 1989; Candelaria et al., 1992). This is potentially a function of biologically-controlled mound and biohermal tendencies of the lower diversity Lower Wolfcampian carbonate factories (Wahlman, 1988). This study also does not document rimmed margin reef facies, restricted back-

reef facies, or a distinct shelf break. However, this does not explain the ability to transport coarse (>2 mm) lithoclasts observed in the Lower Wolfcamp Formation conglomerate facies (Facies 4A), which often are associated with steeper depositional profiles capable of transporting large clasts. Some studies, however, have described Wolfcampian conglomerate formation associated on moderate relief (<3.5°) slopes (Loucks et al., 1985). Others have documented steep, tectonically-modified Wolfcampian ramps with slopes as high as 7 degrees (Playton and Kerans, 2002) and steep Leonardian ramps with slopes as high as 15 degrees (Fitchen, 1996), both in the Sierra Diablo Mountains.

Therefore, the depositional profile interpreted for the Lower Wolfcamp Formation (Figure III-16) in the Glass Mountains is a unique moderate relief carbonate depositional profile on the Southern Shelf in the most proximal margin of the foredeep (possibly in the wedge-top setting *sensu* Decelles and Giles, 1996), which incorporates carbonate-clast conglomerate deposition. This profile is tectonically controlled and reflects extreme proximity to Ouachita-Marathon orogenic wedge. Carbonate-clast conglomerate deposition can occur in marginal marine environments, as part of shelfal channel complexes or non-marine incised valleys (Facies 4A) for the Middle Wolfcamp Formation, or in open marine debris flows or submarine channels (Facies 4B) for the Lower Wolfcamp Formation. The Lower Wolfcamp Formation records no inner shelf facies potentially reflecting partial erosion of the topset of the depositional profile under the Middle Wolfcamp Formation (*sensu* Donovan et al., 2010). Since the axial foredeep developed downdip from the southern shelf (Ross, 1986), the moderate relief profile

may be distally-steepened further north or northwest, towards the western axial trough of the basin, historically termed the Hovey Channel (McKee and Oriel, 1967). The distal margin of the foredeep, here located on the southern margins of the Sierra Diablo and Central Basin Platforms, is more likely to support a low-relief "foreland margin" carbonate ramp (*sensu* Bosence, 2005).

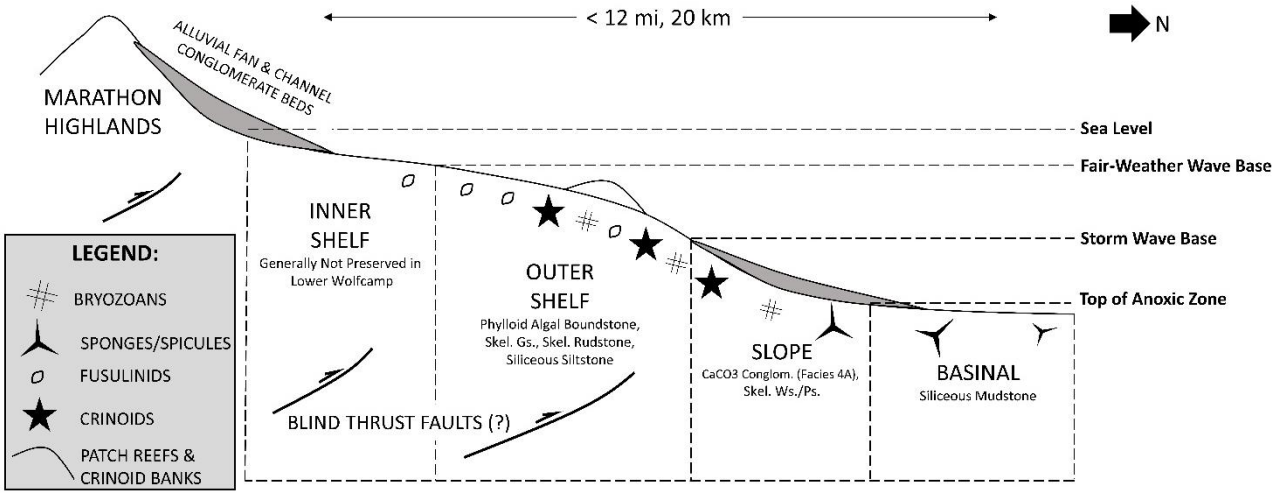

Figure III-16 Schematic moderate relief profile for the Lower Wolfcampian in the Wolf Camp Hills. Angle interpreted as steeper than typical 1° associated with Lower Wolfcampian ramps in order to support transportation of coarse (>2 mm) clasts. This is potentially a function of the tectonic setting on a proximal foreland margin wedge top. The "southern shelf" was narrow (<12 miles or 20 kilometers) as a result of its tectonic setting between the thrust front to the south and the axial trough (foredeep) to the north. During lowstands, sand-sized clastic sediment would mostly bypass the ramp and be deposited in the axial trough (not shown). Subaerial exposure of updip highlands and limestone beds would supply coarse carbonate clasts for short transportation and deposition on the inner shelf. Distal steepening into axial trough is possible but not observed. Modified after Burchette and Wright (1992).

Using this depositional profile (Figure III-16), both carbonate-clast conglomerate facies (Table 1) are interpreted as lowstand facies reflecting drops in relative sea level. The thickly bedded (meter-scale), light gray, boulder to cobble, normally-graded carbonate-clast conglomerate beds (Facies 4A) are only documented at the base of the

Upper Wolfcampian and are not the focus of this study but are tentatively interpreted as possible incised valley or channel complex facies representing extremely proximal, marginal marine (?) depositional environments, consistent with the generalized depositional interpretation by previous workers (e.g., Ross, 1963; Wilde, 1990b; Ross and Ross, 1997). This facies also shows localized high angle cross bedding. These extremely proximal carbonate-clast conglomerate beds sharply overlie an interval of thin, open marine skeletal wackestone and packstone beds (Facies 6) interbedded with mudstone (Facies 7) interpreted as outer shelf or slope facies. The Lower Wolfcamp Formation reddish-brown, cobble to pebble carbonate-clast conglomerate beds with inconsistent grading (Facies 4B) are interpreted as carbonate debris flows, potentially partially channelized, deposited on the upper slope and are only locally erosive, reflecting minor updip subaerial erosion of carbonate factories. These carbonate debris flows (Facies 4A) also sharply overlie outer ramp skeletal wackestone and packstone (Facies 6) and mudstone beds (Facies 7) and also are interpreted as a lowstand response (*sensu* Reijmer et al., 2014). Interpreted debris flow facies are not as proximal or as shallow as the coarser conglomerate facies (Facies 4A) and would therefore represent lower magnitude drops in relative sea level. Rudstone beds could also represent a relative upward shallowing transition where they overlie outer ramp facies. Mudstone (Facies 7) dominated intervals with minor occurrences of skeletal packstone and wackestone beds (Facies 6) are interpreted as transgressive and early highstand facies. Thick skeletal grainstone beds (Facies 5) and associated skeletal packstone beds (Facies 6) are assigned to the middle to late highstand systems tract.

The lack of thick quartz sandstone beds in the Wolf Camp Hills may be due to sediment bypass of sand-sized sediment during regressions, and thick Wolfcampian sandstone deposits are documented downdip in the axial trough of the Val Verde Basin foredeep (Wuellner et al., 1986; Hamlin, 2009). Detrital quartz silt occurs both in rare, thin siltstone beds interbedded with mudstone intervals and as a minor constituent in most limestone facies across all systems tracts. The presence of quartz silt is therefore not diagnostic of relative sea level change, although it may become more commonplace and contain more terrestrial input (e.g., plant material) as relative sea level dropped and deltaic input moved basinward.

Interpretations of Surfaces and Depositional Sequences

Five major surfaces are documented in the Wolf Camp Hills. Of those, four are distinguished chiefly by their sharp transition from interbedded limestone and mudstone beds to carbonate-clast conglomerate beds and their sharp drops in gamma-ray (>50 API units) and are here interpreted as sequence boundaries.

The basal sequence boundary, the base of the Gray Limestone Member, is best documented by the sharp transition to cobble-sized carbonate-clast conglomerate beds (Facies 4A, at 59 feet or 18 meters) in Section C, and caps the *Uddenites* ammonite zone and mudstone interval of the Pennsylvanian Gaptank Formation. This mudstone interval thins and thickens laterally (Section A compared with Section C) providing evidence of differential truncation or erosion. This surface also was documented by recent study of the underlying Pennsylvanian Gaptank Formation (Sleight et al., 2020, in review). This

boundary (the base of the Gray Limestone Member) also was recognized as an erosional sequence boundary representing the base of the Newwellian stage (formerly the Bursumian stage) by previous workers (e.g., Ross and Ross, 2003) but is no longer recognized as the base of the Permian. This study recognizes this basal surface as an erosional sequence boundary defining the base of the Uppermost Pennsylvanian.

The second interpreted sequence boundary, W10sb, occurs towards the top of, but within the prominent "Gray Limestone Member" at 77 feet (23 meters), at the sharp base of a carbonate-clast conglomerate bed (Facies 4A). The base of this conglomerate was previously recognized as an unconformity at the base of the Wolfcampian (Ross, 1963) and a likely candidate for the base of Asselian stage (Ross and Ross, 1987).

The third interpreted sequence boundary, W20sb also is marked by a transition to a carbonate-clast conglomerate bed (Facies 4A) at 200 feet (61 meters) above the base of the Composite Section. This conglomerate bed occurs 10 feet (3 meters) above a prominent siltstone bed (Facies 1) commonly featuring plant fossils that is interpreted as a prodelta turbidite or hyperpycnite (Mulder et al., 2003; Plink-Björklund and Steel, 2004; Saller et al., 2006; Glasspool et al., 2013; Baumgardner et al., 2016). The floral assemblage is interpreted as the initiation of enhanced terrestrial input associated with the early stages of a relative drop in sea level, followed by updip subaerial erosion of carbonate factories which source the polymictic clasts ultimately deposited in the carbonate-clast conglomerate beds (Facies 4A) interpreted as open marine debris flows. This interpreted sequence boundary occurs near a biostratigraphically defined unconformity marking the base of the Sakmarian stage inferred by previous workers

(Wardlaw and Davydov, 2000; Wardlaw and Nestell, 2019). Therefore, this surface (W20sb) is interpreted as a sequence boundary approximately marking the base of the Sakmarian stage.

The fourth sequence boundary, W50sb, is the most significant sequence boundary, marking a sharp transition from beds of Facies 5 (Skeletal Grainstone), Facies 6 (Skeletal Wackestone & Packstone), and Facies 7 (Mudstone), interpreted as outer ramp, open marine facies, to Facies 4B, interpreted as an extremely proximal channel or incised valley facies. Not only does the rapid basinward shift in facies satisfy the traditional definition of a sequence boundary (e.g., Mitchum et al., 1977; Van Wagoner et al., 1987; Van Wagoner et al., 1988), but the magnitude of the shift in facies from is a Waltherian proxy for the magnitude of the relative sea level change in this area (likely > 100 m) and therefore very likely tectonically-enhanced. This supports the findings of Ross (1986) who concludes that the basal unconformity of the Upper Wolfcamp was related to the Dugout Creek thrusting, the last major Marathon-Ouachita orogeny-associated thrust faulting event in the area. Furthermore, a single prominent Mid-Wolfcampian erosional event was noted in the Sierra Diablo Mountains where it's associated with the Pow-Wow Conglomerate (King, 1965; Fitchen, 1997), and using seismic data on the Central Basin Platform (Candelaria et al., 1992). This boundary traditionally was called the "Mid-Wolfcamp Unconformity" (MWU) and often was interpreted as the transition between the Asselian and Sakmarian stages (Ross and Ross, 1988; Candelaria et al., 1992) although recent zircon geochronology of bentonite beds in the Upper Wolfcampian in the subsurface (Tian, 2020, in review) confirm that the Upper

Wolfcampian extends to at least 287 Ma, currently considered mid-Artinskian stage (Lucas and Shen, 2018; Cohen et al., 2013). Similarly, recent conodont work (Wardlaw and Nestell, 2019) places the base of the Artinskian in the Glass Mountains at approximately the base of the Lenox Hills (Wardlaw and Nestell, 2019). This surface (W50sb) is therefore identified as a likely equivalent of the Mid-Wolfcamp Unconformity (MWU) identified in the Sierra Diablo Mountains and on the Central Basin Platform, and as potentially marking the base of the Artinskian stage.

An interpreted transgressive surface (W10ts) occurs at a major break in topography at the top of the "Gray Limestone Member" of King (1931) and beneath a thick (10's of feet, several meters) mudstone interval. The transition from shallow marine limestone beds (Facies 5 and 6) to deep-water marine mudstone beds (Facies 7) is very sharp, and the complete absence of limestone beds above the surface is indicative of a fundamental shift in depositional environment in which limestone deposition ceased, from a shallow marine or shelfal setting to a lower-slope or basinal setting. The overlying mudstone beds are interpreted as onlapping the underlying "Gray Limestone Member" (King, 1931). The extremely sharp inflection in total gamma-ray measurements (>50 API unit increase) here mirrors the sudden shift in lithology. A second interpreted transgressive surface (W20ts) occurs at a major break in topography (forming a narrow ledge along strike) above "Bed 12" of King (1931), over which a thick mudstone interval forms an oblique view of the overlying mudstone interval. A prominent iron-oxide crust marks the surface and is interpreted as a hardground, forming during the maximal rate of marine transgression (e.g., Posamentier and Vail, 1988; Pope

and Read, 1997). The mudstone interval (300-400 feet or 91-128 meters, in the composite section) is more interbedded with minor siltstone (Facies 1) and limestone (Facies 5 and 6) beds than the first major mudstone interval (105-295 feet, 32-90 meters), potentially reflecting a lower-magnitude relative sea level rise.

These surfaces lend themselves toward interpretation of a relative sea level curve (Figure III-17) and three Lower Wolfcamp Formation depositional sequences across the western Wolf Camp Hills (Figure III-18). The system contains both stratal and composition mixing, at multiple scales (*sensu* Chiarella et al., 2017). Specific eustatic interpretations are difficult to interpret given the heavy overprint of tectonic effects associated with the proximity to the Ouachita-Marathon thrust front. The lowermost depositional sequence (W01) in the Lower Wolfcamp Formation is defined by the lower two sequence boundaries (W01sb and W10sb), which approximates the "Gray Limestone Member" (King, 1931). This sequence lacks an obvious internal flooding or maximum flooding surface which would facilitate the internal definition of systems tracts. The second depositional sequence (W10) includes conglomerate beds (Facies 4A) at its base interpreted as a lowstand systems tract (LST), capped by a prominent transgressive surface (W10ts) and a thick mudstone interval which slowly grades into limestone beds, interpreted as a combined transgressive and highstand system tract. A maximum flooding surface (W10mfs) is defined by the highest gamma-ray values within the mudstone interval. The third and final depositional sequence (W20) begins with a thick (100 foot, or 30 meter) interval dominated by skeletal rudstone (Facies 3) and carbonate-clast conglomerate (Facies 4A) beds interpreted as a LST, capped by a

flooding surface (W20ts) and a mixed lithology succession interpreted as a TST (transgressive systems tract). The interpreted LST tract contains numerous conglomerate beds (Facies 4B) and thin sections show potential dissolution effects internally, suggesting a stepped (rather than smooth) drop in relative sea level. This is capped by a prominent maximum flooding surface (W20mfs) and mudstone-rich interval interpreted as an early HST. Then, a thick interval of thinly bedded skeletal wackestone, packstone and grainstone beds (Facies 5 and 6) is interpreted as late HST, before truncation beneath the high relief (at least 66 feet, or 20 meters) Mid-Wolfcamp Unconformity (W50sb). Finally, the light grey to off-white boulder-sized carbonate-clast conglomerate beds (Facies 4B) overlying the Mid-Wolfcamp Unconformity are interpreted as the expression of the basal LST of the Upper Wolfcamp Group.

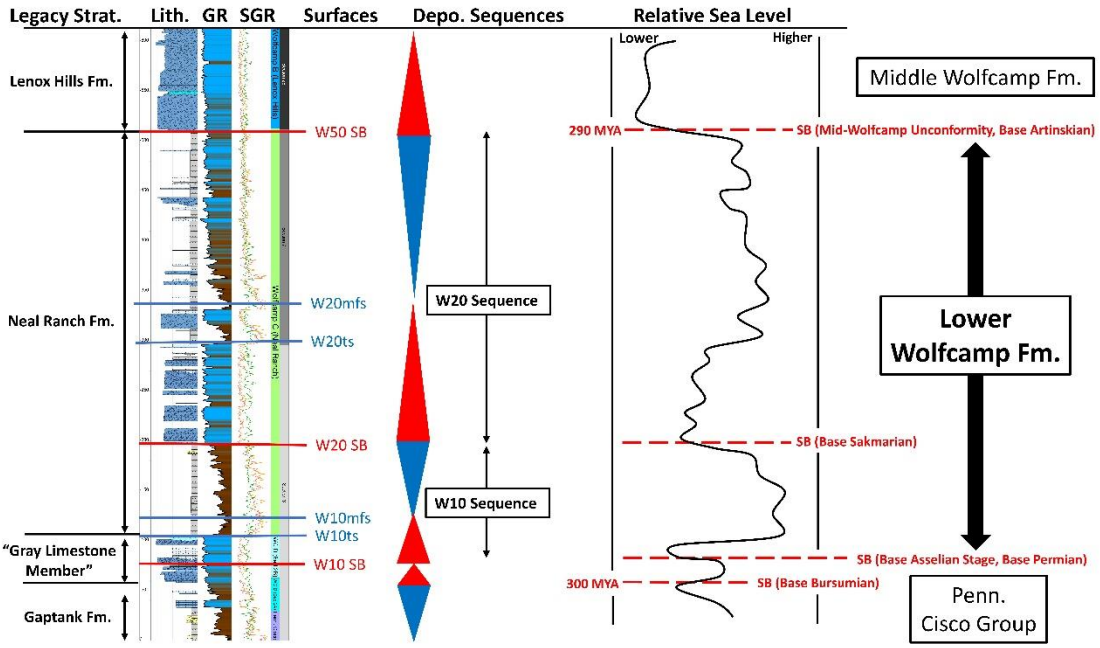

Figure III-17 Relative long term (3rd-order) sea level curve inferred through interpretation of facies and surfaces through the Lower Wolfcampian. Shown with composite section, depositional sequences, and tentative stage boundaries. Note that true eustasy is difficult to

deconvolve from tectonic effects given the proximity to the thrust front. Also note that curve generally aligns with later curves by Ross and Ross (2003).

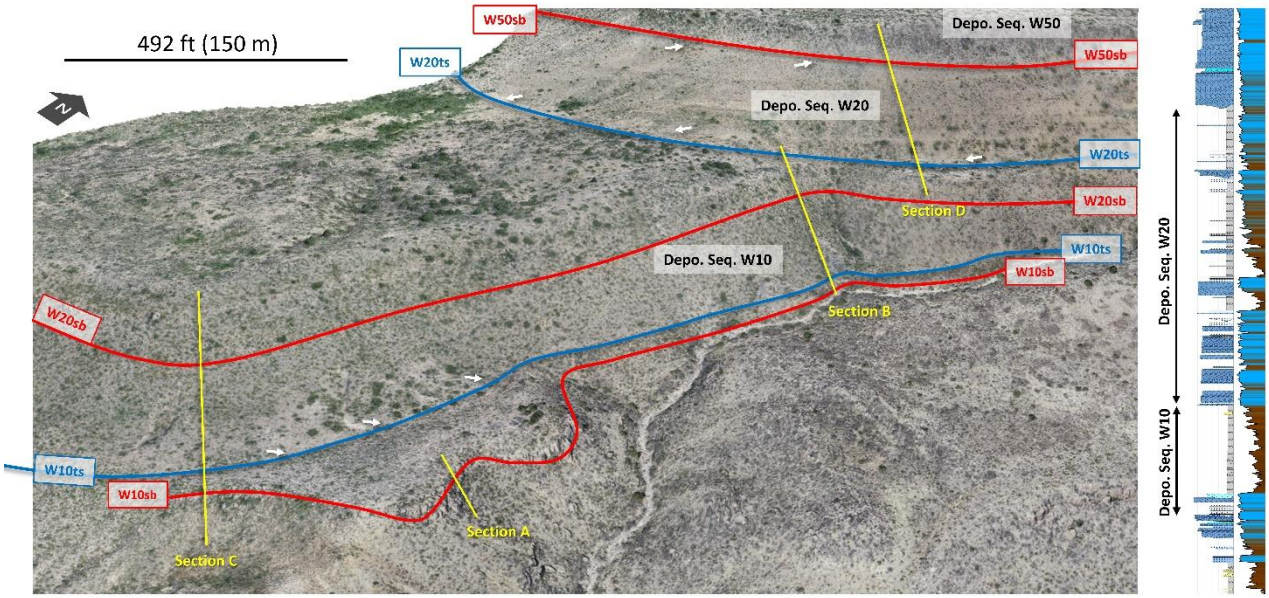

Figure III-18 Drone photogrammetry documenting major surfaces, include onlap surface (W10ts) of Lower Wolfcampian mudstones (base of W10 depositional sequence) on the underlying "Gray Limestone Member" (W01 depositional sequence). The upper interpreted transgressive surface (W20ts) onlaps "Bed 12" of King (1931) and is also shown.

The Lower Wolfcampian, approximately correlative with the Asselian and Sakmarian Stages (Ross and Ross, 1987; Wardlaw and Davydov, 2000; Ross and Ross, 2003), would have a duration of 8.80±0.41 Ma (Cohen et al., 2013). The depositional sequences would therefore likely be on the order of 1 to 5 Ma, each. This also depends on the duration of non-deposition between sequences and the amount of eroded stratigraphy, as well as relative differences in duration between the three depositional sequences. Nonetheless, the interpreted cyclicity would fit within the defined range for 3rd-order sequences (Goldhammer at al., 1991). However, the number of sequences

identified in this study is less than findings by some previous workers. Candelaria et al. (1992) identified four 3rd-order Wolfcampian sequences below the Mid-Wolfcamp Unconformity on the Central Basin Platform and Ross (1997) identified three to four 3rd-order sequences in the Lower Wolfcampian of the Glass Mountains, dependent on the location.

Lateral Thinning and Truncation under the Mid-Wolfcamp Unconformity

The Lower Wolfcamp Formation thins considerably from west to east across the Wolf Camp Hills, with at least 50 feet (15 meters) of thinning above the interpreted flooding surface (W20ts) used as a local datum. This lateral thinning trend also was noted by previous workers (Ross and Ross, 1997; Ross and Ross, 2003). The surface (W50sb) shows distinct truncation of strata under the exposed contact and is supported by thin-section-based evidence (Figure III-15) for dissolution of underlying limestone beds, potentially indicative of subaerial exposure and karsting. The 66 feet (20 meters) of lateral thinning across the Wolf Camp Hills beneath the interpreted sequence boundary (W50sb) also provides a lower bound on the amplitude of relative sea level change associated with this major surface.

Thinning of at least 50 additional feet (15 meters) occurs below the local datum (W20ts) against the top of the underlying "Gray Limestone Member" (W10ts) between Section C (westward) and Section B (eastward). These lap-out relationships are documented by drone photogrammetry, and interpreted as on-lap of the Lower Wolfcamp Formation onto the Latest Pennsylvanian "Gray Limestone Member". These drone-photogrammetry interpretations of thinning due to truncation at the top of the

Lower Wolfcamp Formation and onlap at its base support the interpretations of major differential erosion by Ross and Ross (1995; 2003).

Conclusions

This study presents a new 622 foot (190 meter) composite type section and spectral gamma-ray curve for the Lower Wolfcamp Formation at its type locality in the Wolf Camp Hills in Brewster County, Texas. The formation's strata are comprised of seven lithofacies, dominated by carbonate lithologies which are interbedded with marine mudstone intervals. A variety of coarse carbonate facies occur, including skeletal rudstone beds and carbonate-clast conglomerate beds, the latter of which occur at the base of each depositional sequence and are interpreted as LST deposits. The coarsest and most prominent carbonate-clast conglomerate facies only occurs at the base of the Middle Wolfcamp Formation. Detrital quartz sand is rare, potentially reflected bypass of sand-sized sediment during LST into the axial foredeep, though it is also intermixed with limestone facies. Four sequence boundaries are interpreted; the most prominent in outcrop being the Mid-Wolfcamp Unconformity (W50sb), which is potentially tectonically enhanced and results in differential (eastward) truncation. Two depositional sequences are interpreted within the Lower Wolfcamp Formation (W10 and W20), both of which feature prominent flooding surfaces with distinct high gamma-ray mudstone intervals interpreted as TSTs and initial HSTs. These sequences also record a relative shallowing of facies within the formation. Notably, the tectonic setting for the carbonate factories on the proximal southern shelf, adjacent to axial foredeep creating by the Marathon orogeny, is unique in the Greater Permian Basin.

References

Adams, J. E., M. G. Cheney, R. K. DeFord, R. I. Dickey, C. O. Dunbar, J. M. Hills, R. E. King, E. R. Lloyd, A. K. Miller, and C. E. Needham, 1939, Standard Permian section of North America: AAPG Bulletin, v. 23, no. 11, p. 1673-1678, doi: 10.1306/3D933136-16B1-11D7-8645000102C1865D.

Adams, J. E., 1965, Stratigraphic-tectonic development of Delaware Basin: AAPG bulletin, v. 49, no. 11, p. 2140-2148, doi: 10.1306/A6633888-16C0-11D7-8645000102C1865D.

Ausich, W. I., 1997, Regional encrinites: a vanished lithofacies: Paleontological Events: Stratigraphic, Ecologic, and Evolutionary Implications, p. 509-519.

Baumgardner Jr, R. W., W. A. DiMichele, and N. de Siqueira Vieira, 2016, An early Permian coastal flora dominated by Germaropteris martinsii from basinal sediments in the Midland Basin, West Texas: Palaeogeography, Palaeoclimatology, Palaeoecology, 459, p. 409-422, doi: 10.1016/j.palaeo.2016.07.024.

Blanchard Jr, W. G., and M. J. Davis, 1929, Permian stratigraphy and structure of parts of southeastern New Mexico and southwestern Texas: AAPG Bulletin 13, no. 8, p. 957-995.

Bosence, D., 2005, A genetic classification of carbonate platforms based on their basinal and tectonic settings in the Cenozoic: Sedimentary Geology, v. 175, p. 49-72, doi: 10.1016/j.sedgeo.2004.12.030.

Böse, E., 1917, The Permo-Carboniferous Ammonoids of the Glass Mountains, West Texas and Their Stratigraphical Significance: Univ. Texas Bull. 1762, p. 1-241.

Bostwick, D. A., 1962, Fusulinid stratigraphy of beds near the Gaptank-Wolfcamp boundary, Glass Mountains, Texas: Journal of Paleontology, p. 1189-1200.

Burchette, T. P., and V. P. Wright, 1992, Carbonate ramp depositional systems: Sedimentary geology, v. 79, p. 3-57, doi: 10.1016/0037-0738(92)90003-A.

Campbell, C. V., 1967, Lamina, laminaset, bed and bedset: Sedimentology, v. 8, no. 1, p. 7-26, doi: 10.1111/j.1365-3091.1967.tb01301.x.

Candelaria, M. P., J. F. Sarg, and G. L. Wilde, 1992, Wolfcampian sequence stratigraphy of the eastern Central Basin platform. Permian Basin exploration and production strategies: Applications of sequence-stratigraphic and reservoir characterization concepts: West Texas Geological Society Publication, v. 92(91), p. 27-44, doi: 10.1306/F4C8F606-1712-11D7-8645000102C1865D.

Chen, J., I. P. Montañez, Y. Qi, S. Shen, and X. Wang, 2018, Strontium and carbon isotopic evidence for decoupling of pCO2 from continental weathering at the apex of the late Paleozoic glaciation: Geology, v. 46, no. 5, p. 395-398, doi: 10.1130/G40093.1.

Chiarella, D., S. G. Longhitano, and M. Tropeano, 2017, Types of mixing and heterogeneities in siliciclastic-carbonate sediments: Marine and Petroleum Geology, v. 88, p. 617-627, doi: 10.1016/j.marpetgeo.2017.09.010.

Cohen, K. M., S. C. Finney, P. L. Gibbard, and J. X. Fan, 2013 updated, The ICS International Chronostratigraphic Chart: Episodes v. 36: p. 199-204, doi: 10.18814/epiiugs/2013/v36i3/002.

Cooper, G. A., and R. E. Grant, 1972, Permian brachiopods of west Texas, I. Smithsonian contributions to Paleobiology, doi: 10.5479/si.00810266.14.1.

Covault, J. A., and S. A. Graham, 2010, Submarine fans at all sea-level stands: Tectono-morphologic and climatic controls on terrigenous sediment delivery to the deep sea: Geology, v. 38, no. 10, p. 939-942, doi: 10.1130/G31081.1.

Crain, E. R., 1986, The Log Analysis Handbook; Penn-Well Publishing Company, Tulsa, Oklahoma, USA, 700 p.

Crandall, K. H., 1929, Permian stratigraphy of southeastern New Mexico and adjacent parts of western Texas: AAPG Bulletin, v. 13, no. 8, p. 927-944, doi: 10.1306/3D93286C-16B1-11D7-8645000102C1865D.

Davydov, V. I., 1995, Proposal of Aidaralash as GSSP for the base of the Permian System: Permophiles, v. 26, p. 1-9.

Donovan, A. D., K. Ratcliffe, and B. A. Zaitlin, 2010, The sequence stratigraphy family tree: Understanding the portfolio of sequence methodologies, *in* Application of modern stratigraphic techniques: Theory and case histories, SEPM Special Publication 94, p. 5-33, doi: 10.2110/pec.55.04.0592.

Donovan, A., J. Evenick, and L. Banfield, 2017, An Organofacies-Based Mudstone Classification for Unconventional Tight Rock & Source Rock Plays: Proceedings of the 5th Unconventional Resources Technology Conference, Austin, Texas, July 24-26, p. 3683-3697, doi: 10.15530/URTEC-2017-2715154/.

Dorobek, S. L., 1995, Synorogenic carbonate platforms and reefs in foreland basins: controls on stratigraphic evolution and plat-form/reef morphology, *in* S.L. Dorobek,

G.M. Ross (Eds.), Stratigraphic Evolution of Foreland Basins, Spec. Pub. SEPM, v. 79, p. 127–147, doi: 10.2110/pec.95.52.0127.

Dunbar, C. O., A. A. Baker, G. A. Cooper, P. B. King, E. D. McKee, A. K. Miller, R. C. Moore, N. D. Newell, A. S. Romer, and E. Sellards, 1960, Correlation of the Permian formations of North America: Geological Society of America Bulletin, v. 71, no. 12, p. 1763-1806, doi: 10.1130/0016-7606(1960)71[1763:COTPFO]2.0.CO;2.

Dunham, R. J., 1962, Classification of carbonate rocks according to depositional textures, *in* W.E. Ham., ed., Classification of Carbonate Rocks - a symposium: AAPG Memoir 1, p. 108-121, doi: 10.1306/M1357.

Embry III, A. F., and J. E. Klovan, 1971, A late Devonian reef tract on northeastern Banks Island, NWT: Bulletin of Canadian Petroleum Geology, v. 19, no. 4, p. 730-781, doi: 10.1016/0037-0738(92)90082-3.

Ewing, T. E., 1984, Late Paleozoic Structural Evolution of Permian Basin: AAPG Bulletin, v. 68, no. 4, p. 474-475.

Ewing, T. E., 1993, Erosional margins and patterns of subsidence in the late Paleozoic West Texas Basin and adjoining basins of West Texas and New Mexico: Socorro, New Mexico Geological Society Guidebook, 44th Field Conference, p. 155-166.

Fitchen, W. M., 1996, Strike variability of carbonate platform margin stratal architecture and cycle stacking patterns: Outcrop and seismic examples from lower Permian depositional sequences of the Permian Basin, USA. Proceedings of the 1996 AAPG Annual Convention.

Fitchen, W. M., 1997, Lower Permian sequence stratigraphy of the western Delaware Basin margin. Sierra Diablo, west Texas, Ph.D. dissertation, University of Texas at Austin, Austin, Texas, 263 p.

Flawn, P. T., A. Goldstein Jr., P. B. King, and C. E. Weaver, 1961, The Ouachita System: Texas Univ. Pub. 6120, 401 p, doi:10.26153/tsw/4771.

Galley, J. E., 1958, Oil and Geology in the Permian basin of Texas and New Mexico, in L.G. Weeks, ed., Habitat of oil, a symposium: American Association of Petroleum Geologists, p. 395-446, doi:10.1306/SV18350C16.

Gaswirth, S. B., K. L. French, J. K. Pitman, K. R. Marra, T. J. Mercier, H. M. Leathers-Miller, C. J. Schenk, M. E. Tennyson, C. A. Woodall, M. E. Brownfield, and T. M. Finn, 2018, USGS National and Global Oil and Gas Assessment Project-Permian Basin Province, Delaware Basin, Wolfcamp Shale and Bone Spring Assessment

Units and Input Data: U.S. Geological Survey Data Release, doi: 10.5066/P9WOUJD3.

Glasspool, I., J. Wittry, K. Quick, H. Kerp, and J. Hilton, 2013, A preliminary report on a Wolfcampian age floral assemblage from the type section for the Neal Ranch Formation in the Glass Mountains, Texas: The Carboniferous–Permian Transition. New Mexico Museum of Natural History and Science Bulletin, v. 60, p. 98-102.

Goldhammer, R. K., E. J. Oswald, P. A. Dunn, E. K. Franseen, and W. L. Watney, 1991, Hierarchy of stratigraphic forcing: Example from Middle Pennsylvanian shelf carbonates of the Paradox Basin. Sedimentary Modeling: Computer Simulations and Methods for Improved Parameter Definition: Kansas Geological Survey Bulletin 233, p. 361-413.

Hamlin, H. S., 2009, Ozona sandstone, Val Verde Basin, Texas: Synorogenic stratigraphy and depositional history in a Permian foredeep basin: AAPG Bulletin, v. 93, no. 5, p. 573-594, doi: 10.1306/01200908121.

Harris, A. D., J. A. Covault, A. S. Madof, T. Sun, Z. Sylvester, and D. Granjeon, 2016, Three-dimensional numerical modeling of eustatic control on continental-margin sand distribution: Journal of Sedimentary Research, v. 86, no. 12, p. 1434-1443, doi: 10.2110/jsr.2016.85.

Heckel, P. H., 1986, Sea-level curve for Pennsylvanian eustatic marine transgressive-regressive depositional cycles along midcontinent outcrop belt, North America: Geology, v. 14, p. 330-334, doi: 10.1130/0091-7613(1986)14<330:SCFPEM>2.0.CO;2.

Henderson, C. M., V. I. Davydov, B. R. Wardlaw, F. M. Gradstein, and O. Hammer, 2012, The Permian Period, *in* The Geologic Time Scale, p. 653-679, doi: 10.1016/B978-0-444-59425-9.00024-X.

Hill, R. T., 1887, ART. XXXIV. The Topography and Geology of the Cross Timbers and surrounding regions in Northern Texas. American Journal of Science (1880-1910), v. 33, no. 196, p. 291, doi: 10.2475/ajs.s3-33.196.291.

Hill, R. T., 1903, Physical Geography of the Texas Region: U.S. Geol. Survey Topog. Atlas, Folio 3.

Hills, J. M., 1942, Rhythm of Permian seas—a paleogeographic study: AAPG Bulletin v. 26, no. 2, p. 217-255, doi: 10.1306/3D933444-16B1-11D7-8645000102C1865D.

Hills, J. M., 1972, Late Paleozoic sedimentation in west Texas Permian basin: AAPG Bulletin, v. 56, no. 12, p. 2303-2322, doi: 10.1306/819A421C-16C5-11D7-8645000102C1865D.

Hills, J. M., 1984, Sedimentation, tectonism, and hydrocarbon generation in Delaware Basin, west Texas and southeastern New Mexico: AAPG Bulletin, v. 68, no. 3, p. 250-267, doi: 10.1306/AD460A08-16F7-11D7-8645000102C1865D.

Hills, J. M., 1985, Structural evolution of the Permian basin of west Texas and New Mexico: Structure and tectonics of trans-Pecos Texas, West Texas Geological Society Guidebook, Midland, Texas, 85, p. 81.

Horak, R. L., 1985, Tectonic and hydrocarbon maturation history in the Permian Basin: Oil & gas journal, v. 83, no. 21, p. 124-129.

Horton, B. K., and P. G. DeCelles, 1997, The modern foreland basin system adjacent to the Central Andes: Geology, v. 25, no. 10, p. 895-898, doi: 10.1130/0091-7613(1997)025<0895:TMFBSA>2.3.CO;2.

Jackson, W. E., 1964, Depositional topography and cyclic deposition in west-central Texas: AAPG Bulletin, v. 48, no. 3, p. 317-328, doi: 10.1306/BC743BEF-16BE-11D7-8645000102C1865D.

Janson, X., C. Kerans, J. A. Bellian, and W. Fitchen, 2007, Three-dimensional geological and synthetic seismic model of Early Permian redeposited basinal carbonate deposits, Victorio Canyon, west Texas: AAPG Bulletin 91, no. 10, p. 1405-1436, doi: 10.1306/05210705188.

Jin, Y. G., B. R. Wardlaw, B. F. Glenister, and C. V. Kotlyar, 1997, Permian chronostratigraphic subdivisions: Episodes, v. 20, no. 1, p. 6–10.

Keyte, I. A., W. G. Blanchard, and H. L. Baldwin, 1927, Gaptank-Wolfcamp Problem of the Glass Mountains, Texas: Journal of Paleontology, v. 1, no. 2, p. 175-178.

King, P. B., 1931, Geology of the Glass Mountains, Part I, Descriptive Geology: Univ. Texas Bull. 3038, p. 51-90.

King, P. B., 1937, Geology of the Marathon region, Texas: U.S. Geol. Survey Prof. Paper 187, p. 1-148, doi: 10.3133/pp187.

King, P. B., 1942, Permian of West Texas and southeastern New Mexico: AAPG Bulletin, v. 26, p. 535-763.

King, P. B., 1965, Geology of the Sierra Diablo region, Texas, with special determinative studies of Permian fossils by L.G. Henbest, *et al.*, U.S. Geol. Survey Prof. Paper 215, 183 p.

King, P. B., 1980, Geology of the eastern part of the Marathon basin, Texas: U.S. Geological Survey Professional Paper 1157, 40 p., doi: 10.3133/pp1157.

Koch, J. T., and T. D. Frank, 2011, The Pennsylvanian-Permian Transition in the low-latitude carbonate record and the onset of major Gondwanan glaciation: Paleogeography, Paleoclimatology, Palaeoecology, v. 308, p. 362-372, doi: 10.1016/j.palaeo.2011.05.041.

Kvale, E. P., C. M. Bowie, C. Flenthrope, C. Mace, J. M. Parrish, B. Price, S. Anderson, and W. A. DiMichele, 2020, Facies variability within a mixed carbonate–siliciclastic sea-floor fan (upper Wolfcamp Formation, Permian, Delaware Basin, New Mexico). AAPG Bulletin, v. 104, no. 3, p. 525-563, doi: 10.1306/06121917225.

Lee, W. T., and G. H. Girty, 1909, The Manzano Group of the Rio Grande Valley, New Mexico. Washington: Government Printing Office, doi: 10.3133/b389.

Loucks, R. G., A. A. Brown, C. W. Achauer, and D. A. Budd, 1985, Carbonate gravity-flow sedimentation on low-angle slopes off the Wolfcampian northwest shelf of the Delaware Basin, *in* P. D. Crevello and P. M. Harris, eds., Deep-water carbonates; buildups, turbidites, debris-flows and chalks; a core workshop: SEPM, v. 6, p. 56–92, doi: 10.2110/cor.85.06.0056.

Lucas, S. G., A. B. Heckert, J. W. Estep, and C. W. Cook, 1998, Stratigraphy of the Lower Permian Hueco Group in the Robledo Mountains, Doña Ana County, New Mexico. New Mexico Museum of Natural History and Science Bulletin, v. 12, p. 43-54.

Lucas, S. G., 2013, Reconsideration of the base of the Permian System: New Mexico Museum of Natural History and Science Bulletin 60, p. 230-232.

Lucas, S. G., K. Krainer, S. Voigt, D. S. Berman, and A. Henrici, 2014, The Lower Permian Abo Formation in the northern Sacramento Mountains, southern New Mexico: New Mexico Geological Society, Guidebook, v. 65, p. 287-302.

Lucas, S. G., and S. Z. Shen, 2018, The Permian chronostratigraphic scale: history, status and prospectus. Geological Society, London, Special Publications, v. 450, no. 1, p. 21-50, doi: 10.1144/SP450.3.

Luterbacher, H. P., H. Eichenseer, C. Betzler, and A. M. Van Den Hurk, 1991, Carbonate-Siliciclastic Depositional Systems in the Paleogene of the South Pyrenean Foreland Basin: A Sequence-Stratigraphic Approach: Sedimentation, Tectonics and Eustasy: *in* Sea-Level Changes at Active Margins, p. 391-407, doi: 10.1002/9781444303896.ch21.

Markello, J. R., R. B. Koepnick, L. E. Waite, and J. F. Collins, 2008, The Carbonate Analogs Through Time (CATT) hypothesis and the global atlas of carbonate fields – a systematic and predictive look at the Phanerozoic carbonate systems, *in* J. Lukasik and J. A. Simo, eds., Controls on Carbonate Platform and Reef Development, SEPM Spec. Publ., 89, p. 15–54. SEPM, Tulsa, OK, doi: 10.2110/pec.08.89.0015.

McGowen, J. H., 1971, Gum Hollow fan delta, Nueces Bay, Texas: University of Texas at Austin, Bureau of Economic Geology, Report of Investigations no. 69, 91 p., doi: 10.23867/RI0069D.

McKee, E. D., and S. S. Oriel, 1967, Paleotectonic investigations of the Permian System in the United States: U.S. Geol. Survey Prof. Paper 515, 271 p., doi: 10.3133/pp515.

Mitchum, R. M. Jr., P. R. Vail, and S. Thompson, III, 1977, Seismic stratigraphy and global changes of sea-level, part 2: the depositional sequence as a basic unit for stratigraphic analysis, *in* C. E. Payton, ed., Seismic Stratigraphy – Applications to Hydrocarbon Exploration. American Association of Petroleum Geologists Memoir 26, p. 53–62, doi: 10.1306/M26490C8.

Montañez, I. P., N. J. Tabor, D. Niemeier, W. A. DiMichele, T. D. Frank, C. R. Fielding, J. L. Isbell, L. P. Birgenheier, and M. C. Rygel, 2007, CO2-forced climate and vegetation instability during Late Paleozoic deglaciation: Science, v. 315, no. 5808, p. 87-91, doi: 10.1126/science.1134207.

Montañez, I. P., and C. J. Poulsen, 2013, The Late Paleozoic ice age: an evolving paradigm: Annual Review of Earth and Planetary Sciences, v. 41, p. 629-656, doi: 10.1146/annurev.earth.031208.100118.

Montañez, I. P., J. C. McElwain, C. J. Poulsen, J. D. White, W. A. DiMichele, J. P. Wilson, G. Griggs, and M. T. Hren, 2016, Climate, *p*CO 2 and terrestrial carbon cycle linkages during late Palaeozoic glacial–interglacial cycles: Nature Geoscience, v. 9, no. 11, p. 824-828, doi: 10.1038/ngeo2822.

Mulder, T., J. P. Syvitski, S. Migeon, J. C. Faugeres, and B. Savoye, 2003, Marine hyperpycnal flows: initiation, behavior and related deposits. A review: Marine and Petroleum Geology, v. 20, no. 6-8, p. 861-882, doi: 10.1016/j.marpetgeo.2003.01.003.

Murchison, R. I., 1841, LXII. First sketch of some of the principal results of a second geological survey of Russia: To the editor of the Philosophical Magazine: The London, Edinburgh, and Dublin Philosophical Magazine and Journal of Science, v. 19, no. 126, p. 417-422, doi: 10.1080/14786444108650460.

McKee, E. D., and S. S. Oriel, 1967, Paleotectonic investigations of the Permian System in the United States, No. 515. US Government Printing Office, doi: 10.3133/pp515.

Nelson, W. J.; R. W. Hook, and S. Elrick, 2013, Subsurface Nomenclature in the Permian Basin (Texas – New Mexico): Lithostratigraphic Chaos or Fixable Problem?: The Carboniferous-Permian Transition Bulletin, v. 60, p. 312.

Nemec, W., and R. J. Steel, 1988, What is a fan-delta and how do we recognize it?, *in* "Fan-Deltas: Sedimentology and Tectonic Settings", p. 3-13.

Playton, T. E., and C. Kerans, 2002, Slope and toe-of-slope deposits shed from a late Wolfcampian tectonically active carbonate ramp margin: Gulf Coast Association of Geological Societies, Transactions, v. 52, p. 811-820.

Playton, T. E., X. Janson, C. Kerans, N. P. James, and R. W. Dalrymple, 2010, Carbonate slopes, *in* Facies models 4, p. 449-476.

Plink-Björklund, P., and R. J. Steel, 2004, Initiation of turbidity currents: outcrop evidence for Eocene hyperpycnal flow turbidites: Sedimentary Geology, v. 165, no. 1-2, p. 29-52, doi: 10.1016/j.sedgeo.2003.10.013.

Poole, F. G., W. J. Perry, R. J. Madrid, and R. Amaya-Martínez, 2005, Tectonic synthesis of the Ouachita-Marathon-Sonora orogenic margin of southern Laurentia: Stratigraphic and structural implications for timing of deformational events and plate-tectonic model: Geological Society of America Special Papers, v. 393, p. 543-596, doi: 10.1130/0-8137-2393-0.543.

Pope, M., and J. F. Read, 1997, High-resolution surface and subsurface sequence stratigraphy of late Middle to Late Ordovician (late Mohawkian–Cincinnatian) foreland basin rocks, Kentucky and Virginia: AAPG Bulletin, v. 81, no. 11, p. 1866-1893, doi: 10.1306/3B05C654-172A-11D7-8645000102C1865D.

Posamentier, H. W., and P. R. Vail, 1988, Eustatic controls on clastic deposition II, *in* C. K. Wilgus, H. W. Posamentier, C. K. Ross, and C. G. St. C. Kendall, eds., Sea-level Changes: An integrated approach: Society of Economic Paleontologists and Mineralogists Special Publication 42, p. 125– 154, doi: 10.2110/pec.88.0125.

Pray, L. C., and J. l. Wray, 1963, Porous algal facies (Pennsylvanian), Honaker trail, San Juan Canyon, Utah, *in* R. O. Bass, ed., Shelf Carbonates of the Paradox Basin: Four Corners Geological Society, Fourth Field Conference Guidebook, p. 204–234.

Purser, B. H., 1973, Sedimentation around bathymetric highs in the southern Persian Gulf, in Purser, B.H., ed., The Persian Gulf – Holocene Carbonate Sedimentation and Diagenesis in a Shallow Water Epicontinental Sea: New York, Springer-Verlag, p. 1-9, doi: 10.4319/lo.1974.19.2.0376.

Read, J. F., 1985, Carbonate platform facies models: AAPG bulletin, v. 69, no. 1, p.1-21, doi: 10.1306/AD461B79-16F7-11D7-8645000102C1865D.

Read, J. F., 1998, Phanerozoic carbonate ramps from greenhouse, transitional and ice-house worlds: clues from field and modelling studies: Geological Society, London, Special Publications 149, no. 1, p. 107-135, doi: 10.1144/GSL.SP.1999.149.01.07.

Reijmer, J. J., P. Palmieri, R. Groen, and M. Floquet, 2015, Calciturbidites and calcidebrites: Sea-level variations or tectonic processes?: Sedimentary Geology, v. 317, p. 53-70, doi: 10.1016/j.sedgeo.2014.10.013.

Richardson, G. B., 1904, Report of a reconnaissance in Trans-Pecos Texas north of the Texas and Pacific Railway: University of Texas, Mineral Survey, Bulletin 9, 119 p.

Robertson, A. H. F., S. Eaton, E. J. Follows, and J. E. McCallum, 1991, The role of local tectonics versus global sea-level change in the Neogene evolution of the Cyprus active margin, *in* Sedimentation, tectonics and Eustasy: Sea-level Changes at Active Margins, p. 331-369.

Ross, C. A., 1959, The Wolfcamp series (Permian) and new species of fusulinids, Glass Mountains, Texas: Journal of the Washington Academy of Sciences, v. 49, no. 9, p. 299-316.

Ross, C. A., 1963, Standard Wolfcampian Series (Permian), Glass Mountains, Texas: Geol. Soc. America Mem. 88, 205 p, doi: 10.1130/MEM88-p1.

Ross, C. A., 1986, Paleozoic evolution of southern margin of Permian basin: Geological Society of America Bulletin, v. 97, no. 5, p. 536-554, doi: 10.1130/0016-7606(1986)97<536:PEOSMO>2.0.CO;2.

Ross, C. A., D. Cromwell, and L. Mazzullo, 1987, Leonardian Series (Permian), Glass Mountains, West Texas, The Leonardian Facies *in* West Texas and Southeast New Mexico and Guidebook to the Glass Mountains, West Texas: Midland, Society of Economic Paleontologists and Mineralogists Permian Basin Section, p. 25-33.

Ross, C. A., and J. R. P. Ross, 1987, Late Paleozoic sea levels and depositional sequences: Cushman Foundation for Foraminiferal Research, p. 137.

Ross, C. A., and J. R. P. Ross, 1988, Late Paleozoic transgressive-regressive deposition, *in* Wilgus, C.K., Hastings, B.S., Kendall, C.G.S.C., Poamentier, H.W., Ross, C.A., Van Wagoner, J.C. (Eds.), Sea-Level Changes – an Integrated Approach, SEPM Special Publication v. 42, p. 227-247, doi: 10.2110/pec.88.01.0227.

Ross, C. A., and J. R. P. Ross, 1994, The need for a Bursumian stage, uppermost Carboniferous, North America: Permophiles, no. 24, p. 3-6.

Ross, C. A., and J. R. P. Ross, 1997, Nealian and Lenoxian (Wolfcampian, Lower Permian) Depositional Sequences, Fusulinid Facies and Biostratigraphy, Glass Mountains, Texas: Cushman Foundation for Foraminiferal Research, p. 125.

Ross, C. A., and J. R. P. Ross, 2003, Sequence evolution and sequence extinction: Fusulinid biostratigraphy and species level recognition of depositional sequence, Lower Permian, Glass Mountains, west Texas, U.S.A., *in* H.C. Olson and R. M. Leckie, eds., Micropaleontologic proxies for sea level change and stratigraphic discontinuities: Society for Sedimentary Geology Special Publication 75, p. 317–359.

Ross, J. P. R., and C. A. Ross, 1990, Late Palaeozoic bryozoan biogeography: Geological Society, London, Memoirs, v. 12, no. 1, p. 353-362, doi: 10.1144/GSL.MEM.1990.012.01.34.

Royer, D. L., R. A. Berner, I. P. Montañez, N. J. Tabor, and D. J. Beerling, 2004, CO_2 as a primary driver of phanerozoic climate: GSA today, v. 14, no. 3, p. 4-10, doi: 10.1130/1052-5173(2004)014<0004:CAAPDO>2.0.CO:2.

Rygel, M. C., C. R. Fielding, T. D. Frank, and L. P. Birgenheier, 2008, The magnitude of Late Paleozoic glacioeustatic fluctuations: a synthesis: Journal of Sedimentary Research, v. 78, no. 8, p. 500-511, doi: 10.2110/jsr.2008.058.

Saller, A. H., J. W. Barton, and R. E. Barton, 1989, Slope sedimentation associated with a vertically building shelf, Bone Spring Formation, Mescalero Escarpe Field, south-eastern New Mexico, *in* P. G. Crevello, J. J. Wilson, J. F. Sarg, J. F. Read, eds., Carbonate Platform and Basin Development. Soc. Econ. Petrol. Min. (Society for Sedimentary Geology) Spec. Publ. 44, p. 233–257, doi: 10.2110/pec.89.44.0275.

Saller, A. H., M. J. Frankforter, and S. A. Boyd, 1993, Depositional setting of lowstand carbonates in the BC (Canyon) field, Howard County, Texas, *in* R.E. Crick, ed., Transactions and Abstracts: AAPG Southwest Section Geological Convention Abstracts, p. 81-89.

Saller, A. H., J. A. D. Dickson, E. T. Rasbury, and T. Ebato, 1999, Effects of long-term accommodation change on short-term cycles, upper Paleozoic platform limestones, west Texas, *in* P. M. Harris, A. H. Saller, and J. A. Simo, eds., Advances in carbonate sequence stratigraphy, application to reservoirs, outcrops and models: Society for Sedimentary Geology (SEPM) Special Publication 63, p. 227–246, doi: 10.2110/pec.99.11.0227.

Saller, A. H., R. Lin, and J. Dunham, 2006, Leaves in turbidite sands: The main source of oil and gas in the deep-water Kutei Basin, Indonesia: AAPG bulletin, v. 90, no. 10, p. 1585-1608, doi: 10.1306/04110605127.

Sarg, J. F., 1989, Middle-Late Permian depositional sequences, Permian basin, west Texas-New Mexico, *in* A. W. Bally, ed., Atlas of seismic stratigraphy: AAPG Studies in Geology 27, v. 3, p. 140-154.

Scotese, C. R., and R. P. Langford, 1995, Pangea and the paleogeography of the Permian, *in* The Permian of Northern Pangea, p. 3-19. Springer, Berlin, Heidelberg.

Silver, B. A., and R. G. Todd, 1969, Permian cyclic strata, northern Midland and Delaware Basins, West Texas and southeastern New Mexico: AAPG Bulletin, v. 53, no. 11, p. 2223-2251, doi: 10.1306/5D25C94D-16C1-11D7-8645000102C1865D.

Sonnenfeld, M. D., and T. A. Cross, 1993, Volumetric partitioning and facies differentiation within Permian upper San Andres Formation of Last Chance Canyon, Guadalupe Mountains, New Mexico, in R. G. Loucks and J. F. Sarg, eds., Carbonate sequence stratigraphy recent developments and applications: AAPG Memoir 57, p. 435–474, doi: 10.1306/M57579C17.

Soreghan, G. S., M. J. Soreghan, C. J. Poulsen, R. A. Young, C. F. Eble, D. E. Sweet, and O. C. Davogustto, 2008, Anomalous cold in the Pangaean tropics: Geology, v. 36, no. 8, p. 659-662, doi: 10.1130/G24822A.1.

Sweet, D. E., and G. S. Soreghan, 2012, Estimating magnitudes of relative sea-level change in a coarse-grained fan delta system: Implications for Pennsylvanian glacioeustasy: Geology, v. 40, no. 11, p. 979-982, doi: 10.1130/G33225.1.

Tabor, N. J., and I. P. Montañez, 2002, Shifts in late Paleozoic atmospheric circulation over western equatorial Pangea: Insights from pedogenic mineral δ18O compositions: Geology, v. 30, no. 12, p. 1127-1130, doi: 10.1130/0091-7613(2002)030<1127:SILPAC>2.0.CO;2.

Tabor, N. J., and I. P. Montañez, 2004, Morphology and distribution of fossil soils in the Permo-Pennsylvanian Wichita and Bowie Groups, north-central Texas, USA:

implications for western equatorial Pangean palaeoclimate during icehouse–greenhouse transition: Sedimentology, v. 51, no. 4, p. 851-884, doi: 10.1111/j.1365-3091.2004.00655.x.

Tabor, N. J., I. P. Montañez, C. R. Scotese, C. J. Poulsen, and G. H. Mack, 2008, Paleosol archives of environmental and climatic history in paleotropical western Pangea during the latest Pennsylvanian through early Permian, *in* C. R. Fielding, T. D. Frank, and J. L. Isbell, eds., Resolving the Late Paleozoic Ice Age in Time and Space: Geological Society of America, Special Publication 441, p. 291– 303, doi: 10.1130/2008.2441(20).

Thompson, M. L., 1954, American Wolfcampian fusulinids: University of Kansas Paleontological Contributions, Protozoa Article 5, 226 p.

Udden, J. A., 1917, Notes on the Geology of the Glass Mountains: Texas University Bulletin, no. 1753, p. 3-59.

Vail, P. R., R. M. Mitchum Jr., and S. Thompson, III, 1977, Seismic stratigraphy and global changes of sea level, part four: global cycles of relative changes of sea level: American Association of Petroleum Geologists Memoir 26, p. 83–98.

Van Wagoner, J. C., R. M. Mitchum, H. W. Posamentier, and P. R. Vail, 1987, An overview of sequence stratigraphy and key definitions, *in* A. W. Bally, ed., Atlas of Seismic Stratigraphy, 1, AAPG Studies in Geology 27, p. 11–14.

Van Wagoner, J. C., H. W. Posamentier, R. M. J. Mitchum, P. R. Vail, J. F. Sarg, Loutit, T.S., and Hardenbol, J., 1988, An overview of the fundamentals of sequence stratigraphy and key definitions, *in* C. K. Wilgus, et al., eds. Sea Level Changes: An Integrated Approach: SEPM, Special Publication 42, p. 39-45, doi: 10.2110/pec.88.01.0039.

Van Siclen, D. C., 1958, Depositional topography—examples and theory: AAPG Bulletin v. 42, no. 8, p. 1897-1913, doi: 10.1306/0BDA5B88-16BD-11D7-8645000102C1865D.

Wahlman, G. P., 1988, Subsurface Wolfcampian (Lower Permian) shelf-margin reefs in the Permian Basin of west Texas and southeastern New Mexico: SEPM Midcontinent Section, Special Publication, 1, p.177-204.

Wahlman, G. P., D. R. Tasker, K. Verwer, T. E. Playton, and P. M. Harris, 2013, Lower Permian (Wolfcampian) carbonate shelf-margin and slope facies, Central Basin platform and Hueco Mountains, Permian Basin, west Texas, USA. Deposits, architecture and controls of carbonate margin, slope, and basinal settings: SEPM Special Publication, 105, doi: 10.2110/sepmsp.105.09.

Wardlaw, B. R., and V. I. Davydov, 2000. Preliminary Placement of the International Lower Permian Working Standard to the Glass Mountains, Texas: Permophiles, v. 36, p. 11-14.

Wardlaw, B. R., and M. K. Nestell, 2019, Conodont biostratigraphy of Lower Permian (Wolfcampian-Leonardian) stratotype sections of the Glass and Del Norte Mountains, West Texas, USA, *in* S. C. Ruppel,, ed., Anatomy of a Paleozoic Basin: the Permian Basin, USA (vol. 1, ch. 8): The University of Texas at Austin, Bureau of Economic Geology Report of Investigations 285; AAPG Memoir 118, p. 229-249.

Wilde, G. L., 1975, Fusulinid-defined Permian stages: West Texas Geological Society and Permian Basin Section, Society of Economic Paleontologists and Mineralogists Publication, v. 75, no. 65, p. 67-83.

Wilde, G. L., 1990a, Practical fusulinid zonation: the species concept; with Permian Basin emphasis: West Texas Geological Society Bulletin, v. 29, no. 7, p. 5-34.

Wilde, G. L., 1990b, Stratigraphy and Structure, Gap Tank Area, Southwestern Pecos County, Texas, *in* T. M. Laroche., and L. Higgins, eds., Marathon Thrust Belt, Structure, Stratigraphy and Hydrocarbon Potential: West Texas Geological Society and SEPM, Permian Basin Section, Field Seminar, p. 127-141.

Wilde, G. L., 2002, The Newwellian Substage; rejection of the Bursumian Stage: Permophiles, no. 41.

Wilde, G. L., 2006, The Newwellian Substage: Rejection of the Bursumian Stage: Permophiles, no. 41, p. 53-62.

Wilson, J. L., 1967, Cyclic and reciprocal sedimentation in Virgilian strata of southern New Mexico: Geological Society of America Bulletin, v. 78, no. 7, p. 805–818, doi: 10.1130/0016-7606(1967)78[805:CARSIV]2.0.CO;2.

Wuellner, D. E., L. R. Lehtonen, and W. C. James, 1986, Sedimentary-tectonic development of the Marathon and Val Verde basins, West Texas, USA: a Permo-Carboniferous migrating foredeep: Foreland Basins 8, p. 347-368, doi: 10.1002/9781444303810.ch19.

Yang, K, and S. L. Dorobek, 1995, The Permian Basin of west Texas and New Mexico: Tectonic history of a “composite” foreland basin and its effects on stratigraphic development, *in* S. L. Dorobek and G. M. Ross, eds., Stratigraphic evolution of foreland basins: SEPM (Society for Sedimentary Geology) Special Publication No. 52, p. 149-174, doi: 10.2110/pec.95.52.0149.

Zeller, M., S. B. Reid, G. P. Eberli, R. J. Weger, and J. L. Massaferro, 2015, Sequence architecture and heterogeneities of a field–Scale Vaca Muerta analog (Neuquén Basin, Argentina)–From outcrop to synthetic seismic: Marine and Petroleum Geology v. 66, p. 829-847, doi: 10.1016/j.marpetgeo.2015.07.021.

CHAPTER IV CORRELATING THE WOLFCAMP GROUP STRATA ACROSS THE SUBSURFACE OF THE SOUTHERN PERMIAN BASIN AND INTO THE GLASS MOUNTAINS OUTCROPS, WEST TEXAS

Abstract

The term “Wolfcamp” is used across the Greater Permian Basin, but its internal lithostratigraphic units (Wolfcamp A, B, C and D), as well as its boundaries, vary across the region among and within companies, academia, and government agencies. To provide the first regionally consistent chronostratigraphic framework across the Greater Permian Basin, several regionally correlative sequence stratigraphic surfaces were identified in core, correlated regionally, and tied into the classic Glass Mountains outcrops, where both the Wolfcamp and Leonard Groups were originally defined.

The base of the Wolfcamp Group is defined inconsistently in the literature, but this study identifies a sequence boundary (W01sb) at the base of the Wolfcamp Group in outcrop and in the subsurface. In outcrop, the W01sb is placed at the base of the conglomerate within the Gray Limestone Unit. The base of the Leonard Group (Ln01sb) in this study is placed at the base of the Bone Spring Formation in Delaware Basin, the base of the Dean Formation in Midland Basin, and at the base of the Sullivan Peak Member of the Skinner Ranch Formation in outcrop. This new regional chronostratigraphic framework allows correlations that indicate significant thickening and thinning of the Lowermost Wolfcamp Group, which is related to accommodation and sediment supply associated with Ouachita-Marathon thrusting. Additionally, the top

of the Wolfcamp Group is documented in a structural map using subsurface and outcrop control points, and it indicates a steep depositional profile (20° slope) adjacent to the Southern Shelf in Delaware Basin. This slope is likely steepened as a result of its proximity to the Marathon-Ouachita thrust front.

Introduction

Historically, the Early Permian Wolfcamp Group (Figure IV-1) was studied in limestone-rich, relatively proximal Glass Mountains outcrops (e.g., Udden, 1917; King, 1931; Ross, 1963), and separately in the more mudstone-rich basinal subsurface (e.g., Hall, 1956; Jackson, 1964; Wilshire et al., 1972, Hills, 1984). Although the earliest workers did use limited well data, primarily cuttings, available near the Glass Mountains outcrops (e.g., King, 1931) to aid in the determination of gross lithologies and as a source of fusulinids, they lacked the tools to correlate individual stratigraphic surfaces into the subsurface. Later attempts to connect the Glass Mountains Lower Permian outcrops with the subsurface were limited to the use of sparse fusulinid data which is susceptible to reworking (King, 1980; Bloom, 1988). More well logs were used to correlate the outcrop strata to the subsurface, but focused on the imbricate thrust sheets in southwestern and central Pecos County, very close to the Glass Mountains (Wilde, 1990). Modern handheld gamma-ray spectroscopy data from the Glass Mountains outcrops, in conjunction with recent subsurface data (cores and wireline logs) in southern Delaware and Midland Basins, present a unique opportunity to correlate the Wolfcamp Group from an extremely proximal thrust-front, limestone-rich setting into

the comparatively deep Delaware and Val Verde Basin subsurface for integration into a regional framework.

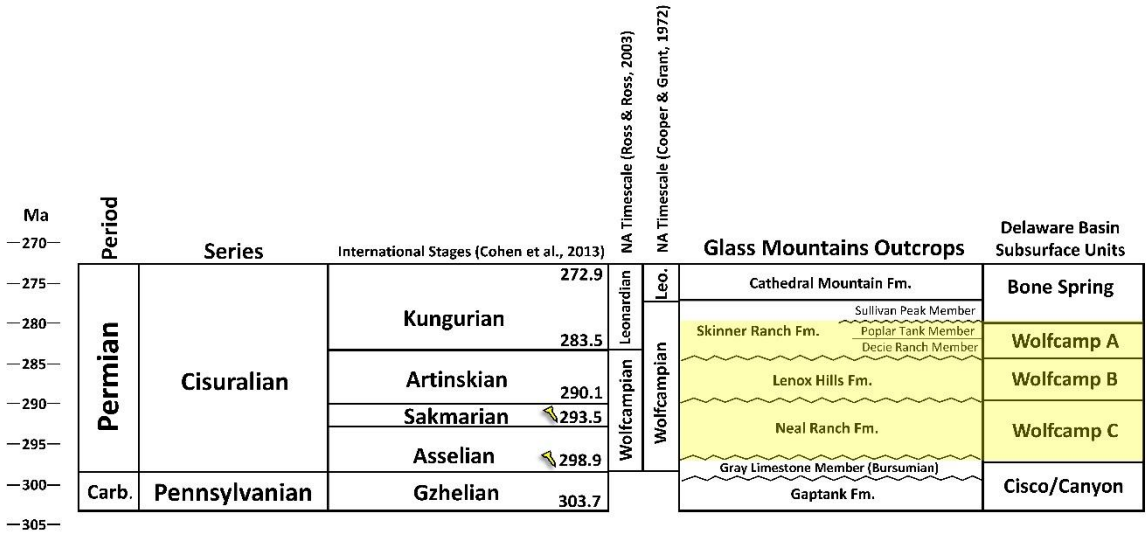

Figure IV-1 Stratigraphic chart for the Lower Permian Wolfcamp Group in outcrop, with international stages, as well as Delaware Basin subsurface divisions. International stage ages from (Cohen et al., 2013; Lucas and Shen, 2018), note that the base of the Asselian and Sakmarian have defined GSSPs. Historically proposed North American Stages shown (Cooper and Grant, 1972; Ross and Ross, 2003). Note that this paper defers to International Stages (Cohen et al., 2013) and does not refer to Wolfcampian as a stage or series.

The physiography of the Early Permian varied considerably across the greater Permian Basin (Figure IV-2), wherein the Eastern Shelf of Midland Basin was especially well studied (Hills, 1942; Rall and Rall, 1958; Van Siclen, 1958; Jackson, 1964; Brown, 1990; Holterhoff, 2010; Sinclair, 2017). This is because of both the abundance of extremely spatially (laterally) dense well data and the low relief (100's of feet) nature of the Eastern Shelf. Early workers, using only this dense well data (Rall and Rall, 1958; Van Siclen, 1958), recognized chronostratigraphic surfaces in the Upper Pennsylvanian and Lower Permian strata separating individual clinoforms prior to the advent of modern

seismic stratigraphy. They recognized that in-situ, proximal carbonate factories or reefs grade into siliciclastic-rich basinal deposits and this led to the development of the "reciprocal sedimentation model" (Van Siclen, 1958; Wilson, 1967). Importantly, clastic deposits in the basin need not be siliciclastic-rich and can instead be comprised of carbonate sediments (Hobson et al., 1985; Reijmer et al., 2012; Kvale et al., 2020), especially in the form of carbonate debrites. Carbonate turbidites, debrites, and hybrid-event beds commonly occur in the basinal Wolfcamp, although their exact relationship with eustasy as a control is not fully understood (Hobson et al., 1985; Kvale et al., 2020).

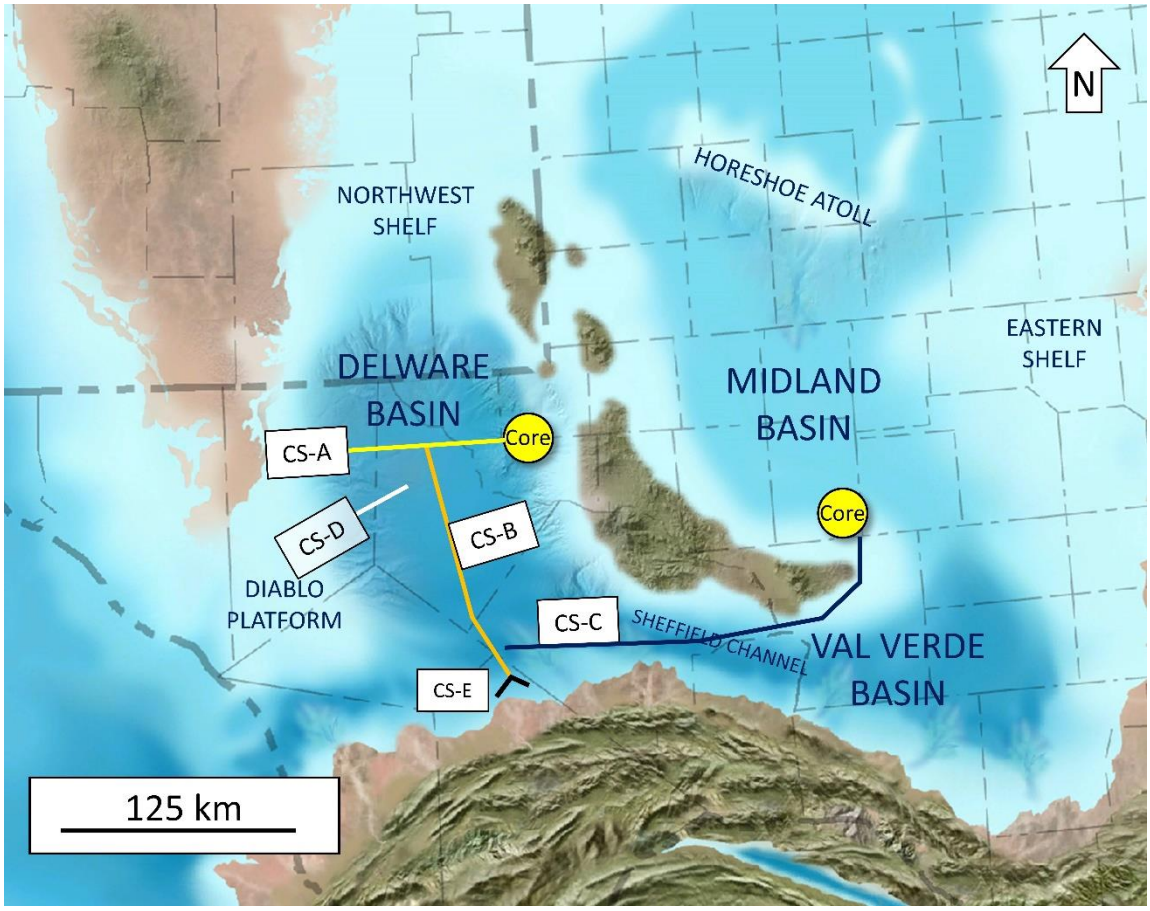

Figure IV-2 Map of the Permian Basin at 295 Ma (Blakey, 2019). Cross sections tie to cores in Delaware and Midland Basins (Cross Sections A and C), with the Glass Mountains outcrops (Cross Section E).

Compared to the Eastern Shelf of Midland Basin, the southernmost Delaware and Val Verde Basins were far less studied, and are much more structurally complex due to their proximity to the Ouachita-Marathon thrust belt (Hall, 1956; King, 1980; Ewing, 1985; Ross, 1986; Wuellner et al., 1986; Yang and Dorobek, 1995; Hamlin, 2009). Furthermore, most classic correlations between Delaware and Midland Basins go across the Central Basin Platform, where strata change facies, as well as lap out, making high-confidence correlations between the Delaware and Midland basins extremely difficult

(Matchus and Jones, 1984) We generated and correlated a regional well-log cross section that was routed through the deeper portions of the Greater Permian Basin through the Delaware, Val Verde and Midland Basins where the Wolfcamp Group could be defined and correlated across the study area. To that end, this study delineates chronostratigraphically-significant surfaces (log markers) interpreted primarily as transgressive and maximum flooding surfaces, from the Glass Mountains into the proximal and distal subsurface. By determining which strata are contemporaneous between Delaware, Val Verde, and Midland Basins, as well as in the type locality outcrops in the Glass Mountains, this study provides a relative chronostratigraphic framework into which absolute age dates (e.g. data from Thermal Ionization Mass Spectrometry, performed on bentonite-derived zircon grains) could be defined and extrapolated across the Greater Permian Basin (e.g., H. Tian, 2020, personal communication). Additionally, potentially unique chemostratigraphic signatures of the various Latest Pennsylvanian and Earliest Permian mudstone intervals, using X-Ray Fluorescence and isotope data derived from outcrop or well samples, might also be used to test and refine this framework (e.g., Gutierrez et al., *in prep*).

Geologic Setting

The Greater Permian Basin formed when, over the course of the Carboniferous and into the Early Permian, the previous Tobosa Basin (passive margin) evolved into a foreland basin and began to tectonically subdivide into distinct sub-regions, especially associated with the uplift of the Central Basin Platform and the extremely pronounced

subsidence of Delaware Basin (Galley, 1958; Adams, 1965; Hills, 1984). The resulting configuration was termed a composite foreland basin (Yang and Dorobek, 1995) with several sub-basins and uplifts. Major physiographic features from west to east include the Diablo Uplift or Platform to the far west, the deep Delaware Basin or Sub-Basin, the Central Basin Platform, the comparatively shallow Midland Basin or Sub-Basin, and the broad, shallowly dipping westward-dipping Eastern Shelf. Other features include the Northwest Shelf north of Delaware Basin, the San Simon Channel connecting the Delaware and Midland Basins north of the Central Basin Platform, the Sheffield Channel connecting the Delaware and Midland Basins south of the Central Basin Platform, and the Hovey Channel connecting the Delaware Basin to open marine waters in the southwest (Hills, 1942; Galley, 1958; Adams, 1965). Finally, the Val Verde Basin or Sub-Basin at the far southern end of Delaware Basin and the Central Basin Platform is a particularly deep region filled with thick syntectonic Pennsylvanian and Permian siliciclastic strata and roughly approximating the foredeep adjacent to the Ouachita-Marathon thrust front (Ross, 1986; Wuellner et al., 1986, Hamlin, 2009).

The Greater Permian Basin was located in western equatorial Pangea after the Carboniferous collision of the Laurasia and Gondwana (Scotese et al., 1979) and the onset of the Permian (coinciding with the start of the Wolfcampian Series) occurred during peak icehouse conditions, wherein extensive glaciation resulted in high-amplitude eustasy (Fielding et al., 2008; Rygel et al., 2008; Isbell et al., 2012, Montañez and Poulsen, 2013; Montañez et al., 2016). This eustatic signal is superimposed on tectonic trends in subsidence associated with the northward directed Ouachita-Marathon thrusting

(Hills, 1984). The intensity of tectonism likely declined over the course of the Wolfcampian (Ross, 1986). The Earliest Permian also coincided with a transition to a more arid climate (Tabor et al., 2008; DiMichele et al., 2010, Tabor, 2013).

Sedimentation patterns also varied greatly across the Greater Permian Basin with multiple siliciclastic sediment sources depositing in different sub-regions at different times through the Permo-Carboniferous (Hamlin, 2009; Liu and Stockli, 2020, Soto-Kerans, 2020). Specifically, the Ouachita-Marathon thrusting resulted in massive subsidence and subsequent thick deposition, exceeding 10,000 feet in places (Hamlin, 2009), in Val Verde Basin immediately northeast of the thrust front, with the axial trough running roughly northwest to south-east from Pecos County to Terrell County (Wuellner et al., 1986). These sandstone-rich basinal deposits are primarily concentrated in the Pennsylvanian and Lower Wolfcampian and were interpreted as synorogenic (Wuellner et al., 1986; Hamlin et al., 1992; Johnson et al., 1998). Later deposits (Leonardian to Guadalupian) have been shown to have significantly lower sediment contributions from southern sources associated with the thrusting south of Delaware Basin (Liu and Stockli, 2020).

Previous Work

The base of the Wolfcampian Series and the Permian Period (Figure IV-1) is contested in outcrop (King, 1931; Ross, 1963, Wardlaw and Davydov, 2000; Lucas, 2013; Sims and Belanger, 2021) and in the subsurface (Jones, 1975; Wilde, 1975; King, 1980). Of particular relevance to this study, the base of the Wolfcamp in the subsurface is picked inconsistently (Figure IV-3). Some workers have included all the strata above

the top of the Middle Pennsylvanian (Desmoinesian) Strawn Formation within the Wolfcamp Group (Sinclair et al., 2017; Barrick and Wahlman, 2019), effectively conceding that the classic Upper Pennsylvanian Cisco and Canyon outcrop equivalents (Adams. 1951) are being grouped with the overlying Wolfcamp Group in the basin. Fusulinid and conodont age control from the strata immediately above the Strawn confirm them as belonging to the Upper Pennsylvanian (Hobson et al., 1985; Barrick and Wahlman, 2019). In this study, we differentiate the Upper Pennsylvanian (Cisco and Canyon equivalents) and trace the overlying base Wolfcamp Group unconformity into the subsurface, thereby excluding these Upper Pennsylvanian strata from the Wolfcamp Group (Figure IV-4). In summary, in this study, Upper Pennsylvanian sediments (overlying the Middle Pennsylvanian Strawn Formation) were excluded the overlying Wolfcamp Group (Figure IV-4).

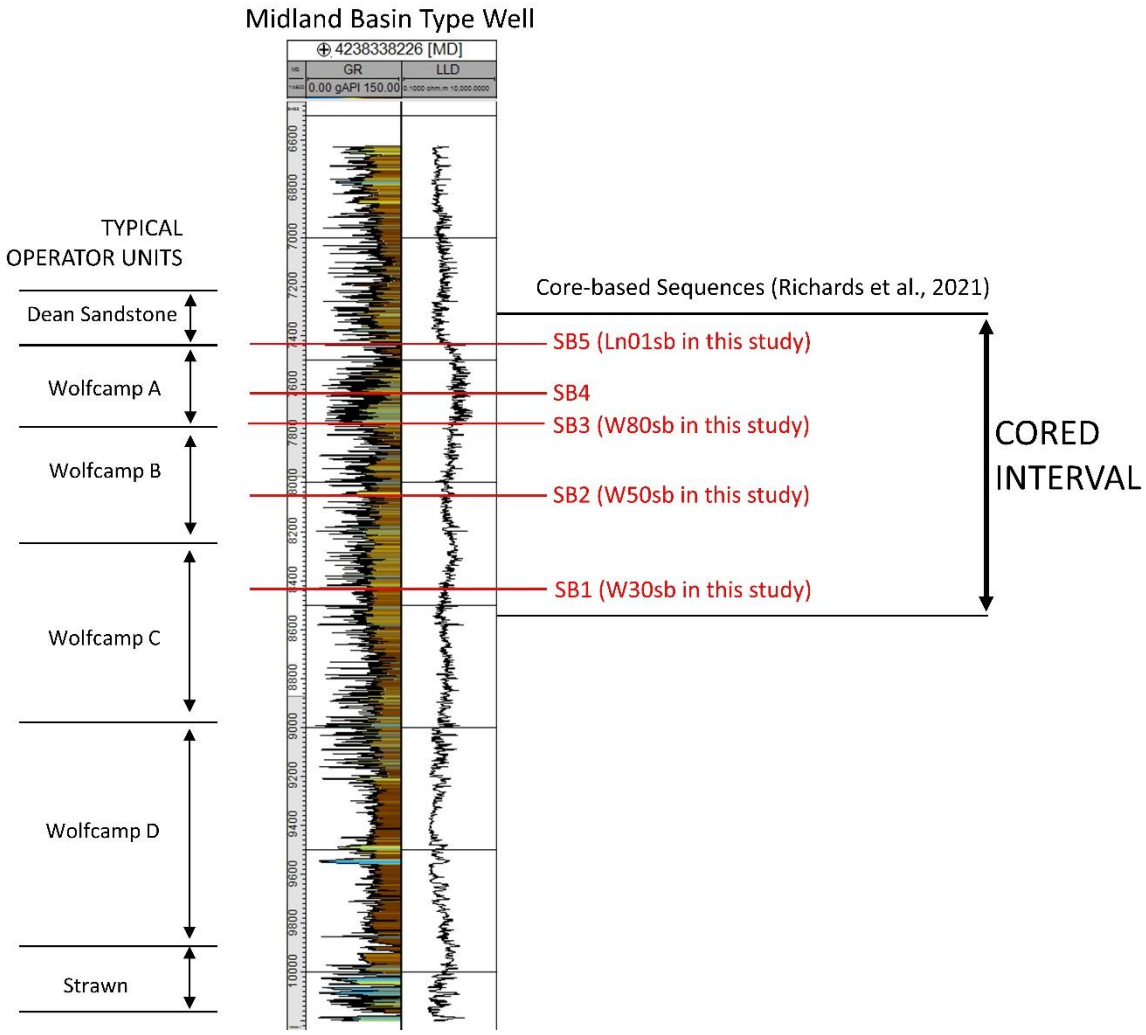

Figure IV-3 Midland Basin type log shown with typical operator picks as well as core-based sequence boundaries from recent study (Richards et al., 2021). Note that the Wolfcamp D is often applied to the Uppermost Pennsylvanian mudstone units, which are Cisco and Canyon equivalent (Sinclair et al., 2017). The Pennsylvanian-Permian boundary therefore likely occurs below cored interval but above Strawn Formation.

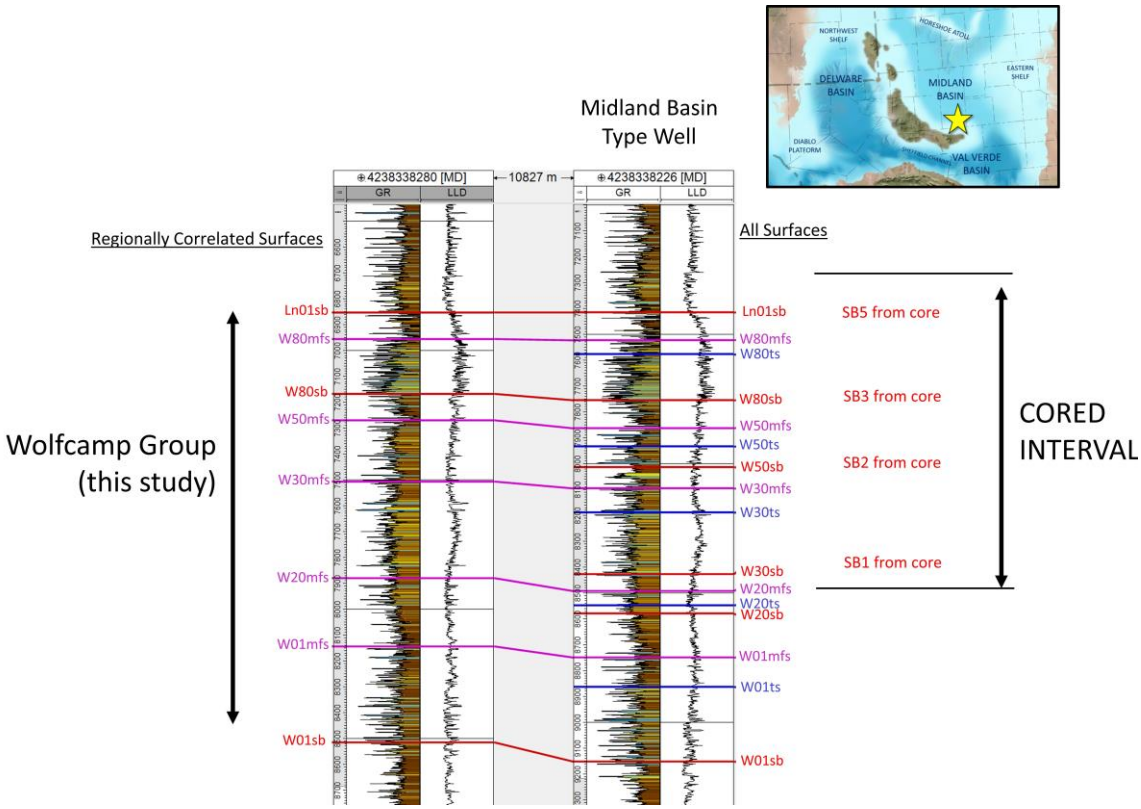

Figure IV-4 The Midland Basin type well (42-383-38226) shown with cored interval and all sixteen surfaces interpreted for the Wolfcamp Group, including several sequence boundaries from recent core work (Richards et al., 2021). Lowermost two sequence boundaries (W01sb, W20sb) correlated on logs, and from outcrops. In the adjacent well (42-383-38280), eight surfaces shown which are correlated regionally, including bounding unconformities (W01sb, Ln01sb), and one internal unconformity (W80sb) which is the most prominent from the studied core. Five maximum flooding surfaces
(W01mfs, W20mfs, W30mfs, W50mfs, W80mfs) also correlated regionally. Type well shown with yellow star in index map.

The top of the Wolfcamp Group also is equally contested in the outcrop (Ross, 1963; Cooper and Grant, 1972), as well as in the subsurface (Mazzullo et al., 1987; Van der Loop, 1990). In this study we place the top of the Wolfcamp Group at an interpreted unconformity at the base of the Sullivan Peak Member of Skinner Ranch Formation in the Glass Mountains. In terms of the subsurface, the base of the Dean Formation in the

Midland Basin, and base of the Third Bone Spring Sandstone in the Delaware Basin were picked as the classic top of the Wolfcamp Group. Recently, however, the top of the Wolfcamp Group was placed stratigraphically lower (Figure IV-3), essentially excluding the economically important Wolfcamp A Zone from the Wolfcamp Group, and terming it the Leonard Shale (Baumgardner et al., 2016). This recent reinterpretation, however, is largely biostratigraphic, focusing on fusulinid and conodont interpretations, and also is related to where the base of the Leonard (top of Wolfcamp) should be placed in the Glass Mountain outcrops. In this study (Figure IV-4), we followed the industry standard sub-surface definition for the top of the Wolfcamp Group (Base Dean/Third Bone Springs), and by doing so place the top of the Wolfcamp Group (base of Leonard) near the Skinner Ranch/Cathedral Mountain contact proposed by Cooper and Grant (1972).

Data and Methodology

This study integrates a variety of subsurface and surficial data. For subsurface data, over 500 wells in the study area have either raster and/or digital data suitable for surface correlation or interpretation. Of these, three (3) were chosen as type logs for the Delaware, Southern Delaware and Midland Basins, for study at regional-scale (Figure IV-5) and for intra-Wolfcamp Group study (Figure IV-6). Forty-seven (47) wells, based on log quality, suite, depth, and location, were used to create 5 well-log cross sections spanning the Greater Permian Basin (Figure IV-2).

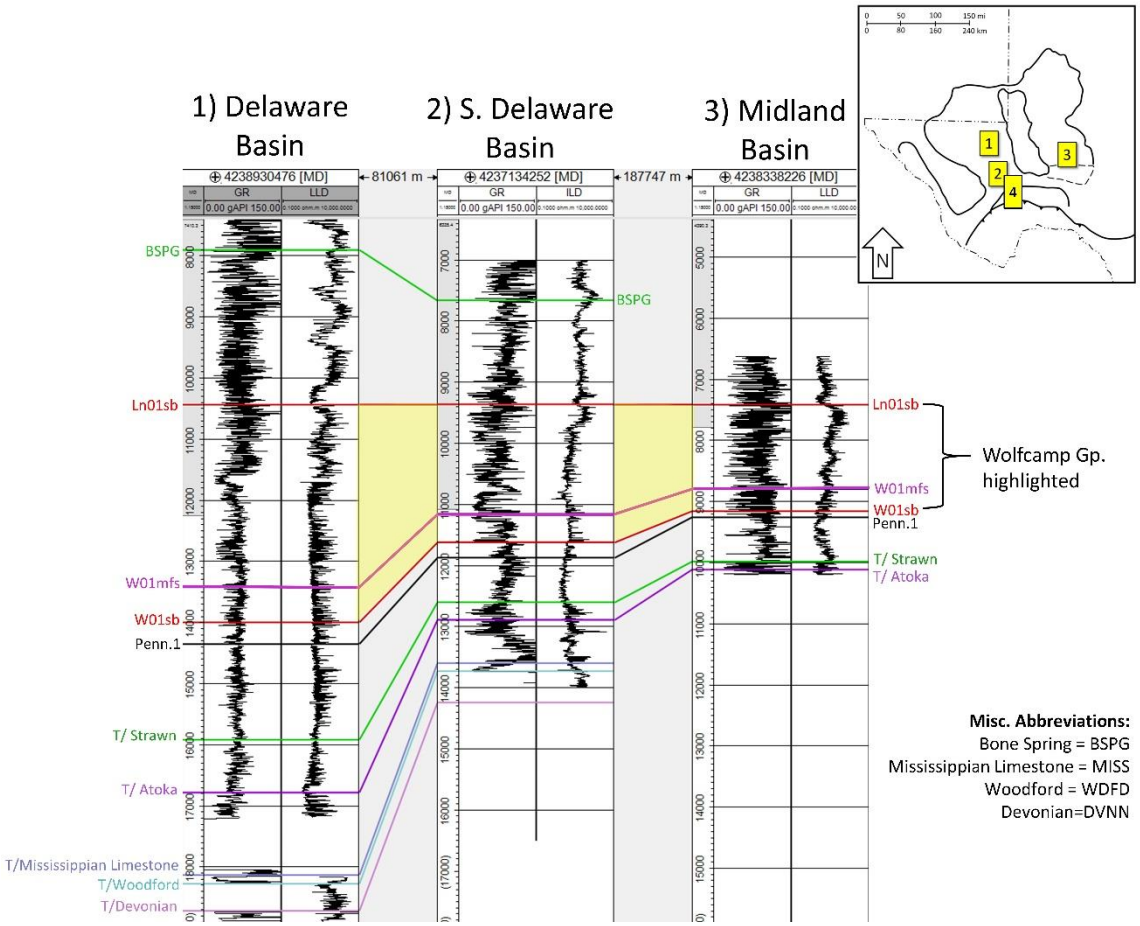

Figure IV-5 Regional-scale type logs for the Wolfcamp Group in central and southern Delaware Basin, as well as Midland Basin. Index map after McKee and Oriel (1967). The base of the Wolfcamp Group often is picked at the lowest maximum flooding surface (W01mfs) but is here picked at an interpreted sequence boundary (W01sb) tied into the Glass Mountains outcrops.

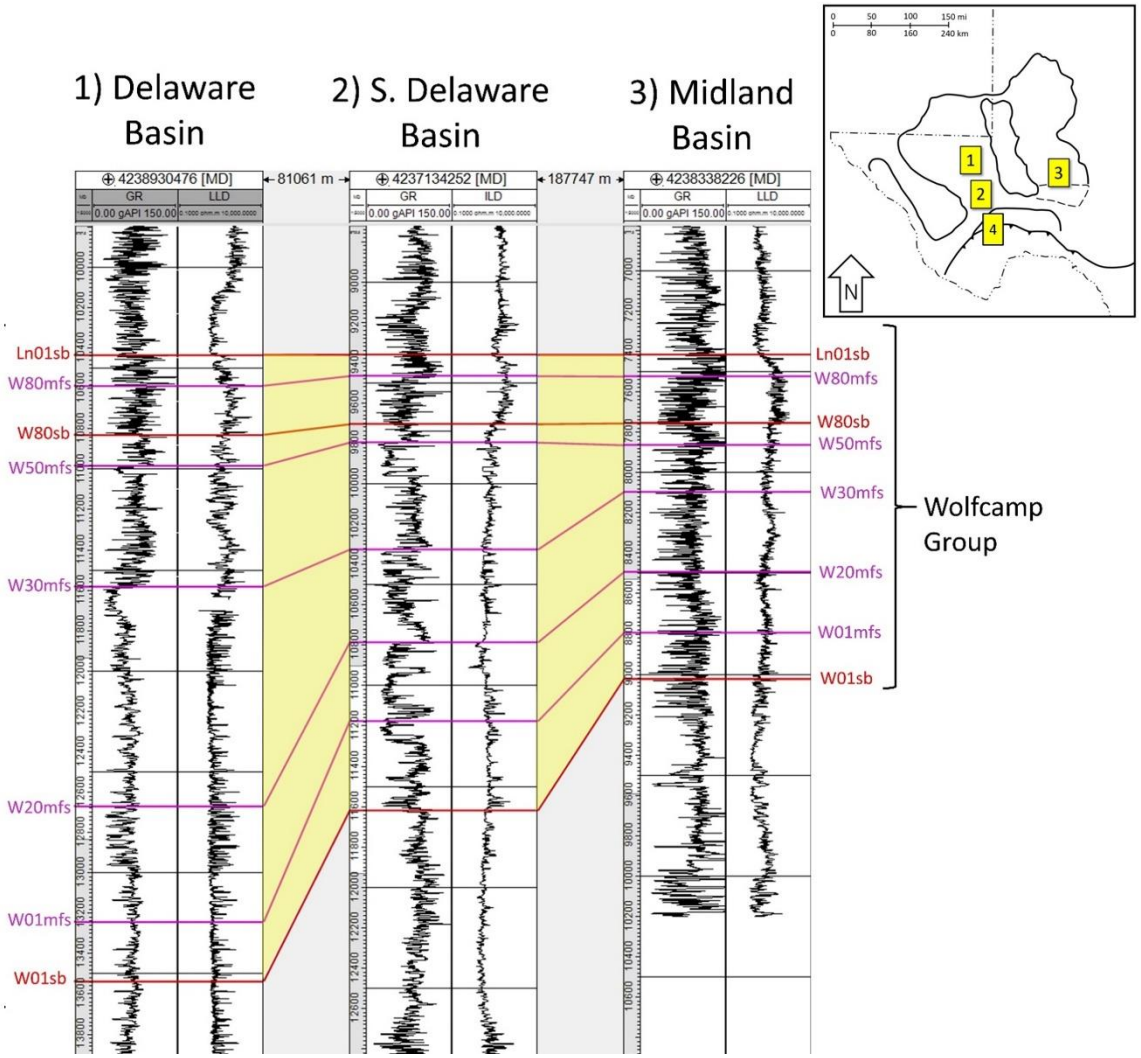

Figure IV-6 Three detailed type logs for the Wolfcamp Group in central and southern Delaware Basin, as well as Midland Basin. Index map after McKee and Oriel (1967).

Surficial data includes four outcrop-derived gamma-ray profiles from measured sections across the Wolfcampian exposures in the western and eastern Glass Mountains (near the Lenox and Wolf Camp Hills, respectively). A composite gamma-ray profile for the Glass Mountains Wolfcamp is assembled (Figure IV-7). These handheld gamma-ray profiles total over 2000 feet of dip-adjusted data and measurements are taken at the bed

scale, approximately every foot. Gamma-ray values were measured with a Radiation Solutions RS-230 BGO Super-SPEC device and the resulting profiles were imported into Schlumberger's Petrel software platform for correlation. These simulated wells are correlated with standard subsurface wireline log data.

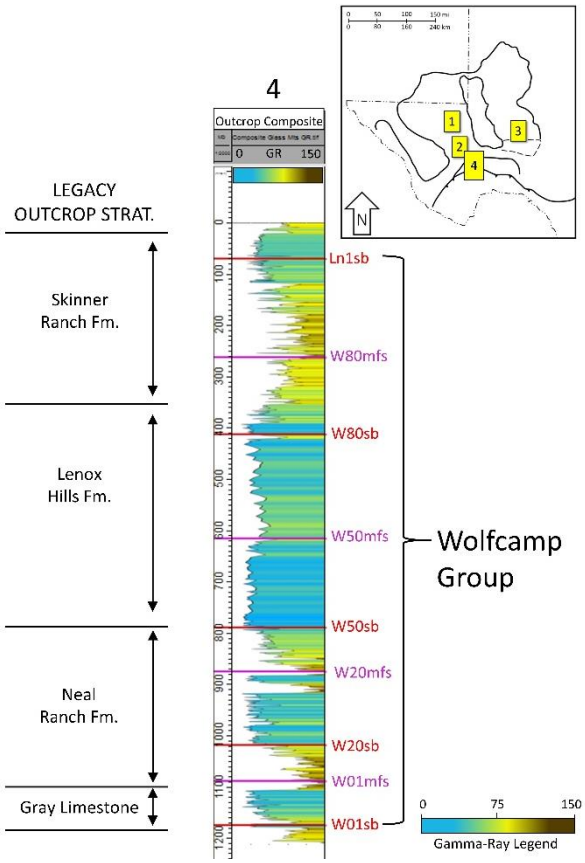

Figure IV-7 Fourth type section is a composite section from the Glass Mountains outcrops. The Skinner Ranch and Lenox Hills portions were measured from Lenox Hills outcrops (Dusak, 2021, *in prep*; Peavey, 2021, *in prep*). The Neal Ranch and Gray Limestone portions were measured in the Wolf Camp Hills (Richards et al., 2021, *in prep*). Index map after McKee and Oriel (1967). GR colored as proxy for lithology where lower values (under 50 API) tend to be limestone beds, 50-100 GR API sections tend to have mixed or silty lithologies, and >100 API intervals are dominated by mudstone beds. Four sequences interpreted for the Wolfcamp Group in outcrop, with one sequence occurring in the Skinner Ranch Formation, one in the Lenox Hills Formation, and two in the Neal Ranch Formation. The fifth sequence, W30, is thought to be eroded under the W50 sequence boundary (W50sb) in proximal outcrop strata.

In terms of the correlation methodology, the first step was to define the base and top of the Wolfcamp Group on the regional-scale across the Southern Delaware Basin (Figure IV-5). This was done by choosing wells which penetrated the entire Permian, as well as underlying Pennsylvanian section, and reach total depth (TD) in the Lower-Middle Paleozoic. Within this succession, the extremely high gamma-ray (>150 API units) Devonian Woodford Formation serves as an important readily recognizable regional marker on both raster and digital logs in the Delaware Basin. After determining the boundaries of the Wolfcamp Group at a regional scale, the Wolfcamp Group's major internal divisions were correlated at a more detailed-scale (Figure IV-6) for correlation into the Glass Mountains outcrops. Some of the informally picked operator-derived surfaces track or parallel maximum flooding surfaces, where gamma-ray peaks often exceed 100 API units (Figure IV-3). The maximum flooding surfaces correlated regionally for this study (Figure IV-3) are interpreted as correlative, as well as chronostratigraphically significant surfaces across the basin (Wilson, 1975; Van Wagoner et al., 1988; Van Wagoner et al., 1990; Bhattacharya, 1993). The top of the Wolfcamp Group in the subsurface was picked at the base of the Dean Sandstone in the Midland Basin and at the 3rd Bone Spring Sandstone in Delaware Basin and is interpreted as representing a sequence boundary at the base of the Leonardian (Richards et al., 2021). The most correlative internal Wolfcamp markers (the W01mfs, W20mfs, W30mfs, W50mfs, W80mfs), can be correlating across the Permian Basin (Figure IV-4). The base of the Wolfcamp Group (Figure IV-5) is interpreted as a sequence boundary,

marked by a sudden upward decrease in gamma-ray values (at least 25 API units) interpreted as a correlative conformity in the basin, representing either a sediment bypass surface or the base of a lowstand wedge (Van Wagoner et al., 1990).

Results

Type Logs and Surfaces Correlated

Regional-Scale Type Logs and Units Correlated

Several major units, formal and informal, were defined in the subsurface, focusing on Permian and Pennsylvanian units (Figure IV-5), while specific stratigraphic surfaces were picked to define the Wolfcamp Group (Figure IV-6). These major units (Figure IV-5) are picked in order to help define the upper and lower bounds of the Wolfcamp Group in the subsurface (the Ln01sb and W01sb surfaces, respectively). The most important units outside of the Wolfcamp Group include the overlying Bone Spring (BSPG) and Dean Sandstone (DEAN), and the underlying Strawn (STRN), Atoka (ATOK), Barnett (BRNT), and Woodford (WDFD) Formations.

Detailed Type Logs and Surfaces Correlated for the Wolfcamp Group

In this study, eight specific stratigraphic surfaces were defined for the Wolfcamp Group (Table 1) in three basinal type logs (Figure IV-6) and in a composite section representing the Glass Mountains outcrops (Figure IV-7). Two sequence boundaries were defined, both at the base and at the top of the Wolfcamp Group (W01sb and Ln01sb, respectively). Additionally, four internal, major maximum flooding surfaces

were defined (from oldest to youngest, W01mfs, W20mfs, W30mfs, W50mfs, W80mfs). In practice, the various markers often serve as the base of the Wolfcamp Group (Jones, 1975) because the lowermost sequence boundary (W01sb) is not as consistent in the basin. The lowermost sequence boundary (W01sb) also was defined in outcrop (Figure IV-7).

The Wolfcamp Group often is defined by operators using a top-down A, B, C, and D nomenclature (Figure IV-3). These informal units vary in their consistency and sometimes follow local transgressive or maximum flooding surfaces, because these markers are reasonably correlative. In particular, the Wolfcamp A and B tend to be picked near reasonably consistent, high gamma-ray intervals (at least 80 API units over at least 100 feet in the basin), though picks occur below, on, and above these intervals (Sinclair et al., 2017). Note that, while some operators utilize the lowermost maximum flooding surface (W01mfs) as the base of the Wolfcamp Group, others have labelled any mudstone interval above the Middle Pennsylvanian (Desmoinesian) Strawn Limestone as belonging to the "Wolfcamp D" (e.g., Sinclair et al., 2017). This paper attempts to delineate the Upper Pennsylvanian in the subsurface as a separate unit and restricts the Wolfcamp Group and its subdivisions to the Lower Permian (Figure IV-1).

Cross Sections

Description of Cross Section A: Culberson County to Winkler County Oasis Core, West to East

Cross section A (Figure IV-8) shows considerable thickening of the Wolfcamp Group into the Delaware Basin axis before thinning again towards the Central Basin Platform. Specifically, the Wolfcamp Group goes from approximately 1,480 feet (450 m) thick in the west, to 3,010 feet (917 m) at its maximum thickness, to 2,200 feet (671 m) to the farthest eastern well penetrating the entire Wolfcamp Group stratigraphy. This cross section also records a relatively consistent signature for the upper portions of the Wolfcamp Group, especially just below the top Wolfcamp (Ln01sb). The upper portions of the Wolfcamp Group contain higher gamma-ray intervals (~90-140 API units) often labelled as Wolfcamp A and B, informally. These intervals are more consistent than the lower portions of the Wolfcamp Group. Deep resistivity values also are significantly higher in the uppermost Wolfcamp Group (10 to 300 ohm-meters) compared with the immediately overlying Bone Spring (5 to 70 ohm-meters). The sequence boundary at the top of the Wolfcamp Group is marked by a consistent inflection at the top of the high-resistivity interval.

Surface Name	Description	Interpretation
Ln01sb	Common top Wolfcamp, aligns with sharp upward drop in GR and resistivity, occurs towards top of Skinner Ranch Formation in outcrop	Sequence boundary, top of Wolfcamp Group
W80mfs	Marked by very high GR values typically exceeding 100 API units for over 100 feet, occurs towards top of informal Wolfcamp A	Maximum Flooding Surface

W80sb	Marked by very sharp drop in GR values (>25 API units) over the "Wolfcamp Shale" marker (Baumgardener et al., 2016), often chosen as Wolfcamp B top, base of Skinner Ranch Formation in outcrop	Sequence Boundary
W50mfs	Typically marked by very high GR values as part of thick (>100 ft) interval similar to that around W80mfs, often picked below (10's of feet) Wolfcamp B top in subsurface and occurs inside the Lenox Hills Formation in outcrop	Maximum Flooding Surface
W30mfs	Thin interval (<50 ft) exceeding 100 GR API units, often occurs in lower portion of Wolfcamp B, does not appear to occur in outcrop	Maximum Flooding Surface
W20mfs	Occurs within thinner interval (often <100 feet) with GR values exceeding 80 API units, lower than in W80 and W50 mfs, occurs in upper half of Neal Ranch Formation in outcrop, sometimes aligns with Wolfcamp D top marker	Maximum Flooding Surface
W01mfs	Typically at least 90 GR API units, base of prominent "funnel" shape, sometimes marked as traditional base of Wolfcamp Group in subsurface, occurs towards base of Neal Ranch Formation in outcrop	Maximum Flooding Surface
W01sb	Marked by sharp upward decrease in GR (>25 API units), marked by higher and more chaotic resistivity above, occurs within Gray Limestone Unit in outcrop, does not align with common subsurface pick from previous work	Sequence boundary, base Wolfcamp Group

Table IV-1 List of 8 key surfaces defining the Wolfcamp Group including bounding unconformities and internal, regionally correlated transgressive surfaces. In cross sections, interpreted sequence boundaries are colored red, interpreted transgressive surfaces are colored blue, and interpreted maximum flooding surfaces are colored purple.

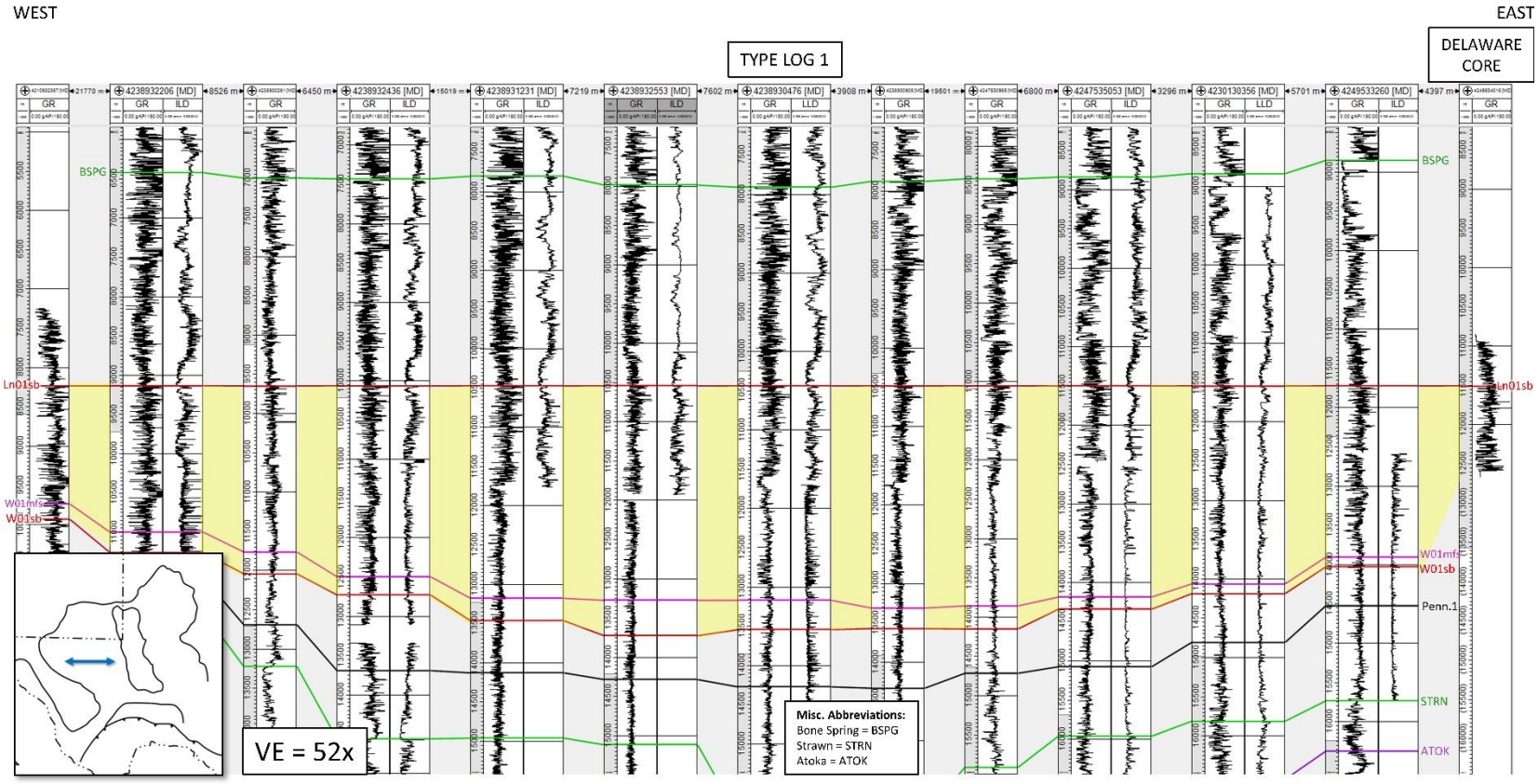

Figure IV-8 Cross Section A goes across central Delaware Basin and displays typical basinal Wolfcamp log signatures. The Wolfcamp Group (bounded by red sequence boundaries W01sb and Ln01sb) thickens in the basin center, though the Pennsylvanian units thicken and thin to a greater degree. The Wolfcamp Group is highlighted between wells. Flattened on top Wolfcamp (Ln01sb).

Interpretation of Cross Section A: Culberson County to Winkler County Oasis Core, West to East

Thickening of the Wolfcamp Group to the east, reaching its maximum value along the basin axis (Figure IV-8), is interpreted as a direct response to basin position and available accommodation space. This reveals asymmetric basin relief wherein the deepest part of Delaware basin occurs towards the east, close to the foot of the Central Basin Platform and the western slope is comparatively shallow. This results aligns with thicknesses and geometries established by previous workers (e.g., Hills, 1984). Variation in lithology is interpreted as a first-order control on the intra-Wolfcamp Group absolute gamma-ray values, in which the beds and bedsets recording over 100 API units are overwhelming dominated by mudstone (of varying mineralogical composition). This was demonstrated by studies of the Wolfcamp Group in Midland Basin (e.g., Richards et al., 2021). Values under 65 API units were interpreted as likely silt- or sandstone beds, or as limestone beds (e.g., Driskill et al., 2018).

Description of Cross Section B: Reeves County Basin Center to Brewster County Glass Mountains, North-South

Beginning in central Delaware Basin, this dip-oriented cross section (Figure IV-9) starts in the approximate basin center and follows the basin axis southward and thinning considerably (from 2,908 to 591 feet, or 886 to 180 meters), while migrating gradually to a structurally higher position. The mid-cross section jump from Collier 52-

14 #1 (42-389-32572) to Dora Robert #1 (42-389-00418) shows more pronounced thinning and change in subsea depth (shallowing) for the total Wolfcamp section (Figure IV-10). That transition occurs across the east-west trending Grisham or Mid-Basin Fault, a prominent normal fault downthrown towards the north (Ewing, 1985; Ewing, 1991; Shumaker, 1992; Yang and Dorobek, 1995). In the far south (Figure IV-10), between the penultimate well, Sibley, Jane #1 (42-043-30231) and the final, southernmost well, Madre Grande #1 (42-043-30266) the Wolfcamp Group thins and shallows dramatically (from 1,337 to 591 feet [408 to 180 m] in thickness, and +1,809 to -2,036 feet [+551 to -621 m] SS TVD, or Sub Sea True Vertical Depth). As picked, the top of the Wolfcamp Group between these wells records a dip of 10.2°. The two previous well-well dips for the top of the Wolfcamp Group record dips of 1.8° and 0.9°, respectively.

The total thickness of the Pennsylvanian thickens dramatically from north to south across Pecos County towards the Ouachita-Marathon thrust front (Figure IV-9). Specifically, the total Pennsylvanian goes from 1,692 feet (516 m) thick (Hayter State 28 #1, 42-371-34252) to 9,010 feet thick (Sibley, Jane #1, 42-043-30231). The Pennsylvanian, as picked, is even thicker in the southernmost, final well where it measures 12,856 feet (3,919 m) thick, although this well contains Pennsylvanian units not present toward the north including the Haymond Formation, and the Dimple Limestone. Other workers have also noticed significant Permo-Carboniferous thickening toward the Ouachita-Marathon Thrust Front (Hamlin, 2009). Conversely, sandstone-rich units in the Upper Wolfcamp (e.g., the informal Wolfcamp X, Y sandstone units) thin and become less prominent across Reeves County (Figure IV-11). It is unclear whether

the sandstone units in the upper Wolfcamp A continue south beyond this point, the gamma-ray profile changes considerably starting with Dora Robert #1 (42-389-00418)

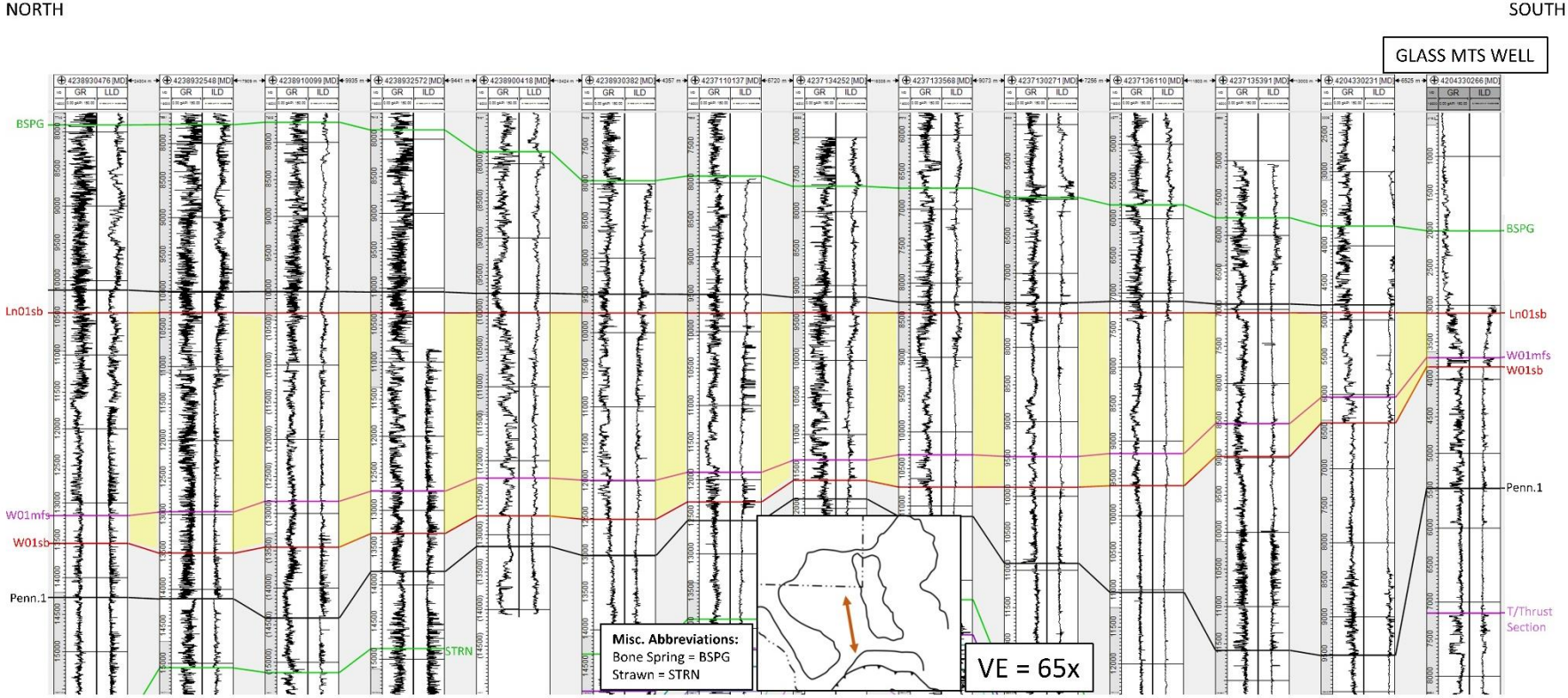

Figure IV-9 Cross Section B (regional scale) goes from central Delaware Basin to the Glass Mountains. Over this distance the Wolfcamp Group thins and shallows considerably whereas Pennsylvanian strata thicken into the Marathon-Ouachita foredeep. The log signature for the top of the Wolfcamp changes considerably towards the south. The Wolfcamp Group is highlighted between wells. Flattened on the top of the Wolfcamp Group (Ln01sb).

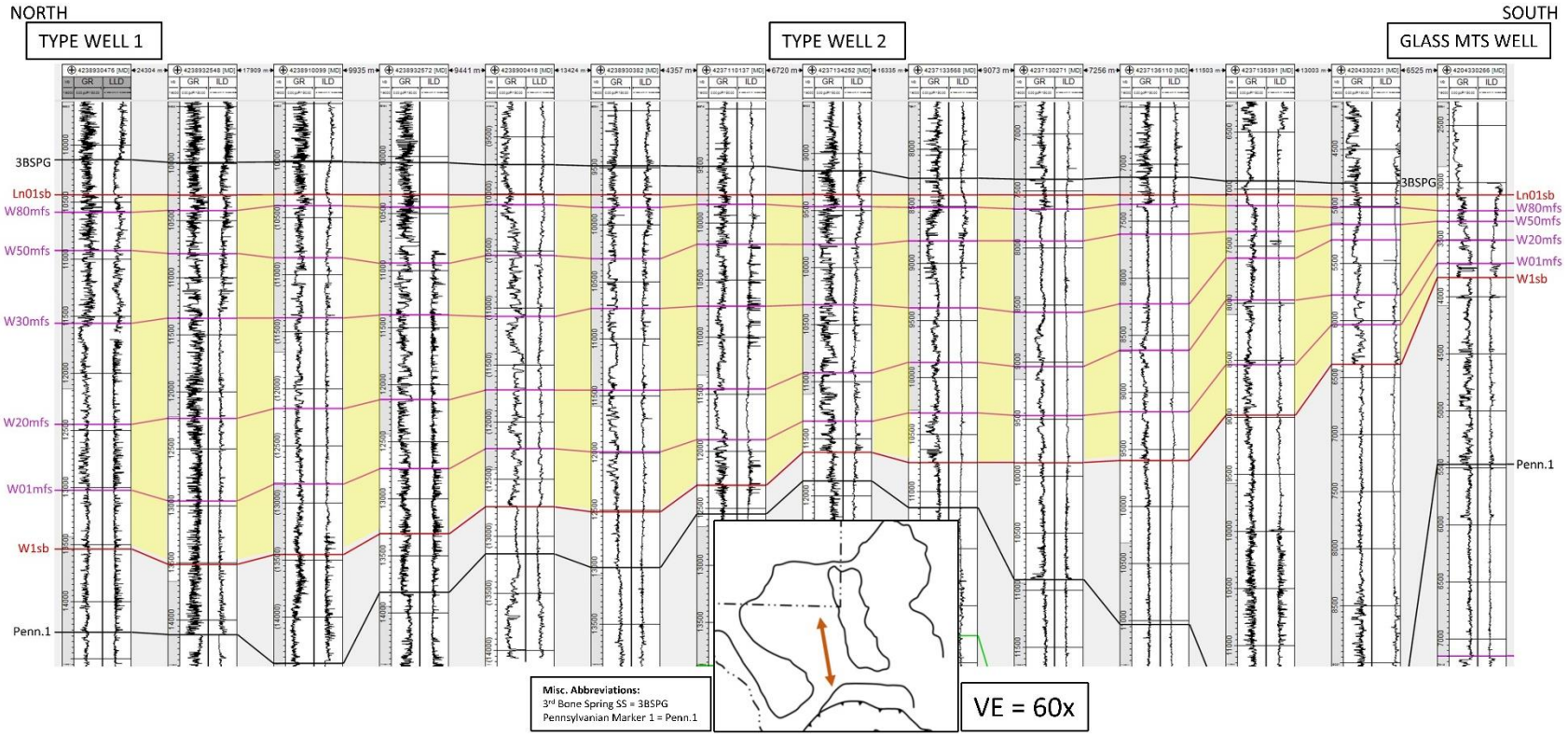

Figure IV-10 Cross Section B (detailed) goes from central Delaware Basin to the Glass Mountains. Over this distance the Wolfcamp Group strata thin and shallow considerably whereas the Pennsylvanian strata thicken into the Marathon-Ouachita foredeep. The log signature for the top of the Wolfcamp changes considerably towards the south. This cross section is flattened on the top of the Wolfcamp (Ln01sb).

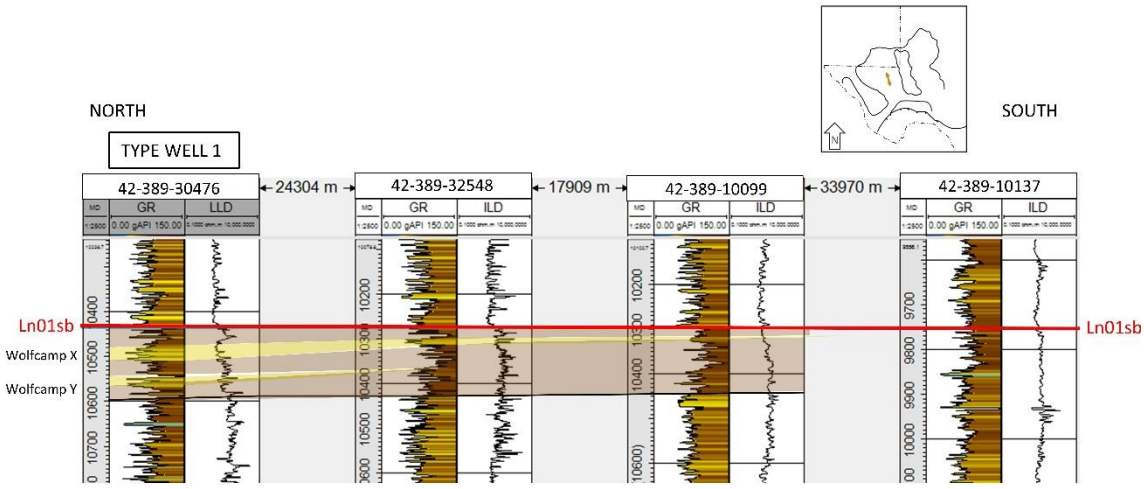

Figure IV-11 Cross Section B (zoomed in, Reeves county only) Wolfcamp XY sandstone intervals thin out towards south in Reeves County. Gamma-ray colored to highlight sandstone intervals in otherwise high gamma-ray upper Wolfcamp A. This cross section is flattened on the top of the Wolfcamp (Ln01sb).

Interpretation of Cross Section B: Reeves County Basin Center to Brewster County Glass Mountains, North-South

The complex pattern of southern thinning and then thickening of the Wolfcamp Group is interpreted as reflecting variable paleobathymetry during the deposition of the Early Permian. Thickening in Pecos County (Figures IV-9, 10) is interpreted as partially isolated from the thickest Wolfcamp stratigraphy north of the Grisham or Mid-Basin Fault (Shumaker, 1992), in the basin center (Ewing, 1991; Shumaker, 1992; Ewing, 2019). The difficulty in correlating the Wolfcamp X/Y sandstone intervals south of this zone (Figure IV-11) is interpreted as potentially indicative of a northern source for these detrital inputs, effectively marking the southern limit of their deposition against the

paleo-high at the Grisham (Mid-Basin) Fault. Conversely, the extreme thickening of the Pennsylvanian strata towards the southernmost end of the cross section (Figure IV-9) is interpreted as reflecting both the extreme subsidence and increased sediment input generated in the foredeep of the Ouachita-Marathon thrusting and orogenesis, as was previously interpreted for Terrell and Crockett Counties to the east (Hamlin, 2009).

Additionally, the pronounced changes in dip at the top of the Wolfcamp Group and at the southern end of the cross section (Figure IV-10) are interpreted as reflecting the paleobathymetry towards the end of Wolfcamp Group deposition, with a distinct, steep relief surface correlated between Sibley Jane #1 (42-043-30231) and Madre Grande #1 (42-043-30266) interpreted as a pronounced slope (10-20°), whereas the shallower dips (< 5°) north of Sibley Jane #1 (42-043-30231) represent the toe of slope and basin floor. This interpretation would preclude the interpretation of a homoclinal ramp (Ahr, 1973) for the Wolfcamp Group, despite the dominance of lower-relief and weakly aggradational algal mound carbonate factories in the Lowermost Permian (Ross, 1986; Mazzullo and Reid, 1989; Sarg, 1989; Candelaria et al., 1992). Finally, at this southernmost position, the overlying Bone Spring formation is much more uniform in gamma-ray log character, with distinctly lower median values (typically <65 API units) interpreted as recording predominately limestone-rich lithologies in the most proximal Bone Spring strata.

Description of Cross Section C: Pecos County to Reagan County, West-East

This cross section (Figure IV-12) connects the Wolfcamp Group between southern Delaware Basin and southern Midland Basin. The chosen route, through central Pecos, northern Terrell and central Crockett, and southern Reagan Counties, avoids the structural highs of the Central Basin Platform in order to correlate only basinal stratigraphy between the Delaware, Val Verde and Midland Basins. Nonetheless, the Wolfcamp Group is significantly structurally higher south of the Central Basin Platform, e.g., along the Puckett uplift between Coates -A- #1 (42-371-31361) and Ranch Hand "8" #3 (42-105-38855), between 3,000 and 3,600 feet (914 to 1,097 m) SS TVD. Conversely, the deepest Wolfcamp Group strata occur in central Pecos County where the top of the Wolfcamp Group occurs at 5,947 feet (1,812 m) SS TVD in University Lands 27-9 #1 (42-371-37746). The Middle Pennsylvanian through Devonian units (Strawn though Devonian picks) vary by more than 5,000 feet (15,000 m) in the western half of the cross section, from above 10,000 feet (3,000 m) SS TVD to below 15,000 feet (5,000 m) SS TVD feet in the basin center. Towards the east, the Middle Pennsylvanian through Devonian Units shallow again, occurring between 5,000 and 10,000 feet (1,500 to 3,000 m) SS TVD in UTP Montgomery Ranch #1 (42-371-31782) and University 10 #2704H (42-383-38226). This mirrors the variation in thickness observed in the Pennsylvanian units, which thicken and thin in tandem with the structural position (depth) and greatly exceed the thickening and thinning in the overlying Wolfcamp Group. Additionally, the Devonian Woodford Formation, typically marked by gamma-ray measurements exceeding 150 API units, is not observed and not therefore picked between Millspaugh

#4201 (42-105-36447) and University 10 #2704H (42-383-38226). Finally, the Third Bone Spring Sandstone and the Dean Sandstone are shown to be equivalent units immediately overlying the Wolfcamp Group between the wells Noelke Kennie #1 (42-443-30017) and University 29-20 #2P towards the east (42-105-42111).

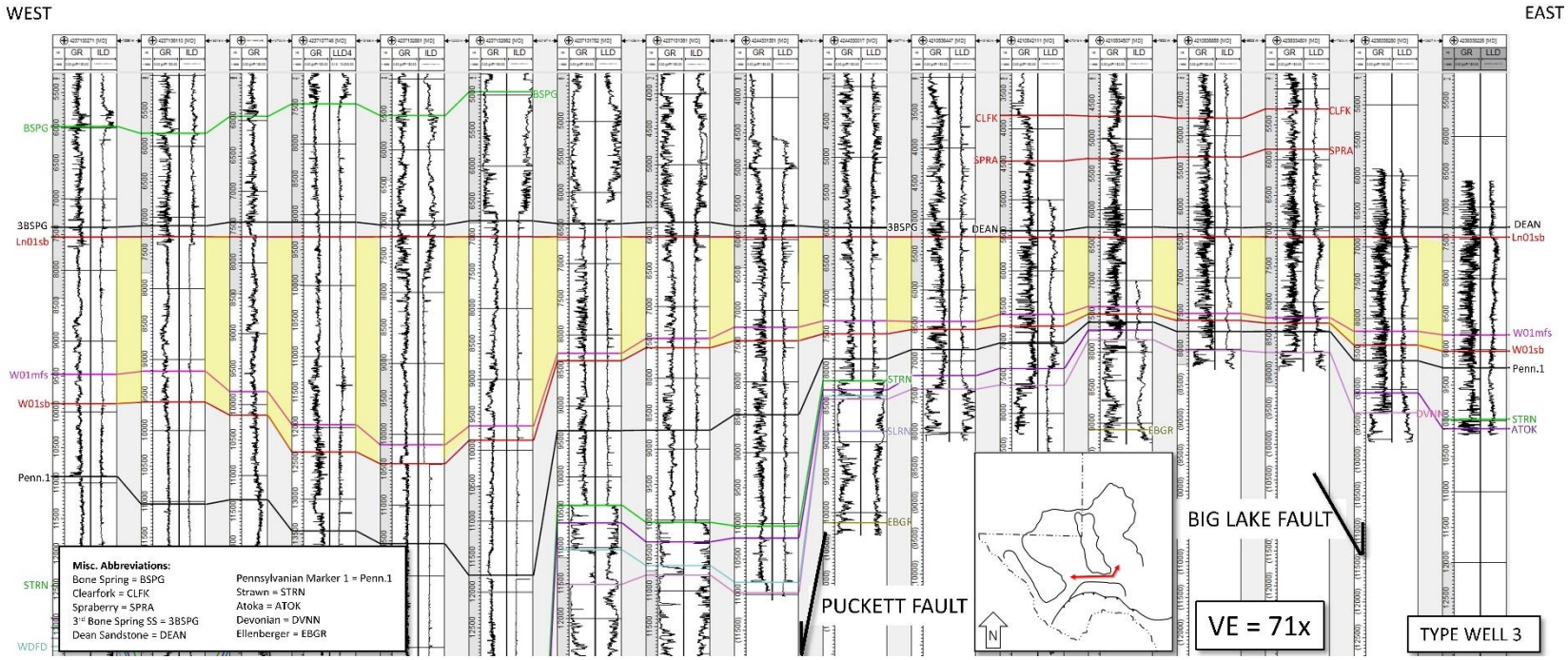

Figure IV-12 Cross Section C from southern Delaware Basin to southern Midland Basin. The three broad regions include the deep Delaware Basin, the thinner Wolfcamp Group strata south of the Central Basin Platform across structural highs, and the comparatively shallow strata in southern Midland Basin to the far east (right). Note that the typical Wolfcamp Group top changes considerably to the far west, whereas the central Delaware Basin log signature more closely matches that of Midland Basin. This cross section is flattened on the top of the Wolfcamp (Ln01sb). Note that Middle-Upper Permian units (e.g. Bone Spring, Spraberry) use local names which are not correlated between Delaware and Midland Basins.

Interpretation of Cross Section C: Pecos County to Reagan County, West-East

This cross section (Figure IV-12) is interpreted to record three fundamentally distinct regions of deposition for the Wolfcamp Group, from west to east, 1) southern Delaware Basin, 2) Puckett uplift and Sheffield Channel south of the Central Basin Platform, and 3) the Ozona Arch and southern Midland Basin. While the Delaware and Midland Basin regions record consistently higher gamma-ray values for the Wolfcamp Group (interpreted as reflecting the dominance of basinal mudstone facies), the structurally higher Sheffield Channel region is interpreted as reflecting a paleo-high suitable for carbonate production, resulting in the increased relative occurrence of low gamma-ray (<65 API units) intervals. Thinning of the Wolfcamp Group across the Sheffield Channel region also is interpreted as resulting from reduced accommodation on the paleo-high(s). The Woodford Formation was interpreted to be eroded by Upper Pennsylvanian or Lower Permian unconformities across the paleo-high(s), given that the Tobosa Basin should have allowed for sufficient accommodation in this region for Woodford Formation deposition during the Devonian (Galley, 1958). Others have shown similar erosion of the Woodford Formation on the Central Basin Platform itself (Comer, 1991). The basinal Wolfcamp Group in southern Midland Basin does show similar broad log character, and trends in gamma-ray and deep resistivity log signature to the Delaware Basin stratigraphy, although the entire Wolfcamp Group is compressed as a function of the reduced accommodation available in the Midland Basin. The maximum flooding surface (W50mfs) in particular is consistent across basins as seen in the

regional and detailed types logs (Figures IV-5, 6) and this prominent marker often occurs just below the operator-selected, informal Wolfcamp B top.

Description of Cross Section D: Culberson to Reeves County Pow-Wow Conglomerate, Southwest-Northeast

This cross section (Figure IV-13) is restricted to Culberson and western Reeves counties and leverages lithology logs documenting the Pow-Wow Conglomerate in the western side of Delaware basin. Here, the Pow-Wow Conglomerate interval is correlated between the base Wolfcamp (W01sb) and first major flooding surface (W10mfs) marker, showing that the top of the Pow-Wow Conglomerate as picked in the lithology log and represents the base of the Wolfcamp Group in this location.

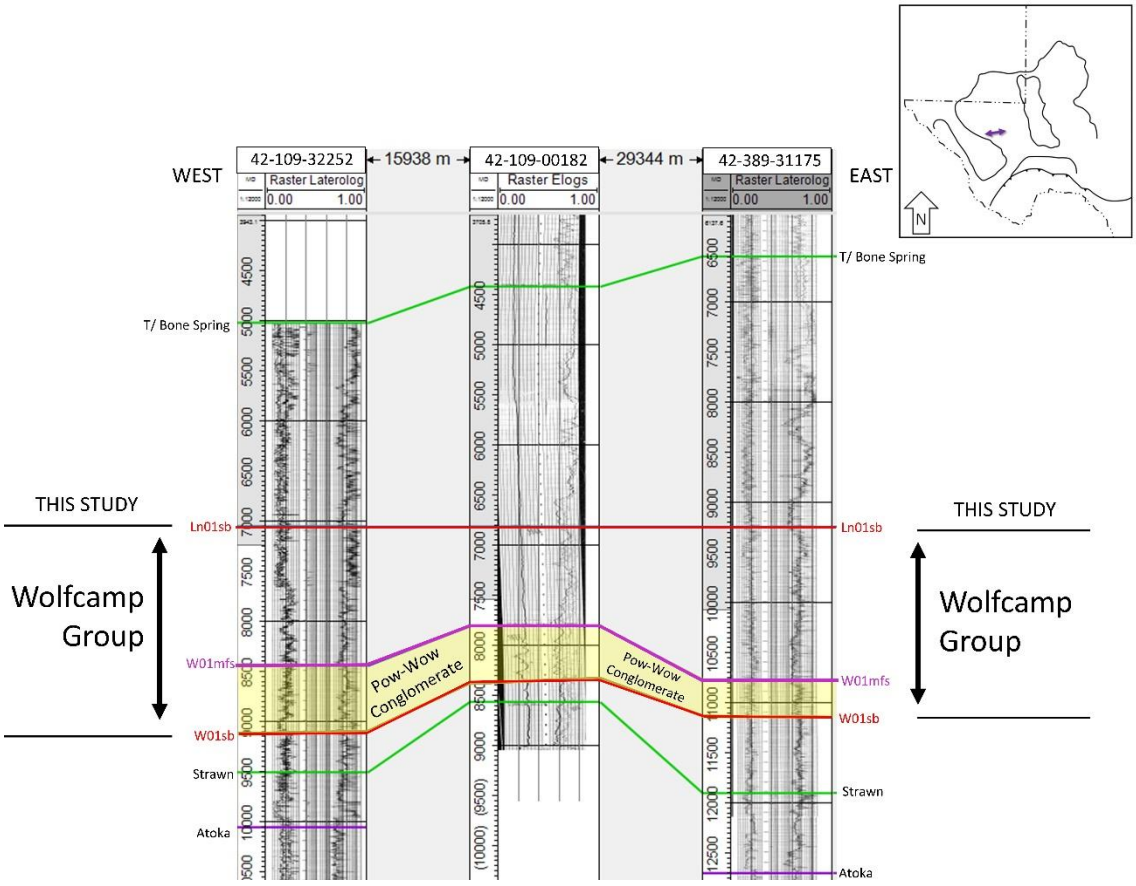

Figure IV-13 Cross Section D is a small portion of western Delaware Basin from Culberson to western Reeves County. The middle well (42-109-00182) contains a lithology log (not shown) which describes and labels an interval the loggers interpret as the "Pow-Wow Conglomerate" (King, 1965) originally mapped in the Sierra Diablo Mountains. Here, this interval is highlighted where it occurs just below the lowermost transgressive surface (W10ts). This study interprets the Pow-Wow conglomerate interval below the transgressive surface (W10ts) as a possible lowstand wedge reflecting updip erosion associated with the base Wolfcamp Group unconformity (W01sb), equivalent to the unconformity in the Glass Mountains (Figure IV-7).

Interpretation of Cross Section D: Culberson to Reeves County Pow-Wow Conglomerate, Southwest-Northeast

The base of the Wolfcamp Group (W01sb) is interpreted as occurring at the base of a conglomeratic lowstand wedge (Figure IV-13) resulting from updip unconformities

occurring at the base of the Permian in the Glass Mountains (King, 1931; Ross, 1963) and in the Hueco and Sierra Diablo Mountains (King et al., 1945; King, 1965; Playton and Kerans, 2002). This interpretation supports the delivery of conglomeratic clasts by debris flows and other processes downdip and onto the proximal basin floor. The lowermost flooding surface surface (W01mfs) would then, as picked, represent the top of a lowstand wedge and the basal Wolfcamp unconformity (W01sb) would be its base, a likely correlative conformity in this area. The chaotic log signatures between these markers is interpreted as indicating the complex lowstand wedge associated with updip erosion rather than quiescent, basinal hemipelgaic or pelagic fallout occurring during highstands.

Description of Cross Section E: Brewster County Outcrops to Nearest Basinward Well, West-East

The provincial outcrop formations and members (from older to younger, the Gaptank, Neal Ranch, Lenox Hills, Skinner Ranch and Cathedral Mountains Formations) were measured and an outcrop-based composite gamma-ray profile correlated (Figure IV-14) with the nearest basinward well, Madre Grande #1 (42-043-30266). The stratigraphic framework enables the comparison of the informal divisions and the outcrop stratigraphy. As correlated, the Skinner Ranch Formation roughly overlaps with the Wolfcamp A, the Lenox Hills Formation overlaps with the Wolfcamp B and the Neal Ranch Formation overlaps with the Wolfcamp D.

Finally, the high gamma-ray surface inside the Wolfcamp C (W20mfs) can be traced between the Wolf Camp Hills and Madre Grande #1 (42-043-30266), and this surface has a seven degree dip. This dip is calculated simply by measuring present day change in elevation over present day distance and is therefore uncorrected for compaction effects.

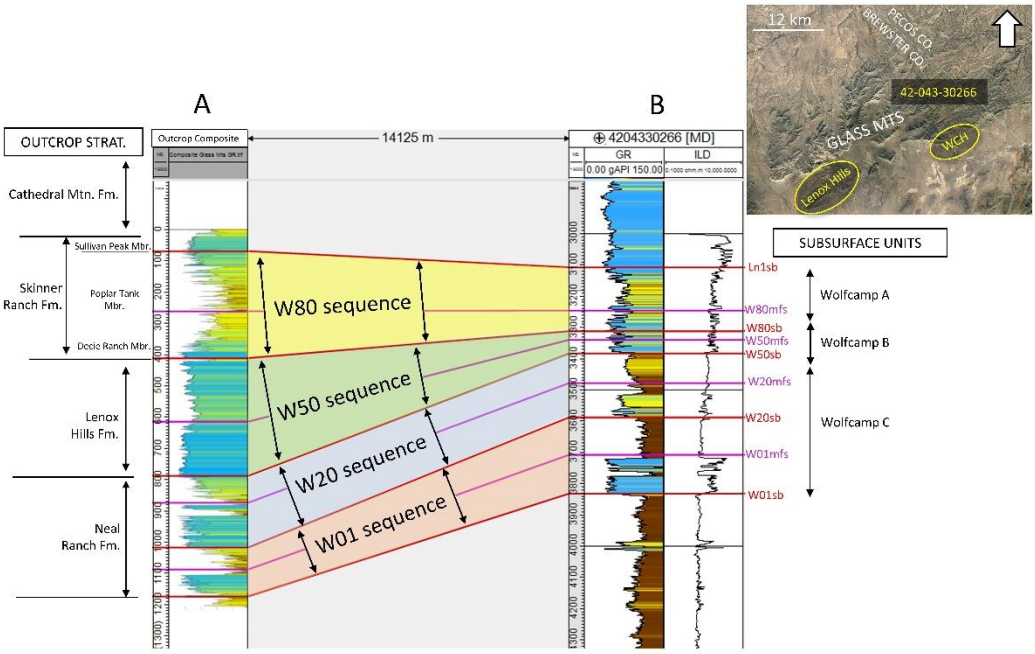

Figure IV-14 Cross section E correlates the Glass Mountains outcrop composite section (A) into a nearby basinward well (B). The base of the Lenox Hills Formation is a prominent angular unconformity (W50sb) in outcrop, and the overlying Lenox Hills Formation thickens and thins dramatically across the Glass Mountains (Ross, 1963). Composite section includes the Neal Ranch Formation in the eastern Wolf Camp Hills and the Lenox Hills and Skinner Ranch Formations in the western Lenox Hills. Correlation indicates location of traditional operator-derived units relative to outcrop formations.

Interpretation of Cross Section E: Brewster County Outcrops to Nearest Basinward Well, West-East

This cross section (Figure IV-14) shows consistent high gamma-ray signatures for the Gaptank, Neal Ranch and Skinner Ranch formations as correlated here, whereas the Lenox Hills Formation shows considerable variation in thickness and log character from the Glass Mountains into the subsurface. This matches the description of Ross (1963) who noted the variable nature of the Lenox Hills Formation in outcrop, especially the basal conglomeratic intervals. Given that the base of the Lenox Hills represents an angular unconformity (Ross, 1963), the varying thickness of conglomeratic fill may be consistent with variable erosion and creation of accommodation space during subaerial exposure. This interpretation also supports previous work (Ross, 1963) placing the base of the Wolfcamp Group at the flooding surface close to the top of the Gray Limestone Member of King (1931). The Gaptank Formation, including the Gray Limestone Member, would therefore be interpreted as Upper Pennsylvanian Canyon and Cisco equivalent.

Finally, the sudden transition to a high gamma ray interval in the Neal Ranch formation (W20mfs) is interpreted as a flooding surface and because this dip of 7° is steep, but less so than at the southern end of Cross Section B (Figure IV-10), one possible interpretation is that this dip records the shelf-slope transition where the outcrops represent the middle or outer shelf and the Madre Grande #1 (42-043-30266) penetrates the upper slope, at least during deposition of the lower interval(s) of the Wolfcamp Group. Another possibility is that the reduced occurrence of mudstones in the

proximal Glass Mountains outcrops reduces compaction effects, and this 7° is closer to depositional dip during the deposition of the Wolfcamp Group.

Structure Maps

Description of Structure Map 1: Top Wolfcamp Structure across Paleo-Slope, Brewster and Pecos Counties

In the map, 465 well logs (shown as black squares) in the southern Delaware Basin were used to reconstruct the top of the Wolfcamp Group. This assumes post-depositional tectonic alteration was minimal, but tectonic intensity associated with the Marathon-Ouachita orogeny had decreased significantly by the Leonardian (Hills, 1984). The hotter colors represent shallower values and the deeper values are shown with cooler colors. Numeric annotations shown are relative to sea level. The outline of Delaware Basin and the southernmost portion of Midland Basin are clearly visible. Although the Central Basin Platform was not the focus of these picks the general outline is nonetheless visible in the structure map. Absolute values range from 3000 feet (1000 m) above sea level (yellow-orange color) to 8000 feet (2500 m) below sea level in the central Delaware Basin. The Wolfcamp Group south of the Central Basin Platform is positioned significantly structurally higher (i.e., shallower) than the Wolfcamp Group in Delaware Basin and slightly higher or shallower than in Midland Basin. The Wolfcamp towards the Glass Mountains shows significant and rapid shallowing, manifesting as tightly spaced 1000 foot contours. The top of the Wolfcamp Group in the basin does

continue to deepen toward the north, but with a significantly lower dip compared with the area near the western Pecos-eastern Brewster County boundary.

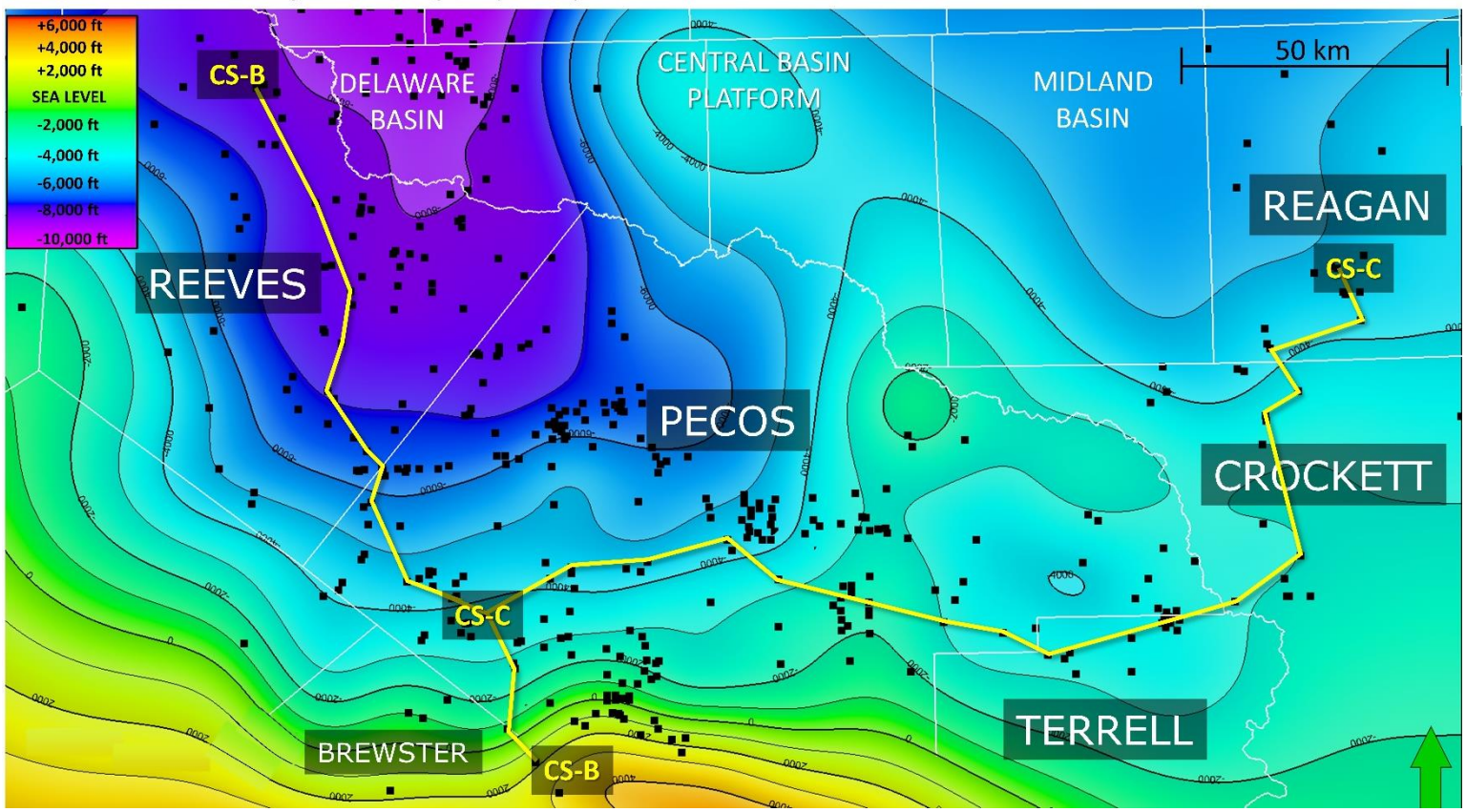

Figure IV-15 Structure map for the top of the Wolfcamp generated in Petrel using 465 well tops (black squares) picked for this study. Well density deliberately higher in southern Delaware Basin. Note defined slope in southern Pecos County approaching southern shelf. Counties in white, contour is 1000 feet, datum is sea level. Cross sections 2 and 3 are shown in green and orange, respectively. Select counties labelled in white.

Interpretation of Structure Map 1: Top Wolfcamp Structure across Paleo-Slope, Brewster and Pecos Counties

The general structural configuration of the Permian Basin (i.e., the general outlines of Delaware, Midland Basins and Central Basin Platform is well established in the literature (e.g., Galley, 1958) but the detail shown here around the southern shelf, integrating several outcrop-based picks for the top of the Wolfcamp Group, clarifies the appriximate structural configuration at the end of Wolfcamp Deposition. Additionally, the cluster of wells north of the Glass Mountains recording a steep transition from approximately +2,000 to -2,000 feet (+600 to -600 m) SS TVD is interpreted as recording a well-defined paleo-slope, where the Glass Mountains outcrops were positioned close to the apparent top of the slope. The positioning and dip of the slope are interpreted as being at least partially a function of the Ouachita-Marathon thrust front, where the most northern thrust fault(s), e.g., the Dugout Creek Thrust (King, 1980), tip out somewhere beneath the Glass Mountains, although this could be tested with 3D seismic data In this scenario, the carbonate depositional profile for the Wolfcamp Group at the southern shelf of Delaware Basin could be interpreted as a "wedge-top" thrust front (DeCelles and Giles, 1996; Bosence, 2005).

Discussion

How does the outcrop to basin correlation affect the understanding of the age of the uppermost Wolfcamp Group?

As previously noted, both the top and bottom boundaries of the Wolfcamp Group are controversial. Regarding the top of the Wolfcamp Group, this study uses the stratigraphic framework to correlate the informal subsurface nomenclature from operators with the outcrop formations. This work suggests that the informal Wolfcamp A in the basin is, in general, equivalent to the Skinner Ranch Formation in outcrop (Figure IV-14). Debate around this interval revolves around whether this interval is Leonardian or older, and which rocks constitute the Leonardian in outcrop (Ross, 1963; Cooper and Grant, 1972). By deferring to the well-defined international time-scale, this discussion is avoided, and the outcrop to subsurface correlation is established wherein the Skinner Ranch Formation in outcrop corresponds to the informal Wolfcamp A in the basin. Skinner Ranch Formation deposition occurred during the upper Artinskian or lower Kungurian (Henderson et al., 2012), similarly to the informal Wolfcamp A in the subsurface (Tian et al., 2019). The absolute ages of both the surface and subsurface strata, however, needs to be better constrained with more geochronology established using TIMS dating on bentonite-derived zircon grains. Finally, whatever the age of the Wolfcamp A in the Midland Basin it should equivalent to the Wolfcamp A in Delaware Basin (Figure IV-12) because both are shown to be equivalent, as are their overlying Leonardian sandstone units, the Dean and the Third Bone Spring units, respectively.

Are the markers delineating the top of the Wolfcamp Group in the basin chronostratigraphically significant?

By comparing the type wells from the central and southern Delaware Basin, and the Midland Basin, (Figure IV-6) the well log signatures for the basinal Wolfcamp Group can be compared at the regional scale. The continuity of the transgressive surfaces between basins strongly suggests that these intervals represent time-stratigraphic surfaces because the log signatures show not just similar lithologies (i.e., mudstone-dominated bedsets) but have the same gamma-ray and especially deep resistivity spikes and inflection points occurring at the same stratigraphic heights in all three wells. This suggests that individual events are responsible for those individual log signatures (e.g., changes in marine geochemistry) which are recorded in both basins and at approximately the same time. If the correlation were purely lithostratigraphic (i.e., not representing basinal mudstones of the same age), the gross lithofacies might be comparable, but the individual events and resulting wireline log signatures complete with matching spikes and inflection points would not align. In fact, the log signature observed for the Uppermost Wolfcamp Group here occurs through Delaware Basin and southern Midland Basin, and its correlation only breaks down across the paleo-highs along the Sheffield Channel where the lithofacies do not record the same signals as the basinal mudrock intervals in the basin.

What is the nature of the depositional profile for the Wolfcamp Group across Southern Delaware Basin?

While early workers were able to delineate individual clinoforms in the Wolfcamp Group using very closely spaced well logs (≤ 1 mile spacing) on the Eastern Shelf (e.g., Rall and Rall, 1958; Van Siclen, 1958), this study correlates flooding surfaces in the Wolfcamp Group using available wireline log data which remains relatively sparse, and records depositional topography across the tectonically complex Ouachita-Marathon thrust front. The dips for the top of the Wolfcamp Group (Figure IV-15) greatly exceed those of Lower Wolfcamp Group ramps studied by previous workers (Mazzullo and Reid, 1989; Sinclair et al., 2017). This may reflect changes in the primary reef builders over time from less aggradational phylloid algae to more strongly aggradational corals (Mazzullo and Reid, 1989). Studies of Midland Basin have invoked changes in sediment supply over time, concluding the times of higher sediment supply (e.g., collisional phases) result in shelf progradation and slope margin flattening, while lower sediment supply times result in carbonate aggradation and slope steepening (Liu et al., 2021). The tectonic setting could also explain the steep depositional profile (10-20° slope), where the Wolfcamp Group previously was measured as having steep relief across tectonically enhanced margins, as occurs on the western side of Delaware Basin or across deep normal faults bounding the Central Basin Platform (Yang and Dorobek, 1995; Playton and Kerans, 2002; Sinclair, 2017). In the western Delaware Basin, modern Sierra Diablo Mountains, tectonically-enhanced relief across the Wolfcamp Group was recorded as being as steep as 7°, whereas Leonardian profiles measured as dipping as

steeply as 15° (Fitchen, 1996). Additionally, work in the southern Delaware Basin previously interpreted the Lower Permian shelf as being perched atop paleo-highs controlled by imbricate blind thrusts (Ross, 1986) creating more tectonically-enhanced relief between the shelf and the basin than would otherwise occur purely as a function of carbonate factory reef building. This type of carbonate depositional profile was termed a "wedge-top" profile forming in a tectonically active part of a foreland basin (DeCelles and Giles, 1996; Bosence, 2005). In relation to recent conclusions from Midland Basin regarding sediment supply as the primary control on slope, Delaware Basin generally, and especially adjacent to the thrust front, has comparatively extreme accommodation space available for sediment fill, potentially dampening any flattening effect akin to that observed due to sediment outbuilding in Midland Basin (Liu et al., 2021). Similarly, if the shelf margin is sufficiently steepened by tectonics to act as a continuous bypass surface during the deposition of the Wolfcamp Group in Southern Delaware Basin, this "shelf margin" would not prograde normally, even with a very high sediment supply with the Marathon highlands, because it had not yet filled the available accommodation space in the foredeep.

Occurrence of Detrital Silt- and Sandstone Units with Relation to Sediment Provenance

The Wolfcamp Group X and Y sandstone intervals are most prominent in the northern Delaware Basin (Figure IV-11), the Upper Pennsylvanian and Lower Wolfcamp (the informal Wolfcamp C, especially) detrital packages thicken towards the south (Van Der Loop, 2017) and the Ouachita-Marathon thrust front (Hall, 1956). This

suggests that at different periods in time, sources of sediment to the basin changed significantly, from the south to the north and that input on one side of the basin may not be observed elsewhere in the basin. This is supported by recent work on detrital zircons (Gao et al., 2020; Soto-Kerans et al., 2020) which specifically supports a southern source associated with the Ouachita-Marathon highlands in Uppermost Pennsylvanian and Lowermost Permian detrital sediments in southern Delaware Basin. Other recent studies highlight the persistent importance of southern sediment sources in Delaware Basin through the Leonardian (e.g., Liu and Stockli, 2020). Finally, distance from a sediment source might record not just the thickening or thinning of units, but might record changes in sediment size or uniformity which affect reservoir quality and occurrence (Montgomery, 1997; Driskill et al., 2018; Liu et al., 2021).

Thickening and Thinning of the Permo-Carboniferous as a Function of Tectonism Associated with the Ouachita-Marathon Orogeny

These cross sections, especially cross section B (Figures IV-9, 10), record significant thickening and thinning across the Pennsylvanian units and some thickening and thinning in the Lower Wolfcamp. Conversely, thickening in Upper Wolfcamp Group is comparatively minimal. This upward reduction in thickening aligns with interpretations by previous workers that the uppermost Wolfcamp Group is likely predominantly post-tectonic, whereas the lowermost Wolfcamp Group is likely syn-tectonic (Hills, 1984; Fitchen, 1997; Sinclair et al., 2017). Since the changes in accommodation and sediment supply are strongest adjacent to the thrust front, the

Pennsylvanian units in the southern portions of cross section B (Figure IV-10) likely record the most extreme subsidence and sediment delivery to the basin documented in these cross sections, representing the western edge of the Ouachita-Marathon foredeep (Liu et al., 2021). This is partially responsible for the difficulty in comparing the lower portions of the Wolfcamp Group, below the W50mfs surface, between the southern Delaware and southern Midland Basins. This is because of the strong, localized tectonic influence on the relative sea level curves for the Lower Wolfcamp Group, whereas the relative sea level curve associated with the comparatively quiescent Upper Wolfcamp Group is more likely to reflect eustasy, and the resulting Upper Wolfcamp Group sediment patterns are therefore more likely to be comparable between basins.

Conclusions

New correlations for the Wolfcamp Group, connecting southern Delaware Basin with the type locality outcrops in the Glass Mountains and with southern Midland Basin, yield several key insights. They show that the Wolfcamp Group can be defined and correlated consistently using chronostratigraphically-significant surfaces on a regional scale, especially by identifying and correlating specific high gamma-ray markers, within mudstone-prone intervals. They also show that the Wolfcamp Group is correlative across the tectonically complex southern Delaware Basin, as well as the outcrop belt. Furthermore, this work also revealed that sandstone units in the Upper Pennsylvanian units and the lower parts of the Wolfcamp Group do not follow the thickening and thinning pattern of sandstone units in the upper Wolfcamp Group (e.g., the XY

sandstone intervals), demonstrating significance of varying sediment provenance through time. The outcropping Neal Ranch Formation is correlative with the operator-derived Wolfcamp C unit while the overlying Lenox Hills and Skinner Ranch Formations are correlative with the Wolfcamp B and A units, respectively. Finally, these correlations yield a three-dimensional understanding of the paleo-topography at the end of Wolfcamp Group deposition in the southern Delaware Basin, supporting a wedge-top carbonate depositional model, wherein the paleo-highs of the southern shelf were influenced by the Ouachita-Marathon thrust front and locally hosted carbonate platforms adjacent to the southern Delaware Basin.

References

Adams, J.E., 1951, Starved Pennsylvanian Midland basin: AAPG bulletin, v. 35, no. 12, p. 2600-2607.

Adams, J.E., 1965, Stratigraphic-tectonic development of Delaware Basin: AAPG bulletin, v. 49, no. 11, p. 2140-2148.

Barrick, J.E., and G.P. Wahlman, 2019, Conodont and fusulinid biostratigraphy of the Strawn Group (Desmoinesian, Middle Pennsylvanian) and lower part of the "Wolfcamp Shale" (Missourian-Virgilian, Late Pennsylvanian) in the northern Midland Basin, West Texas: Stratigraphy, v. 16, no. 2, p. 65-86, doi: 10.29041/strat.16.2.65-86.

Baumgardner, R.W., Hamlin, H.S., and H. Rowe, 2016, Lithofacies of the Wolfcamp and Lower Leonard Intervals, Southern Midland Basin, Texas; The University of Texas at Austin, Bureau of Economic Geology, Report of Investigations, no. 281, 61 p.

Bessa, F., Jerath, K., Ginn, C., Johnston, P., Zhao, Y., Brown, T., Lopez, R., Kessler, J., Nicklen, B., and V. Sahni, 2021, Subsurface Characterization of Hydraulic Fracture Test Site-2 (HFTS-2), Delaware Basin, Proceedings of the 2021 Unconventional Resources Technology Conference, Houston, Texas, July, doi:10.1016/j.sedgeo.2004.12.030.

Bhattacharya, J. P., 1993, The expression and interpretation of marine flooding surface and erosional surfaces in core; examples from the Upper Cretaceous Dunvegan Formation, Alberta foreland basin, Canada, *in* Posamentier, H.W., Summerhayes, C.P., Haq, B.U., and G.P. Allen, eds., Sequence Stratigraphy and Facies Associations: International Association of Sedimentologists, Special Publication 18, p. 125-160, 10.1002/9781444304015.ch8.

Bloom, M.A., 1988, A subsurface geologic study of northern Brewster County, Texas: Master's thesis, Sul Ross State University, Alpine, Texas, 157 p.

Bosence, D., 2005, A genetic classification of carbonate platforms based on their basinal and tectonic settings in the Cenozoic: Sedimentary Geology, v. 175, p. 49-72, doi: doi:10.1016/j.sedgeo.2004.12.030.

Brown, Jr., L.F., R.F. Solis Iriarte, and D.A. Johns, 1990, Regional depositional systems tracts, paleogeography, and sequence stratigraphy, Upper Pennsylvanian and Lower Permian strata, north-and west-central Texas: The University of Texas at Austin, Bureau of Economic Geology, Report of Investigations No. 197, 116 p. + oversized plates.

Candelaria, M. P., Sarg, J. F., and Wilde, G. L., 1992, Wolfcampian sequence stratigraphy of the eastern Central Basin platform. Permian Basin exploration and production strategies: Applications of sequence-stratigraphic and reservoir characterization concepts: West Texas Geological Society Publication, v. 92, no. 91, p. 27-44.

Cohen, K.M., Finney, S.C., Gibbard, P.L. & Fan, J.-X., 2013; updated, The ICS International Chronostratigraphic Chart: Episodes v. 36: p. 199-204.

Comer, J. B, 1991, Stratigraphic analysis of the Upper Devonian Woodford Formation, Permian Basin, West Texas and Southeastern New Mexico: Texas Bureau of Economic Geology Report of Investigations 201, 63 p.

Cooper, G. A., and R. E. Grant, 1972, Permian brachiopods of west Texas, I. Smithsonian contributions to Paleobiology.

DeCelles, P.G., and K.A. Giles, 1996, Foreland basins: Basin Research, v. 8, p. 105-123, doi: 10.1046/j.1365-2117.1996.01491.x.

DiMichele, W.A., Cecil, C.B., Montañez, I.P., and H.J. Falon-Lang, 2010, Cyclic changes in Pennsylvanian paleoclimate and effects on floristic dynamics in tropical Pangea: International Journal of Coal Geology, v. 83, no. 2-3, p. 329-344, doi: 10.1016/j.coal.2010.01.007.

Driskill, B., Pickering, J., and H. Rowe, 2018, Interpretation of high resolution XRF data from the Bone Spring and Upper Wolfcamp, Delaware Basin, USA. Proceedings of the 2018 Unconventional Resources Technology Conference, Houston, Texas, July, doi: 10.15530/URTEC-2018-2901968.

Ewing, T. E., 1984, Late Paleozoic Structural Evolution of Permian Basin: AAPG Bulletin, v. 68, no. 4, p. 474-475.

Ewing, T.E., 1985, Westward expansion of the Devils River uplift – implications for the Paleozoic evolution of the southern margin of North America: Geology, v. 13, p. 433-436.

Ewing, T.E., 1991, The tectonic framework of Texas: Text to accompany "The Tectonic Map of Texas": Austin, Bureau of Economic Geology, The University of Texas at Austin, 36 p.

Ewing, T.E., 1993, Erosional margins and patterns of subsidence in the late Paleozoic West Texas Basin and adjoining basins of West Texas and New Mexico: Socorro, New Mexico Geological Society Guidebook, 44th Field Conference, p. 155-166.

Fielding, C.R., Frank, T.D., Birgenheier, L.P., Rygel, M.C., Jones, A.T. and J. Roberts, 2008. Stratigraphic imprint of the Late Palaeozoic Ice Age in eastern Australia: a record of alternating glacial and nonglacial climate regime: Journal of the Geological Society, v. 165, no. 1, p. 129-140.

Fitchen, W.M., 1996, Strike variability of carbonate platform margin stratal architecture and cycle stacking patterns: Outcrop and seismic examples from lower Permian depositional sequences of the Permian Basin, USA. Proceedings of the 1996 AAPG Annual Convention.

Fitchen, W.M., 1997, Lower Permian sequence stratigraphy of the western Delaware Basin margin. Sierra Diablo, west Texas, Ph.D. dissertation, University of Texas at Austin, Austin, Texas, 263 p.

Galley, J.E., 1958, Oil and Geology in the Permian basin of Texas and New Mexico, in L.G. Weeks, ed., Habitat of oil, a symposium: American Association of Petroleum Geologists, p. 395-446.

Gao, Z., N.D. Perez, B. Miller, and M.C. Pope, 2020, Competing sediment sources during Paleozoic closure of the Marathon-Ouachita remnant ocean basin: GSA Bulletin, v. 132, no. 1-2, p. 3-16.

Hall, W.E., 1956, Marathon folded belt in Big Bend area of Texas: AAPG Bulletin, v. 40, p. 2247-2255.

Hamlin, H.S., 2009, Ozona sandstone, Val Verde Basin, Texas: Synorogenic stratigraphy and depositional history in a Permian foredeep basin: AAPG bulletin, v. 93, no. 5, p.573-594.

Henderson, C.M., V.I. Davydov, and B.R. Wardlaw, 2012, The Permian Period, *in* Gradstein, F.M., J.G. Ogg, M.D. Schmitz, and G.M. Ogg (eds) The Geologic Time Scale 2012, v. 2. Elsevier, p. 653-679.

Hills, J.M., 1942, Rhythm of Permian seas—a paleogeographic study: AAPG Bulletin v. 26, no. 2, p. 217-255.

Hills, J. M., 1984, Sedimentation, tectonism, and hydrocarbon generation in Delaware Basin, west Texas and southeastern New Mexico: AAPG bulletin, v. 68, no. 3, p. 250-267.

Hobson, J.P., C.D. Caldwell and D.F. Toomey, 1985, Early Permian deep-water allocthonous limestone facies and reservoir, west Texas: AAPG Bulletin, v. 69, p. 2130-2147.

Holterhoff, P. F., 2010, Sequence Stratigraphy and Depositional Systems of the Eastern Shelf Lower Permian, Central Texas: Examining the Tropical Record of Late Paleozoic Climate Change. Permian Basin Section, SEPM Publication, 2010, 124 p.

Horak, R. L., 1985, Tectonic and hydrocarbon maturation history in the Permian Basin: Oil & gas journal, v. 83, no. 21, p. 124-129.

Isbell, J.L., Henry, L.C., Gulbranson, E.L., Limarino, C.O., Fraiser, M.L., Koch, Z.J., Ciccioli, P.L. and Dineen, A.A., 2012, Glacial paradoxes during the late Paleozoic ice age: Evaluating the equilibrium line altitude as a control on glaciation: Gondwana Research, v. 22, no. 1, p. 1-19.

Jackson, W. E., 1964, Depositional topography and cyclic deposition in west-central Texas: AAPG Bulletin, v. 48, no. 3, p. 317-328.

Johnson, R.L., Walters, W.W., Conway, M.W., Burdett, B.S. and R. G. Stanley, 1998, CO2 energized and remedial 100% CO2 treatments improve productivity in Wolfcamp intervals, Val Verde Basin, West Texas. Proceedings of the 1998 SPE Permian Basin Oil and Gas Recovery Conference, doi: 10.2118/39778-MS.

Jones, T.S., 1975, Base of the Permian in Midland and Delaware Basins from logs, *in* Permian Exploration, Boundaries, and Stratigraphy: WTGS and PBS-SEPM Publ. No. 62-7, p. 51-66.

King, P.B., 1931, Geology of the Glass Mountains, Part I, Descriptive Geology: Univ. Texas Bull. 3038, p. 51-90.

King, P. B., King, R. E., and Knight, J. B., 1945, Geology of the Hueco Mountains, El Paso and Hudspeth Counties, Texas: U. S. Geological Survey Oil and Gas Investigations Preliminary Map 36, 2 sheets.

King, P.B., 1965, Geology of the Sierra Diablo region, Texas, with special determinative studies of Permian fossils by L.G. Henbest, *et al.*, U.S. Geol. Survey Prof. Paper 215, 183 p.

King, P. B., 1980, Geology of the eastern part of the Marathon basin, Texas: U.S. Geological Survey Professional Paper 1157, 40 p.

Kohn, J., Barrick, J.E., Wahlman, G.P., and R. Baumgardner, 2019, Late Pennsylvanian (Virgilian) to Early Permian (Leonardian) conodont biostratigraphy of the "Wolfcamp Shale", northern Midland Basin, Texas, *in* Denne, R.A., and Kahn, A., eds., Geologic Problem Solving with Microfossils IV: Society for Sedimentary Geology, SEPM Special Publication No. 111, p. 245-261, doi: 10.2110/sepmsp.111.11.

Kvale, E. P., Bowie, C. M., Flenthrope, C., Mace, C., Parrish, J. M., Price, B., Anderson, S. and DiMichele, W. A., 2020, Facies variability within a mixed carbonate–siliciclastic sea-floor fan (upper Wolfcamp Formation, Permian, Delaware Basin, New Mexico). AAPG Bulletin, v. 104, no. 3, p. 525-563, doi: 10.1306/06121917225**.**

Liu, L., and D.F. Stockli, 2020, U-Pb ages of detrital zircons in lower Permian sandstone and siltstone of the Permian Basin, west Texas, USA: Evidence of dominant Gondwanan and peri-Gondwanan sediment input to Laurentia: AAPG Bulletin, v. 132, no. 1-2, p. 245-262.

Liu, L., W.A. Ambrose, T.F. Lawton, and D.F. Stockli, 2021, Tectonic controls on the evolution of mixed carbonate-siliciclastic systems: Insights from the late Palaeozoic Ouachita-Marathon Foreland, United States: Basin Research, v. 33, p. 2281-2302.

Lucas, S. G., Heckert, A. B., Estep, J. W., and C.W. Cook, 1998, Stratigraphy of the Lower Permian Hueco Group in the Robledo Mountains, Doña Ana County, New Mexico. New Mexico Museum of Natural History and Science Bulletin, 12, p. 43-54.

Lucas, S. G., Barrick, J. E., Krainer, K. and Schneider, J. W., 2013, The Carboniferous-Permian boundary at Carrizo Arroyo, Central New Mexico, USA: Stratigraphy, v. 10, no. 3, pp.153-170.

Lucas, S. G., Krainer, K., Voigt, S., Berman, D. S., and A. Henrici, 2014, The Lower Permian Abo Formation in the northern Sacramento Mountains, southern New Mexico. New Mexico Geological Society, Guidebook, 65, p. 287-302.

Lucas, S. G., and S. Z. Shen, 2018, The Permian chronostratigraphic scale: history, status and prospectus. Geological Society, London, Special Publications, v. 450(1), p. 21-50, doi: 10.1144/SP450.3.

Matchus, E. J., and T. S. Jones (co-chairmen), 1984, East to west cross section through Permian basin west Texas: West Texas Geological Society Special Publication No. 84-79, 1 sheet.

Mazzullo, S. J., L. J. Mazzullo, and A. M. Reid, 1987, Basinal Lower Permian Facies, Permian Basin: Part I – Stratigraphy of the Wolfcampian-Leonardian Boundary: WTGS Bulletin, v. 26, no. 7, p. 5-9.

Mazzullo, S. J., and A. M. Reid, 1989, Lower Permian platform and basin depositional systems, northern Midland Basin, Texas, in P. Crevello, J. L. Wilson, J. F. Sarg, and J. F. Read, eds., Controls on Carbonate Platform and Basin Development: SEPM Special Publication 44, p. 305–320.

McKee, E. D., and S. S. Oriel, 1967, Paleotectonic investigations of the Permian System in the United States: U.S. Geol. Survey Prof. Paper 515, 271 p., doi: 10.3133/pp515.

Montañez, I. P., and C.J. Poulsen, 2013, The Late Paleozoic ice age: an evolving paradigm: Annual Review of Earth and Planetary Sciences, v. 41, p. 629-656.

Montañez, I. P., McElwain, J. C., Poulsen, C. J., White, J. D., DiMichele, W. A., Wilson, J. P., Griggs, G., and Hren, M. T., 2016, Climate, *p*CO 2 and terrestrial carbon cycle linkages during late Palaeozoic glacial–interglacial cycles: Nature Geoscience, v. 9, no. 11, p. 824-828, doi: 10.1038/ngeo2822.

Montgomery, S.L., 1997, Permian Bone Spring formation: sandstone play in the Delaware basin, part II—basin: AAPG bulletin, v. 81, no. 9, p. 1432-1434.

Playton, T.E., and C. Kerans, 2002, Slope and toe-of-slope deposits shed from a late Wolfcampian tectonically active carbonate ramp margin: Gulf Coast Association of Geological Societies, Transactions, v. 52, p. 811-820.

Rall, R. W., and E. P. Rall, 1958, Pennsylvanian subsurface geology of Sutton and Schleicher counties, Texas: AAPG Bulletin, v. 42, p. 839-870.

Richards, B. H., Wehner, M., Pope, M. C., Donovan, A. D., 2021, An Integrated Chemo- and Sequence Stratigraphic Analysis of Extended (>1000 ft) Lower Permian Wolfcamp Cores, Reagan County, Southern Midland Basin, AAPG Bulletin, *in review*.

Ross, C. A., 1963, Standard Wolfcampian Series (Permian), Glass Mountains, Texas: Geol. Soc. America Mem. 88, 205 p.

Ross, C. A., 1986, Paleozoic evolution of southern margin of Permian basin: Geological Society of America Bulletin, v. 97, no. 5, p. 536-554.

Ross, C.A., Cromwell, D., and L. Mazzullo, 1987, Leonardian Series (Permian), Glass Mountains, West Texas, The Leonardian Facies in west Texas and southeast New Mexico and guidebook to the Glass Mountains, West Texas: Midland, Society of Economic Paleontologists and Mineralogists Permian Basin Section, p. 25-33.

Ross, C. A., and J. R. P. Ross, 1987, Late Paleozoic sea levels and depositional sequences: Cushman Foundation for Foraminiferal Research, p. 137.

Ross, C.A., and J.R.P. Ross, 1988, Late Paleozoic transgressive-regressive deposition, *in* Wilgus, C.K., Hastings, B.S., Kendall, C.G.S.C., Poamentier, H.W., Ross, C.A., Van Wagoner, J.C. (Eds.), Sea-Level Changes – an Integrated Approach, SEPM Special Publication vol. 42, p. 227-247.

Rygel, M. C., Fielding, C. R., Frank, T. D., and L.P. Birgenheier, 2008, The magnitude of Late Paleozoic glacioeustatic fluctuations: a synthesis: Journal of Sedimentary Research, v. 78, no. 8, p. 500-511.

Sarg, J.F., 1989, Middle-Late Permian depositional sequences, Permian basin, west Texas-New Mexico, in A. W. Bally, ed., Atlas of seismic stratigraphy: AAPG Studies in Geology 27, v. 3, p. 140-154.

Scotese, C.R., Bambach, R.K., Barton, C., Van der Voo, R. and Ziegler, A.M., 1979, Paleozoic base maps: The Journal of Geology, v. 87, no. 3, p. 217-277.

Scotese, C. R., and R.P. Langford, 1995, Pangea and the paleogeography of the Permian, in The Permian of Northern Pangea, p. 3-19. Springer, Berlin, Heidelberg.

Shumaker, R.C., 1992, Paleozoic structure of the Central Basin uplift and adjacent Delaware basin, west Texas: AAPG Bulletin, v. 76, no. 11, p. 1804-1824, doi: 10.1306/BDFF8AD8-1718-11D7-8645000102C1865D.

Silver, B.A., and R.G. Todd, 1969, Permian cyclic strata, northern Midland and Delaware Basins, West Texas and southeastern New Mexico: AAPG Bulletin, v. 53, no. 11, p. 2223-2251, doi: 10.1306/5D25C94D-16C1-11D7-8645000102C1865D.

Sims, E. R., and Belanger, C. L., 2021, Quantifying Late Pennsylvanian multivariate morphological change in the fusulinid genus *Triticites* from the central and southwestern United States: Journal of Foraminiferal Research, v. 51, no. 3, p. 165-181.

Sinclair, S., L. Crespo, L. Waite, K. Smith, and C. Leslie, 2017, Resource assessment in the northern Midland Basin: Detailed mapping of Late Pennsylvanian, Wolfcampian, and Early Leonardian margins and flooding surfaces using well logs and seismic data: Proceedings of the 5th Unconventional Resources Technology Conference, Austin, Texas, July 24–26, p. 2781–2793, doi:10.15530/urtec-2017-2692102.

Soto-Kerans, G.M., Stockli, D.F., Janson, X., Lawton, T.F. and Covault, J.A., 2020. Orogen proximal sedimentation in the Permian foreland basin: Geosphere, v. 16, no. 2, p. 567-593, doi: 10.1130/GES02108.1.

Tabor, N.J., Montañez, I.P., Scotese, C.R., Poulsen C.J., and G.H. Mack, 2008, Paleosol archives of environmental and climatic history in paleotropical western Pangea during the latest Pennsylvanian through early Permian. See Fielding et al. 2008c, p. 291–304.

Tian, H., M. Fan, L. Waite, and R.J. Stern, Revise the Paleozoic Norther American Regional Time Scales by Volcanic Ashes in the Midland Basin: AAPG Search and Discovery Article, no. 11247.

Udden, J. A., 1917, Notes on the Geology of the Glass Mountains, Texas University Bulletin 1753, p. 3-59.

Van Der Loop, M., 1990, Amacker Tippett Wolfcamp field, Upton County, Texas, *in* Flis, J. E., and Price, R. C., eds., Permian Basin oil and gas fields: innovative ideas in exploration and development: West Texas Geological Society, Publication No. 90-87, p. 133–151.

Van Wagoner, J. C., Posamentier, H. W., Mitchum, R. M. J., Vail, P. R., Sarg, J. F., Loutit, T. S., and J. Hardenbol, 1988, An overview of the fundamentals of sequence stratigraphy and key definitions, in Wilgus, C.K., et al., eds. Sea Level Changes: An Integrated Approach: SEPM, Spec. Publ. 42, p. 39-45.

Van Wagoner, J.C., Mitchum, R.M., Campion, K.M. and Rahmanian, V.D., 1990, Siliciclastic sequence stratigraphy in well logs, cores, and outcrops: concepts for

high-resolution correlation of time and facies: American Association of Petroleum Geologists Methods in Exploration Series, vol. 7, 55 p.

Van Siclen, D. C., 1958, Depositional topography—examples and theory: AAPG Bulletin v. 42, no. 8, p. 1897-1913.

Wardlaw, B.R., and V.I. Davydov, 2000. Preliminary Placement of the International Lower Permian Working Standard to the Glass Mountains, Texas: Permophiles, v. 36, p. 11-14.

Wilde, G. L., 1975, Fusulinid-defined Permian stages: West Texas Geological Society and Permian Basin Section, Society of Economic Paleontologists and Mineralogists Publication, v. 75, no. 65, p. 67-83.

Wilde, G. L., 1990, Practical fusulinid zonation: the species concept; with Permian Basin emphasis: West Texas Geological Society Bulletin, v. 29, no. 7, p. 5-34.

Wilde, G. L., 1990, Surface to Subsurface Structure and Stratigraphy of the Marathon Fold Belt, Brewster, Pecos, and Terrell Counties, Texas: WTGS and PBS-SEPM Field Seminar, May 10-12, 1990, p. 65-82.

Wilshire, H.G., Offield, T.W., Howard, K.A., Cummings, D., 1972, Geology of the Sierra Madera cryptoexplosion structure, Pecos County, Texas. U.S. Geological Survey Professional Paper, H1–H42.

Wilson, J. L., 1967, Cyclic and reciprocal sedimentation in Virgilian strata of southern New Mexico: Geological Society of America Bulletin, v. 78, no. 7, p. 805–818.

Wilson, J. L., 1975, Carbonate facies in geologic history: New York, Springer-Verlag, 471 p

Wuellner, D.E., Lehtonen, L.R., and W.C. James, 1986, Sedimentary-tectonic development of the Marathon and Val Verde basins, West Texas, USA: a Permo-Carboniferous migrating foredeep: Foreland Basins 8, p. 347-368.

Yang, K, and Dorobek, S.L., 1995, The Permian Basin of west Texas and New Mexico: Tectonic history of a “composite” foreland basin and its effects on stratigraphic development, *in* Dorobek, S.L. and Ross, G.M., eds., Stratigraphic evolution of foreland basins: SEPM (Society for Sedimentary Geology) Special Publication No. 52, p. 149-174, doi: 10.2110/pec.95.52.0149.

CHAPTER V

CONCLUSIONS

In describing over 2,000 feet (over 600 meters) of core data bed-by-bed, in conjunction with elemental data, this study was consistently able to differentiate between various populations of Wolfcamp Group mudstone facies, as well coarser sedimentary lithologies. At the bedset scale, these facies tend to cluster compositionally, and the Wolfcamp Group alternates between intervals which are more or less enriched in carbonate lithologies. These alternations were interpreted through a novel stratigraphic model which recognizes that, depending upon antecedent topography and on fluvial sediment availability, detrital carbonate production and/or delivery to the basin can actually be enhanced during sea level lowstands while siliceous intervals, when driven by productivity of siliceous radilaria, need not be associated with lowstands and fluvial input to the deep basin. Using this framework, four depositional sequences were interpreted across the two cores. Additional findings from the core data include the efficacy of nickel as proxy for TOC, the upward fining of carbonate lithologies through the Wolfcamp Group, and the quantification of the dimensions of detrital carbonate beds correlated between the cores.

Study of the Lower Wolfcamp (Neal Ranch Formation) outcrops in the Wolf Camp Hills resulted in the identification of four major sequence boundaries, each overlain by carbonate-clast conglomerates and interpreted to be the updip equivalent of lowstand wedges in the basin. The first and lowermost sequence boundary occurs below the Bursumian Gray Limestone Member, the second occurs at the base of the Permian

and the base of the Wolfcamp Group. The third is internal to the Lower Wolfcamp, while the fourth caps the Lower Wolfcamp (Neal Ranch Formation) and marks the onset of the Lenox Hills Formation. Two major flooding surfaces were also identified as part of two 3rd-order sequences interpreted for the Lower Wolfcamp in the Wolf Camp Hills. These sequences, overlain by prominent carbonate-clast conglomerates, are interpreted as reflecting relative sea level oscillations across a unique wedge-top depositional environment, itself a function of the antecedent topography controlled by the extreme proximity to the Ouachita-Marathon thrust front.

Finally, new correlations for the Wolfcamp Group correlate the relatively consistent basinal stratigraphy with the underdeveloped and structurally complex Southern Delaware Basin, complete with a tie to the Glass Mountains exposures. Delaware Basin is then correlated with the studied cores from Midland Basin using prominent flooding surfaces which are correlative through the comparatively shallow Sheffield Channel, rather than attempting to correlate the basinal strata across the dramatically uplifted Central Basin Platform. In aggregate, these correlations yield a unifying framework for Wolfcamp Group stratigraphy. This stratigraphic framework enables the extrapolation of absolute age data through the Wolfcamp Group. Finally, a structure map of Southern Delaware Basin shows a relatively steep depositional profile for the Wolfcamp Group adjacent to the Ouachita-Marathon thrust front, potentially supporting the aforementioned wedge-top depositional model interpreted in outcrop.

APPENDIX A

MEASURED SECTION LOCATIONS IN WOLF CAMP HILLS

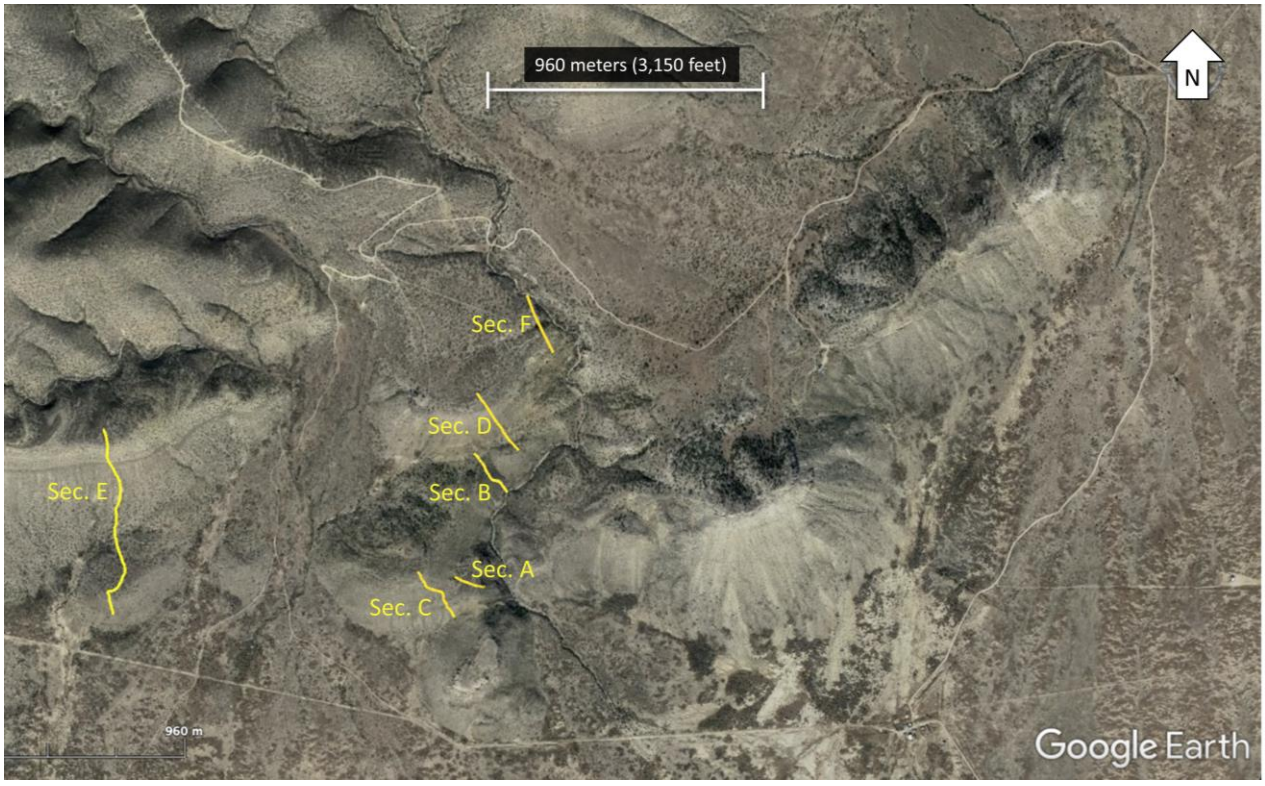

Location	Latitude	Longitude
Section A Base	30.35020	-103.13359
Section A Top	30.35003	-103.13372
Section B Base	30.35302	-103.13285
Section B Top	30.35350	-103.13380
Section C Base	30.34903	-103.13433
Section C Top	30.35040	-103.13590
Section D Base	30.35410	-103.13260
Section D Top	30.35566	-103.13380
Section E Base	30.34970	-103.14630
Section E Top	30.35460	-103.14751
Section F Base	30.35736	-103.13124
Section F Top	30.35908	-103.13224

APPENDIX B

WELL LOG TOPS PICKED FOR SUBSURFACE CORRELATIONS

UWI	Surface	MD
4249534016	Ln01sb	11510
4249534016	WC X SS	11539
4249534016	WC Y SS	11603
4249534016	W80sb	11775
4249534016	W50mfs	11796
4249534016	W30mfs	12270
4249533261	Ln01sb	11774
4249533261	W50mfs	12106
4249533261	W30mfs	12567
4249533261	W01mfs	13208
4249533261	Penn. 1	14246
4249533260	Ln01sb	11719
4249533260	WC X SS	11757
4249533260	WC Y SS	11831
4249533260	W80sb	12011
4249533260	W50mfs	12066
4249533260	W30mfs	12550
4249533260	W20mfs	13307
4249533260	W01mfs	13902
4249533260	W01sb	14025
4249533260	Penn. 1	14523
4249533040	W30mfs	12482
4249533040	W20mfs	13305
4249533040	W01mfs	13857
4249532996	W30mfs	12538
4249532996	W20mfs	13340
4249532996	W01mfs	14215
4249532864	Ln01sb	10925
4249532686	Ln01sb	11698
4249532686	W50mfs	12007
4249532686	W30mfs	12371
4249531442	Ln01sb	11747
4249531442	W50mfs	12040
4249531442	W30mfs	12470

UWI	Surface	MD
4237136246	Ln01sb	2026
4237136130	Ln01sb	5202
4237136130	Penn. 1	9283
4237136110	Ln01sb	7268
4237136110	W80mfs	7353
4237136110	W80sb	7546
4237136110	W50mfs	7613
4237136110	W30mfs	8223
4237136110	W20mfs	8630
4237136110	W01mfs	9163
4237136110	W50sb	7956
4237136110	W01sb	9597
4237136110	Penn. 1	11033
4237135908	Ln01sb	5679
4237135908	W01mfs	7279
4237135864	Ln01sb	10201
4237135619	Ln01sb	9506
4237135619	W50mfs	9954
4237135391	Ln01sb	7047
4237135391	W80mfs	7144
4237135391	W80sb	7318
4237135391	W50mfs	7370
4237135391	W30mfs	7604
4237135391	W20mfs	7971
4237135391	W01mfs	8537
4237135391	W01sb	8980
4237135391	Penn. 1	11592
4237135372	Ln01sb	5249
4237135372	Penn. 1	6443
4237135209	W30mfs	4877
4237135209	W01mfs	6396
4237135113	Ln01sb	6222
4237135078	Ln01sb	5960
4237135078	W50mfs	6329

4249531442	W01mfs	13203
4249530889	Ln01sb	11535
4249530889	W50mfs	11884
4249530889	W30mfs	12299
4249530889	W20mfs	12953
4249530889	W01mfs	13359
4249530889	Penn. 1	14116
4249530195	Ln01sb	11108
4249520231	Ln01sb	11433
4249520231	W50mfs	11841
4249520231	W30mfs	12371
4249520231	W20mfs	12745
4249520231	W01mfs	12996
4249520231	Penn. 1	13222
4247535053	Ln01sb	11495
4247535053	WC X SS	11553
4247535053	WC Y SS	11627
4247535053	W80sb	11960
4247535053	W50mfs	12021
4247535053	W30mfs	12489
4247535053	W20mfs	13444
4247535053	W01mfs	14184
4247535053	W01sb	14338
4247535053	Penn. 1	15071
4247533677	Ln01sb	10481
4247533527	Ln01sb	11344
4247533097	Ln01sb	9525
4247533097	W50mfs	9738
4247532690	Ln01sb	7301
4247532690	Penn. 1	8451
4247530965	Ln01sb	11054
4247530965	WC X SS	11107
4247530965	WC Y SS	11173
4247530965	W80sb	11528
4247530965	W50mfs	11658
4247530965	W30mfs	12257
4247530965	W20mfs	13255
4247530965	W01mfs	13856
4247530965	W01sb	14149
4247530965	Penn. 1	14714
4237135078	W30mfs	6885
4237135078	W20mfs	7210
4237135078	W01mfs	7455
4237135078	Penn. 1	8707
4237135076	Ln01sb	6242
4237135076	Penn. 1	6559
4237134962	Ln01sb	10099
4237134345	Ln01sb	9477
4237134252	Ln01sb	9360
4237134252	W80mfs	9465
4237134252	W80sb	9732
4237134252	W50mfs	9795
4237134252	W30mfs	10325
4237134252	W20mfs	10922
4237134252	W01mfs	11345
4237134252	W01sb	11618
4237134252	Penn. 1	11869
4237134213	Ln01sb	5601
4237134213	W50mfs	6156
4237134213	W30mfs	7054
4237134213	W20mfs	7829
4237134213	Penn. 1	8935
4237134132	Ln01sb	1850
4237133837	Ln01sb	9323
4237133837	W50mfs	9793
4237133837	W30mfs	10722
4237133837	W01mfs	11655
4237133837	Penn. 1	12596
4237133755	Ln01sb	9368
4237133755	W50mfs	10026
4237133755	W30mfs	10952
4237133755	W01mfs	11485
4237133755	W01mfs	12784
4237133685	Ln01sb	7818
4237133685	W50mfs	8052
4237133685	W30mfs	8489
4237133685	W20mfs	8992
4237133685	W01mfs	9334
4237133677	Ln01sb	7940
4237133677	W80mfs	8336

4247530937	Ln01sb	11162	4237133677	W50mfs	8555
4247530937	W50mfs	11424	4237133677	W30mfs	9549
4247530937	W30mfs	12053	4237133677	W20mfs	10078
4247530937	W01mfs	12793	4237133677	W01mfs	10294
4247530639	Ln01sb	11243	4237133677	Penn. 1	10652
4247530632	Ln01sb	11376	4237133669	Ln01sb	7901
4247530626	Ln01sb	10784	4237133669	W50mfs	8622
4247530617	Ln01sb	11122	4237133568	Ln01sb	8399
4247530617	W50mfs	11383	4237133568	W80mfs	8509
4247530617	W30mfs	11868	4237133568	W80sb	8728
4247530617	W20mfs	12463	4237133568	W50mfs	8802
4247530617	W01mfs	12598	4237133568	W30mfs	9388
4247530617	Penn. 1	12611	4237133568	W20mfs	9866
4247530605	Ln01sb	11365	4237133568	W01mfs	10310
4247530605	W50mfs	11850	4237133568	W01sb	10745
4247530605	W30mfs	12457	4237133568	Penn. 1	11139
4247530605	W01mfs	13252	4237133554	Ln01sb	8869
4247530593	Ln01sb	10790	4237133463	Ln01sb	7710
4247530593	W50mfs	11132	4237133463	W50mfs	8079
4247530593	W30mfs	11965	4237133463	W30mfs	8635
4247530593	W01mfs	12610	4237133463	W20mfs	9264
4247530584	Ln01sb	11238	4237133463	W01mfs	9746
4247530584	W50mfs	11578	4237133463	Penn. 1	10194
4247530584	W30mfs	12194	4237133395	Ln01sb	8886
4247530584	W01mfs	12854	4237133395	W50mfs	9445
4247530551	Ln01sb	10654	4237133395	W30mfs	9788
4247530551	W50mfs	11133	4237133395	W01mfs	10247
4247530551	W30mfs	11871	4237132990	Ln01sb	6635
4247530551	W01mfs	12383	4237132990	W50mfs	7069
4247530513	Ln01sb	11328	4237132928	Ln01sb	9531
4247530513	W50mfs	11626	4237132928	W50mfs	10019
4247530513	W30mfs	12141	4237132928	W30mfs	10936
4247530513	W01mfs	12843	4237132928	W20mfs	11370
4247530511	Ln01sb	10633	4237132928	W01mfs	11707
4247530511	W50mfs	11112	4237132928	Penn. 1	12695
4247530511	W30mfs	11789	4237132881	Ln01sb	7217
4247530511	W20mfs	12560	4237132881	W80mfs	7306
4247530511	W01mfs	13435	4237132881	W80sb	7813
4247530137	Ln01sb	11114	4237132881	W50mfs	8009
4247511138	Ln01sb	10991	4237132881	W30mfs	8706

4247511138	W50mfs	11513
4247511138	W30mfs	12745
4247511138	W01mfs	13969
4244531242	Ln01sb	9232
4244531021	Ln01sb	9336
4244331351	Ln01sb	5965
4244331351	W80mfs	6097
4244331351	W80sb	6262
4244331351	W50mfs	6353
4244331351	W30mfs	6559
4244331351	W20mfs	6852
4244331351	W01mfs	7234
4244331351	W50sb	6462
4244331351	W01sb	7425
4244331351	Penn. 1	8465
4244331349	Ln01sb	6259
4244331349	W50mfs	6731
4244331349	W30mfs	7136
4244331349	W20mfs	7365
4244331349	W01mfs	7764
4244331349	Penn. 1	8509
4244331345	Ln01sb	6306
4244331345	W80mfs	6423
4244331345	W50mfs	6745
4244331345	W30mfs	7183
4244331345	W20mfs	7380
4244331345	W01mfs	7660
4244331345	Penn. 1	8156
4244330999	Ln01sb	5957
4244330999	W80mfs	6239
4244330999	W50mfs	6443
4244330999	W30mfs	6804
4244330999	W01mfs	7294
4244330945	Ln01sb	6272
4244330945	W80mfs	6449
4244330945	W50mfs	6736
4244330945	W30mfs	7135
4244330945	W01mfs	7652
4244330908	Ln01sb	6099
4244330908	W80mfs	6316

4237132881	W20mfs	9444
4237132881	W01mfs	10146
4237132881	W50sb	8278
4237132881	W01sb	10414
4237132881	Penn. 1	11537
4237132876	Ln01sb	10376
4237132876	W50mfs	10663
4237132876	W30mfs	11514
4237132876	W01mfs	13212
4237132862	Ln01sb	6990
4237132862	W80mfs	7157
4237132862	W80sb	7489
4237132862	W50mfs	7639
4237132862	W30mfs	8077
4237132862	W20mfs	9006
4237132862	W01mfs	9655
4237132862	W50sb	7730
4237132862	W01sb	9857
4237132862	Penn. 1	11757
4237132812	Ln01sb	2901
4237132735	Ln01sb	8880
4237132735	W50mfs	9065
4237132735	W30mfs	9212
4237132735	W20mfs	9329
4237132735	W01mfs	9475
4237132733	Ln01sb	9711
4237132733	W50mfs	10142
4237132733	W30mfs	11140
4237132733	W20mfs	11809
4237132733	W01mfs	12592
4237132733	Penn. 1	12590
4237132727	Ln01sb	6211
4237132695	Ln01sb	2270
4237132695	W50sb	3528
4237132682	Ln01sb	9671
4237132682	W50mfs	10515
4237132682	W30mfs	11307
4237132682	W20mfs	11952
4237132666	Ln01sb	2405
4237132666	W50mfs	3373

4244330908	W50mfs	6481
4244330908	W30mfs	6863
4244330908	W01mfs	7371
4244330905	Ln01sb	6073
4244330905	W50mfs	6524
4244330905	W30mfs	6915
4244330905	W01mfs	7497
4244330471	W01mfs	7841
4244330068	Ln01sb	5576
4244330025	Ln01sb	6325
4244330025	W80mfs	6542
4244330025	W50mfs	6655
4244330025	W30mfs	7102
4244330025	W01mfs	7536
4244330025	Penn. 1	8039
4244330017	Ln01sb	6117
4244330017	W80mfs	6199
4244330017	W80sb	6303
4244330017	W50mfs	6466
4244330017	W30mfs	6748
4244330017	W20mfs	6951
4244330017	W01mfs	7300
4244330017	W50sb	6588
4244330017	W01sb	7482
4244330017	Penn. 1	7835
4244330009	Ln01sb	6306
4244330009	W50mfs	6753
4244330009	W30mfs	7113
4244330009	W01mfs	7625
4244330009	Penn. 1	8146
4244310020	Ln01sb	5922
4244310020	W50mfs	6529
4244310020	W30mfs	7024
4244310020	W01mfs	8118
4244310020	Penn. 1	9317
4244300055	Ln01sb	5798
4244300055	W50mfs	6245
4244300055	W30mfs	6626
4244300055	W20mfs	6860
4244300055	W01mfs	7224

4237132660	Ln01sb	7643
4237132640	Ln01sb	7462
4237132640	W50mfs	8243
4237132640	W30mfs	9415
4237132640	W20mfs	10092
4237132640	W01mfs	10540
4237132640	Penn. 1	10704
4237132623	Ln01sb	7358
4237132623	W50mfs	7783
4237132623	W30mfs	8450
4237132623	W20mfs	8939
4237132623	W01mfs	9726
4237132623	Penn. 1	10252
4237132606	Ln01sb	2128
4237132600	Ln01sb	4118
4237132529	Ln01sb	6440
4237132529	Ln01sb	6526
4237132513	W80mfs	3256
4237132504	Ln01sb	7695
4237132504	W50mfs	8062
4237132504	W30mfs	8578
4237132504	W20mfs	9578
4237132504	W01mfs	10857
4237132480	Ln01sb	9599
4237132468	Ln01sb	7787
4237132468	W50mfs	8356
4237132450	Ln01sb	10241
4237132436	Ln01sb	6958
4237132436	W50mfs	7806
4237132436	W30mfs	8817
4237132436	W01mfs	10348
4237132433	Ln01sb	10204
4237132433	W50mfs	10395
4237132433	W30mfs	11687
4237132423	Ln01sb	5798
4237132418	Ln01sb	5077
4237132418	W50mfs	5336
4237132418	W30mfs	5709
4237132418	W20mfs	6047
4237132418	Penn. 1	6212

4244300055	Penn. 1	8436
4244300023	Ln01sb	5911
4244300023	W50mfs	6476
4244300023	W30mfs	6797
4244300023	W20mfs	7066
4244300023	W01mfs	7378
4244300023	Penn. 1	8733
4238935371	Ln01sb	10373
4238935371	W50mfs	11066
4238935371	Penn. 1	15613
4238935175	Ln01sb	8919
4238935066	Ln01sb	10539
4238934991	Ln01sb	10759
4238934991	W80mfs	11696
4238934693	Ln01sb	10047
4238934629	Ln01sb	10575
4238934629	W50mfs	10854
4238934254	Ln01sb	10233
4238934117	Ln01sb	10412
4238934070	Ln01sb	10463
4238934001	Ln01sb	10221
4238934001	W30mfs	10528
4238933926	Ln01sb	10533
4238933926	W50mfs	10813
4238933926	W30mfs	11221
4238933926	W01mfs	11594
4238933848	Ln01sb	10402
4238933848	W50mfs	10684
4238933747	Ln01sb	10496
4238933747	W50mfs	10785
4238933747	W30mfs	11093
4238933747	W01mfs	11518
4238933725	Ln01sb	9684
4238933725	W50mfs	10074
4238933708	Ln01sb	10464
4238933708	W50mfs	10757
4238933708	W30mfs	11061
4238933708	W01mfs	11404
4238933657	Ln01sb	10521
4238933657	W50mfs	10803

4237132401	Ln01sb	6289
4237132401	W50mfs	7462
4237132401	W30mfs	8516
4237132401	W20mfs	9884
4237132401	Penn. 1	10533
4237132310	W80mfs	3443
4237131880	Ln01sb	9445
4237131880	W50mfs	9851
4237131853	Ln01sb	6541
4237131837	Ln01sb	3994
4237131833	Ln01sb	10152
4237131782	Ln01sb	6624
4237131782	W80mfs	6756
4237131782	W80sb	6949
4237131782	W50mfs	7081
4237131782	W30mfs	7484
4237131782	W20mfs	7861
4237131782	W01mfs	8261
4237131782	W50sb	7251
4237131782	W01sb	8366
4237131782	Penn. 1	9349
4237131778	Ln01sb	9838
4237131778	W50mfs	10064
4237131778	W30mfs	11087
4237131777	Ln01sb	5249
4237131766	Ln01sb	6644
4237131766	Penn. 1	7065
4237131764	Ln01sb	9603
4237131764	W80mfs	9664
4237131764	W50mfs	9863
4237131764	W30mfs	11148
4237131751	Ln01sb	9555
4237131751	W50mfs	9849
4237131748	Ln01sb	4058
4237131736	Ln01sb	9146
4237131692	Ln01sb	9411
4237131692	W50mfs	9740
4237131684	Ln01sb	5505
4237131684	W50mfs	6552
4237131684	W30mfs	7837

4238933657	W30mfs	11100	4237131684	W20mfs	9341
4238933657	W01mfs	11512	4237131684	Penn. 1	10294
4238933627	Ln01sb	10555	4237131626	Ln01sb	5543
4238933627	W50mfs	10963	4237131626	W50mfs	6570
4238933627	W30mfs	11648	4237131626	W30mfs	7930
4238933627	W20mfs	12334	4237131626	W20mfs	9414
4238933627	W01mfs	13072	4237131626	Penn. 1	10327
4238933592	Ln01sb	10508	4237131620	Ln01sb	4994
4238933558	Ln01sb	10527	4237131620	W50mfs	5320
4238933558	W50mfs	10767	4237131620	W30mfs	6492
4238933558	W30mfs	11068	4237131620	W01mfs	7667
4238933558	W20mfs	11446	4237131620	Penn. 1	8341
4238933558	W01mfs	11600	4237131611	Ln01sb	9382
4238933424	Ln01sb	10271	4237131611	W50mfs	9962
4238933424	W50mfs	10555	4237131610	Ln01sb	7558
4238933424	W30mfs	10783	4237131610	W50mfs	7979
4238933419	Ln01sb	11390	4237131610	W30mfs	8543
4238933332	Ln01sb	10632	4237131610	W20mfs	8946
4238933332	W50mfs	10884	4237131610	W01mfs	10146
4238933332	W30mfs	11030	4237131600	Ln01sb	10047
4238933332	W01mfs	11261	4237131581	Ln01sb	3960
4238933293	Ln01sb	10569	4237131544	Ln01sb	9235
4238933173	Ln01sb	10737	4237131411	Ln01sb	5341
4238932880	Ln01sb	9081	4237131394	Ln01sb	8155
4238932867	Ln01sb	10252	4237131394	W50mfs	8546
4238932867	W50mfs	10536	4237131394	W30mfs	13475
4238932867	W30mfs	10851	4237131394	Penn. 1	10727
4238932867	W01mfs	11202	4237131361	Ln01sb	6015
4238932812	Ln01sb	10422	4237131361	W80mfs	6086
4238932802	Ln01sb	10421	4237131361	W80sb	6207
4238932726	Ln01sb	10555	4237131361	W50mfs	6307
4238932658	Ln01sb	10224	4237131361	W30mfs	6758
4238932658	W50mfs	10606	4237131361	W20mfs	7088
4238932658	W01mfs	11621	4237131361	W01mfs	7443
4238932658	W01mfs	11621	4237131361	W50sb	6581
4238932637	Ln01sb	10030	4237131361	W01sb	7575
4238932608	Ln01sb	9813	4237131361	Penn. 1	8734
4238932608	W50mfs	10231	4237131295	Ln01sb	4551
4238932608	W30mfs	10716	4237131295	W50mfs	4801
4238932608	W01mfs	12093	4237131295	W30mfs	5769

4238932604	Ln01sb	9797
4238932604	W50mfs	10372
4238932604	W30mfs	10812
4238932604	W20mfs	11354
4238932604	W01mfs	12110
4238932604	Penn. 1	13126
4238932572	Ln01sb	10333
4238932572	W80mfs	10443
4238932572	W80sb	10682
4238932572	W50mfs	10933
4238932572	W30mfs	11387
4238932572	W20mfs	12129
4238932572	W01mfs	12735
4238932572	W01sb	13305
4238932572	Penn. 1	13818
4238932567	Ln01sb	9656
4238932567	W50mfs	10272
4238932567	W30mfs	11005
4238932567	W20mfs	11400
4238932567	W01mfs	11637
4238932567	Penn. 1	12450
4238932553	Ln01sb	10538
4238932553	WC X SS	10577
4238932553	WC Y SS	10664
4238932553	W80sb	10994
4238932553	W50mfs	11124
4238932553	W30mfs	11726
4238932553	W20mfs	12607
4238932553	W01mfs	13268
4238932553	W01sb	13720
4238932553	Penn. 1	14278
4238932548	Ln01sb	10275
4238932548	WC X SS	10300
4238932548	W80mfs	10411
4238932548	W80sb	10845
4238932548	W50mfs	10788
4238932548	W30mfs	11355
4238932548	W20mfs	12232
4238932548	W01mfs	12956
4238932548	W01sb	13512
4237131295	Penn. 1	7292
4237131236	Ln01sb	10198
4237131222	Ln01sb	3863
4237131197	Ln01sb	7212
4237131197	W01mfs	11035
4237131061	Penn. 1	9867
4237131017	Ln01sb	5694
4237131017	W01mfs	10456
4237131017	Penn. 1	12184
4237130997	Ln01sb	6090
4237130997	W50mfs	6810
4237130997	W30mfs	8068
4237130997	W20mfs	10477
4237130997	W01mfs	11552
4237130981	Ln01sb	9379
4237130974	Ln01sb	6627
4237130967	Ln01sb	4014
4237130959	Ln01sb	5149
4237130959	W50mfs	6032
4237130959	W30mfs	7764
4237130959	Penn. 1	10264
4237130940	Ln01sb	7808
4237130940	W50mfs	8028
4237130940	W30mfs	8375
4237130940	W20mfs	8886
4237130940	W01mfs	10317
4237130873	Ln01sb	8149
4237130873	W50mfs	8646
4237130873	W30mfs	9386
4237130873	W01mfs	10605
4237130873	Penn. 1	11536
4237130872	Ln01sb	5608
4237130872	Penn. 1	10666
4237130857	Ln01sb	6826
4237130852	Ln01sb	3907
4237130795	Ln01sb	4999
4237130794	Ln01sb	7115
4237130658	Ln01sb	5487
4237130658	W50mfs	5642
4237130658	W30mfs	6207

4238932548	Penn. 1	14128
4238932520	Ln01sb	10227
4238932517	Ln01sb	9674
4238932517	W01mfs	12643
4238932509	Ln01sb	8221
4238932436	Ln01sb	10064
4238932436	WC X SS	10103
4238932436	WC Y SS	10192
4238932436	W80sb	10433
4238932436	W50mfs	10520
4238932436	W30mfs	10982
4238932436	W20mfs	11580
4238932436	W01mfs	12494
4238932436	W01sb	12725
4238932436	Penn. 1	13690
4238932388	Ln01sb	9585
4238932235	Ln01sb	9756
4238932235	W50mfs	10400
4238932235	W30mfs	10952
4238932235	W01mfs	11754
4238932235	Penn. 1	12589
4238932225	Ln01sb	9447
4238932225	W50mfs	9759
4238932225	W30mfs	10181
4238932225	Penn. 1	10806
4238932213	Ln01sb	9311
4238932213	W01mfs	12040
4238932206	Ln01sb	9134
4238932206	WC X SS	9182
4238932206	WC Y SS	9273
4238932206	W80sb	9495
4238932206	W50mfs	9573
4238932206	W30mfs	10052
4238932206	W20mfs	10562
4238932206	W01mfs	10997
4238932206	W01sb	11257
4238932206	Penn. 1	11575
4238932200	Ln01sb	9274
4238932024	Ln01sb	10039
4238932024	W50mfs	10339
4237130658	W20mfs	6741
4237130658	W01mfs	7639
4237130658	Penn. 1	10053
4237130645	Ln01sb	6665
4237130645	W50mfs	7136
4237130505	Ln01sb	9408
4237130505	W01mfs	12262
4237130503	Penn. 1	5854
4237130480	Ln01sb	9979
4237130480	W30mfs	11622
4237130480	W01mfs	12695
4237130443	Ln01sb	8537
4237130388	Ln01sb	9298
4237130327	Ln01sb	9518
4237130327	W50mfs	10013
4237130327	W30mfs	10707
4237130327	W01mfs	11870
4237130327	Penn. 1	12677
4237130312	Ln01sb	4938
4237130298	W50mfs	10969
4237130298	W30mfs	11677
4237130298	W01mfs	13943
4237130271	Ln01sb	7535
4237130271	W80mfs	7658
4237130271	W80sb	7819
4237130271	W50mfs	7938
4237130271	W30mfs	8563
4237130271	W20mfs	9038
4237130271	W01mfs	9468
4237130271	W50sb	8387
4237130271	W01sb	9881
4237130271	Penn. 1	10906
4237130251	Ln01sb	6806
4237130235	Ln01sb	6959
4237130235	W50mfs	7966
4237130235	W30mfs	9173
4237130144	Ln01sb	9395
4237130144	W50mfs	9884
4237120329	Ln01sb	10093
4237120148	Ln01sb	7892

4238932024	W30mfs	10886
4238932024	W01mfs	11010
4238931670	Ln01sb	9686
4238931670	W50mfs	10094
4238931670	W30mfs	10675
4238931670	W20mfs	11248
4238931670	W01mfs	11596
4238931669	Ln01sb	9873
4238931669	W50mfs	10505
4238931669	W30mfs	10888
4238931669	W30mfs	10900
4238931669	W01mfs	12017
4238931557	Ln01sb	8589
4238931557	W50mfs	8789
4238931295	Ln01sb	10722
4238931295	W50mfs	11528
4238931295	W30mfs	12387
4238931295	W01mfs	13281
4238931231	Ln01sb	10469
4238931231	WC X SS	10507
4238931231	WC Y SS	10593
4238931231	W80sb	10865
4238931231	W50mfs	11064
4238931231	W30mfs	11650
4238931231	W20mfs	12375
4238931231	W01mfs	13175
4238931231	W01sb	13460
4238931231	Penn. 1	14124
4238931175	Ln01sb	9246
4238931175	W50mfs	9619
4238931175	W30mfs	10027
4238931175	W20mfs	10349
4238931175	W01mfs	10774
4238931175	Penn. 1	11486
4238931058	Ln01sb	9844
4238931058	W50mfs	10260
4238931058	W30mfs	10941
4238931058	W20mfs	11805
4238931058	W01mfs	11566
4238931058	Penn. 1	12426
4237120148	Penn. 1	13747
4237120089	Ln01sb	8605
4237111374	Ln01sb	9697
4237111374	W50mfs	10062
4237111343	Ln01sb	4837
4237111343	W50mfs	5028
4237111343	W30mfs	5306
4237111343	W01mfs	5991
4237111343	Penn. 1	9333
4237111342	Ln01sb	6602
4237111342	W50mfs	7526
4237111342	W30mfs	8663
4237111342	W01mfs	11015
4237111188	Ln01sb	7577
4237111121	Ln01sb	9109
4237111098	Ln01sb	7798
4237111098	W50mfs	8044
4237111098	W30mfs	8439
4237111098	W20mfs	8899
4237111098	W01mfs	10377
4237110966	Ln01sb	9466
4237110966	W50mfs	9935
4237110966	W30mfs	10587
4237110966	W01mfs	11501
4237110966	Penn. 1	12413
4237110931	Ln01sb	7923
4237110931	W50mfs	8134
4237110931	W30mfs	8534
4237110931	W20mfs	9220
4237110931	W01mfs	10480
4237110929	Ln01sb	7107
4237110922	Ln01sb	10007
4237110907	Ln01sb	8482
4237110882	Ln01sb	9143
4237110882	W50mfs	9602
4237110882	W30mfs	10352
4237110882	W01mfs	11321
4237110882	Penn. 1	11913
4237110863	Ln01sb	10068
4237110836	Ln01sb	6629

4238930905	Ln01sb	10482
4238930905	WC X SS	10525
4238930905	WC Y SS	10600
4238930905	W80sb	10923
4238930905	W50mfs	11086
4238930905	W30mfs	11628
4238930905	W20mfs	12683
4238930905	W01mfs	13312
4238930905	W01sb	13572
4238930905	Penn. 1	14332
4238930507	Ln01sb	10978
4238930507	W50mfs	11573
4238930507	W30mfs	12328
4238930507	W20mfs	13172
4238930507	W01mfs	14130
4238930507	Penn. 1	15062
4238930476	Ln01sb	10435
4238930476	WC X SS	10481
4238930476	WC Y SS	10548
4238930476	W80mfs	10587
4238930476	W80sb	10830
4238930476	W50mfs	10922
4238930476	W30mfs	11516
4238930476	W20mfs	12446
4238930476	W01mfs	13165
4238930476	W01sb	13538
4238930476	Penn. 1	14268
4238930392	Ln01sb	10791
4238930384	Ln01sb	10442
4238930384	W50mfs	10919
4238930384	W30mfs	11621
4238930384	W20mfs	12662
4238930384	W01mfs	13373
4238930384	Penn. 1	14413
4238930382	Ln01sb	9737
4238930382	W80mfs	9847
4238930382	W80sb	10060
4238930382	W50mfs	10296
4238930382	W30mfs	10732
4238930382	W20mfs	11448

4237110836	W50mfs	6963
4237110836	Penn. 1	8165
4237110752	Ln01sb	9302
4237110729	Ln01sb	7235
4237110729	Penn. 1	7334
4237110689	Ln01sb	9354
4237110689	W50mfs	9727
4237110689	W30mfs	10477
4237110689	W01mfs	11425
4237110689	Penn. 1	12186
4237110686	Ln01sb	9467
4237110686	W50mfs	9710
4237110686	W30mfs	11220
4237110686	W01mfs	15534
4237110684	Ln01sb	6223
4237110664	Ln01sb	8331
4237110664	W50mfs	8819
4237110664	W30mfs	9704
4237110662	Ln01sb	7635
4237110662	W80mfs	7750
4237110662	W80sb	8231
4237110662	W50mfs	8349
4237110662	W30mfs	8836
4237110662	W20mfs	9360
4237110662	W01mfs	9814
4237110662	W50sb	8644
4237110662	W01sb	10146
4237110662	Penn. 1	11337
4237110659	Ln01sb	10050
4237110659	W50mfs	10437
4237110659	W30mfs	11140
4237110659	W01mfs	12068
4237110659	Penn. 1	12922
4237110520	Ln01sb	10043
4237110520	W50mfs	10418
4237110520	W30mfs	11189
4237110520	W01mfs	12105
4237110520	Penn. 1	13386
4237110464	Ln01sb	7451
4237110464	W50mfs	8048

4238930382	W01mfs	11989
4238930382	W01sb	12514
4238930382	Penn. 1	13002
4238930261	Ln01sb	9651
4238930261	WC X SS	9699
4238930261	WC Y SS	9777
4238930261	W80sb	9994
4238930261	W50mfs	10102
4238930261	W30mfs	10542
4238930261	W20mfs	11031
4238930261	W01mfs	11764
4238930261	W01sb	12043
4238930261	Penn. 1	12690
4238930191	Ln01sb	9925
4238930191	W50mfs	10252
4238930191	W30mfs	10782
4238930191	W20mfs	11877
4238930191	W01mfs	11414
4238930191	Penn. 1	12610
4238930088	Ln01sb	10908
4238930081	Ln01sb	9951
4238920042	Ln01sb	10333
4238920042	W50mfs	10639
4238920042	W30mfs	11800
4238920042	W01mfs	13531
4238910530	Ln01sb	10362
4238910530	W50mfs	10723
4238910530	W30mfs	11425
4238910530	W20mfs	12286
4238910530	W01mfs	12913
4238910530	Penn. 1	14386
4238910496	Ln01sb	10333
4238910496	W50mfs	10819
4238910458	Ln01sb	10405
4238910458	W80mfs	10432
4238910458	W50mfs	10697
4238910458	W30mfs	11211
4238910458	W20mfs	11911
4238910458	W01mfs	12272
4238910458	Penn. 1	12272
4237110464	W30mfs	8599
4237110464	W20mfs	9415
4237110464	Penn. 1	10496
4237110422	Ln01sb	7191
4237110333	Ln01sb	9475
4237110333	W50mfs	9807
4237110333	W30mfs	10411
4237110333	W01mfs	11796
4237110213	Ln01sb	6607
4237110139	Ln01sb	9302
4237110139	W50mfs	9781
4237110139	W30mfs	10323
4237110139	W01mfs	11510
4237110139	Penn. 1	12110
4237110137	Ln01sb	9752
4237110137	W80mfs	9836
4237110137	W80sb	10088
4237110137	W50mfs	10185
4237110137	W30mfs	10728
4237110137	W20mfs	11453
4237110137	W01mfs	11898
4237110137	W01sb	12297
4237110137	Penn. 1	12548
4237105736	Ln01sb	10316
4237104844	Ln01sb	7753
4237104442	Ln01sb	6650
4237104442	W50mfs	7058
4237104442	W30mfs	7629
4237104442	W01mfs	8387
4237104442	Penn. 1	9393
4237104440	Ln01sb	5724
4237104440	W50mfs	6245
4237104440	W30mfs	7034
4237104440	W20mfs	7932
4237104440	W01mfs	8268
4237104440	Penn. 1	9069
4237104418	Ln01sb	5121
4237104418	Penn. 1	6363
4237104415	Ln01sb	5694
4237104415	W50mfs	6209

4238910234	Ln01sb	10326	4237104415	W30mfs	7237
4238910099	Ln01sb	10296	4237104415	W20mfs	8050
4238910099	WC X SS	10315	4237104415	Penn. 1	8988
4238910099	W80mfs	10394	4237104302	Ln01sb	5313
4238910099	W80sb	10763	4237103874	Ln01sb	8249
4238910099	W50mfs	10849	4237103813	Ln01sb	5131
4238910099	W30mfs	11377	4237103784	Ln01sb	5244
4238910099	W20mfs	12171	4237103784	W50mfs	6014
4238910099	W01mfs	12833	4237103784	W30mfs	7394
4238910099	W01sb	13451	4237103750	Ln01sb	7713
4238910099	Penn. 1	14405	4237103650	Ln01sb	5489
4238910084	Ln01sb	7905	4237103650	W50mfs	5832
4238910084	W50mfs	8474	4237103650	W30mfs	6874
4238910084	W30mfs	8922	4237103650	W01mfs	7728
4238910084	W01mfs	9143	4237103650	Penn. 1	9208
4238901128	Ln01sb	9379	4237103603	Ln01sb	7004
4238901128	W50mfs	9999	4237103603	Penn. 1	16425
4238901128	W30mfs	10583	4237103037	Ln01sb	5106
4238901128	W01mfs	10983	4237103037	W50mfs	5894
4238901128	Penn. 1	11321	4237103037	W30mfs	7203
4238900905	Ln01sb	7128	4237103037	Penn. 1	10146
4238900546	Ln01sb	9277	4237102821	Ln01sb	3951
4238900546	W50mfs	9846	4237102819	Ln01sb	7306
4238900546	W30mfs	10280	4237102819	W01mfs	9305
4238900546	Penn. 1	10749	4237102819	Penn. 1	11128
4238900418	Ln01sb	10005	4237102816	Ln01sb	6507
4238900418	W80mfs	10094	4237102813	Ln01sb	5226
4238900418	W80sb	10276	4237102813	Ln01sb	5228
4238900418	W50mfs	10538	4237102812	Ln01sb	6351
4238900418	W30mfs	11072	4237102812	W50mfs	7470
4238900418	W20mfs	11717	4237102812	W30mfs	8772
4238900418	W01mfs	12231	4237102812	W01mfs	11238
4238900418	W01sb	12740	4237102515	Ln01sb	5864
4238900418	Penn. 1	13154	4237102443	Ln01sb	5202
4238900375	Ln01sb	10367	4237102439	Ln01sb	6507
4238900375	W80mfs	10438	4237102439	W50mfs	6906
4238900375	W50mfs	10625	4237102439	W30mfs	7479
4238900375	W30mfs	11687	4237102439	W20mfs	8009
4238900375	W01mfs	12439	4237102439	W01mfs	8347
4238339293	Ln01sb	8086	4237102439	Penn. 1	9398

4238339293	W50mfs	8390
4238339293	W50mfs	8394
4238338629	Ln01sb	8069
4238338629	W50mfs	8452
4238338629	W30mfs	8917
4238338280	Ln01sb	6853
4238338280	W80mfs	6956
4238338280	W80sb	7168
4238338280	W50mfs	7270
4238338280	W30mfs	7507
4238338280	W20mfs	7880
4238338280	W01mfs	8144
4238338280	W50sb	7419
4238338280	W01sb	8465
4238338280	Penn. 1	8600
4238338226	Ln01sb	7415
4238338226	W80mfs	7522
4238338226	W80ts	7576
4238338226	W80sb	7754
4238338226	W50mfs	7863
4238338226	W50ts	7933
4238338226	W30mfs	8095
4238338226	W30sb	8427
4238338226	W20mfs	8492
4238338226	W20sb	8579
4238338226	W01mfs	8749
4238338226	W50sb	8013
4238338226	W30ts	8188
4238338226	W20ts	8547
4238338226	W01ts	8863
4238338226	W01sb	9158
4238338226	Penn. 1	9256
4238338223	Ln01sb	7962
4238338223	W50mfs	8413
4238338223	W30mfs	8925
4238338223	W20mfs	9298
4238338223	W01mfs	9515
4238338223	Penn. 1	9750
4238338086	Ln01sb	7715
4238337491	Ln01sb	7183
4237102155	W01mfs	7921
4237102153	Ln01sb	6439
4237102153	W50mfs	6903
4237102153	W30mfs	7567
4237102153	W01mfs	8278
4237102153	Penn. 1	9339
4237100369	Ln01sb	9750
4237100369	W50mfs	10224
4237100369	W30mfs	11726
4237100363	Ln01sb	9548
4237100363	W50mfs	10100
4237100363	W30mfs	11077
4237100363	W20mfs	11521
4237100363	W01mfs	11841
4237100363	Penn. 1	12437
4237100361	Ln01sb	9606
4237100361	W50mfs	10081
4237100361	W30mfs	10561
4237100361	W20mfs	10943
4237100361	W01mfs	11912
4237100361	Penn. 1	12959
4232935643	Ln01sb	9284
4232935216	Ln01sb	8756
4232935216	W50mfs	9117
4232935216	W30mfs	9555
4232935216	W01mfs	9837
4232935097	Ln01sb	9316
4232934715	Ln01sb	8477
4232934715	W50mfs	8864
4232934715	W30mfs	9359
4232934715	W01mfs	9671
4232931988	Ln01sb	9205
4231740190	Ln01sb	9753
4231739550	Ln01sb	9584
4231739342	Ln01sb	9782
4231739193	Ln01sb	9248
4231734762	Ln01sb	9529
4231734658	Ln01sb	9546
4231733913	Ln01sb	9229
4230530516	Ln01sb	8849

4238337491	W50mfs	7526
4238337491	W30mfs	7904
4238337491	W20mfs	8229
4238337491	W01mfs	8533
4238337491	Penn. 1	9184
4238336145	Ln01sb	8182
4238336145	W50mfs	8500
4238336145	W30mfs	9038
4238336145	W01mfs	9333
4238335872	Ln01sb	7123
4238335872	W50mfs	7409
4238335872	W30mfs	7840
4238335872	W20mfs	8082
4238335872	W01mfs	8343
4238335872	Penn. 1	8825
4238335557	Ln01sb	7197
4238335557	W50mfs	7546
4238335557	W30mfs	7958
4238335557	W01mfs	8192
4238334801	Ln01sb	7083
4238334801	W80mfs	7180
4238334801	W80sb	7369
4238334801	W50mfs	7444
4238334801	W30mfs	7698
4238334801	W20mfs	7993
4238334801	W01mfs	8235
4238334801	W50sb	7636
4238334801	W01sb	8426
4238334801	Penn. 1	8482
4238334799	Ln01sb	6992
4238334799	W50mfs	7315
4238334799	W30mfs	7608
4238334799	W20mfs	8104
4238334799	Penn. 1	8305
4238333796	Ln01sb	7598
4238333796	W50mfs	7902
4238333796	W30mfs	8250
4238333796	W20mfs	8541
4238333796	W01mfs	8814
4238333796	Penn. 1	9191

4230530516	W01mfs	9448
4230530467	Ln01sb	8754
4230530467	W01mfs	9430
4230530457	Ln01sb	8771
4230530457	W01mfs	9409
4230530456	Ln01sb	8580
4230530456	W01mfs	9274
4230530455	Ln01sb	8627
4230530455	W01mfs	9265
4230530452	Ln01sb	8635
4230530452	W01mfs	9284
4230131374	Ln01sb	11505
4230131374	WC X SS	11545
4230131374	WC Y SS	11619
4230131374	W50mfs	11873
4230131325	Ln01sb	11999
4230131270	Ln01sb	11627
4230131269	Ln01sb	11509
4230131269	W50mfs	11799
4230131269	W30mfs	12412
4230131269	W01mfs	13078
4230131224	Ln01sb	10659
4230131224	W50mfs	11243
4230131223	Ln01sb	11706
4230131223	W50mfs	12155
4230131223	W30mfs	12593
4230131223	W20mfs	13298
4230131223	Penn. 1	13991
4230131185	Ln01sb	11418
4230131185	W50mfs	11729
4230131185	W30mfs	12301
4230131185	W01mfs	12983
4230131169	Ln01sb	11367
4230131169	W50mfs	11731
4230131169	W30mfs	12475
4230131169	W01mfs	13525
4230130356	Ln01sb	11543
4230130356	WC X SS	11582
4230130356	WC Y SS	11651
4230130356	W80sb	11991

4238332006	Ln01sb	8030
4238332006	W80mfs	8169
4238332006	W80sb	8409
4238332006	W50mfs	8487
4238332006	W30mfs	8739
4238332006	W01mfs	9263
4238332006	W01sb	9451
4238332006	Penn. 1	9732
4238310104	Ln01sb	7629
4238310104	W50mfs	7960
4238310104	W30mfs	8302
4238310104	Penn. 1	8515
4238301721	Ln01sb	6909
4238301721	W50mfs	7215
4238301721	W30mfs	7610
4238301721	W20mfs	7966
4238301721	Penn. 1	8322
4238301716	Ln01sb	6855
4238301716	W50mfs	7185
4238301716	W30mfs	7567
4238301716	W20mfs	7797
4238301716	W01mfs	8248
4238301716	Penn. 1	8257
4237183181	Ln01sb	5653
4237183181	W50mfs	6634
4237183181	W30mfs	7771
4237183181	W01mfs	11324
4237183111	Ln01sb	7387
4237170836	Ln01sb	5533
4237170836	Penn. 1	10926
4237170827	Ln01sb	5112
4237170827	Penn. 1	12755
4237139387	Ln01sb	6333
4237139387	Penn. 1	10035
4237139383	Ln01sb	5602
4237139315	Ln01sb	7919
4237139306	Ln01sb	7519
4237139306	W50mfs	7906
4237139306	W30mfs	8279
4237139306	W20mfs	9117
4230130356	W50mfs	12051
4230130356	W30mfs	12535
4230130356	W20mfs	13475
4230130356	W01mfs	14063
4230130356	W01sb	14187
4230130356	Penn. 1	14808
4230130045	Ln01sb	10540
4230130020	Ln01sb	10937
4230110170	Ln01sb	12972
4224330101	Ln01sb	8307
4224300015	Ln01sb	5484
4224300015	W50sb	5740
4224300015	Penn. 1	6335
4217337266	Ln01sb	9234
4216536674	Ln01sb	9806
4216536674	W50mfs	10223
4216535905	Ln01sb	9090
4216533544	Ln01sb	9944
4216533544	W50mfs	10369
4210932538	Ln01sb	9288
4210932367	Ln01sb	8232
4210932367	WC X SS	8262
4210932367	WC Y SS	8334
4210932367	W80sb	8617
4210932367	W50mfs	8679
4210932367	W30mfs	8977
4210932367	W20mfs	9225
4210932367	W01mfs	9734
4210932367	W01sb	9929
4210932367	Penn. 1	10403
4210932346	Ln01sb	7776
4210932346	Penn. 1	10128
4210932287	Ln01sb	6393
4210932278	Ln01sb	6405
4210932271	Ln01sb	3998
4210932271	W50mfs	4302
4210932271	W30mfs	4563
4210932271	W01mfs	5127
4210932271	Penn. 1	6030
4210932255	Ln01sb	7627

4237139301	Ln01sb	7521	4210932255	W50mfs	8678
4237139288	Ln01sb	6303	4210932255	W30mfs	9528
4237139238	Ln01sb	7600	4210932252	Ln01sb	7052
4237139238	W50mfs	8774	4210932252	W50mfs	7642
4237139236	Ln01sb	7797	4210932252	W30mfs	8171
4237139229	Ln01sb	7452	4210932252	W01mfs	8441
4237139229	W50mfs	7804	4210931362	Ln01sb	10460
4237139229	W30mfs	8103	4210931362	W50mfs	10833
4237139229	W20mfs	8455	4210931362	Penn. 1	13368
4237139223	Ln01sb	7473	4210931359	Ln01sb	7745
4237139223	W50mfs	7755	4210931359	Penn. 1	10766
4237139223	W30mfs	8146	4210900289	Ln01sb	4907
4237139223	W20mfs	8528	4210900182	Ln01sb	6814
4237139223	W01mfs	8568	4210900182	W50mfs	7000
4237139210	Ln01sb	5045	4210900182	W30mfs	7391
4237139210	W50mfs	5430	4210900182	W01mfs	7805
4237139210	W30mfs	5994	4210542111	Ln01sb	5523
4237139210	W20mfs	6402	4210542111	W80mfs	5649
4237139210	Penn. 1	6923	4210542111	W80sb	5855
4237139188	Ln01sb	8639	4210542111	W50mfs	5950
4237139151	Ln01sb	7546	4210542111	W30mfs	6231
4237139146	Ln01sb	7850	4210542111	W20mfs	6443
4237139140	Ln01sb	7070	4210542111	W01mfs	6612
4237139133	Ln01sb	8922	4210542111	W50sb	6124
4237139133	W50mfs	9373	4210542111	W01sb	6801
4237139112	Ln01sb	7548	4210542111	Penn. 1	7016
4237139108	Ln01sb	8151	4210541549	Ln01sb	6813
4237139080	Ln01sb	6808	4210541353	Ln01sb	6087
4237139070	Ln01sb	7841	4210541353	W30mfs	6513
4237139069	Ln01sb	9649	4210541353	W01mfs	7097
4237139069	W50mfs	10154	4210540823	Ln01sb	5285
4237139069	W30mfs	10745	4210540823	W50mfs	5489
4237139061	Ln01sb	6402	4210540823	W30mfs	5698
4237139056	Ln01sb	9432	4210540823	W20mfs	5962
4237139028	Ln01sb	8072	4210540823	Penn. 1	6312
4237139005	Ln01sb	7483	4210540542	Ln01sb	7327
4237138985	Ln01sb	7351	4210540108	Ln01sb	7448
4237138893	Ln01sb	10308	4210539814	Ln01sb	6896
4237138891	Ln01sb	9136	4210539468	Ln01sb	4863
4237138891	W50mfs	9346	4210539468	W50mfs	5231

4237138891	W30mfs	9899
4237138886	Ln01sb	8070
4237138886	W50mfs	8656
4237138886	W30mfs	9934
4237138753	Ln01sb	8804
4237138753	W50mfs	9203
4237138659	Ln01sb	3167
4237138416	Ln01sb	5282
4237138416	Penn. 1	6221
4237138380	W01mfs	4635
4237138218	Ln01sb	9275
4237138192	Ln01sb	7110
4237138192	W50mfs	7667
4237138192	W30mfs	8188
4237138192	W20mfs	8939
4237138192	W01mfs	9657
4237138192	Penn. 1	10178
4237137987	Ln01sb	6640
4237137987	Ln01sb	6640
4237137987	W50mfs	7047
4237137987	W30mfs	7944
4237137987	W20mfs	8440
4237137987	W01mfs	9253
4237137987	Penn. 1	10031
4237137875	Ln01sb	1616
4237137875	W50sb	1945
4237137829	Ln01sb	6551
4237137829	W01mfs	9999
4237137790	Ln01sb	8990
4237137790	W50mfs	9397
4237137790	W30mfs	9790
4237137790	W20mfs	10344
4237137790	W01mfs	10971
4237137790	W50sb	9395
4237137790	Penn. 1	10988
4237137746	Ln01sb	9312
4237137746	W80mfs	9418
4237137746	W80sb	9929
4237137746	W50mfs	10078
4237137746	W30mfs	10772

4210539468	W30mfs	5672
4210539468	W20mfs	5975
4210539468	Penn. 1	6208
4210538855	Ln01sb	6419
4210538855	W80mfs	6500
4210538855	W80sb	6723
4210538855	W50mfs	6801
4210538855	W30mfs	7059
4210538855	W20mfs	7297
4210538855	W01mfs	7498
4210538855	W50sb	6979
4210538855	W01sb	7597
4210538855	Penn. 1	7684
4210537472	Ln01sb	6891
4210537472	W50mfs	7213
4210537472	W30mfs	7507
4210537472	W20mfs	7720
4210537472	W01mfs	7720
4210537472	Penn. 1	7728
4210537472	Penn. 1	7808
4210536447	Ln01sb	5249
4210536447	W80mfs	5135
4210536447	W80sb	5494
4210536447	W50mfs	5572
4210536447	W30mfs	5813
4210536447	W20mfs	6108
4210536447	W01mfs	6440
4210536447	W50sb	5702
4210536447	W01sb	6553
4210536447	Penn. 1	6796
4210534795	Ln01sb	5629
4210534608	W30mfs	6205
4210534608	W20mfs	6438
4210534608	Penn. 1	6681
4210534507	Ln01sb	6383
4210534507	W80mfs	6479
4210534507	W80sb	6706
4210534507	W50mfs	6766
4210534507	W30mfs	7028
4210534507	W20mfs	7250

4237137746	W20mfs	11337	4210534507	W01mfs	7344
4237137746	W01mfs	11956	4210534507	W50sb	6949
4237137746	W50sb	10477	4210534507	W01sb	7465
4237137746	W01sb	12339	4210534507	Penn. 1	7579
4237137746	Penn. 1	13451	4210534491	Ln01sb	6325
4237137709	Ln01sb	7446	4210534491	W50mfs	6625
4237137709	W50mfs	7940	4210534491	W30mfs	7117
4237137709	W30mfs	8531	4210534491	W20mfs	7613
4237137709	W20mfs	9069	4210534491	Penn. 1	7896
4237137709	W01mfs	10151	4210532896	Ln01sb	5051
4237137709	Penn. 1	11881	4210532896	W80mfs	5192
4237137640	Ln01sb	8219	4210532896	W50mfs	5367
4237137640	W50mfs	8715	4210532896	W30mfs	5656
4237137640	W30mfs	9306	4210532896	W30mfs	5656
4237137640	W20mfs	11090	4210532896	W01mfs	5769
4237137640	W01mfs	12229	4210532896	Penn. 1	5882
4237137570	Ln01sb	7054	4210532603	Ln01sb	5528
4237137570	W50mfs	7855	4210531620	Ln01sb	6481
4237137570	W30mfs	8955	4210501247	Ln01sb	4747
4237137570	W01mfs	10391	4204399999	W20mfs	324
4237137538	Ln01sb	5676	4204399999	W01mfs	518
4237137532	W50mfs	8429	4204399999	W50sb	205
4237137459	Ln01sb	10365	4204399999	W20ts	330
4237137400	Ln01sb	6106	4204399999	W01sb	551
4237137397	Ln01sb	7479	4204399998	Ln01sb	88
4237137334	Ln01sb	5495	4204399998	W50sb	764
4237137331	Ln01sb	1910	4204399997	Ln01sb	117
4237137331	W50mfs	2036	4204399996	Ln01sb	71
4237137331	W30mfs	2186	4204399996	W50mfs	266
4237137331	W20mfs	2314	4204399996	W30mfs	361
4237137331	W01mfs	2455	4204399996	W50sb	792
4237137275	Ln01sb	6437	4204399995	Ln01sb	159
4237137275	W50mfs	6664	4204399995	W50mfs	241
4237137275	W30mfs	7274	4204399995	W30mfs	321
4237137275	W20mfs	7656	4204399994	Ln01sb	94
4237137275	W01mfs	7983	4204399994	W50mfs	177
4237137275	Penn. 1	8980	4204399991	Ln01sb	40
4237137268	Ln01sb	9653	4204399989	Ln01sb	69
4237137268	W50mfs	10122	4204399989	W80mfs	261
4237137265	Ln01sb	3924	4204399989	W80ts	358

4237137230	Ln01sb	3317
4237137230	W01mfs	4041
4237137226	Ln01sb	10090
4237137152	Ln01sb	10047
4237137135	W01mfs	3987
4237137061	Ln01sb	4928
4237137025	Ln01sb	8992
4237137021	Ln01sb	8411
4237137021	W50mfs	8841
4237137021	W30mfs	9726
4237137021	W01mfs	10976
4237137021	Penn. 1	11913
4237137003	Ln01sb	6096
4237136979	Ln01sb	9403
4237136976	Ln01sb	5684
4237136971	Ln01sb	4210
4237136971	Penn. 1	4897
4237136892	Ln01sb	12469
4237136892	W50mfs	13157
4237136892	W30mfs	13778
4237136892	W01mfs	15132
4237136892	Penn. 1	16701
4237136854	Ln01sb	6096
4237136854	Penn. 1	6601
4237136828	Ln01sb	6395
4237136819	Ln01sb	10365
4237136819	W50mfs	10648
4237136819	W30mfs	11929
4237136774	Ln01sb	7118
4237136764	Ln01sb	9320
4237136756	Ln01sb	7951
4237136590	Ln01sb	6575
4237136590	W50mfs	7812
4237136549	Ln01sb	9358
4237136549	W50mfs	9792
4237136549	W30mfs	10495
4237136549	W01mfs	11485
4237136549	Penn. 1	12146
4237136545	Ln01sb	4136
4237136545	W50mfs	5049

4204399989	W80sb	412
4204399989	W50mfs	615
4204399989	W20mfs	874
4204399989	W20sb	1017
4204399989	W01mfs	1088
4204399989	W50sb	788
4204399989	W01sb	1174
4204370000	Ln01sb	270
4204330319	Ln01sb	8180
4204330293	Ln01sb	4703
4204330293	W50mfs	5284
4204330293	W30mfs	5770
4204330293	W20mfs	6439
4204330293	W01mfs	6632
4204330288	Ln01sb	3201
4204330266	Ln01sb	3108
4204330266	W80mfs	3246
4204330266	W80sb	3312
4204330266	W50mfs	3340
4204330266	W20mfs	3478
4204330266	W20sb	3588
4204330266	W01mfs	3708
4204330266	W50sb	3383
4204330266	W20ts	3515
4204330266	W01sb	3832
4204330266	Penn. 1	5468
4204330265	Ln01sb	6093
4204330265	W50mfs	6727
4204330265	W30mfs	7547
4204330265	W20mfs	9019
4204330265	W01mfs	10412
4204330265	Penn. 1	10412
4204330231	Ln01sb	4897
4204330231	W80mfs	5008
4204330231	W80sb	5107
4204330231	W50mfs	5157
4204330231	W30mfs	5292
4204330231	W20mfs	5776
4204330231	W01mfs	6036
4204330231	W01sb	6383

4237136545	W30mfs	5905
4237136545	W20mfs	6967
4237136532	Ln01sb	4995
4237136521	Ln01sb	9196
4237136521	W50mfs	9957
4237136521	W30mfs	10528
4237136423	W01mfs	11965
4237136272	Ln01sb	8037
4237136272	W50mfs	8454
4237136272	W30mfs	8984
4237136272	W20mfs	9392
4237136272	W01mfs	9904
4237136272	Penn. 1	10286

4204330231	Penn. 1	9512
4204310103	Ln01sb	3663
4204300023	Ln01sb	4851
4200345081	Ln01sb	9659
4200345081	W01mfs	10492
4200342107	Ln01sb	9817
4200342107	W50mfs	10242